Universitat d'Alacant
Universidad de Alicante

Oxidación de etanol y ácido fórmico en nanocristales de platino: Electrocatálisis y reactividad superficial

Ethanol and formic acid oxidation in platinum nanocrystals: Electrocatalysis and surface reactivity

Carlos Antonio Busó Rogero

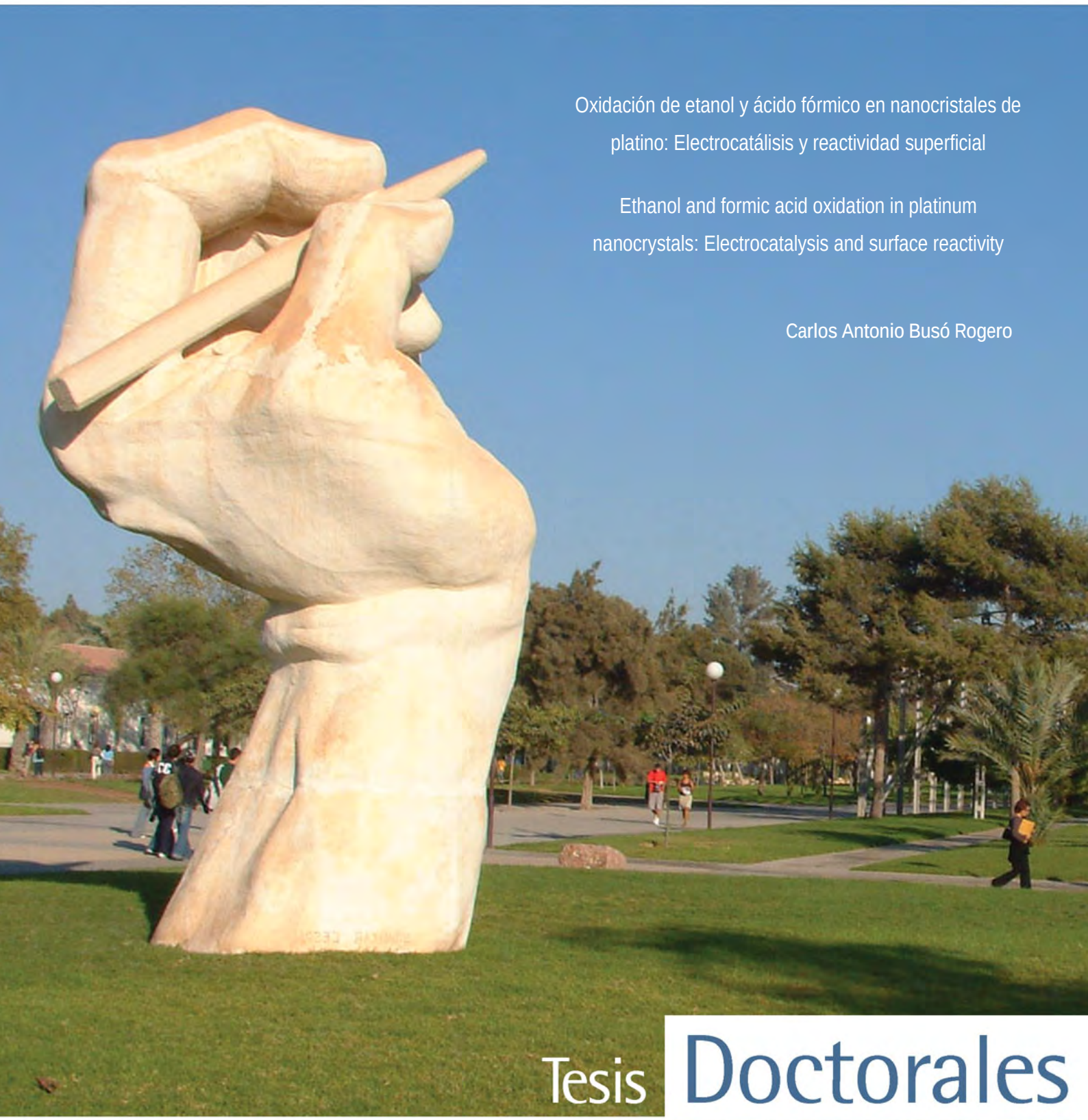

Tesis Doctorales

www.eltallerdigital.com

UNIVERSIDAD de ALICANTE

Universitat d'Alacant
Universidad de Alicante

Instituto Universitario de Electroquímica

Facultad de Ciencias

Oxidación de etanol y ácido fórmico en nanocristales de platino: Electrocatálisis y reactividad superficial

Ethanol and formic acid oxidation in platinum nanocrystals: Electrocatalysis and surface reactivity

Carlos Antonio Busó Rogero

Tesis presentada para aspirar al grado de

DOCTOR POR LA UNIVERSIDAD DE ALICANTE

MENCIÓN DE DOCTOR INTERNACIONAL

Programa de Doctorado Electroquímica, Ciencia y Tecnología RD 99/2011

Dirigida por:

Enrique Herrero Rodríguez

Catedrático de Universidad en el Dpto. de Química Física de la Universidad de Alicante

Juan Miguel Feliu Martínez

Catedrático de Universidad en el Dpto. de Química Física de la Universidad de Alicante

Alicante, Mayo 2016

Agradecimientos/Acknowledgements

Los años en los cuales se realiza la tesis doctoral son un período de continuo aprendizaje tanto desde el punto de vista formativo como en el personal. Su realización requiere indudablemente de una gran cantidad de trabajo imposible de realizar sin ayuda. Por ello, me gustaría agradecer a todas las personas que hayan contribuido con su granito de arena a esta tesis doctoral, especialmente a:

- Enrique Herrero, por introducirme en el laboratorio hace ya unos años, y por haber sido el principal supervisor de mi tesis. A pesar de ser una de las personas más atareadas que conozco, gracias por estar siempre dispuesto a ayudarme en lo necesario y a resolverme cualquier duda (y no sólo de Electroquímica).
- Juan M. Feliu, la persona que más pasión demuestra hacia la Electroquímica de Superficies, por ser codirector de la tesis, por el suministro de nuevos electrodos monocristalinos siempre que hayan sido necesarios y por los consejos dados durante estos años.
- José Solla y Fran Vidal, por toda la ayuda al proporcionarme las muestras de nanopartículas necesarias para llevar a cabo gran parte de los trabajos aquí presentados, por la enseñanza del método para trabajar correctamente con nanopartículas y por la rápida resolución de cualquier duda surgida al trabajar con ellas. También quisiera agradecer a ambos vuestra involucración en casi todos los trabajos que he logrado publicar.
- Prof. Behm, for accepting me in the Ulm University and for his contribution in the DEMS experiments discussion presented in this thesis. Thanks also to Sylvain Brimaud for supervising my work there and to Zenonas Jusys for his useful help in the laboratory during the performance of the experiments.
- Victor Climent, por su ayuda ante cualquier problema relacionado con la Electroquímica o cualquier cuestión general del laboratorio. También gracias a Antonio Rodes por sus útiles consejos para la correcta elaboración de experimentos espectroelectroquímicos.
- Manuel J.S. Farías y Vitali Grozovski, por la contribución directa en la elaboración de estos trabajos y por poner siempre a mi disposición vuestra experiencia en investigación relacionada con la Electroquímica.

- A todas las personas que han colaborado en la asistencia técnica durante la realización del doctorado, ya sean técnicos de laboratorio, vidrieros o técnicos del taller mecánico, por la paciencia que han tenido conmigo, por las ideas aportadas y por la rapidez en entregar el material requerido.
- A compañeros del laboratorio que han contribuido directamente a la mejora de los resultados experimentales de la tesis: Antonio Berná, que tuvo mucha paciencia en mis inicios y me enseñó muchos 'trucos' trabajando en el laboratorio; Marta Figueiredo, también por sus sugerencias que han influido en el éxito de mis experimentos y que sigo utilizando a día de hoy; el excéntrico William Cheuquepan, por su colaboración en el laboratorio de IR, resolviendo cualquier duda y buscando la perfección en los experimentos; y a Ana Boronat, una de las personas con más bondad que conozco, por ofrecerme su ayuda en todo momento sin esperar nada a cambio.
- A todos mis compañeros de la Universidad de Alicante, que de una forma u otra han hecho estos años más agradables y que se han llegado a convertir en buenos amigos tras compartir tanto tiempo de trabajo y risas: Rubén G, Alberto V, Sara Chumillas, Jonnathan, Juan Victor, Betzhy, Ricardo, Rosi, Rubén R., Valentín, Fran, Gisele, Paula, Andrea, Ana María, Miguel Ángel, Naiara, Leti, Alicia, David S., Alonso, Paco Montilla, Ana C., María P., María José, Sara L., Carolina, Omar O., Ariadna, Nacho, David V, Irene, Milena, Dejan, Fabián, Néstor, Laura P, Aroldo, Moha.… Habéis creado en mí grandes recuerdos, como las cenas de San Alberto o los derbys de fútbol sala entre el grupo de Superficies y el de Polímeros.
- Mis amigos (vosotros sabéis quiénes sois), ya sea de la carrera, los del grupo de Alicante o los que he tenido la suerte de conocer durante los años de doctorado gracias a actividades derivadas de esta tesis, los cuales siempre me han ofrecido su apoyo comprendiendo la dificultad de la exhaustiva dedicación a una tesis doctoral. Especial agradecimiento a Bea y Mayer por sus continuos ánimos y por las risas en las quedadas que hemos realizado en estos años.
- Mi familia, especialmente mi madre, mi padre y mi hermana, que también me han apoyado y han soportado mi mal humor en épocas con alta cargas de estrés y, simplemente, por quererme tal como soy.

A mis padres y mi hermana

Índice

Abstract

Abstract

In the present thesis, fundamental studies for the oxidation of small organic molecules (ethanol and formic acid) have been performed. These molecules can be used as reactive in the anode for the fuel cell technology. For this purpose, platinum catalysts in the form of single crystal surfaces and nanoparticles have been employed. The final aim is to find the best catalyst for achieving the highest possible activity at the lower overpotential, avoiding the formation of undesired products, such as CO in the formic acid oxidation process and acetic acid/acetate in the case of ethanol oxidation. The results presented here will allow a better understanding of these oxidation processes, and how different factors, such the surface structure, the solution pH, and the agglomeration of the nanoparticles, affect to the catalytic response of the electrodes and can help to develop better electrocatalysts. In addition, the modification of the surface reactivity by deposition of foreign adatoms, seeking an enhancement in the catalytic activity of the nanoparticles for the considered reactions, will be also studied.

In these studies, electrochemical techniques, such as cyclic voltammetry and chronoamperometry, have been used for characterizing the platinum electrodes and studying the reactivity of the electrodes for the two reactions. The possible intermediates and final products of the reaction have been characterized using the spectroelectrochemical techniques Fourier Transformed-Infrared Reflection-Absorption Spectroscopy (FT-IRRAS) with external reflection and Attenuated Total Reflection-Fourier Transform Infrared (ATR-FTIR). Differential Electrochemical Mass Spectrometry (DEMS) is also employed for obtaining quantitative data about the oxidation mechanism.

The results of Colmati *et. al.* [1] with single crystal electrodes in acidic solutions demonstrated that ethanol oxidation reaction on platinum is a structure sensitive reaction. For Pt(111) electrodes only acetic acid is produced, whereas for Pt(110) and, especially, Pt(100) electrodes the C-C bond scission is also taking place, leading to the formation of adsorbed CO before the complete oxidation to CO_2. Chapter 2 shows the extension of these studies to practical catalysts, using nanoparticles with preferential shape [2, 3] by means of electrochemical and spectroscopic techniques. The results show that the behavior of the

nanoparticles can be rationalized using the data obtained with the single crystal electrodes. On the other hand, anion adsorption effects are also investigated. It is found that there are no significant differences in the oxidation currents in H_2SO_4 and $HClO_4$ electrolytes, *i.e.*, irrespectively of the presence of specifically adsorbed anions in the electrolyte. The formation of acetic acid, which is adsorbed specifically on the electrode surface as acetate and is always formed regardless of the presence of {111} or {100} domains, justifies the absence of differences.

The oxidation mechanism for ethanol oxidation is strongly affected by the solution pH. For this reason, chapter 3 studies how pH influences the ratio of products using DEMS in flow cell conditions [4]. The pH is always maintained below 4 for avoiding carbonate formation, which can interfere in the analysis of the results. Preferentially shaped (100)Pt and (111)Pt nanoparticles samples are used for these experiments. These two samples were selected because they represent the paradigm of the two distinct behaviors shown in chapter 2. (100)Pt nanoparticles are more active than (111)Pt nanoparticles for the formation of C1 fragments (CO or CH_x), as the better efficiency for CO_2 production demonstrates, 10% vs. 5% respectively. The results also indicate that the increase of pH leads to a lower rate for the C-C bond breaking and a stabilization of the CH_x fragments.

Continuing with the pH effect on ethanol oxidation, the studies in alkaline solutions are started in chapter 4. These studies can be important for the development of alkaline fuel cells, where the lower corrosive properties of the medium will allow the use of non-noble metals as catalysts. First of all, single crystal electrodes with a well-known crystallographic structure are used for a better understanding of the reaction, following the same strategy used in the studies in acidic media [1, 5], that is, the behavior of the low index planes and the effect of the presence of {100} and {110} steps on {111} terraces for ethanol oxidation will be studied. The results, which are compared with previous works done in similar conditions [6-8], show that the Pt(111) electrode has the highest activity, followed by the Pt(110) and Pt(100) electrodes. This reactivity trend is the opposite to that found in acidic medium. Similarly, the {100} and {110} steps in {111} terraces do not increase the currents for ethanol oxidation in alkaline solutions, despite lower onset potential values are obtained. In addition, IR experiments confirm the poor selectivity of the platinum electrodes for the CO_2 formation, producing quasi exclusively acetate. The IR spectra,

which was analyzed using a similar strategy than that employed in ref. [9], demonstrate that the amount of carbonate formed on the three electrodes is negligible. On the other hand, the huge deactivation detected for all the platinum surfaces is attributed to the polymerization of the acetaldehyde produced from the ethanol oxidation reaction. The deactivation process affects especially the {111} ordered domains.

In the same way as in chapter 2, ethanol oxidation on shape-controlled platinum nanoparticles is studied in chapter 5 for alkaline solutions, in the same conditions of the previous results with single crystal electrodes. The affinity for the acetate formation observed in chapter 4 is corroborated with the shape-controlled platinum nanoparticle samples, and the trend for the activity in the Pt nanoparticles electrodes also agrees with the previous results. In addition to the surface structure effect, the agglomeration effects in the reactivity are also attempted. For that purpose, nanoparticle samples dispersed in carbon are employed. The importance of attaining a good dispersion of the nanoparticles on the support for measuring the correct catalytic activity is highlighted. This good dispersion of the nanoparticles on the support assures that all of them could participate in the reaction. The best dispersion are obtained using the method of Garsany and co-workers [10], which used a slow rotation of the support during the deposition of the nanoparticles.

The effects of the modification of the shape-controlled platinum nanoparticles composition, specifically the (100)Pt and (111)Pt nanoparticles, with adatoms in its reactivity are studied in chapters 6 and 7. The first studies are conducted for the formic acid oxidation reaction, trying to increase the rate for CO_2 production and avoiding the CO formation. Modifications of the Pt electrodes with adsorbed Bi, As or Pd have been shown large enhancement in the currents measured for the formic acid oxidation reaction [11-13]. In the present case, Tl is deposited on the platinum surfaces. For both (100)Pt and (111)Pt nanoparticles, Tl adsorption shows a positive effect, shifting the onset potential to lower values (around 0.1 V), with the absence of CO formation. Specifically, (100)Pt nanoparticles show higher activity than (111)Pt nanoparticles. FTIR experiments indicate that the presence of Tl inhibits the formation of CO. Moreover, the effect of formic acid concentration for the Tl-modified Pt nanoparticles electrodes is also investigated, displaying some complexity in the oxidation mechanism and suggesting additional species involved in this reaction.

Finally, chapter 7 deals with the effect of adatoms for ethanol oxidation. The study was carried out both in acidic and alkaline media using (100)Pt or (111)Pt nanoparticles. From the different adatoms studied in the literature for this reaction (Sn [14], Ru [15], Os [16], Bi [17] or Pb [18, 19]), Sn, Rh, Ru and Pb were selected since they show higher catalysis. As before, the target is an electrode which displays higher currents and lower overpotentials for the ethanol oxidation reaction. In 0.5 M H_2SO_4, the best activity is found for Pt-Sn; the onset potential shifts towards more negative values, mainly for the (100)Pt nanoparticles. This effect is attributed to the catalysis of the oxidation of CO to CO_2. For the (111)Pt nanoparticles, higher currents are also observed, due to a catalytic effect in the oxidation of ethanol to acetic acid at high Sn coverages [20]. For 0.1 M NaOH, very minor positive effects are found for the Pt-Rh, Pt-Sn and Pt-Pb surfaces, mainly in the (100)Pt nanoparticles samples.

In summary, fundamental studies about the effect of the surface structure and composition for the ethanol oxidation reaction are carried out in this thesis. These studies have used shape-controlled platinum nanoparticles, which is the form of the catalysts more interesting from the applied point of view. These works have been complemented with studies on single crystal electrodes, to better understand the reaction mechanism. The important effect of the solution pH in the reaction mechanism is highlighted. Finally, the effect of the surface composition is studied. The catalysis of the formic acid oxidation is more effective, due to the simpler reaction mechanism. For the ethanol oxidation, the different steps in the reaction (dehydrogenation, C-C bond scission, oxidation to CO and finally to CO_2) probably requires complex strategies to find a suitable electrocatalyst.

References

[1] F. Colmati, G. Tremiliosi-Filho, E. R. Gonzalez, A. Berná, E. Herrero and J. M. Feliu, "Surface structure effects on the electrochemical oxidation of ethanol on platinum single crystal electrodes" *Faraday Discussions* **2008**, 140, 379-397.

[2] J. Solla-Gullón, F. J. Vidal-Iglesias, A. López-Cudero, E. Garnier, J. M. Feliu and A. Aldaz, "Shape-dependent electrocatalysis: methanol and formic acid electrooxidation on preferentially oriented Pt nanoparticles" *Physical Chemistry Chemical Physics* **2008**, 10, 3689-3698.

[3] V. Grozovski, J. Solla-Gullón, V. Climent, E. Herrero and J. M. Feliu, "Formic Acid Oxidation on Shape-Controlled Pt Nanoparticles Studied by Pulsed Voltammetry" *Journal of Physical Chemistry C* **2010**, 114, 13802-13812.

[4] M. Heinen, Y. X. Chen, Z. Jusys and R. J. Behm, "In situ ATR-FTIRS coupled with on-line DEMS under controlled mass transport conditions - A novel tool for electrocatalytic reaction studies" *Electrochimica Acta* **2007**, 52, 5634-5643.

[5] F. Colmati, G. Tremiliosi-Filho, E. R. Gonzalez, A. Berná, E. Herrero and J. M. Feliu, "The role of the steps in the cleavage of the C-C bond during ethanol oxidation on platinum electrodes" *Physical Chemistry Chemical Physics* **2009**, 11, 9114-9123.

[6] M. López-Atalaya, E. Morallón, F. Cases, J. L. Vázquez and J. M. Pérez, "Electrochemical oxidation of ethanol on Pt(hkl) basal surfaces in NaOH and Na_2CO_3 media" *Journal of Power Sources* **1994**, 52, 109-117.

[7] S. C. S. Lai and M. T. M. Koper, "Ethanol electro-oxidation on platinum in alkaline media" *Physical Chemistry Chemical Physics* **2009**, 11, 10446-10456.

[8] P. A. Christensen, S. W. M. Jones and A. Hamnett, "In Situ FTIR Studies of Ethanol Oxidation at Polycrystalline Pt in Alkaline Solution" *Journal of Physical Chemistry C* **2012**, 116, 24681-24689.

[9] Z.-Y. Zhou, Q. Wang, J.-L. Lin, N. Tian and S.-G. Sun, "In situ FTIR spectroscopic studies of electrooxidation of ethanol on Pd electrode in alkaline media" *Electrochimica Acta* **2010**, 55, 7995-7999.

[10] Y. Garsany, I. L. Singer and K. E. Swider-Lyons, "Impact of film drying procedures on RDE characterization of Pt/VC electrocatalysts" *Journal of Electroanalytical Chemistry* **2011**, 662, 396-406.

[11] S. A. Campbell and R. Parsons, "Effect of Bi and Sn adatoms on formic acid and methanol oxidation at well defined platinum surfaces" *Journal of the Chemical Society, Faraday Transactions* **1992**, 88, 833-841.

[12] F. J. Vidal-Iglesias, A. López-Cudero, J. Solla-Gullón and J. M. Feliu, "Towards More Active and Stable Electrocatalysts for Formic Acid Electrooxidation: Antimony-Decorated Octahedral Platinum Nanoparticles" *Angewandte Chemie-International Edition* **2013**, 52, 964-967.

[13] F. J. Vidal-Iglesias, J. Solla-Gullón, E. Herrero, A. Aldaz and J. M. Feliu, "Pd Adatom Decorated (100) Preferentially Oriented Pt Nanoparticles for Formic Acid Electrooxidation" *Angewandte Chemie-International Edition* **2010**, 49, 6998-7001.

[14] Q. W. Zheng, C. H. Fan, C. H. Zhen, Z. Y. Zhou and S. G. Sun, "Irreversible adsorption of Sn adatoms on basal planes of Pt single crystal and its impact on electrooxidation of ethanol" *Electrochimica Acta* **2008**, 53, 6081-6088.

[15] V. Del Colle, A. Berná, G. Tremiliosi-Filho, E. Herrero and J. M. Feliu, "Ethanol electrooxidation onto stepped surfaces modified by Ru deposition: electrochemical and spectroscopic studies" *Physical Chemistry Chemical Physics* **2008**, 10, 3766-3773.

[16] V. Del Colle, V. Santos and G. Tremiliosi-Filho, "Comparative Electrochemical and Spectroscopic Studies of Ethanol Oxidation on Pt(h,k,l) Modified by Osmium Nanoislands" *Electrocatalysis* **2010**, 1, 144-158.

[17] M. C. Figueiredo, A. Santasalo-Aarnio, F. J. Vidal-Iglesias, J. Solla-Gullón, J. M. Feliu, K. Kontturi and T. Kallio, "Tailoring properties of platinum supported catalysts by irreversible adsorbed adatoms toward ethanol oxidation for direct ethanol fuel cells" *Applied Catalysis B-Environmental* **2013**, 140, 378-385.

[18] Q. G. He, B. Shyam, K. Macounova, P. Krtil, D. Ramaker and S. Mukerjee, "Dramatically Enhanced Cleavage of the C-C Bond Using an Electrocatalytically Coupled Reaction" *Journal of the American Chemical Society* **2012**, 134, 8655-8661.

[19] P. A. Christensen, S. W. M. Jones and A. Hamnett, "An in situ FTIR spectroscopic study of the electrochemical oxidation of ethanol at a Pb-modified polycrystalline Pt electrode immersed in aqueous KOH" *Physical Chemistry Chemical Physics* **2013**, 15, 17268-17276.

[20] V. Del Colle, J. Souza-Garcia, G. Tremiliosi-Filho, E. Herrero and J. M. Feliu, "Electrochemical and spectroscopic studies of ethanol oxidation on Pt stepped surfaces modified by tin adatoms" *Physical Chemistry Chemical Physics* **2011**, 13, 12163-12172.

Capítulo 1:

Síntesis

Capítulo 1: Síntesis

1.1 Introducción

La Electroquímica focaliza sus estudios en los procesos de transferencia de carga que ocurren en la interfase entre un conductor electrónico y un conductor iónico o directamente entre dos conductores iónicos [1]. De acuerdo con Bockris y Reddy [2], históricamente los estudios de la Electroquímica se dividen en dos grandes grupos:

- *Iónica:* Trata de sistemas homogéneos relacionados con iones en disolución (acuosa o no), sales iónicas o electrolitos sólidos.

- *Electródica:* Estudia lo que sucede en una interfase electrodo/electrolito a través de una transferencia de electrones.

Después de los primeros experimentos que evidenciaban la existencia de la electroquímica (Galvani en 1791, Volta en 1799 y Faraday en 1831), los estudios posteriores vinieron marcados por la publicación de Nernst sobre la termodinámica de las pilas galvánicas (1891), que decantaron la investigación hacia las reacciones en equilibrio y las propiedades termodinámicas de las disoluciones. Esta situación cambia cuando se empiezan a considerar algunas publicaciones realizadas anteriormente acerca de la cinética electroquímica (Butler en 1924, Volmer en 1930 o Frumkin en la década de los años 30), lo cual provocó una orientación de todas las investigaciones electroquímicas hacia la cinética electródica a partir de entonces.

La Electroquímica electródica también se considera una parte de la ciencia de superficies, ya que estudia los fenómenos físicos y químicos ocurridos en la interfase metal-disolución, atendiendo tanto a sus propiedades macroscópicas (normalmente carga, potencial y corriente eléctrica) como a las microscópicas. Por tanto, es importante realizar un análisis adecuado de la estructura metálica a nivel atómico. Para un correcto estudio de

la interfase metálica hasta niveles microscópicos, en primera aproximación, son necesarias técnicas de caracterización superficial que precisan condiciones de ultra alto vacío (*ultra high vacuum*, UHV, en sus siglas en inglés). Estas técnicas favorecen el control del máximo número de variables posibles para mejorar la caracterización, como por ejemplo trabajar a bajas presiones para evitar la contaminación de la superficie metálica (en la sección 1.3 se presentan algunos ejemplos de estas técnicas). Esta metodología deberá extenderse posteriormente a las condiciones electroquímicas *in-situ*: en disolución y con potencial aplicado. Sin embargo, esa caracterización UHV-Electroquímica requiere técnicas experimentales muy costosas y no siempre el resultado es satisfactorio, por lo que conviene algún método alternativo más sencillo para realizarla, siendo capaz de encontrar las relaciones existentes entre las propiedades macroscópicas y microscópicas de una superficie metálica en condiciones electroquímicas (por ejemplo, mediante una simple voltametría cíclica). De este modo será posible obtener información relevante en Electroquímica de Superficies.

En la actualidad, la Electroquímica está presente en muchos aspectos de la vida cotidiana, como en el caso de la fabricación de biosensores [3, 4], electroanálisis [5, 6], células solares [7], tratamiento de aguas [8], electrosíntesis [9, 10], corrosión [11] y almacenamiento de energía [12, 13], entre otras. No obstante, una de las aplicaciones más importantes de la Electroquímica es la de la obtención de energía a partir de baterías, las cuales se clasifican en dos tipos: primarias (donde la batería produce energía hasta que el reactivo químico encargado de ello se agota) o secundarias, las cuales se pueden recargar. Ejemplos de baterías son los acumuladores, las baterías de flujo o las pilas de combustible [14-17]. Dentro de los dispositivos electroquímicos primarios para la obtención de energía, el grupo particular de las pilas de combustible tiene por objeto generar electricidad a partir de un suministro de combustible externo y oxígeno mediante una reacción química controlada, originando la formación de productos y el abastecimiento de energía eléctrica a un circuito externo. Su funcionamiento es similar al de las baterías, con la salvedad de que necesitan un suministro continuo de los reactivos empleados.

Las pilas de combustible presentan ventajas respecto a otras fuentes de energía, como el nulo deterioro de los electrodos y la baja contaminación para el medio ambiente producto de las disoluciones utilizadas, además de las altas eficiencias observadas debido a

la inexistencia de procesos térmicos o mecánicos asociados a la producción de la energía eléctrica. Por tanto, las pilas de combustible se pueden considerar como un recurso energético alternativo, limpio y útil para el futuro teniendo en cuenta el agotamiento de las fuentes de energía fósiles.

Desde la primera pila de combustible fabricada a partir de hidrógeno y oxígeno empleando electrodos de platino, publicada por Groove en 1839, se han diseñado multitud de pilas de combustible utilizando pequeñas moléculas orgánicas e inorgánicas en el ánodo, además del citado hidrógeno. Las principales tecnologías desarrolladas para estos dispositivos actualmente se pueden clasificar atendiendo al reactivo o al tipo de electrolito utilizado [17, 18]:

- *Pilas de combustible alcalinas (AFC)*: Una de las razones para el uso de electrolitos alcalinos es el de abrir la posibilidad a la utilización de catalizadores menos nobles. Como en las pilas de combustible más habituales, utilizan hidrógeno en el ánodo y oxígeno en el cátodo. Se han llegado a obtener potencias de hasta 0.8 W cm^{-2} en prototipos realizados para la NASA, con eficiencias en torno al 50% y un tiempo de vida de hasta 10000 horas.

- *Pilas de combustible de ácido fosfórico (PAFC)*: En estas pilas de combustible, el ácido fosfórico actúa como electrolito iónico y como disolvente y trabajan a temperaturas en torno a los 170-200 º C. Utiliza Pt como catalizador para el ánodo, donde se sigue empleando hidrógeno como reactivo, aunque en el cátodo se usa Pt-Co-Cr como catalizador. Se han llegado a alcanzar potencias de 0.2 W cm^{-2} y eficiencias en torno al 40-50%, con un tiempo de vida largo (hasta 40000 horas).

- *Pilas de combustible de membrana de intercambio protónico (PEMFC)*: Utilizan una membrana sólida, fabricada con un polímero capaz de conducir protones (el cual constituye el electrolito sólido), intercalada entre dos electrodos de platino porosos que permiten la difusión del hidrógeno y del oxígeno. Entre todas las membranas fabricadas para este tipo de pila de

combustible destacan las de Nafion, permitiendo alcanzar potencias de hasta 0.7 W cm^{-2}, con eficiencias y tiempo de vida similares a las AFC.

- *Pilas de combustible de metanol directa (DMFC)*: Usan metanol en lugar de hidrógeno como reactivo en el ánodo. Se han fabricado DMFC con ácido sulfúrico como electrolito soporte empleando ánodos de metales nobles como Pt, Ru, Pd o combinación entre ellos. Además de la lenta cinética de electrodo, un problema a solventar en esta pila de combustible es el conocido como *crossover* del metanol, que pasa del ánodo al cátodo a través de la membrana. Al igual que las PEMFC, se han preparado DMFC con membranas poliméricas como el Nafion, llegando a obtener potencias de alrededor de 0.2 W cm^{-2} con un tiempo de vida hasta 1000 horas y eficiencias en torno al 30-35%.

- *Pilas de combustible de carbonato fundido (MCFC)*: En estos dispositivos, la reacción catódica consume oxígeno y dióxido de carbono produciendo carbonatos, que son conducidos hacia el ánodo donde se une con el hidrógeno para formar agua y dióxido de carbono, el cual retorna al compartimento catódico. La temperatura operativa es muy elevada, 650ºC, favoreciendo sobrepotenciales más bajos para el inicio de las reacciones de la pila de combustible y la no necesidad de metales muy nobles. La eficiencia y tiempo de vida es similar al de las pilas PEMFC y AFC, mientras que la potencia es de 0.12 W cm^{-2}.

- *Pilas de combustible de óxido sólido (SOFC)*: Estas pilas de combustible utilizan una tecnología diferente con un sistema de cátodos y ánodos porosos de lantano dopados con cationes divalentes y un electrolito formado por óxidos de ytrio y zirconio. Para asegurar buenas conductividades iónicas y electrónicas, se necesitan temperaturas muy elevadas (entre 800 y 1000ºC). El combustible es hidrógeno, la potencia obtenida puede llegar a ser hasta de 1.2 W cm^{-2}, la eficiencia está en torno al 50% y el tiempo de vida alcanza las 10000 horas.

Además de las anteriores pilas de combustible, se han desarrollado otros prototipos no comercializados, como por ejemplo *la pila de combustible de etanol directa (DEFC)* [19] similar a las DMFCs, pero con algunas ventajas como su mayor densidad energética, su nula toxicidad y su casi inexistente crossover a través de la membrana comparándolo con el metanol [20]. Sin embargo, todavía presentan el inconveniente de que su potencia está lejos de la de las pilas de hidrógeno. Por otra parte, se han propuesto otras alternativas como combustible, como es el caso de ácido fórmico [21], compuestos nitrogenados como amoníaco [22] o hidracina [23], hidruros metálicos como el borohidruro [24] o pilas de combustible que utilizan catalizadores como enzimas o bacterias [25, 26].

Actualmente, para el desarrollo de nuevas pilas de combustible, los estudios fundamentales de oxidación de pequeñas moléculas orgánicas en diferentes catalizadores son interesantes de cara a su uso como reacción anódica, especialmente con alcoholes de hasta 3 átomos de carbono como el glicerol. De manera análoga, se llevan a cabo investigaciones similares para la reducción de oxígeno, la reacción catódica más común en las pilas de combustibles. Estos estudios se hacen prestando atención a diferentes parámetros como el pH del medio, la temperatura de trabajo o el catalizador utilizado. En la presente tesis, se aborda el estudio de catalizadores para la oxidación de ácido fórmico y, especialmente, para el etanol, de interés medioambiental debido a la posibilidad de producirlo a partir de la fermentación de azúcares.

Un catalizador modifica la velocidad de una reacción química sin consumirse durante el proceso. Si ese catalizador se utiliza en el cátodo o en el ánodo de una pila de combustible, contribuye a acelerar la correspondiente reacción electródica. El electrodo actúa como sustrato para facilitar la transformación electroquímica, lo que se conoce como electrocatalizador [2], que permite aumentar la velocidad de reacción manteniendo la diferencia de potencial aplicada en la interfase, el denominado sobrepotencial. Con respecto a los tradicionales catalizadores químicos, la electrocatálisis tiene lugar a temperaturas operativas más bajas, siendo el potencial el responsable de incidir en la energía de activación necesaria para el inicio de las reacciones electroquímicas.

Desde mediados del siglo pasado existen numerosos estudios con diferentes metales nobles buscando el mejor catalizador para la oxidación de pequeñas moléculas orgánicas.

Ejemplos claros de estos catalizadores para la oxidación de alcoholes son el oro, el platino, el paladio y el rodio, generalmente usando electrolitos alcalinos, un ambiente menos corrosivo y más favorable desde el punto de vista de la economía, ya que abre la posibilidad del uso de materiales más baratos [27, 28]. Como ejemplo de la capacidad electrocatalítica de varios metales nobles, se presenta la oxidación de n-butanol en medio alcalino (Fig. 1.1) para los cuatro metales mencionados [29].

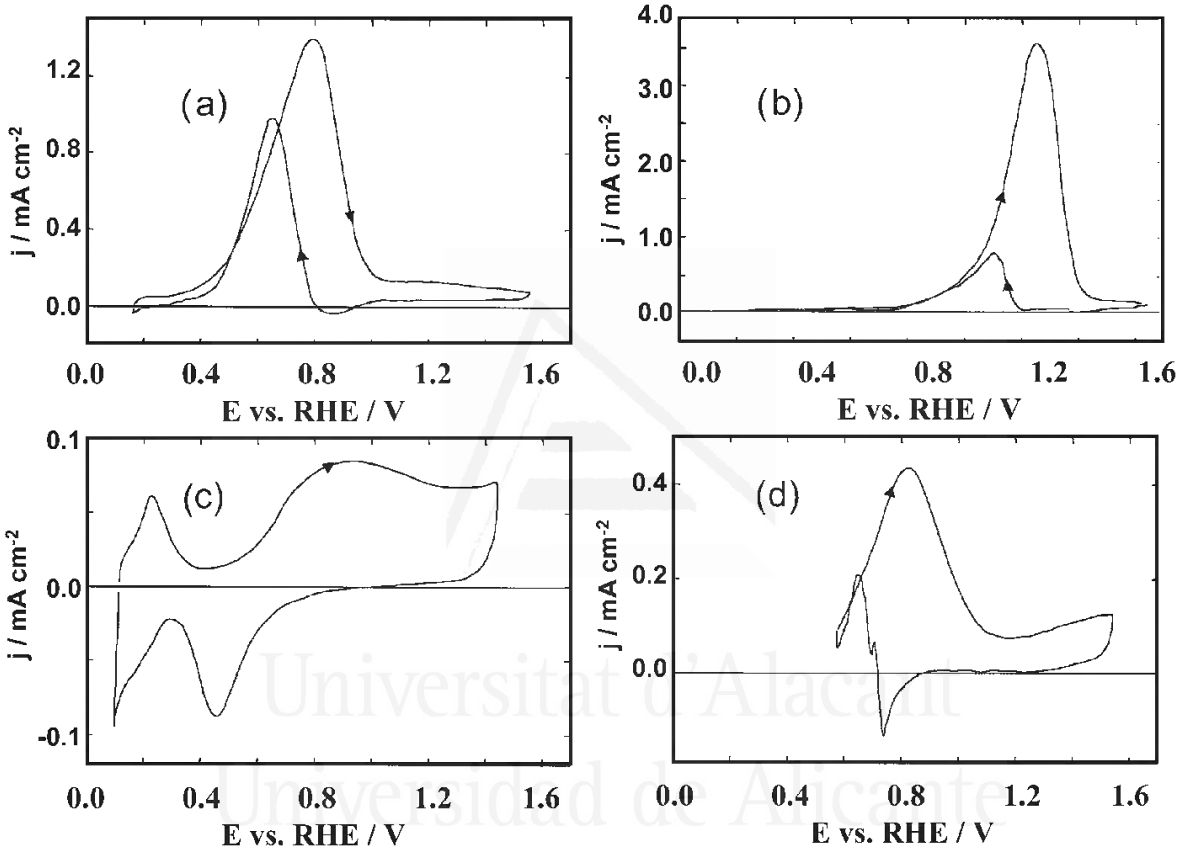

Fig. 1.1. Voltametría cíclica para la oxidación de 0.1 M n-butanol en 0.1 M NaOH a 25ºC y una velocidad de barrido de 50 mV s^{-1} para diferentes electrodos metálicos: (a) Platino, (b) Oro, (c) Rodio y (d) Paladio. Datos publicados de la ref. [28].

La mayor actividad total la presenta el oro, aunque los menores sobrepotenciales para iniciar la oxidación del n-butanol se dan en el platino, lo cual es conveniente de cara a su utilización en sistemas de generación de energía. El paladio se muestra menos activo que los otros dos metales, mientras que el rodio apenas presenta actividad en estas condiciones. A pesar de que el oro y el platino son catalizadores bastante activos en medio alcalino, sin duda, el platino es el único metal noble que presenta actividades catalíticas importantes

para la oxidación de casi todos estos compuestos a pHs ácidos [30]. Por ello, los estudios electrocatalíticos, objeto de esta tesis, están enfocados en los electrodos de platino en electrolitos con diferentes pHs, tratando de racionalizar los cambios en la reactividad de los alcoholes al cambiar de medio ácido a medio básico.

Al oxidar moléculas orgánicas como el ácido fórmico, el metanol, el etanol o el etilenglicol en platino, uno de los mayores problemas es el del envenenamiento del catalizador producto del CO formado durante la oxidación [31], el cual bloquea la superficie y retarda el potencial al cual se produce la oxidación de estas moléculas a CO_2, producto principal de la oxidación. En el caso de moléculas de más de un átomo de carbono, se forman otros productos no deseados debido a la dificultad de romper el enlace C-C, produciendo moléculas como el ácido acético [32], la cual es muy complicada de oxidar. Todas estas reacciones electroquímicas, estudiadas en platino, son sensibles a la estructura superficial del electrodo, es decir, dependiendo de cómo sea la orientación cristalográfica de los átomos en el catalizador, la reactividad cambia, variando la cantidad de CO producido y, por ende, la cantidad de CO_2 total formado.

Para entender cómo afecta la estructura superficial en platino a la reactividad se utilizan electrodos monocristalinos con superficies bien definidas preparados según el método de Clavilier, el cual se explicará en la sección 1.3 de esta síntesis. Estas investigaciones dan información fundamental muy interesante acerca de cómo varía la relación entre los productos formados en la oxidación de pequeñas moléculas orgánicas en función de la orientación cristalográfica de los electrodos. Sin embargo, desde un punto de vista aplicado como el de las pilas de combustible, el coste de grandes catalizadores a partir de superficies monocristalinas sería prohibitivo, lo que hace que su aplicación sea inviable debido al alto coste del platino. Una manera de abaratar el coste del catalizador es el del uso de nanopartículas, que optimizan el área activa usando la menor cantidad posible de platino. Hay métodos desarrollados en la actualidad mediante los cuales se sintetizan nanopartículas con tamaños entre 5 y 10 nm y en las cuales se puede controlar la estructura superficial para que tenga preferencia por distintas formas, que indican la presencia de diferentes estructuras superficiales [33, 34], encontrándose una buena relación entre la reactividad de estas nanopartículas y la observada en superficies monocristalinas de platino.

1.1.1 Oxidación de ácido fórmico en Pt

La oxidación del ácido fórmico es una reacción de gran interés, ya que sirve como modelo para el estudio de oxidaciones similares con moléculas orgánicas más complejas, y ha sido objeto de abundantes estudios en los últimos 50 años. De cara a su uso como combustible, el ácido fórmico presenta como ventajas una cinética relativamente rápida, una disminución en el 'crossover', comparándolo con otros alcoholes, o su baja temperatura operativa, ventajas que compensan otros inconvenientes como su baja densidad energética teórica (1.63 kW h kg^{-1}) [21, 35]. La reacción global de la oxidación es un proceso simple en el que se intercambian dos electrones:

$$HCOOH \longrightarrow CO_2 + 2H^+ + 2e^- \quad (1.1)$$

Termodinámicamente, el potencial estándar de esta reacción es -0.25 V frente al electrodo normal de hidrógeno (NHE, en sus siglas en inglés). No obstante, en platino, la reacción necesita sobrepotenciales de hasta 0.6 V sobre el potencial termodinámico para el inicio de la oxidación, debido a la producción de intermedios que bloquean los sitios activos del platino y disminuyen su eficiencia, principalmente CO.

La oxidación del ácido fórmico en platino ocurre mediante un mecanismo dual hasta el CO_2 [36, 37] como se sugiere en el esquema:

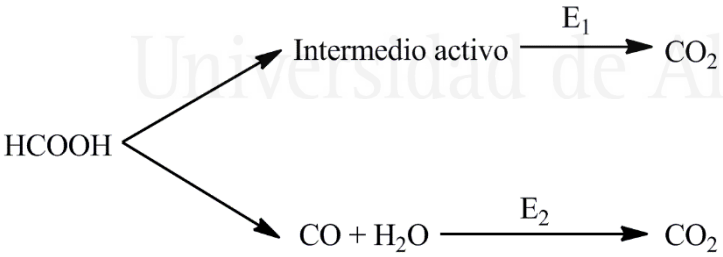

(1.2)

siendo $E_1 < E_2$. En la ruta del intermedio venenoso, el CO se ha detectado como la especie inhibidora mediante técnicas de IR [38, 39]. En este camino, el ácido fórmico descompone espontáneamente sobre la superficie de platino:

$$HCOOH \longrightarrow CO_{ads} + H_2O \quad (1.3)$$

Para oxidar el CO_{ads} son necesarias especies OH_{ads}, que se originan a partir de moléculas de agua [37]:

$$H_2O \longrightarrow OH_{ads} + H^+ + e^- \quad (1.4)$$

Una vez formadas las especies OH_{ads}, se completa la oxidación hasta CO_2:

$$CO_{ads} + OH_{ads} \longrightarrow CO_2 + H^+ + e^- \quad (1.5)$$

En cuanto a la otra ruta, la naturaleza del intermedio activo no está tan clara. Utilizando experimentos de IR en configuración de reflexión externa, se han propuesto intermedios como –COOH [30] y, más recientemente, se ha detectado la presencia de formiato ($HCOO_{ads}$), que se postula mayoritariamente como la especie activa previa al CO_2 [36, 40]. Osawa *et. al* confirman con experimentos en configuración de ATR la presencia de formiato con un enlace tipo 'bridge' a los átomos de platino [41-43], siendo el mecanismo de oxidación propuesto el representado en el siguiente esquema:

$$HCOOH \longrightarrow HCOO_{ads} + H^+ + e^- \quad (1.6)$$

$$HCOO_{ads} \longrightarrow CO_2 + H^+ + e^- \quad (1.7)$$

Sin embargo, Behm *et. al.* sugieren que dicho anión formiato también puede bloquear sitios activos del platino [44, 45], aconsejando una tercera vía en la oxidación del ácido fórmico mediante la cual se produce directamente la oxidación hasta CO_2. Además, el pH del sistema también influye en la reactividad del sistema, aunque existen ciertas discrepancias en cuanto a su efecto. Joo *et. al.* [46] proponen la importancia de la presencia de aniones formiato en la disolución que provoca un aumento de la actividad hasta valores de pH cercanos al pK del ácido fórmico (3.75), mientras que Brimaud *et. al.* [47] observan un aumento de las actividades en un rango de pHs entre 0 y 7. Sin embargo, ambos trabajos concuerdan en la importancia de la presencia de los aniones formiato para una mejora en la actividad de la reacción.

Todas estas rutas son sensibles a la estructura superficial del platino [37, 48, 49], mostrándose el Pt(100) como la superficie más activa pero a la vez más propensa a la formación de CO, por lo que prácticamente siempre está inhibido. Sin embargo, el Pt(111), que es menos activo, se envenena menos y consigue la oxidación completa mediante la ruta del intermedio activo a potenciales más bajos. La Fig. 1.2 muestra las voltametrías cíclicas características para estas superficies de platino:

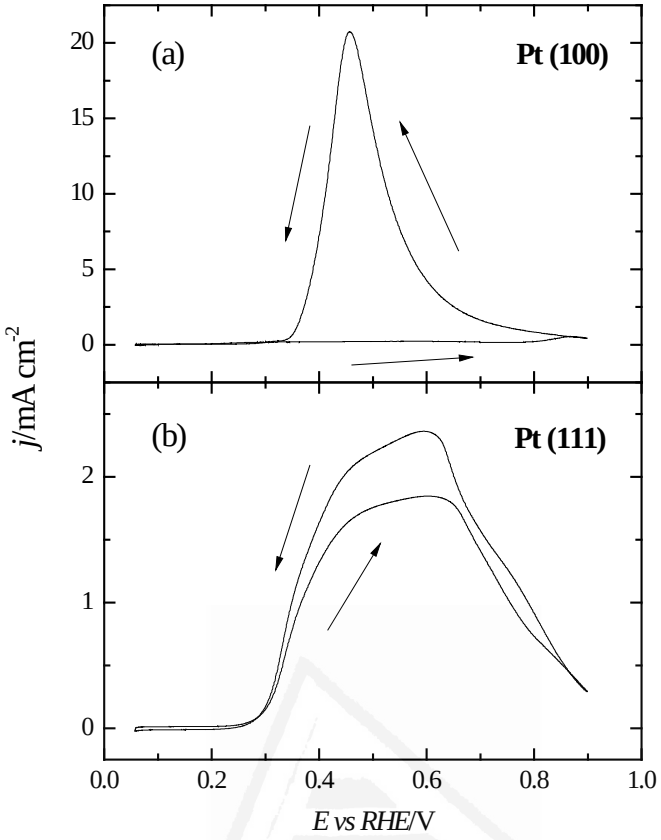

Fig. 1.2. Voltametría cíclica para el primer ciclo en la oxidación de 0.1 M HCOOH + 0.5 M H_2SO_4 en: (a) Pt(111) y (b) Pt(100). Velocidad de barrido: 0.02 V s^{-1}.

Para evitar la formación de CO y favorecer la actividad a bajos potenciales, una opción es modificar la composición de la superficie de platino con algún átomo de diferente naturaleza tanto sobre los planes base del platino como sobre superficies escalonadas, por ejemplo Bi [50-52], Sb [53, 54], Pb [55], Pd [56], Te [57], Se [58], As [59] o combinaciones de varios átomos [60]. La catálisis hasta la completa oxidación a CO_2 en estos electrodos modificados se explica a través de diferentes efectos: a) efectos de tercer cuerpo, donde los adátomos bloquean varios sitios activos contiguos, necesarios para la formación del CO, b) efectos electrónicos, donde la presencia del adátomo disminuye la energía de activación entre el adsorbato y el sustrato facilitando la oxidación del CO o favoreciendo la ruta a través del intermedio activo o c) por un mecanismo bifuncional, donde las especies dadoras de oxígeno están presentes a potenciales más bajos en el electrodo modificado, produciendo una disminución del sobrepotencial necesario para la oxidación del CO respecto a los electrodos de platino sin modificar.

1.1.2 Oxidación de etanol en Pt

Al igual que el ácido fórmico, el estudio de la electrooxidación de etanol en platino ha recibido mucha atención, debido a su facilidad para el almacenamiento y sus beneficios medioambientales, comentados anteriormente. Además, comparando con otros alcoholes como el metanol, presenta ventajas adicionales, como su mayor densidad energética teórica (8.00 kW h kg^{-1} frente a 6.10 kW h kg^{-1}) y su menor toxicidad. En la reacción para la completa oxidación del etanol, se intercambian 12 e^-:

$$CH_3CH_2OH + 3H_2O \longrightarrow 2CO_2 + 12H^+ + 12e^- \quad (1.8)$$

El potencial termodinámico para la oxidación del etanol es 0.085 V vs NHE, pero, al igual que el ácido fórmico, la reacción cinéticamente es más lenta, necesita mayores sobrepotenciales para llevarse a cabo, debido al CO que bloquea los sitios activos, y además forma productos no deseados como el ácido acético.

El mecanismo de oxidación en platino es más complejo que el del ácido fórmico, ya que requiere que se rompa el enlace C-C antes de llegar a la oxidación completa [61, 62]:

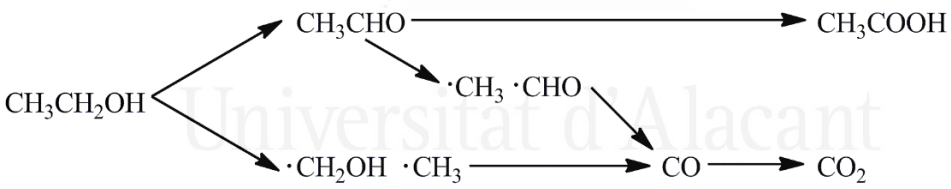

(1.9)

En este mecanismo se consideran dos rutas principales, la de la formación de ácido acético y la deseada hasta CO_2. A pesar de que ambos caminos son termodinámicamente favorables, la formación de ácido acético es mayoritaria respecto a la formación de CO_2, debido a que la energía de activación requerida para que se produzca la rotura del enlace C-C es muy elevada [63]. En medio ácido, la ruta de formación de ácido acético, con únicamente 4 e^- producidos por molécula, es considerada no deseada ya que es un producto estable casi imposible de oxidar hasta CO_2 a temperatura ambiente [64]. Además de ácido acético, se detecta la formación de acetaldehído, también característico de la ruta incompleta de oxidación de etanol [65]. El acetaldehído se genera mediante una adsorción disociativa del etanol [29]:

$$CH_3\text{-}CH_2OH \longrightarrow (CHOH\text{-}CH_3)_{ads} + H^+ + e^- \quad (1.10)$$

$$(CHOH\text{-}CH_3)_{ads} \longrightarrow CHO\text{-}CH_3 + H^+ + e^- \quad (1.11)$$

Posteriormente, dicho acetaldehído se adsorbe en la superficie de platino formando la denominada especie acetil adsorbida [66], que, con la ayuda de OH_{ads} procedentes de moléculas de H_2O formados de la misma manera que en la reacción (1.4), producen el ácido acético a potenciales alrededor de 0.6 V:

$$CHO\text{-}CH_3 \longrightarrow (CO\text{-}CH_3)_{ads} + H^+ + e^- \quad (1.12)$$

$$(CO\text{-}CH_3)_{ads} + OH_{ads} \longrightarrow CH_3\text{-}COOH \quad (1.13)$$

Recapitulando, en la ruta de la oxidación incompleta se produce ácido acético como producto final, intercambiando 4 e^- en su reacción global:

$$CH_3CH_2OH + H_2O \longrightarrow CH_3COOH + 4H^+ + 4e^- \quad (1.14)$$

La oxidación completa de etanol, que implica la rotura del enlace C-C, se produce también a partir de la especie acetil adsorbida formada en la reacción (1.12), la cual disocia a bajos potenciales [66, 67]:

$$(CO\text{-}CH_3)_{ads} \longrightarrow (CO)_{ads} + (CH_x)_{ads} \qquad 0.2\ V < E < 0.6\ V \quad (1.15)$$

Para los fragmentos $(CH_x)_{ads}$, el valor de *x* será 2 o 3 dependiendo de si el enlace con el Pt es de tipo linear o tipo 'bridge'. Dichos fragmentos forman metano entre 0.1 V y 0.4 V, como se ha podido detectar mediante experimentos de espectrometría de masas diferencial electroquímica (DEMS, en sus siglas en inglés) [65]:

$$(CH_x)_{ads} + (4\text{-}x)\ H_{ads} \longrightarrow CH_4 \qquad E < 0.4\ V \quad (1.16)$$

Además, esos mismos fragmentos $(CH_x)_{ads}$ pueden producir CO a potenciales superiores a 0.4 V [68], de acuerdo con la reacción:

$$(CH_x)_{ads} + OH_{ads} \longrightarrow (CO)_{ads} + (x+1)\ H^+ + (x+1)\ e^- \qquad E > 0.4\ V \quad (1.17)$$

Dicho $(CO)_{ads}$, junto al formado en la reacción (1.15), reaccionará con OH_{ads} a potenciales más altos de 0.6 V para formar CO_2 mediante un mecanismo Langmuir-Hinshelwood, de igual manera que en la reacción (1.5).

En cuanto a la influencia de la estructura superficial del platino, al igual que en la oxidación de ácido fórmico, en medio ácido las superficies de Pt(100) favorecen la

formación de CO mientras que en los dominios {111} únicamente se produce la oxidación incompleta hasta ácido acético [69-72]. Además, en esta superficie, el anión acetato adsorbido a partir de la ruta de formación de ácido acético inhibe la reacción de oxidación [73]. El Pt(110) muestra un comportamiento intermedio entre el Pt(100) y el Pt(111), esto es, produce la rotura del enlace C-C formando CO pero en menos proporción que el Pt(100), además de grandes cantidades de ácido acético mediante la ruta de oxidación incompleta. Los perfiles voltamétricos de los tres planos bases del platino para la oxidación de etanol 0.2 M se muestran en la Fig. 1.3:

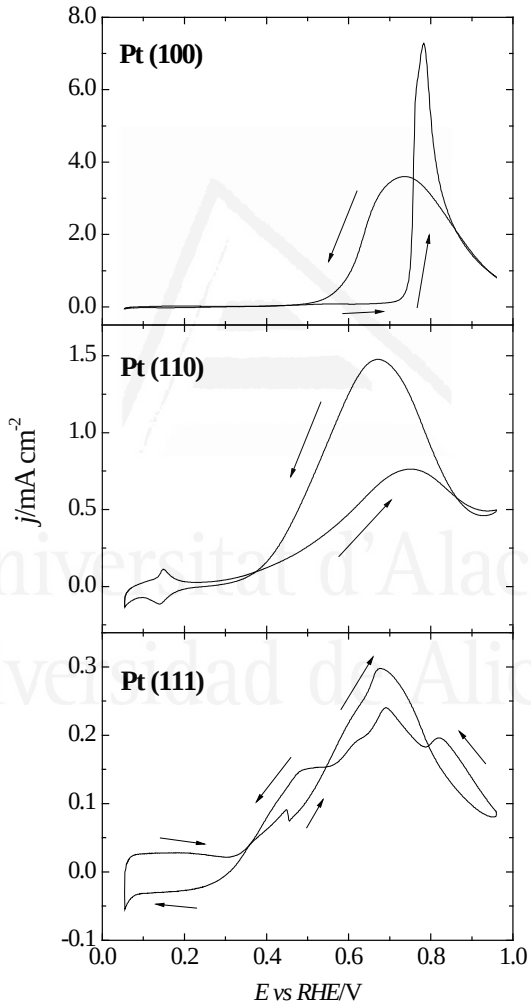

Fig. 1.3. Voltametría cíclica para la oxidación de 0.2 M CH_3CH_2OH + 0.5 M H_2SO_4 en los tres planos base del platino. Velocidad de barrido: 0.02 V s^{-1}.

Para mejorar la actividad hacia la oxidación completa de etanol, una opción clara es la de utilizar superficies escalonadas, concretamente con largas terrazas {111} separadas

por escalones {110} o {100} [74-76], donde las moléculas de CO adsorbidas sobre los sitios de escalón se oxidan hasta CO_2 a potenciales más bajos, e incluso, en el caso de las superficies con escalones {110}, se produce una doble mejora para la electrooxidación de etanol: a potenciales por debajo de 0.7 V, se cataliza la escisión del enlace C-C y su oxidación hasta CO_2, mientras que a altos potenciales se beneficia la formación de acetaldehído y ácido acético. Por otra parte, al igual que en el ácido fórmico, la adsorción de un átomo diferente sobre dichos sitios de escalón, puede beneficiar todavía más la oxidación de etanol a potenciales más negativos [77, 78], favoreciendo la oxidación del CO adsorbido a CO_2 a bajos recubrimientos de adátomo, ya que a altos recubrimientos se inhibe la rotura del enlace C-C produciendo únicamente el ácido acético, no deseado.

La decoración de las superficies de platino con un átomo diferente persigue un doble efecto [79]: (1) mejorar la fracción de moléculas de etanol en las que se produce la escisión del enlace C-C, como es el caso del rodio [80] y (2) favorecer la oxidación del CO hasta CO_2, como ocurre por ejemplo con el rutenio, el estaño o el paladio, apoyando la adsorción del OH [81]. Partiendo de la formación de la especie acetil en la reacción (1.12), el mecanismo de oxidación de etanol se beneficia de la presencia de otros átomos para alcanzar la formación de CO_2:

$$Pt\text{-}(CO\text{-}CH_3) + Rh_{ads} \longrightarrow Pt\text{-}(CO) + Rh_{ads}\text{-}(CH_3) \quad (1.18)$$

$$Sn_{ads} + 2\,H_2O \longrightarrow Sn_{ads}\text{-}(OH)_2 + 2\,H^+ + 2\,e^- \quad (1.19)$$

$$Rh_{ads}\text{-}(CH_3) + Sn_{ads}\text{-}(OH)_2 \longrightarrow Rh_{ads} + Sn_{ads} + CO_2 + 5\,H^+ + 5\,e^- \quad (1.20)$$

$$Pt\text{-}(CO) + Sn_{ads}\text{-}(OH)_2 \longrightarrow Pt + Sn_{ads} + CO_2 + 2\,H^+ + 2\,e^- \quad (1.21)$$

Además del estaño o el rutenio, la adición de otros átomos como el osmio, iridio o wolframio parecen ejercer un efecto similar de optimizar la cantidad de CO_2 formado en la oxidación de etanol [82-84].

En medio alcalino, el mecanismo es diferente y menos estudiado en la bibliografía, pero se ha propuesto que la adsorción del etanol en el platino ocurre a través del oxígeno y no a través del C1 [85, 86], formando especies *etoxi* adsorbidas sobre el platino:

$$CH_3CH_2OH + OH^- \longrightarrow (CH_3\text{-}CH_2O)_{ads} + H_2O + e^- \quad (1.22)$$

A partir de este intermedio, sin producirse la rotura del enlace C-C, se originan acetaldehído y aniones acetato, especie mayoritaria y casi exclusiva para la oxidación de etanol en este medio independientemente de la estructura superficial del platino, proponiéndose distintos mecanismos para su formación:

- La especie *etoxi* es la única adsorbida a pHs elevados [85], oxidándose a acetaldehído según la reacción:

$$(CH_3CH_2O)_{ads} + OH^- \longrightarrow CH_3CHO + H_2O + e^- \quad (1.23)$$

  El acetaldehído se transforma en acetato con la ayuda de un OH_{ads}, siguiendo un mecanismo Eley-Rideal:

$$CH_3CHO + OH_{ads} + 2\ OH^- \longrightarrow CH_3COO^- + 2\ H_2O + e^- \quad (1.24)$$

- Partiendo de la misma especie *etoxi*, ésta se oxida sucesivamente hasta producir acetato adsorbido sobre el electrodo [86]:

$$(CH_3CH_2O)_{ads} + 2\ OH^- \longrightarrow (CH_3CHOHO)_{ads} + 2\ H_2O + 2\ e^- \quad (1.25)$$

$$(CH_3CHOHO)_{ads} + 2\ OH^- \longrightarrow (CH_3COO)_{ads} + 2\ H_2O + 2\ e^- \quad (1.26)$$

  De acuerdo con estas reacciones, de la desorción de las especies adsorbidas formadas en las reacciones (1.25) y (1.26) se producirán acetaldehído y acetato respectivamente:

$$(CH_3CHOHO)_{ads} + e^- \longrightarrow CH_3CHO + OH^- \quad (1.27)$$

$$(CH_3COO)_{ads} + e^- \longrightarrow CH_3COO^- \quad (1.28)$$

1.2 Técnicas experimentales

Durante la tesis doctoral se emplearon diversas técnicas experimentales con el objetivo de obtener la mayor información posible acerca de las oxidaciones de etanol y ácido fórmico. Las técnicas electroquímicas permiten adquirir de una forma rápida información acerca de la dependencia con el potencial de las reacciones electroquímicas estudiadas. Para obtener detalles acerca de la naturaleza de los adsorbatos formados durante las oxidaciones se hizo uso de la espectroscopía infrarroja *in situ* de reflexión externa en configuración de capa fina.

Además, se utilizó la técnica de espectroscopía infrarroja de reflexión interna acoplada con la espectrometría de masas, la cual permite simultáneamente averiguar las especies formadas en un proceso electroquímico mediante experimentos IR junto a información cuantitativa del mecanismo de reacción con la espectrometría de masas.

1.2.1 Técnicas electroquímicas

Las técnicas electroquímicas manejadas durante esta tesis doctoral son, principalmente, la voltametría cíclica y la cronoamperometría, las cuales permiten una caracterización superficial de los electrodos empleados y, posteriormente, el estudio de parámetros acerca de su reactividad electroquímica.

Antes de comenzar con la descripción de las técnicas, para realizar estos experimentos se siguió un protocolo experimental común para una celda de tres electrodos:

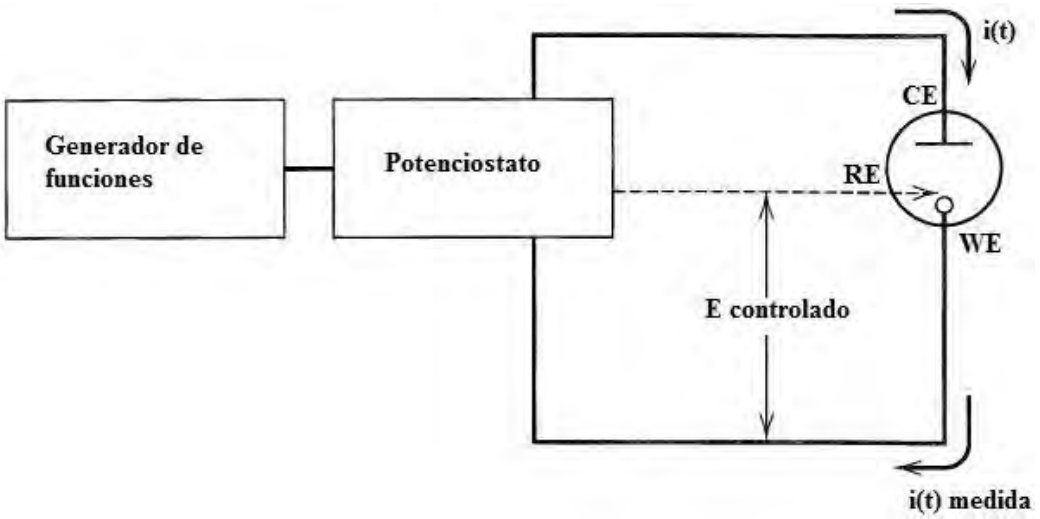

Fig. 1.4. Disposición experimental utilizada durante los experimentos con técnicas electroquímicas (CE: Contraelectrodo, RE: Electrodo de referencia, WE: Electrodo de trabajo). Esquema adaptado de la ref. [87].

En esta disposición, el generador de funciones crea un programa de potenciales que se aplica entre el electrodo de trabajo y el de referencia a través del potenciostato, modificando la corriente que circula a través del electrodo de trabajo y el contraelectrodo para mantener el potencial deseado entre el electrodo de trabajo y el electrodo de referencia. La corriente registrada es la variable, que mide la velocidad de respuesta a la perturbación de potencial producida en las técnicas electroquímicas. Como contraelectrodo se usa un hilo de Pt, el electrodo de referencia es un hilo de negro de Pt en contacto con la misma disolución de trabajo al cual se burbujea hidrógeno y, finalmente, como electrodo de trabajo se utiliza la superficie de platino objeto de estudio, ya sea una superficie monocristalina o nanopartículas depositadas en un sustrato conductor.

La voltametría cíclica [87, 88] es la técnica más popular para estudios iniciales en un sistema con especies redox. En ella se puede obtener información sobre procesos electródicos complicados. Es una técnica no estacionaria, que consiste en realizar un barrido de potenciales a una determinada velocidad de barrido entre un potencial inferior y un potencial superior, registrando al mismo tiempo la corriente obtenida. En los resultados se presentan las curvas E-i, representaciones conocidas como voltamogramas o voltamperogramas. En la Fig. 1.5 se muestra un ejemplo de un voltamograma para un electrodo de platino poliorientado utilizando como electrolito soporte 0.5 M H_2SO_4:

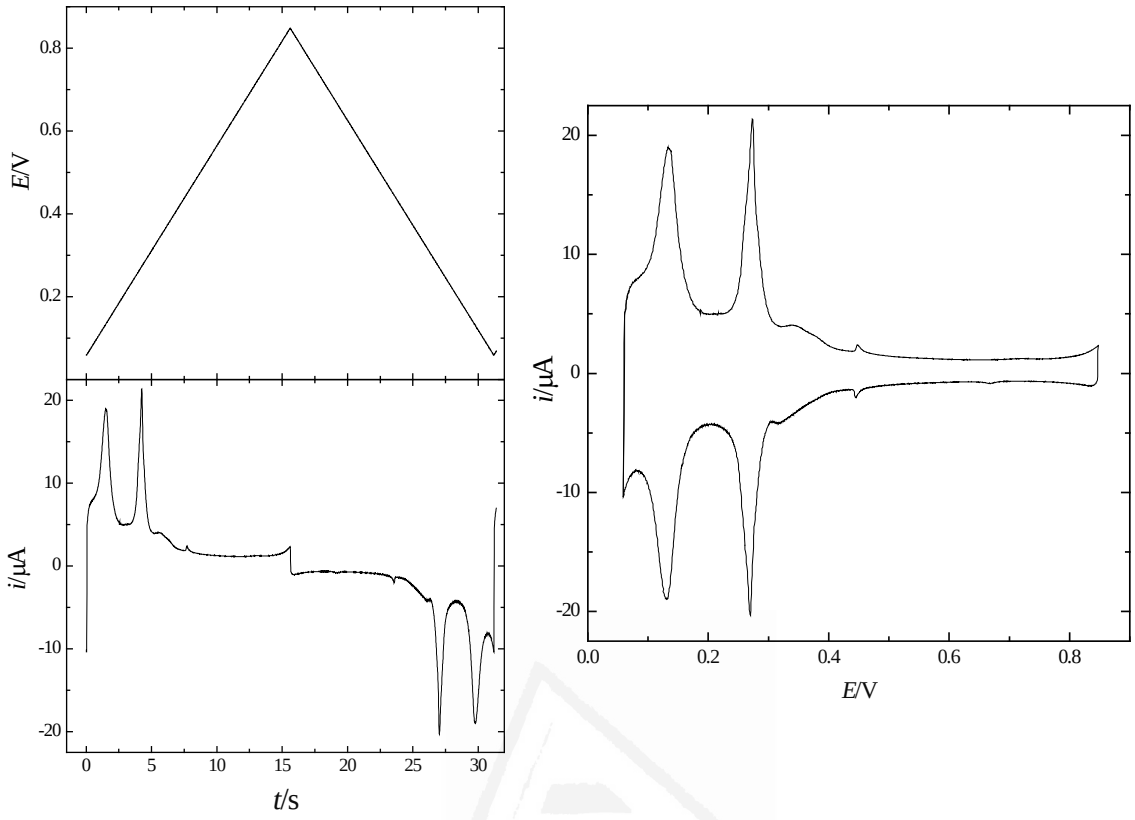

Fig. 1.5. Programa de barrido de potenciales y corriente obtenida frente al tiempo (izqda.) y representación común de i vs E (dcha.) en una voltametría cíclica. Sistema test: Electrodo Pt poly en 0.5 M H_2SO_4.

El empleo de esta técnica en experiencias electroquímicas es extenso, tanto para caracterizar la superficie de los electrodos monocristalinos de Pt a partir de los picos de adsorción de hidrógeno como para detectar la presencia de posibles impurezas. Las corrientes de pico proporcionan información acerca de la naturaleza de la reacción electroquímica. Modificando las velocidades de barrido se puede conocer si el proceso está controlado por la transferencia de carga de especies adsorbidas en el electrodo o si, por el contrario, el proceso viene marcado por la difusión de especies electroactivas procedentes de la disolución hacia el electrodo. Concretamente, las relaciones entre las corrientes de pico (i_p) y la velocidad de barrido (v) son $i_p \propto v$ para el caso de procesos con especies adsorbidas involucradas e $i_p \propto v^{1/2}$ en casos donde intervienen especies en disolución. Además, la diferencia entre los potenciales de pico en el barrido positivo y en el barrido negativo de una voltametría cíclica da una idea acerca de la reversibilidad del sistema.

La cronoamperometría [87, 89] es una técnica en el que se aplica un salto entre un potencial donde no hay reacción faradaica hasta un potencial donde se produce la reducción/oxidación estudiada. Es más sencilla que la voltametría cíclica, ya que mantiene el potencial constante. Se mide la corriente producida y su evolución con el tiempo:

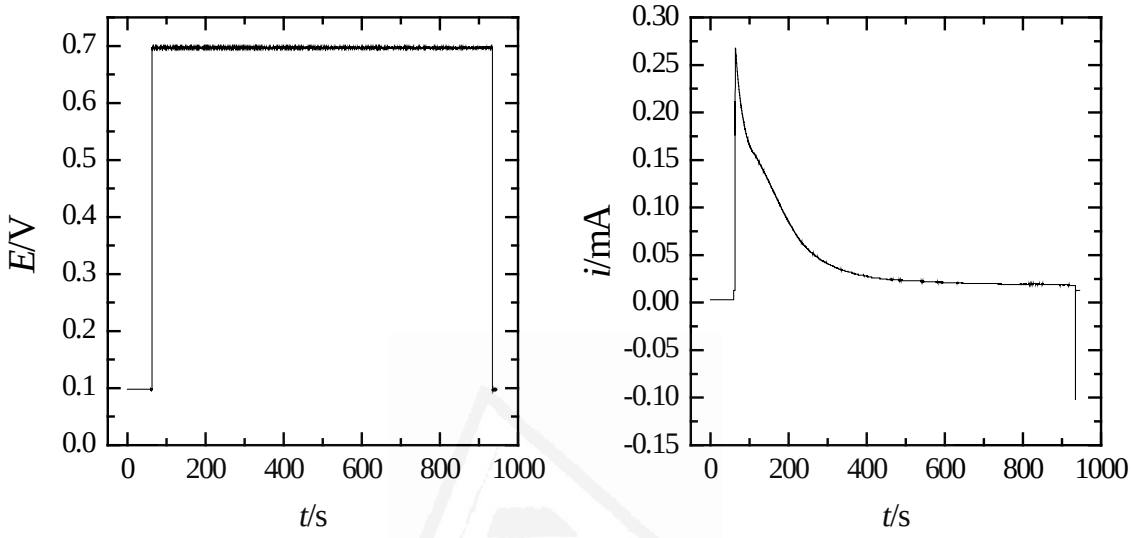

Fig. 1.6. Representación de un salto de potencial entre 0.1 V y 0.7 V frente al tiempo (izqda.), además de las corrientes registradas durante ese salto. Sistema test: Electrodo Pt(111) en 0.2 M CH_3CH_2OH + 0.1 M NaOH.

Al realizar el salto, la corriente crece instantáneamente debido al gradiente de concentración creado, que produce un flujo continuo de especie electroactiva hacia el electrodo. Para un electrodo plano, la disminución de la corriente transitoria con el tiempo refleja generalmente problemas de difusión del reactivo hacia el electrodo, o bien que la adsorción de alguna especie bloquea la reacción de estudio. La cronoamperometría es útil para aclarar aspectos mecanísticos de una reacción, ajustando los datos con un modelo cinético, como en el caso del CO en electrodos de Pt [90, 91], o simplemente para ver si el efecto electrocatalítico se mantiene estable con el tiempo [92, 93].

Las medidas se han realizado con un generador de funciones (EG&G PARC 175) junto a un potenciostato (eDAQ 161 o AMEL Model 2053) y un registrador (eDAQ ED401), o directamente con un µAutolab type III. El potenciostato AMEL Model 2053 se utiliza en el caso de que hayan sido necesarias correcciones de caída óhmica,

principalmente al trabajar con electrodos de platino para la oxidación de etanol en medio alcalino, debido a las altas corrientes registradas y a la menor conductividad en este tipo de disoluciones. El potencial real aplicado en la interfase de estudio función del potencial impuesto por el potenciostato viene dado por la expresión:

$$E_{real} = E_{aplicado} - iR \tag{1.29}$$

donde i es la corriente medida y R se refiere a la resistencia del sistema, que en la célula empleada se atribuye principalmente a la disolución. El objetivo de la corrección de la caída óhmica es que el potencial real sea igual al potencial aplicado, por lo que el término iR de la ecuación (1.29) debe ser anulado. Para ello, el potenciostato aplica una resistencia externa calibrada previamente que en todo momento compensa ese término. La calibración de esta resistencia se realiza estableciendo ciclos a altas velocidades de barrido en zona de doble capa, aplicando resistencias crecientes hasta comprobar que el perfil voltamétrico recupera la forma capacitiva característica de esa zona.

1.2.2 Espectroscopía infrarroja (IR) in situ

La espectroscopía IR se puede utilizar como técnica complementaria a las experiencias de voltametría cíclica y cronoamperometría, proporcionando datos que ayudan a la identificación de las especies formadas, consumidas o adsorbidas en la superficie del electrodo conforme se varía el campo eléctrico de la doble capa, además de proveer información sobre su geometría de adsorción [94-96]. Para ello, un sistema electroquímico como el expuesto en la Fig. 1.4 se acopla con un espectrómetro IR, conformando el sistema para la realización de experiencias espectroelectroquímicas.

Para realizar los espectros IR, se emplea un espectrómetro de FTIR acoplado con un interferómetro de Michelson [97, 98], por el cual circula un haz IR policromático cuya intensidad disminuye al pasar a través de la muestra debido a la radiación absorbida. El interferómetro de Michelson está compuesto por dos espejos, uno fijo y otro móvil en la dirección del haz de luz. Entre los dos espejos se sitúa un divisor de haz, donde la radiación es parcialmente reflejada al espejo móvil y parcialmente transmitida al espejo

fijo. Ambas partes del haz regresan al divisor recorriendo diferentes caminos ópticos, originando una interferencia. A la representación entre ese retraso óptico medido por el interferómetro de Michelson con la intensidad de la radiación alcanzada se le denomina interferograma. La transformación de los interferogramas en espectros se logra mediante una operación matemática denominada transformada de Fourier (FT, en sus siglas en inglés). La principal ventaja de los espectrómetros que utilizan transformada de Fourier es la velocidad con la que obtienen un interferograma, ya que son capaces de medir todas las longitudes de onda del haz de luz simultáneamente, al contrario que otros espectrómetros denominados dispersivos, que las miden consecutivamente.

La configuración empleada para la realización de los espectros con monocristales de platino o el soporte de oro en el cual se depositan las nanopartículas de platino es la de reflexión externa, IRRAS (siglas en inglés de espectroscopía infrarroja de reflexión-absorción), en la que se analiza la intensidad de la radiación en función de la longitud de onda de un haz de luz que es reflejado en un metal en contacto con una disolución. Una característica de las experiencias IRRAS es la del obligado cumplimiento de la regla de selección superficial [99], esto es, *solamente los modos de vibración que posean una componente del momento dipolar perpendicular a la superficie metálica interactúan con el campo eléctrico de la radiación IR*. De acuerdo a este principio, la luz polarizada *s* (perpendicular al plano de reflexión) únicamente se muestra activa para especies presentes en disolución, mientras que la luz polarizada *p* (paralelo al plano de reflexión), además de las especies presentes en disolución, presenta contribuciones de modos vibracionales con cambios en el momento dipolar perpendicular a la superficie de las especies adsorbidas en superficie.

En el modo de reflexión externa, el electrodo monocristalino se pone en contacto con un prisma transparente a la radiación IR y con un bajo índice de refracción, procurando que el espesor de la capa de disolución sea el mínimo posible, para minimizar los efectos de absorción IR por la disolución. En la Fig. 1.7 se muestra el prisma acoplado por una junta de teflón a una célula electroquímica similar a la empleada en las experiencias de voltametría cíclica y cronoamperometría. La pequeña porción de disolución confinada entre el electrodo y el prisma conforman la estructura de capa fina con un espesor entre 1 y 10 μm.

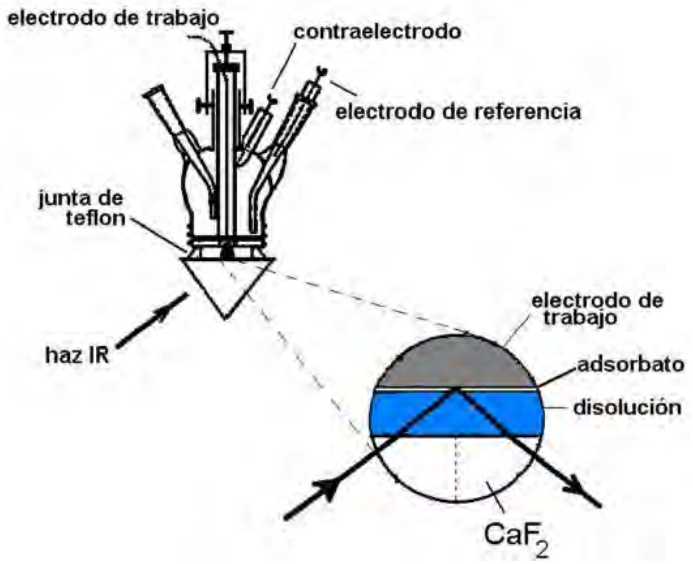

Fig. 1.7. Configuración de la célula electroquímica y del prisma de CaF_2 durante los experimentos de IRRAS con los electrodos monocristalinos de Pt.

A pesar de que el espesor de la capa de difusión es pequeño, las principales bandas observadas en el espectro pertenecen al disolvente, que en todos los casos presentados en esta tesis es agua. La Fig. 1.8 muestra el espectro 'Single Beam' habitual obtenido en cada experiencia IRRAS con electrodos de platino. En ella, se ven modos de vibración característicos de los enlaces O-H del agua como las tensiones simétrica y asimétrica por encima de 3500 cm^{-1} y la flexión simétrica sobre 1600 cm^{-1}.

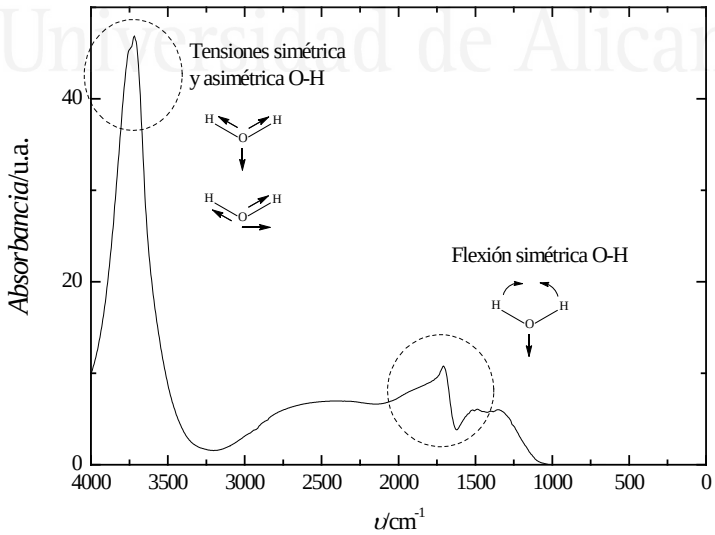

Fig. 1.8. Forma general de un espectro 'Single Beam' para una configuración de capa fina en un electrodo de platino monocristalino acoplado con un prisma de CaF_2.

Al tomar varios espectros a diferentes potenciales, éstos son aparentemente iguales, ya que la contribución de las moléculas adsorbidas a la radiación IR es muy pequeña comparada con la del disolvente, produciéndose variaciones de menos de 0.01 unidades de absorbancia. Para eliminar en la medida de lo posible la contribución del disolvente y centrarse en las especies adsorbidas sobre el electrodo y en los productos formados, la estrategia seguida consiste en tomar varios espectros a diferentes potenciales y en un corto espacio de tiempo, utilizando uno de ellos como referencia y observando sus variaciones al modificar el potencial. Los espectros resultantes se presentan en términos de unidades de absorbancia $A = -\log(R/R_0)$, donde R y R_0 son los valores de intensidad de la luz reflejada al potencial de trabajo y al de referencia respectivamente. Para las pequeñas variaciones esperadas en estos valores, se considera que $A = -(R - R_0)/R_0$. Los espectros se realizan siguiendo el esquema de la Fig. 1.9, que muestra un ejemplo para el caso de la oxidación de CO adsorbido en un electrodo de Pt(111) en 0.5 M H_2SO_4.

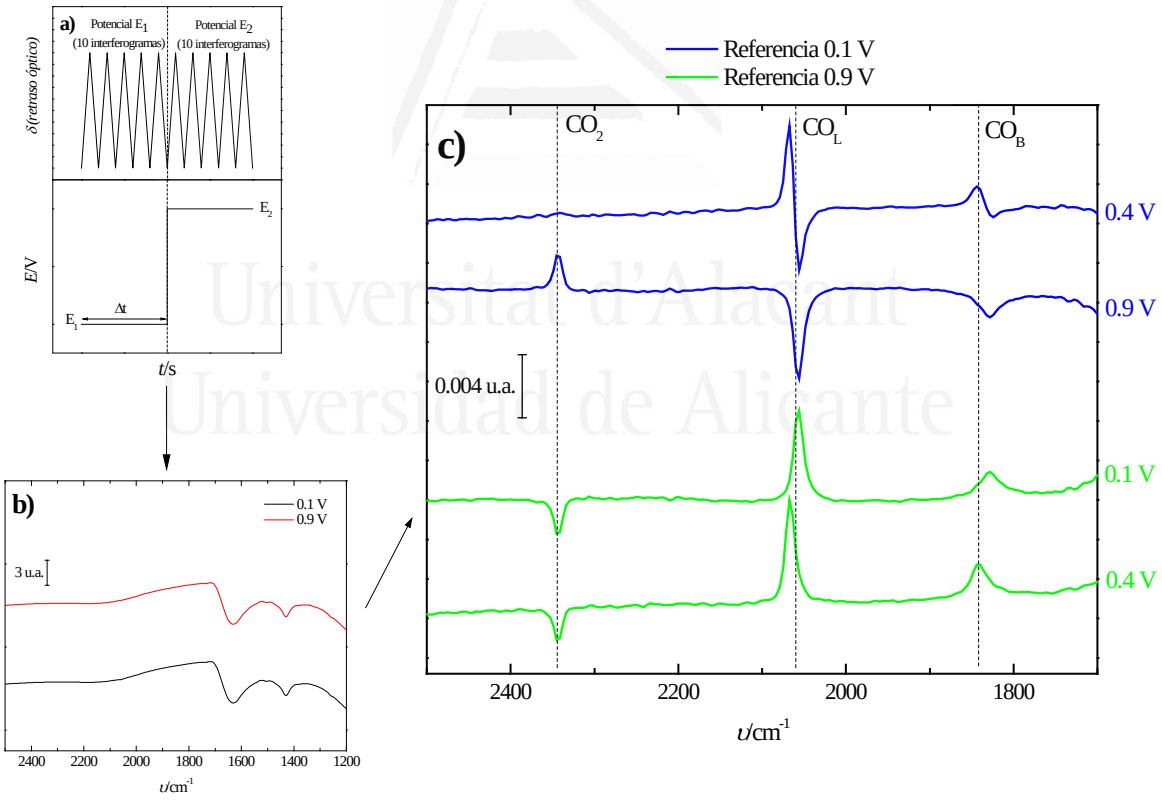

Fig. 1.9. Esquema con los pasos seguidos a la hora de realizar espectros: (a) modo de adquisición de espectros a un potencial estático, (b) espectros 'Single Beam' medidos a diferentes potenciales y (c) espectros procesados utilizando como referencia el espectro a 0.1 V (azul) y a 0.9 V (verde) para la oxidación de CO con Pt(111) en una disolución 0.5 M H_2SO_4.

El potencial deseado se establece manualmente, potencial en el cual se miden un número fijo de interferogramas, que en el caso del ejemplo presentado en la Fig. 1.9a son 10. El espectro 'Single Beam' resultante se adquiere del promedio de todos los interferogramas obtenidos. Cuanto más alto sea el número de interferogramas tomados, mejor relación señal/ruido se logrará. Por ello, en todos los espectros realizados durante esta tesis se toman, al menos, 100 interferogramas. El Δt indicado en el esquema se corresponde con el tiempo que se necesita para medir los interferogramas, que para el caso en que se tomen 100 es de 43 segundos.

Los espectros 'Single Beam' de la Fig. 1.9b muestran la diferencia inapreciable entre las medidas tomadas a diferentes potenciales. La Fig. 1.9c expone los espectros resultantes después de restarlos con los espectros a los potenciales de referencia escogidos (0.1 V o 0.9 V). Las bandas positivas indican la presencia de una especie respecto al potencial de referencia, como es el caso de las bandas de CO lineal sobre 2050 cm^{-1} en los dos potenciales calculados con el referencia a 0.9 V. Las bandas negativas se refieren a especies consumidas respecto al potencial de referencia, como las bandas de CO_2 a 2340 cm^{-1} en el mismo caso del ejemplo con el referencia a 0.9 V o en la banda de CO lineal en el espectro a 0.9 V utilizando el referencia a 0.1 V. En el caso en el que aparecen bandas bipolares, éstas se refieren a especies adsorbidas que están presentes tanto en el potencial de referencia como en el potencial estudiado. Como la frecuencia de la banda se ve afectada por el potencial de trabajo, la diferencia con el espectro de referencia da lugar a una banda bipolar, como en el mostrado en la banda de CO lineal del espectro a 0.4 V, con el referencia establecido a 0.1 V.

Los espectros FT-IRRAS se han adquirido utilizando espectrómetros Nicolet Nexus (modelo 8700) o Nicolet Magna modelo 850, especificando el espectrómetro empleado en cada capítulo. En ambos casos, un detector MCT (Telururo de Mercurio y Cadmio) se acopla al espectrómetro, que además está dotado de un sistema Veemax de Spectra-Tech como sistema de reflectancia especular. Como ventana óptica, en todos los experimentos de reflexión externa se ha utilizado un prisma de CaF_2, que es capaz de detectar bandas por encima de 900 cm^{-1} [95], suficiente para los casos estudiados. El prisma fue biselado a 60º, lo cual provoca un ángulo de incidencia con el electrodo de trabajo de alrededor de 70º, cercano al ángulo crítico del material que se encuentra sobre 77º. Cuanto más cercano esté

el ángulo de incidencia al ángulo límite del material, mejor relación entre las intensidades de la luz reflejada ($(R - R_0)/R_0$) se obtendrá y, por tanto, mejor señal de absorbancia [100].

Para asignar las bandas de los espectros, los resultados se comparan con espectros de transmisión realizados con posibles productos o intermedios de las reacciones de oxidación estudiadas. Dichos espectros de transmisión se tomaron con un prisma de ZnSe, el cual puede mostrar modos de vibración que aparezcan a partir de 500 cm^{-1}. La resolución de los espectros fue de 8 cm^{-1} empleando luz polarizada *p* en la toma de los espectros.

1.2.3 Espectroscopía infrarroja ATR acoplada con espectrometría de masas DEMS

A pesar de las ventajas de la técnica IRRAS, existen también algunas limitaciones al trabajar con esta configuración. En primer lugar, a pesar de que la capa de disolución entre el electrodo y el prisma de CaF_2 es de un espesor muy pequeño (entre 1 y 10 µm), la absorción de la radiación IR por parte de la disolución es mucho mayor comparándola con la de la capa de adsorbatos (suponiendo que la capa de adsorbato fuera de 1 nm, la absorción por parte de la disolución sería entre 3 y 4 órdenes de magnitud mayor). Por ello, es importante reducir la absorción IR de fondo en los espectros, la cual se asigna al disolvente. Por otra parte, los problemas de difusión de especies en la configuración de capa fina provocan que, en el caso de que los productos de la reacción sean gases, éstos queden atrapados dentro de la capa de disolución entre el electrodo y el prisma, provocando impedimentos en las medidas espectrales y electroquímicas. De acuerdo con estos hechos, la configuración FT-IRRAS no se considera como la más adecuada para el estudio de reacciones rápidas en superficie.

Los problemas anteriores pueden solucionarse con la configuración de reflexión interna o ATR (reflexión total atenuada en sus siglas en inglés) [101, 102]. Sobre un prisma transparente para el infrarrojo y con un índice de refracción suficientemente alto como para permitir la reflexión total, por ejemplo silicio o germanio, se deposita una fina

película de un metal que se usa como electrodo de trabajo, constituyendo la denominada configuración de Kretschmann que viene representada en la Fig. 1.10. La radiación IR se focaliza directamente sobre el prisma alcanzando la película de metal y formando una onda evanescente que penetra solo unos cientos de nanómetros sobre la muestra, lo cual permite que la aportación de las bandas IR procedentes de la disolución sea reducida considerablemente respecto a lo observado en la configuración FT-IRRAS. Además, si la película presenta rugosidades de hasta 10 nm se produce una intensificación de la señal conocida como SEIRAS, que es capaz de producir un aumento de hasta 1000 órdenes de magnitud en la intensidad de la señal [103].

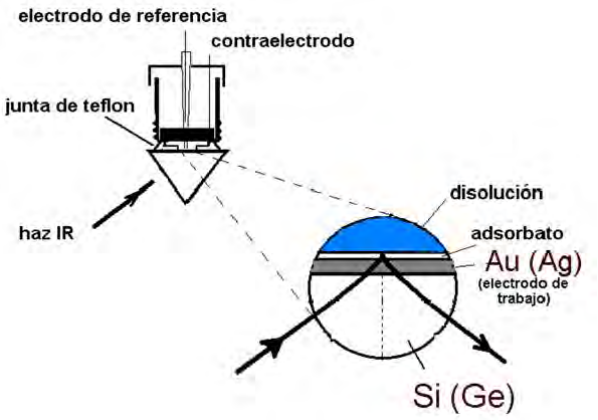

Fig. 1.10. Dispositivo experimental para experimentos de ATR-SEIRAS utilizando la configuración de Kretschmann.

Por otro lado, la espectrometría de masas diferencial electroquímica (DEMS) [104, 105] permite la rápida detección de productos gaseosos volátiles formados en reacciones electroquímicas. La instrumentación consiste básicamente en una célula electroquímica, donde está ubicado el electrodo de trabajo, una membrana de teflón y un sistema de vacío donde se incluye el espectrómetro de masas:

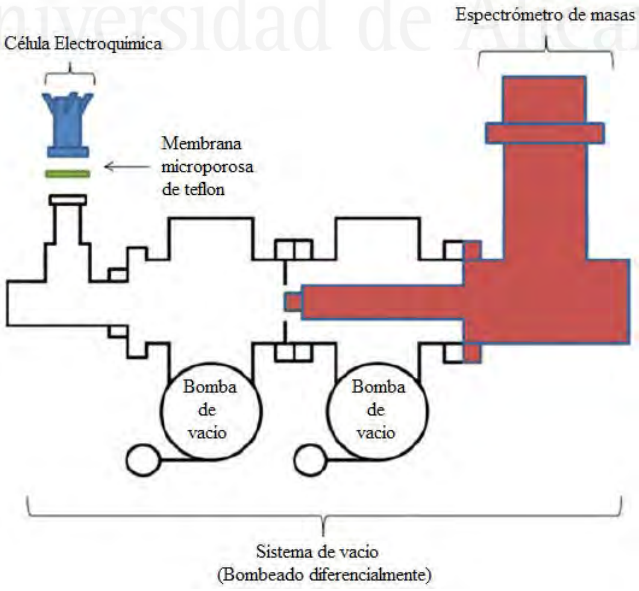

Fig. 1.11. Dispositivo convencional para experimentos DEMS, tomado de la ref. [106].

Es conveniente que la célula electroquímica sea de un material como el vidrio, diferente al teflón, cuya porosidad puede provocar la absorción de especies orgánicas. Su función es la de controlar las condiciones electroquímicas sobre el electrodo de trabajo, permitiendo el transporte de los productos gaseosos volátiles hacia la membrana de teflón. El carácter hidrofóbico de este material impide el paso del electrolito hacia el sistema de vacío, mientras que sí es permeable a gases volátiles y relativamente no polares, que son conducidos hacia el espectrómetro de masas, el cual necesita condiciones de alto vacío (< 10^{-5} mbar) para su correcto funcionamiento, condiciones obtenidas con la ayuda de dos bombas de vacío.

En un experimento DEMS típico, al mismo tiempo que se mide la corriente faradaica realizando una voltametría cíclica normal, se registran las corrientes correspondientes a las masas que contengan información acerca de los iones que se desean detectar. El registro de estas corrientes frente al potencial se conoce como voltametría cíclica de espectrometría de masas (MSCV en sus siglas en inglés). Las aplicaciones de esta técnica son variadas, como la caracterización de adsorbatos orgánicos, la detección de especies nitrogenadas, la evolución de hidrógeno en una reacción tan complicada como la oxidación de formaldehído o, la aplicación más interesante desde nuestro punto de vista, el seguimiento de las reacciones de oxidación de pequeñas moléculas orgánicas como el ácido fórmico o el etanol.

La principal ventaja de las técnicas DEMS respecto a técnicas ATR es la posibilidad de detectar especies inactivas en el IR, como la formación de hidrógeno. Sin embargo, el DEMS está más limitado ya que solamente es capaz de medir productos gaseosos volátiles, mientras que el ATR permite medir intermedios de reacción adsorbidos sobre el electrodo de trabajo y productos no volátiles. Por ello, las técnicas de ATR y DEMS se consideran complementarias, y su combinación es de mucha utilidad para estudios de electrocatálisis como los realizados en esta tesis. Además, si se acopla con una célula de flujo electroquímica de doble capa fina, la cual trabaja en condiciones de transporte de masa, se obtiene información acerca de la cinética de las reacciones ocurridas en el electrodo [107].

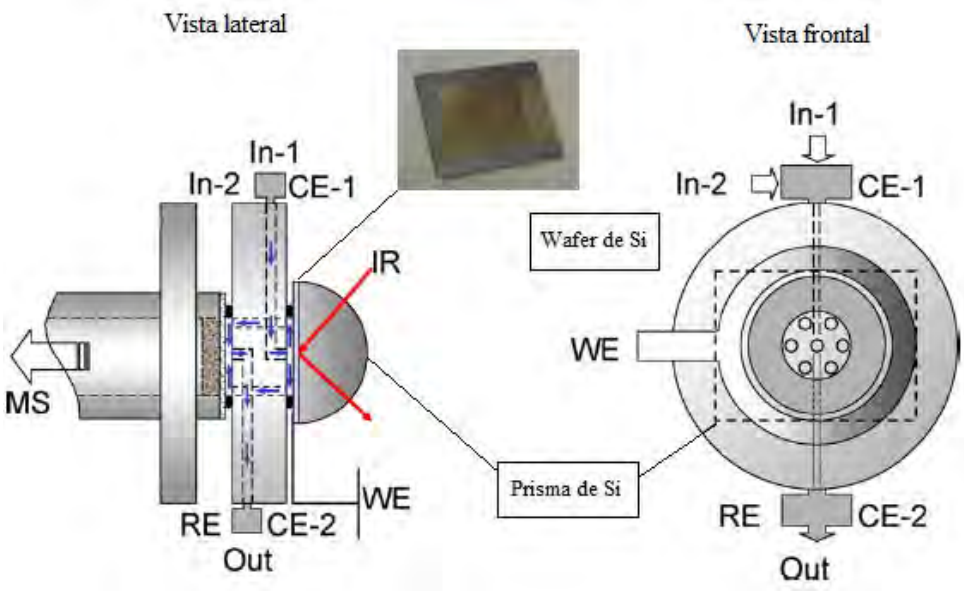

Fig. 1.12. Diagrama esquemático de la célula de flujo de capa fina para medidas ATR-FTIRS y on-line DEMS junto a una imagen con los wafers de Si acoplados con el prisma (ver texto para más detalles). In-1 e In-2: puntos de entrada del electrolito; CE-1 y CE-2: puntos de conexión de los dos contraelectrodos; WE y RE: puntos donde se conectan el electrodo de trabajo y de referencia; Out: punto de salida del electrolito. Esquema adaptado de la ref. [107].

La Fig. 1.12 muestra un esquema orientativo del dispositivo experimental usado en los experimentos ATR-FTIR acoplados con DEMS. El electrodo de trabajo es un 'wafer' con el depósito de nanopartículas acoplado con el prisma semicilíndrico de silicio. El 'wafer' de silicio consiste en una pieza rectangular a la cual se le deposita una película de Au mediante la técnica de 'electroless' [108], sobre la cual se deposita la muestra de nanopartículas de platino. El principal requisito que tiene que cumplir es ser lo suficientemente fino como para permitir el paso del haz IR que viene a través del prisma y, a su vez, suficientemente grueso para proporcionar una conductividad adecuada. El conjunto del prisma y el wafer son presionados sobre la célula espectroelectroquímica mediante una junta circular de Parafilm® y una hoja fina circular de cobre que se emplea para hacer contacto.

La célula espectroelectroquímica está fabricada con Kel-F® y presenta dos compartimentos diferentes: en el primero, la disolución llega hasta el conjunto del electrodo de trabajo en el centro de la celda, que está rodeada por seis pequeños capilares por los cuales fluye la disolución en dirección al segundo compartimento, permitiendo un

flujo laminar continuo hacia el electrodo de trabajo. El volumen aproximado de la célula es de 10 µL. En el segundo compartimento de la célula, el electrolito es conducido hacia la membrana porosa de teflón antes de llegar al punto de salida de la disolución. Como se ha explicado, la membrana permite el paso de los gases volátiles formados en las nanopartículas de platino y los conduce hacia el espectrómetro de masas. El retraso entre la señal de corriente faradaica y la respuesta del espectrómetro de masas es de alrededor de 1 s, que es el tiempo que tarda el electrolito en fluir desde el primer al segundo compartimento de la célula espectroelectroquímica.

Como electrodo de referencia se usa un electrodo saturado de calomelanos (SCE, en sus siglas en inglés), aunque los resultados están corregidos y presentados respecto al electrodo reversible de hidrógeno (RHE, en sus siglas en inglés) para una comparación más cómoda con los demás resultados de la tesis. Además, en el sistema se introducen dos contraelectrodos de platino en la entrada y la salida de la célula de flujo, con el objetivo de favorecer una distribución más homogénea del campo eléctrico en las células de flujo de capa fina.

En estas experiencias se registran simultáneamente la voltametría cíclica, los espectros y la voltametría cíclica de espectroscopía de masas de una manera potenciodinámica con un barrido de potencial a una velocidad lenta de 5 mVs^{-1}. El potenciostato utilizado fue un 'Pine instruments potentiostat', mientras que el registro de datos fue computerizado. Los experimentos *in-situ* ATR-FTIRS fueron llevados a cabo en un espectrómetro BioRad FTS-6000 equipado con un accesorio de reflexión no comercial con un ángulo de incidencia del haz IR de 70º y un detector de telururo de mercurio y cadmio (MCT). Se toman espectros cada 10 s con una resolución de 4 cm^{-1} a la vez que se realiza un barrido de potenciales, aunque los espectros ATR presentados se midieron de manera potenciostática para mejorar la relación señal/ruido. Los espectros se presentan igualmente en valores de absorbancia, aunque, al contrario que las experiencias de IRRAS, las bandas negativas indican especies formadas en el potencial de estudio, mientras que las bandas positivas muestran especies consumidas respecto al espectro de referencia.

La configuración DEMS [109] está basada en un sistema de bombeo con dos cámaras de vacío similar al de la Fig. 1.11 equipado con un espectrómetro 'Balzers QMS

112 quadrupole mass spectrometer'. Se obtiene una mayor sensibilidad producto de las dos bombas de vacío que favorece el alcance de las condiciones de alto vacío necesario y del posicionamiento de la fuente de iones del espectrómetro entre las dos bombas, lo cual beneficia la mayor eficiencia de ionización en las especies estudiadas.

1.2.4 Microscopia electrónica de transmisión (TEM)

Las muestras de nanopartículas de platino se caracterizaron usando la microscopía electrónica de transmisión (TEM), que da información acerca del tamaño y del grado de aglomeración. La técnica se basa en la interacción de un haz de electrones con la muestra para su visualización, haciendo uso de la trasmisión/dispersión de los electrones para formar la imagen, la difracción de los electrones para conocer la estructura cristalina y la emisión de rayos X característicos para obtener información acerca de la composición. El microscopio está compuesto por un cañón que emite los electrones hacia la muestra, lentes especiales que son capaces de crear campos magnéticos que dirigen y enfocan el haz de electrones, un sistema de vacío para evitar las interacciones de los electrones con las moléculas del aire, una pantalla fluorescente que permita visualizar la imagen aumentada y un ordenador como sistema de registro de la imagen. Las muestras se preparan depositando unas gotas de la disolución micelar en rejillas de microscopía, que posteriormente se dejan secar. El sistema utilizado fue un Microscopio Electrónico de Transmisión JEOL modelo JEM-2010 con un detector de rayos X marca OXFORD modelo INCA Energy TEM 100 disponible en los Servicios Técnicos de la Universidad de Alicante.

1.3 Caracterización superficial

Una parte importante, previa a los estudios de electrocatálisis, es la caracterización física de las superficies de platino estudiadas, con el objetivo de averiguar la disposición cristalográfica de los átomos en el catalizador. En condiciones de UHV, la caracterización física se puede realizar con técnicas de difracción de rayos X o difracción de electrones de baja o de alta energía (en sus siglas en inglés, LEED o HEED respectivamente), donde se hace incidir sobre la muestra un haz de electrones de energía definida y se registra la intensidad del haz dispersado en función de la energía y del ángulo de incidencia [110].

Por otra parte, una técnica muy común para la caracterización superficial es la microscopía de efecto túnel (STM), donde una punta metálica barre la superficie de materiales conductores registrándose la corriente túnel como medida de la distancia de la punta a la superficie. El STM se puede considerar como una técnica *'in situ'* donde la caracterización se realiza en presencia del electrolito. Tanto las técnicas de difracción de electrones que funcionan en condiciones de UHV como el STM requieren demasiado tiempo y son costosas para ser prácticas en un trabajo frecuente. Por ello, es beneficioso usar otros métodos de caracterización indirectos más sencillos, preferiblemente *in situ*. A partir de la utilización del tratamiento a la llama desarrollado por Clavilier a partir de los años 80, se obtuvieron superficies limpias y ordenadas de electrodos metálicos monocristalinos sin necesidad de utilizar sistemas de UHV y consiguiendo caracterizar las superficies de platino con una simple voltametría cíclica.

1.3.1 Monocristales de platino

Los electrodos monocristalinos de platino se preparan siguiendo el método desarrollado por Clavilier [111, 112], el cual también es válido para la preparación de electrodos monocristalinos de oro [113, 114], rodio [115, 116], iridio [117-119] o paladio [120, 121]. En dicho método, un hilo de platino de elevada pureza y de unos 0.5 mm de diámetro es fundido por uno de los extremos mediante una llama de oxígeno-propano, produciendo una gota de metal fundido de unos 2-3 mm de diámetro para los electrodos de

trabajo utilizados en experimentos electroquímicos, y 5-6 mm para los electrodos empleados en experimentos espectroelectroquímicos. La gota de metal fundido se enfría muy lentamente, tratando de producir únicamente la cristalización en un único cristal. Posteriormente, la esfera monocristalina, unida al hilo de platino, se coloca en un banco óptico con un goniómetro y un láser que permiten identificar las facetas del cristal y la orientación del monocristal en la dirección deseada. A continuación se realiza el corte y pulido, mediante un sistema que permite la operación manteniendo la dirección perpendicular al eje del banco óptico. Para el pulido del monocristal, se utilizaron materiales abrasivos como carburo de silicio o pasta de diamante de hasta 0.25 µm.

Antes de la publicación del procedimiento de trabajo con monocristales de platino de Clavilier, la forma más habitual para limpiar la superficie era mediante ciclos de oxidación-reducción [122-125]. A pesar de la correcta preparación de las superficies monocristalinas en condiciones UHV, al realizar el transvase a la célula electroquímica se observaban impurezas adsorbidas sobre el electrodo que se eliminaban recurriendo a ciclos de oxidación hasta potenciales superiores más altos de 1 V, donde se empiezan a formar óxidos de platino. El problema de alcanzar estos potenciales es la alteración de la superficie del electrodo al llegar a la zona de oxidación del platino, lo que se refleja en la carga de adsorción a potenciales bajos, que involucra más de un átomo de hidrógeno por átomo de platino [122].

El tratamiento a la llama de Clavilier [111] dio solución a este problema. El procedimiento se basa en calentar el electrodo con un mechero Bunsen para oxidar las impurezas adsorbidas procedentes del ambiente, aprovechando las propiedades catalíticas del platino, y favoreciendo además la reorganización de la superficie. Posteriormente, el electrodo, todavía a altas temperaturas, se introduce en un balón de enfriamiento dejándolo en una atmósfera libre de oxígeno. Antes de que la temperatura del electrodo disminuya lo suficiente como para verse afectado de nuevo por la adsorción de impurezas presentes en la atmósfera, el electrodo se sumerge en agua ultrapura contenida en el balón de enfriamiento, quedando protegido con una gota de dicha agua e impidiendo su contaminación durante el traslado a la célula electroquímica.

Un factor importante a tener en cuenta es el de la naturaleza de la atmósfera en la cual se produce el enfriamiento del electrodo, ya que la adsorción de oxígeno en algunas superficies puede afectar a la correcta ordenación de la estructura final debido a la formación de óxidos térmicos. Por ello, el enfriamiento se lleva a cabo en una atmósfera reductora H_2 + Ar para preservar la superficie, sobre todo en el caso de los electrodos de Pt(110), Pt(100) y las escalonadas con terrazas {111} y escalones {110} o {100}. En el caso de los electrodos de Pt(111), el enfriamiento del electrodo en atmósfera de Ar es suficiente para obtener la correcta ordenación de la superficie monocristalina, debido a que es la orientación con mayor densidad atómica superficial y, por tanto, la más estable y menos sensible a la formación de óxidos superficiales.

La notación empleada en el párrafo anterior para nombrar los diferentes planos cristalográficos son los denominados índices de Miller, que se definen como el producto entre la recíproca de la intersección del plano cristalográfico y los ejes de coordenadas (x,y,z) con el mínimo común múltiplo de dichas recíprocas, con el objetivo de que siempre sean números enteros. Los índices de Miller constan de tres números (h,k,l) para estructuras cúbicas y cuatro en el caso de estructuras hexagonales compactas (w,x,y,z). Como el platino presenta estructura cúbica centrada en las caras (fcc, en sus siglas en inglés), durante toda la tesis los índices de Miller indicados se representan como tres números referidos a planos cristalográficos del platino.

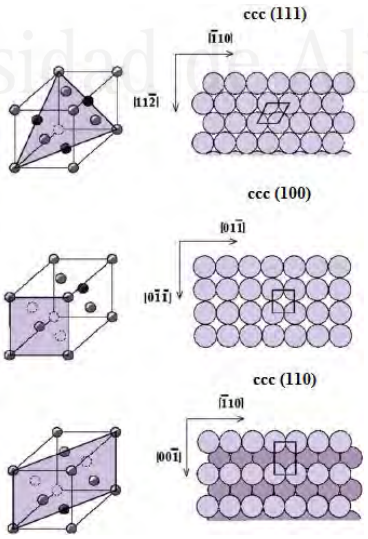

Fig. 1.13. Representación de los planos base de índice de Miller {111}, {100} y {110} para una estructura cúbica centrada en las caras, mostrando la disposición de los átomos y la celdilla unidad característica de cada plano. Figura tomada de la referencia [110].

La Fig. 1.13 muestra las distribuciones de los átomos en la celdilla unidad cúbica centrada en las caras para las superficies más sencillas con los índices de Miller más bajos, denominados planos base, y caracterizados por tener solamente un tipo de simetría, hexagonal para las {111}, cuadradas para las {100} y rectangular en el caso de las superficies {110}. Además, en cada superficie se muestran entre corchetes los vectores que indican la dirección de los ejes que forman cada superficie. Todas las superficies están formadas por diferentes contribuciones de los tres planos base, las cuales vienen representadas en el triángulo estereográfico:

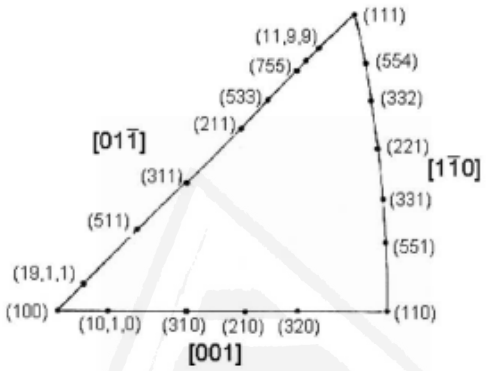

Fig. 1.14. Triángulo estereográfico.

Las tres esquinas del triángulo se corresponden con electrodos que poseen terrazas de longitud infinita de una superficie de cada plano base. En los lados del triángulo, se indican superficies con contribuciones de los planos base que forman el lado del triángulo. Por ejemplo, la superficie Pt(554) presenta terrazas de nueve átomos de terraza {111}, separados por escalones monoatómicos {110}. A este tipo de superficies se conoce como escalonadas, compuestas por átomos de terraza con una orientación determinada separados por escalones monoatómicos con otra ordenación. Por último, los índices de Miller que aparecen en el interior del triángulo estereográfico contienen contribuciones de los tres planos base, donde los escalones no son rectos y pueden presentarse diferentes esquinas.

Volviendo a las superficies escalonadas, la nomenclatura habitual con la que se conocen es la propuesta por Lang [126]:

$$M\,(S) - [n\,(h,k,l) \times (h',k',l')] \qquad (1.30)$$

donde M es el metal, *n* es el número de átomos presentes en la terraza, (h,k,l) es el índice de Miller para la orientación de los átomos de terraza y (h',k',l') es el índice de Miller correspondiente a la orientación de los átomos de escalón. La Tabla 1.1 muestra la relación entre la nomenclatura instruida por Lang y los índices de Miller para cada superficie escalonada:

Superficies escalonadas	**Índices de Miller**
n (111) x (111)	(n, n, n-2)
n (111) x (100)	(n+1, n-1, n-1)
n (100) x (111)	(2n-1, 1, 1)
n (100) x (110)	(n,1,0)
n (110) x (111)	(2n-1, 2n-1, 1)
n (110) x (100)	(n, n-1, 0)

Tabla 1.1. Relación entre la notación de superficies escalonadas propuesta por Lang y los índices de Miller.

En el caso de algunas superficies escalonadas {111}, son correctas dos notaciones para indicar su simetría. Por ejemplo, la superficie con índice {553} se puede nombrar como [5 (111) x (111)] o [4 (111) x (110)], ya que en una estructura cúbica centrada en las caras una estructura {110} es equivalente a una superficie escalonada que presenta una terrraza monoatómica con orientación {111} y un escalón monoatómico {111}. La asignación dependerá de su reactividad. Por otro lado, al moverse a través de los lados del triángulo estereográfico, conforme más se alejan de los vértices, menor es la proporción de esas terrazas a las superficies escalonadas. En el punto medio entre dos vértices, se encuentra el denominado 'turning point', donde la relación entre los átomos de terraza y escalón es de 1:1. Estas superficies son la {331}, la {311} y la {210}.

La correcta ordenación de todas las superficies y la limpieza de las disoluciones utilizadas se comprueba con una voltametría cíclica previa, cuya respuesta está

perfectamente detallada en la literatura [127, 128]. Se adjunta como ejemplo la caracterización electroquímica del Pt(111) en 0.5 M H_2SO_4.

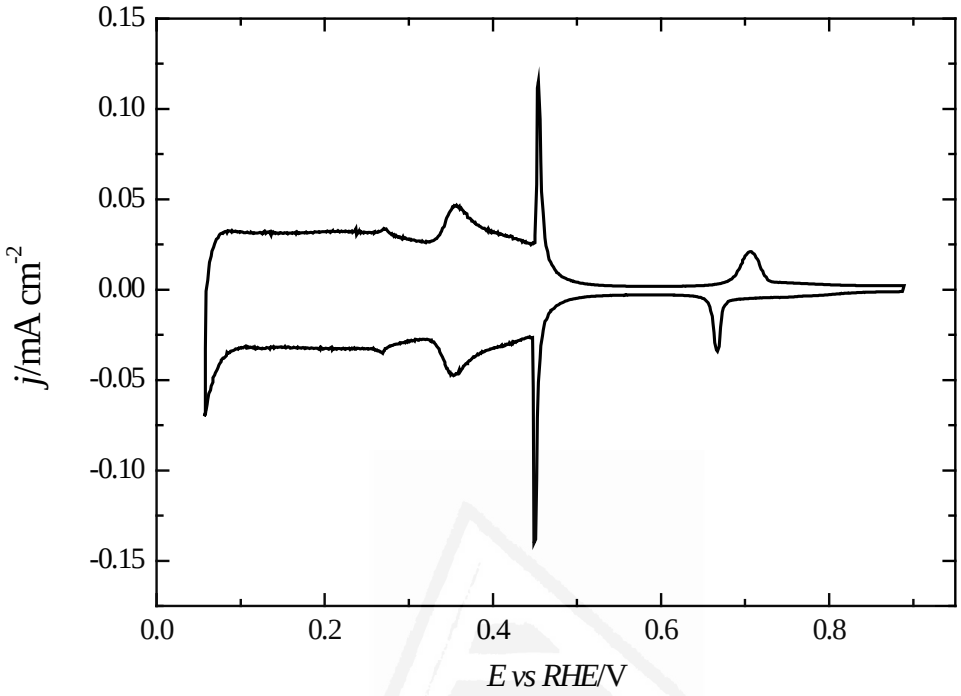

Fig. 1.15. Voltametría cíclica para un electrodo de Pt(111) en 0.5 M H_2SO_4. v = 0.05 V s^{-1}.

Las características de la voltametría del Pt(111) son una señal plana desde 0.05 hasta 0.25 V correspondiente con la zona de adsorción/desorción de hidrógeno. Al incrementar el potencial hacia valores más positivos, a partir de 0.3 V la adsorción del anión sulfato empieza a tener lugar sobre los sitios liberados por el hidrógeno entrando en la denominada región de mariposa. El par de picos reversibles a 0.45 V se corresponde con una transición de fase desorden-orden de la adcapa de SO_4^{2-} [129], mientras que el par de picos irreversibles que aparecen a 0.70 V en el barrido positivo y 0.67 V en el negativo no tiene un origen del todo claro. Experiencias de desplazamiento de carga con CO sugieren que son debidos mayoritariamente al anión sulfato [130, 131], resultados confirmados con posteriores análisis termodinámicos [132, 133]. Además, los cationes presentes en el electrolito ejercen una clara influencia en estos picos.

1.3.2 Nanopartículas de platino

Como se ha mencionado anteriormente, los catalizadores de platino preparados a partir de superficies monocristalinas son inviables en aplicaciones como pilas de combustible, por lo que el platino se dispersa en forma de nanopartículas tratando de optimizar la cantidad utilizada. El uso de nanopartículas como catalizadores en la tecnología de las pilas de combustible ha sido ampliamente investigado en la bibliografía [134-137].

Un parámetro importante a tener en cuenta en los estudios con nanopartículas es el de su tamaño, afectando a la relación entre átomos presentes en la superficie y en el seno del material. Si esta relación es muy alta, pueden producirse variaciones en las propiedades electrónicas superficiales de los catalizadores. Por otra parte, conviene controlar la estructura superficial de las nanopartículas, debido a su efecto en reacciones estudiadas en electrocatálisis. En el año 1969, Van Hardeveld y Hartog [138] propusieron diferentes modelos geométricos a partir de un número variable de átomos, los cuales indicaban la relación entre las formas de las partículas y las orientaciones superficiales ideales para una estructura cúbica centrada en las caras como la del platino. La Fig. 1.16 muestra dicha relación para varias estructuras cristalográficas a partir del triángulo estereográfico:

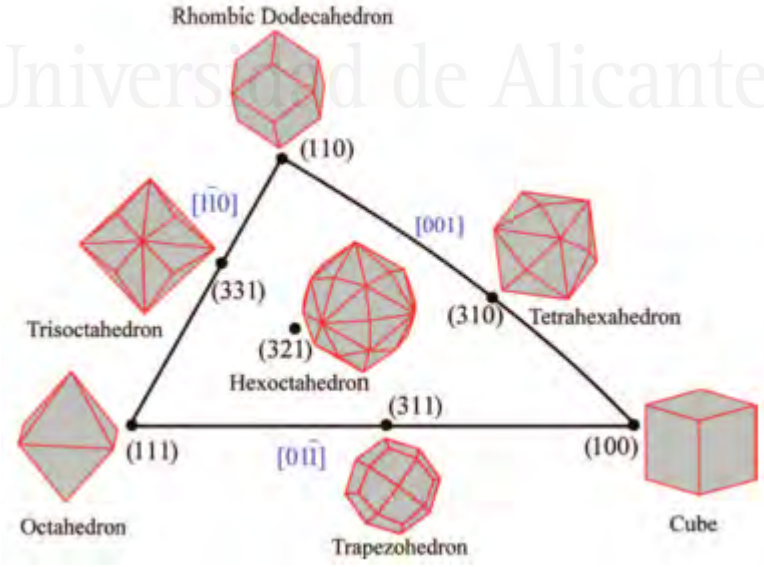

Fig. 1.16. Relación entre las formas de las nanopartículas y su estructura cristalográfica ideal para estructuras cúbicas centradas en las caras. Tomado de la referencia [139].

De acuerdo a la anterior figura, los dominios {111} se presentan en las formas tetraédricas u octaédricas, los dominios {100} aparecen en partículas con forma de cubo y los dominios {110} se presentarán idealmente en formas dodecaédricas truncadas rómbicamente. El problema de las muestras de nanopartículas es la no posibilidad de sintetizar por completo una única forma, pudiendo conseguirse alguna forma mayoritaria pero siempre con presencia de partículas de otras formas. Además, las nanopartículas contienen necesariamente otros tipos de sitio en bordes y esquinas. La notación empleada en toda la tesis se refiere a nombrar como (100)Pt a las muestras que contienen mayoritariamente forma cúbica, (111)Pt a las que presentan preferencia por las formas octaédricas, (100)-(111)Pt para muestras que contienen mezcla de partículas con forma octaédrica truncadas por cubos y (poly)Pt para las nanopartículas esféricas que no presentan preferencia por ningún dominio. Además, se utilizan unas nanopartículas esféricas soportadas en carbón Vulcan, señalando en cada muestra un porcentaje entre paréntesis, el cual indica la masa de platino presente respecto a la masa total de catalizador.

Para la síntesis de las nanopartículas utilizadas en la tesis, se emplearon tres métodos diferentes, dependiendo si se preparan nanopartículas con forma controlada u otras donde no sea tan importante la forma debido a que el objetivo es el estudio de otros efectos como la agregación de partículas. Estos métodos son:

- Método de microemulsión [140] para la preparación de nanopartículas de platino esféricas poliorientadas, (poly)Pt, usadas en los capítulos en los que se estudia el efecto de la estructura superficial.

- Método coloidal [34] para la realización de las nanopartículas de platino preferencialmente cúbicas (100)Pt, octaédricas (111)Pt y las mezcladas (100)-(111)Pt presentes en los estudios del efecto de la estructura superficial.

- Método citrato [141], para la elaboración de las muestras de platino con diferente carga soportadas en carbón Vulcan, utilizadas en el capítulo 5 en el estudio del efecto de la agregación de partículas en la oxidación de etanol.

Otra parte importante al preparar los electrodos de trabajo a partir de nanopartículas es la del soporte escogido para depositar las muestras. La característica principal que ha de cumplir el soporte es el de no presentar ninguna señal faradaica que interfiera en el intervalo de trabajo de las nanopartículas de Pt. Para preservar la estructura superficial de las nanopartículas, al igual que en el caso de las superficies monocristalinas, no es conveniente llegar a potenciales superiores a 0.95 V, ya que se entra en zona de formación de óxidos de platino, que, al reducirse en el barrido negativo, podrían producir la variación no deseada de la superficie inicial.

Los soportes empleados sobre los cuales se depositan las muestras de nanopartículas son un sustrato hemisférico de oro poliorientado o un carbón vítreo comercial. Ambos soportes no presentan corrientes faradaicas reseñables entre 0.05 y 1 V vs RHE, potenciales a los cuales se estudian las reacciones de oxidación con etanol y con ácido fórmico.

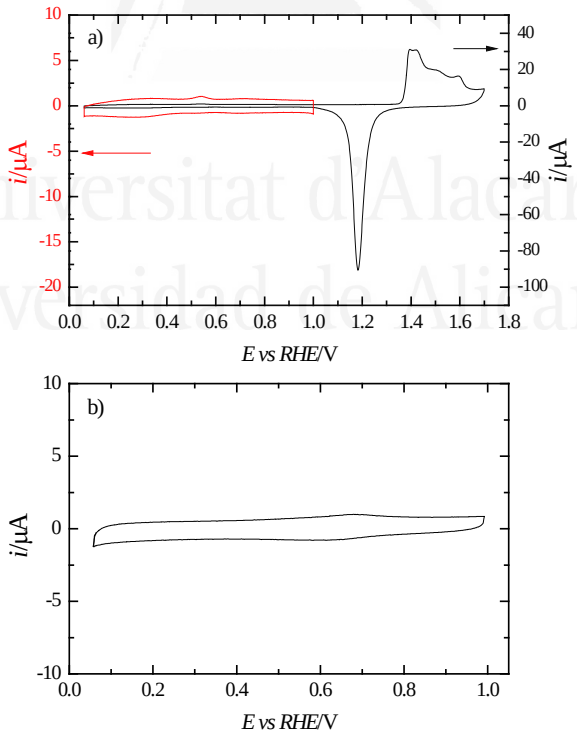

Fig. 1.17. Voltametría cíclica para: a) Soporte de Au policristalino, con la escala de la doble capa aumentada (línea roja) y b) Soporte de carbón vítreo. Disolución test: 0.5 M H_2SO_4. Velocidad de barrido: 0.05 V s^{-1}.

En un electrodo de Au policristalino, la evolución de hidrógeno se produce a potenciales más negativos que en el platino. En la zona entre 0.05 y 1 V, en la que se realizarán los experimentos, prácticamente sólo existe corriente capacitiva, independientemente de la orientación superficial [114], confirmando su utilidad como soporte para las nanopartículas. En el caso del carbón vítreo, tampoco se observan señales faradaicas importantes, únicamente se distinguen un par de picos irreversibles a 0.68 V y 0.63 V que se asignan a la incorporación de grupos quinona a la estructura del carbón vítreo [142]. Este último sustrato es menos conocido, particularmente en lo relacionado con su limpieza.

Una vez realizados los experimentos, los soportes se pulen con alúmina preparada de grano 0.3 micras para eliminar las nanopartículas del oro o del carbón vítreo. La recuperación del perfil voltamétrico de la Fig. 1.17 corrobora la completa eliminación de las nanopartículas después del pulido.

Un problema muy común cuando se trabaja con nanopartículas metálicas es el de la correcta limpieza de la superficie manteniendo su estructura superficial. Muchos métodos de síntesis [34, 140, 141, 143-146] utilizan surfactantes que han de ser eliminados antes de comenzar con los estudios, con el objetivo de trabajar en superficies limpias para conseguir reproducibilidad en los resultados. Como métodos de limpieza se han propuesto el ciclado de las nanopartículas hasta potenciales superiores a la formación de óxidos superficiales [147], la adición de disolventes orgánicos como hexano o ácido acético [146, 148] o el tratamiento en una atmósfera en presencia de ozono [149]. El problema de estos métodos de limpieza es que en muchas ocasiones provocan la modificación de la forma de las nanopartículas. En nuestro grupo de investigación, la técnica de desplazamiento de carga con CO sobre superficies monocristalinas de Pt [150, 151] muestra una total recuperación del perfil voltamétrico correspondiente a un electrodo totalmente limpio después de su adsorción con CO. De acuerdo a estos experimentos, a principio de la década de los 2000, Solla-Gullón *et. al.* [152] propusieron un método sencillo basado en el desplazamiento de las especies contaminantes de la superficie de las nanopartículas mediante la adsorción con CO, el cual se oxida posteriormente, quedando la superficie limpia y sin problemas de variación en la estructura superficial de las partículas. Todos los experimentos con

nanopartículas realizados en la tesis se hicieron después de su limpieza de acuerdo a este tratamiento en una disolución 0.5 M H_2SO_4.

Además, en las experiencias realizadas con electrodos de trabajo compuestos por nanopartículas de platino modificados por un adátomo diferente, el depósito se hizo mediante una voltametría cíclica en una disolución que contenía el precursor metálico con una concentración 10^{-5}-10^{-6} M en 0.5 M H_2SO_4, realizando un barrido de potenciales entre 0.06 y 0.8 V. No obstante, la forma en la que se modifica la superficie de platino es diferente dependiendo del adátomo adsorbido:

- UPD (*under potential deposition* en sus siglas en inglés), donde el átomo de la segunda especie se deposita a potenciales más positivos al termodinámico, como en el caso del Tl, Sn y Pb. En este caso, el enlace entre el metal substrato (Pt en forma de nanopartículas) y los átomos depositados de la segunda especie (adátomos) es más fuerte que en el caso de un depósito másico normal a potenciales más negativos [153, 154]. Esta técnica permite un control preciso y reproducible del recubrimiento de metal depositado sobre el sustrato. Además, la existencia de equilibrio entre el precursor metálico presente en la disolución y el adátomo implica una relación entre el potencial del electrodo y su recubrimiento superficial.

- Adsorción irreversible de adátomos [155, 156], como en el caso del Rh y el Ru, donde dichos adátomos se adsorben de manera irreversible sobre la superficie de las nanopartículas de platino, permaneciendo sobre el sustrato de platino aún en ausencia del precursor metálico. No hay equilibrio entre las especies presentes en disolución y el adátomo correspondiente, por lo que el potencial puede variarse sin efecto alguno sobre el recubrimiento superficial del adátomo en las nanopartículas de platino, dentro de ciertos límites.

El control del recubrimiento del adátomo se lleva a cabo mediante voltametría cíclica, generalmente con la disminución de la carga de adsorción de hidrógeno característica del Pt. En todos los casos planteados en esta tesis, únicamente para la adsorción de Rh no se puede utilizar dicha carga para el cálculo del recubrimiento, debido

a que su voltagrama presenta picos para la adsorción de hidrógeno a potenciales similares a los del platino.

Al igual que en el caso de los monocristales de platino, la manera de caracterizar las nanopartículas de platino es mediante una simple voltametría cíclica, una vez realizados los procesos de limpieza con CO indicados en esta sección. La caracterización electroquímica de las nanopartículas utilizadas ha sido publicada en los últimos años por nuestro grupo de investigación [33, 145, 157, 158]. Dichos resultados coinciden con nuestras caracterizaciones, las cuales vienen representadas en cada capítulo de la tesis en que se hayan empleado nanopartículas de platino como electrodo de trabajo.

1.4 Objetivo de la tesis

La investigación efectuada en esta tesis se engloba dentro de los estudios de electrocatálisis para la oxidación de pequeñas moléculas orgánicas de interés en la tecnología de las pilas de combustible. Concretamente, se emplean el etanol y el ácido fórmico como moléculas de estudio, realizando investigaciones fundamentales a temperatura ambiente usando superficies de platino como catalizadores, ya sean superficies monocristalinas o nanopartículas de platino. Estos estudios fundamentales buscan maximizar la cantidad de CO_2 formado a potenciales bajos, evitando en lo posible la formación de especies que envenenen la superficie inhibiendo la actividad catalítica del platino, como CO en el caso del ácido fórmico o CO y aniones acetato en el etanol.

Para llevar a cabo los estudios de electrocatálisis de oxidación de etanol y ácido fórmico se han recurrido a técnicas electroquímicas (voltametría cíclica y cronoamperometría) donde se obtiene información acerca de qué superficies son más activas y requieren menos sobrepotenciales para llevar a cabo las oxidaciones. La espectroscopía FTIR de reflexión externa se emplea para conocer con exactitud las especies adsorbidas o formadas a cada potencial a medida que prosigue la oxidación, pudiendo, por ejemplo, distinguir entre la cantidad de CO adsorbido o acetato formado (no deseado) en el caso del etanol o si en la oxidación de ácido fórmico se consigue catalizar la conversión de CO a CO_2. Por último, las experiencias con espectrometría de masas electroquímica en condiciones de flujo permiten la obtención de datos cuantitativos muy útiles para conocer con mayor exactitud las diferencias entre catalizadores de platino preparados a partir de nanopartículas de platino con diferentes estructuras superficiales.

Tomando como base los resultados publicados por Colmati *et.al.* para la oxidación de etanol utilizando superficies monocristalinas de platino [71], el capítulo 2 de la tesis tiene como objetivo comprobar si el mismo comportamiento observado respecto al efecto de la estructura superficial en electrodos monocristalinos de platino se conserva en el caso de nanopartículas de platino con orientación preferencial, sintetizadas en nuestro grupo de investigación de la Universidad de Alicante y utilizadas en estudios de electrocatálisis [33, 159, 160]. Además, también se investiga la influencia de la posible adsorción de aniones presentes en el electrolito soporte en la misma oxidación de etanol.

El mecanismo de oxidación de etanol varía si se modifica el pH de la disolución de trabajo. Manteniendo en todo momento pHs ácidos y una concentración constante de electrolito soporte, el capítulo 3 estudia los cambios producidos en dicho mecanismo al aumentar ligeramente el pH, trabajando con dos muestras de nanopartículas de platino: con preferencia por dominios {100} y con preferencia por dominios {111}. Solo se utilizan estas dos muestras porque son las que muestran comportamientos más extremos en cuanto a la oxidación de etanol. Estos estudios se hacen en un sistema con células de flujo [107], una situación más parecida a la empleada en las pilas de combustible. En este sentido, debe pensarse que un aumento del pH aumentará la resistencia del electrolito.

En el capítulo 4 se comienza con el estudio de la oxidación de etanol en medio alcalino. Primero de todo, para una mejor comprensión de la reacción, se emplean superficies monocristalinas de platino con la estructura cristalográfica perfectamente conocida. Las investigaciones realizadas son similares a las efectuadas por Colmati *et. al.* en medio ácido [71, 76], en primer lugar con los planos basales para conocer como varía la actividad al trabajar en pHs opuestos y posteriormente con superficies escalonadas {100} o {110} en terrazas {111} para ver su efecto para la catálisis de etanol. Por otra parte, se comparan los espectros IR obtenidos con espectros de transmisión de probables productos a un mismo pH, de igual manera a lo realizado por experimentos del grupo de Sun [161]. Los resultados se comparan con trabajos similares para la oxidación de etanol en platino a pH alcalino [86, 162, 163].

En la misma línea de los estudios realizados en el capítulo 2 de la tesis, el capítulo 5 busca confirmar los mismos resultados de electrocatálisis con superficies monocristalinas de platino en medio alcalino con las nanopartículas de platino con orientación preferencial, incidiendo además en la estabilidad de la catálisis de las nanopartículas de platino con el tiempo a un potencial fijo. Este capítulo presenta además otra parte, donde se investiga el efecto de agregación en nanopartículas poliorientadas soportadas en carbón con diferentes cantidades de platino en las muestras, que en medio ácido inhibe las reacciones de oxidación de etanol y ácido fórmico [164].

A partir del capítulo 6 se inicia el estudio de la influencia de la adsorción de un metal diferente al platino sobre las nanopartículas de platino. La adición de adátomos como el

Sb, el Bi, o el Pd entre otros provoca una mejora en cuanto a la actividad total y al potencial al cual se inicia la oxidación de ácido fórmico en superficies monocristalinas [53, 54, 56, 165]. Se ha observado el mismo efecto catalítico en las muestras de nanopartículas de platino con orientaciones preferenciales {100} y orientaciones preferenciales {111} decorada con Sb o Pd [92, 166]. En este capítulo se estudia el efecto de la adsorción de talio sobre las mismas muestras de nanopartículas cúbicas y octaédricas en medio ácido para la oxidación de ácido fórmico.

Por último, en el capítulo 7 de la tesis se realizan investigaciones similares con adátomos sobre las superficies de las nanopartículas de platino, pero para la oxidación de etanol. Los catalizadores preparados con la combinación entre Pt y otro metal se muestran muy beneficiosas para la optimización de la reacción de oxidación de etanol, como por ejemplo Rh o Sn [80, 167-169] o la combinación entre diferentes metales con el platino [93, 170]. Siguiendo la estrategia de adsorber átomos de diferentes metales sobre las nanopartículas de platino, trabajos previos realizados con superficies de platino muestran el efecto positivo de la adición de otros átomos junto al platino para la eliminación del veneno, como es el caso de Sn [78], Ru [77, 171], Os [82, 172] o Pb [173, 174]. En este capítulo, se busca algún adátomo que funcione de forma similar con las nanopartículas de platino a pHs ácidos y a pHs alcalinos, tratando de encontrar la combinación óptima para cada electrolito soporte.

1.5 Referencias

[1] W. Schmickler, "Interfacial Electrochemistry", Oxford University Press, New York, **1996**.

[2] J. O. M. Bockris and A. K. N. Reddy, "Modern Electrochemistry", Plenum, New York, **1970**.

[3] W. Schuhmann and E. M. Bonsen, "Biosensors", in *Encyclopedia of Electrochemistry*, Wiley, **2007**.

[4] Y. Li, H. J. Schluesener and S. Xu, "Gold nanoparticle-based biosensors" *Gold Bulletin* **2010**, 43, 29-41.

[5] F. W. Campbell and R. G. Compton, "The use of nanoparticles in electroanalysis: An updated review" *Analytical and Bioanalytical Chemistry* **2010**, 396, 241-259.

[6] J. M. Pingarrón Carrazón and P. Sánchez Batanero, "Química electroanalítica: fundamentos y aplicaciones", Síntesis, **1999**.

[7] B. Oregan and M. Grätzel, "A low-cost, high-efficiency solar cell based on dye-sensitized colloidal TiO_2 films" *Nature* **1991**, 353, 737-740.

[8] I. Sirés and E. Brillas, "Remediation of water pollution caused by pharmaceutical residues based on electrochemical separation and degradation technologies: A review" *Environment International* **2012**, 40, 212-229.

[9] T. Shono, "Electroorganic chemistry in organic synthesis" *Tetrahedron* **1984**, 40, 811-850.

[10] J. Yoshida, K. Kataoka, R. Horcajada and A. Nagaki, "Modern strategies in electroorganic synthesis" *Chemical Reviews* **2008**, 108, 2265-2299.

[11] A. J. Bard, M. Stratmann and G. S. Frankel, "Corrosion and Oxide Films", *Encyclopedia of Electrochemistry vol. 4* A. J. Bard, M. Stratmann and G. S. Frankel (Eds.), Wiley VCH, **2003**.

[12] P. Simon and Y. Gogotsi, "Materials for electrochemical capacitors" *Nature Materials* **2008**, 7, 845-854.

[13] E. Frackowiak and F. Beguin, "Carbon materials for the electrochemical storage of energy in capacitors" *Carbon* **2001**, 39, 937-950.

[14] M. S. Whittingham and T. Zawodzinski, "Introduction: Batteries and Fuel Cells" *Chemical Reviews* **2004**, 104, 4243-4244.

[15] J. M. Tarascon and M. Armand, "Issues and challenges facing rechargeable lithium batteries" *Nature* **2001**, 414, 359-367.

[16] C. P. de León, A. Frías-Ferrer, J. González-García, D. A. Szanto and F. C. Walsh, "Redox flow cells for energy conversion" *Journal of Power Sources* **2006**, 160, 716-732.

[17] S. Srinivasan, "Fuel Cells: From fundamental to Applications", Springer, **2006**.

[18] "Fuel Cell Handbook", U.S. Department of Energy, Morgantown, West Virginia, **2000**.

[19] S. Rousseau, C. Coutanceau, C. Lamy and J. M. Léger, "Direct ethanol fuel cell (DEFC): Electrical performances and reaction products distribution under operating conditions with different platinum-based anodes" *Journal of Power Sources* **2006**, 158, 18-24.

[20] S. Song, W. Zhou, Z. Liang, R. Cai, G. Sun, Q. Xin, V. Stergiopoulos and P. Tsiakaras, "The effect of methanol and ethanol cross-over on the performance of PtRu/C-based anode DAFCs" *Applied Catalysis B: Environmental* **2005**, 55, 65-72.

[21] C. Rice, R. I. Ha, R. I. Masel, P. Waszczuk, A. Wieckowski and T. Barnard, "Direct formic acid fuel cells" *Journal of Power Sources* **2002**, 111, 83-89.

[22] A. Wojcik, H. Middleton, I. Damopoulos and J. Van Herle, "Ammonia as a fuel in solid oxide fuel cells" *Journal of Power Sources* **2003**, 118, 342-348.

[23] K. Yamada, K. Asazawa, K. Yasuda, T. Ioroi, H. Tanaka, Y. Miyazaki and T. Kobayashi, "Investigation of PEM type direct hydrazine fuel cell" *Journal of Power Sources* **2003**, 115, 236-242.

[24] S. C. Amendola, P. Onnerud, M. T. Kelly, P. J. Petillo, S. L. Sharp-Goldman and M. Binder, "A novel high power density borohydride-air cell" *Journal of Power Sources* **1999**, 84, 130-133.

[25] I. Willner, Y. M. Yan, B. Willner and R. Tel-Vered, "Integrated Enzyme-Based Biofuel Cells-A Review" *Fuel Cells* **2009**, 9, 7-24.

[26] Z. W. Du, H. R. Li and T. Y. Gu, "A state of the art review on microbial fuel cells: A promising technology for wastewater treatment and bioenergy" *Biotechnology Advances* **2007**, 25, 464-482.

[27] J. S. Spendelow and A. Wieckowski, "Electrocatalysis of oxygen reduction and small alcohol oxidation in alkaline media" *Physical Chemistry Chemical Physics* **2007**, 9, 2654-2675.

[28] D. Takky, B. Beden, J. M. Léger and C. Lamy, "Evidence for the effect of molecular structure on the electrochemical reactivity of alcohols: Part I. Electrooxidation of the butanol isomers on noble metal electrodes in alkaline medium" *Journal of Electroanalytical Chemistry* **1983**, 145, 461-466.

[29] C. Lamy and C. Coutanceau, "Electrocatalysis of Alcohol Oxidation Reactions at Platinum Group Metals", in *Catalysts for Alcohol-Fuelled Direct Oxidation Fuel Cells, vol. 6*, Z.-X. Liang and T. S. Zhao (Eds.) RSC Energy and Enviroment Series **2012**.

[30] C. Lamy and J. M. Léger, "Electrocatalytic oxidation of small organic molecules at platinum single crystals" *Journal de Chimie Physique et de Physico-Chimie Biologique* **1991**, 88, 1649-1671.

[31] Y. Ishikawa, M. S. Liao and C. R. Cabrera, "Oxidation of methanol on platinum, ruthenium and mixed Pt-M metals (M = Ru, Sn): a theoretical study" *Surface Science* **2000**, 463, 66-80.

[32] G. A. Camara and T. Iwasita, "Parallel pathways of ethanol oxidation: The effect of ethanol concentration" *Journal of Electroanalytical Chemistry* **2005**, 578, 315-321.

[33] J. Solla-Gullón, P. Rodríguez, E. Herrero, A. Aldaz and J. M. Feliu, "Surface characterization of platinum electrodes" *Physical Chemistry Chemical Physics* **2008**, 10, 1359-1373.

[34] T. S. Ahmadi, Z. L. Wang, T. C. Green, A. Henglein and M. A. El-Sayed, "Shape-controlled synthesis of colloidal platinum nanoparticles" *Science* **1996**, 272, 1924-1926.

[35] S. Uhm, H. J. Lee and J. Lee, "Understanding underlying processes in formic acid fuel cells" *Physical Chemistry Chemical Physics* **2009**, 11, 9326-9336.

[36] A. Capon and R. Parsons, "The oxidation of formic acid at noble metal electrodes Part III. Intermediates and mechanism on platinum electrodes" *Journal of Electroanalytical Chemistry* **1973**, 45, 205-231.

[37] J. M. Feliu and E. Herrero, "Formic acid oxidation", in *Handbook of Fuel Cells - Fundamentals, Technology and Applications, vol. 2*, W. Vielstich, H. Gasteiger and A. Lamm (Eds.) Wiley, Chichester, **2003**, pp. 625-634.

[38] K. Kunimatsu, "Infrared spectroscopic study of methanol and formic acid adsorbates on a platinum electrode: Part I. Comparison of the infrared absorption intensities of linear CO(a) derived from CO, CH_3OH and HCOOH" *Journal of Electroanalytical Chemistry* **1986**, 213, 149-157.

[39] S. G. Sun, J. Clavilier and A. Bewick, "The mechanism of electrocatalytic oxidation of formic acid on Pt (100) and Pt (111) in sulphuric acid solution: an EMIRS study" *Journal of Electroanalytical Chemistry* **1988**, 240, 147-159.

[40] Y. X. Chen, M. Heinen, Z. Jusys and R. J. Behm, "Bridge-bonded formate: Active intermediate or spectator species in formic acid oxidation on a Pt film electrode?" *Langmuir* **2006**, 22, 10399-10408.

[41] S. C. Chang, L. W. H. Leung and M. J. Weaver, "Metal crystallinity effects in electrocatalysis as probed by real-time FTIR spectroscopy: electrooxidation of formic acid, methanol, and ethanol on ordered low-index platinum surfaces" *Journal of Physical Chemistry* **1990**, 94, 6013-6021.

[42] A. Miki, S. Ye and M. Osawa, "Surface-enhanced IR absorption on platinum nanoparticles: an application to real-time monitoring of electrocatalytic reactions" *Chemical Communications (Cambridge, United Kingdom)* **2002**, 1500-1501.

[43] A. Cuesta, G. Cabello, M. Osawa and C. Gutiérrez, "Mechanism of the Electrocatalytic Oxidation of Formic Acid on Metals" *ACS Catalysis* **2012**, 2, 728-738.

[44] Y. X. Chen, M. Heinen, Z. Jusys and R. B. Behm, "Kinetics and mechanism of the electrooxidation of formic acid - Spectroelectrochemical studies in a flow cell" *Angewandte Chemie, International Edition in English* **2006**, 45, 981-985.

[45] Y. X. Chen, M. Heinen, Z. Jusys and R. J. Behm, "Kinetic isotope effects in complex reaction networks: Formic acid electro-oxidation" *ChemPhysChem* **2007**, 8, 380-385.

[46] J. Joo, T. Uchida, A. Cuesta, M. T. M. Koper and M. Osawa, "Importance of Acid-Base Equilibrium in Electrocatalytic Oxidation of Formic Acid on Platinum" *Journal of the American Chemical Society* **2013**, 135, 9991-9994.

[47] S. Brimaud, J. Solla-Gullón, I. Weber, J. M. Feliu and R. J. Behm, "Formic Acid Electrooxidation on Noble-Metal Electrodes: Role and Mechanistic Implications of pH, Surface Structure, and Anion Adsorption" *ChemElectroChem* **2014**, 1, 1075-1083.

[48] J. Clavilier, R. Parsons, R. Durand, C. Lamy and J. M. Léger, "Formic acid oxidation on single crystal platinum electrodes. Comparison with polycrystalline platinum" *Journal of Electroanalytical Chemistry* **1981**, 124, 321-326.

[49] N. M. Markovic and P. N. Ross, "Surface science studies of model fuel cell electrocatalysts" *Surface Science Reports* **2002**, 45, 117-229.

[50] J. Clavilier, A. Fernández-Vega, J. M. Feliu and A. Aldaz, "Heterogeneous electrocatalysis on well defined platinum surfaces modified by controlled amounts of irreversibly adsorbed adatoms: Part I. Formic-acid oxidation on the Pt (111) - Bi system" *Journal of Electroanalytical Chemistry* **1989**, 258, 89-100.

[51] J. Clavilier, A. Fernández-Vega, J. M. Feliu and A. Aldaz, "Heterogeneous electrocatalysis on well-defined platinum surfaces modified by controlled amounts of irreversibly adsorbed adatoms: Part III. Formic-acid oxidation on the Pt(100)-Bi system" *Journal of Electroanalytical Chemistry* **1989**, 261, 113-125.

[52] S. A. Campbell and R. Parsons, "Effect of Bi and Sn adatoms on formic acid and methanol oxidation at well defined platinum surfaces" *Journal of the Chemical Society, Faraday Transactions* **1992**, 88, 833-841.

[53] E. Herrero, J. M. Feliu and A. Aldaz, "Poison formation reaction from formic acid on Pt(100) electrodes modified by irreversibly adsorbed bismuth and antimony" *Journal of Electroanalytical Chemistry* **1994**, 368, 101-108.

[54] Y.-Y. Yang, S.-G. Sun, Y.-J. Gu, Z.-Y. Zhou and C.-H. Zhen, "Surface modification and electrocatalytic properties of Pt(100), Pt(110), Pt(320) and Pt(331) electrodes with Sb towards HCOOH oxidation" *Electrochimica Acta* **2001**, 46, 4339-4348.

[55] H. W. Lei, H. Hattori and H. Kita, "Electrocatalysis by Pb adatoms of HCOOH oxidation at Pt(111) in acidic solution" *Electrochimica Acta* **1996**, 41, 1619-1628.

[56] F. J. Vidal-Iglesias, J. Solla-Gullón, E. Herrero, A. Aldaz and J. M. Feliu, "Formic acid oxidation on Pd-modified Pt(100) and Pt(111) electrodes: A DEMS study" *Journal of Applied Electrochemistry* **2006**, 36, 1207-1214.

[57] E. Herrero, M. J. Llorca, J. M. Feliu and A. Aldaz, "Oxidation of formic acid on Pt(100) electrodes modified by irreversibly adsorbed tellurium" *Journal of Electroanalytical Chemistry* **1995**, 383, 145-154.

[58] M. J. Llorca, E. Herrero, J. M. Feliu and A. Aldaz, "Formic acid oxidation on Pt(111) electrodes modified by irreversibly adsorbed selenium" *Journal of Electroanalytical Chemistry* **1994**, 373, 217-225.

[59] A. Fernández-Vega, J. M. Feliu, A. Aldaz and J. Clavilier, "Heterogeneous electrocatalysis on well-defined platinum surfaces modified by controlled amounts of irreversibly adsorbed adatoms: Part IV. Formic acid oxidation on the Pt(111)-As system" *Journal of Electroanalytical Chemistry* **1991**, 305, 229-240.

[60] A. Boronat-González, E. Herrero and J. M. Feliu, "Fundamental aspects of HCOOH oxidation at platinum single crystal surfaces with basal orientations and modified by irreversibly adsorbed adatoms" *Journal of Solid State Electrochemistry* **2014**, 18, 1181-1193.

[61] T. Iwasita, B. Rasch, E. Cattaneo and W. Vielstich, "A SNIFTIRS study of ethanol oxidation on platinum" *Electrochimica Acta* **1989**, 34, 1073-1079.

[62] J. Willsau and J. Heitbaum, "Elementary steps of ethanol oxidation on Pt in sulfuric acid as evidenced by isotope labeling" *Journal of Electroanalytical Chemistry* **1985**, 194, 27-35.

[63] R. Kavanagh, X.-M. Cao, W.-F. Lin, C. Hardacre and P. Hu, "Origin of Low CO_2 Selectivity on Platinum in the Direct Ethanol Fuel Cell" *Angewandte Chemie International Edition* **2012**, 51, 1572-1575.

[64] A. Rodes, E. Pastor and T. Iwasita, "An FTIR Study on the Adsorption of Acetate at the Basal Planes of Platinum Single-Crystal Electrodes" *Journal of Electroanalytical Chemistry* **1994**, 376, 109-118.

[65] T. Iwasita and E. Pastor, "A DEMS and FTIR spectroscopic investigation of adsorbed ethanol on polycrystalline platinum" *Electrochimica Acta* **1994**, 39, 531-537.

[66] H. Wang, Z. Jusys and R. J. Behm, "Ethanol electrooxidation on a carbon-supported Pt catalyst: Reaction kinetics and product yields" *Journal of Physical Chemistry B* **2004**, 108, 19413-19424.

[67] M. Heinen, Z. Jusys and R. J. Behm, "Ethanol, Acetaldehyde and Acetic Acid Adsorption/Electrooxidation on a Pt Thin Film Electrode under Continuous Electrolyte Flow: An in Situ ATR-FTIRS Flow Cell Study" *Journal of Physical Chemistry C* **2010**, 114, 9850-9864.

[68] J. Souza-Garcia, E. Herrero and J. M. Feliu, "Breaking the C-C Bond in the Ethanol Oxidation Reaction on Platinum Electrodes: Effect of Steps and Ruthenium Adatoms" *ChemPhysChem* **2010**, 11, 1391-1394.

[69] X. H. Xia, H. D. Liess and T. Iwasita, "Early stages in the oxidation of ethanol at low index single crystal platinum electrodes" *Journal of Electroanalytical Chemistry* **1997**, 437, 233-240.

[70] S. C. S. Lai and M. T. M. Koper, "Electro-oxidation of ethanol and acetaldehyde on platinum single-crystal electrodes" *Faraday Discussions* **2008**, 140, 399-416.

[71] F. Colmati, G. Tremiliosi-Filho, E. R. Gonzalez, A. Berná, E. Herrero and J. M. Feliu, "Surface structure effects on the electrochemical oxidation of ethanol on platinum single crystal electrodes" *Faraday Discussions* **2008**, 140, 379-397.

[72] U. Schmiemann, U. Müller and H. Baltruschat, "The Influence of the Surface-Structure on the Adsorption of Ethene, Ethanol and Cyclohexene as Studied by DEMS" *Electrochimica Acta* **1995**, 40, 99-107.

[73] M. J. Prieto and G. Tremiliosi-Filho, "The influence of acetic acid on the ethanol electrooxidation on a platinum electrode" *Electrochemistry Communications* **2011**, 13, 527-529.

[74] D. J. Tarnowski and C. Korzeniewski, "Effects of surface step density on the electrochemical oxidation of ethanol to acetic acid" *Journal of Physical Chemistry B* **1997**, 101, 253-258.

[75] S. C. S. Lai and M. T. M. Koper, "The Influence of Surface Structure on Selectivity in the Ethanol Electro-oxidation Reaction on Platinum" *Journal of Physical Chemistry Letters* **2010**, 1, 1122-1125.

[76] F. Colmati, G. Tremiliosi-Filho, E. R. Gonzalez, A. Berná, E. Herrero and J. M. Feliu, "The role of the steps in the cleavage of the C-C bond during ethanol oxidation on platinum electrodes" *Physical Chemistry Chemical Physics* **2009**, 11, 9114-9123.

[77] V. Del Colle, A. Berná, G. Tremiliosi-Filho, E. Herrero and J. M. Feliu, "Ethanol electrooxidation onto stepped surfaces modified by Ru deposition: electrochemical and spectroscopic studies" *Physical Chemistry Chemical Physics* **2008**, 10, 3766-3773.

[78] V. Del Colle, J. Souza-Garcia, G. Tremiliosi-Filho, E. Herrero and J. M. Feliu, "Electrochemical and spectroscopic studies of ethanol oxidation on Pt stepped surfaces modified by tin adatoms" *Physical Chemistry Chemical Physics* **2011**, 13, 12163-12172.

[79] W. Zhu, J. Ke, S. B. Wang, J. Ren, H. H. Wang, Z. Y. Zhou, R. Si, Y. W. Zhang and C. H. Yan, "Shaping Single-Crystalline Trimetallic Pt-Pd-Rh Nanocrystals toward High-Efficiency C-C Splitting of Ethanol in Conversion to CO_2" *ACS Catalysis* **2015**, 5, 1995-2008.

[80] J. P. I. de Souza, S. L. Queiroz, K. Bergamaski, E. R. Gonzalez and F. C. Nart, "Electro-oxidation of ethanol on Pt, Rh, and PtRh electrodes. A study using DEMS and in-situ FTIR techniques" *Journal of Physical Chemistry B* **2002**, 106, 9825-9830.

[81] T. E. Shubina and M. T. M. Koper, "Quantum-chemical calculations of CO and OH interacting with bimetallic surfaces" *Electrochimica Acta* **2002**, 47, 3621-3628.

[82] V. Del Colle, V. Santos and G. Tremiliosi-Filho, "Comparative Electrochemical and Spectroscopic Studies of Ethanol Oxidation on Pt(h,k,l) Modified by Osmium Nanoislands" *Electrocatalysis* **2010**, 1, 144-158.

[83] J. Tayal, B. Rawat and S. Basu, "Bi-metallic and tri-metallic Pt-Sn/C, Pt-Ir/C, Pt-Ir-Sn/C catalysts for electro-oxidation of ethanol in direct ethanol fuel cell" *International Journal of Hydrogen Energy* **2011**, 36, 14884-14897.

[84] W. Zhou, Z. Zhou, S. Song, W. Li, G. Sun, P. Tsiakaras and Q. Xin, "Pt based anode catalysts for direct ethanol fuel cells" *Applied Catalysis B: Environmental* **2003**, 46, 273-285.

[85] S. C. S. Lai, S. E. F. Kleijn, F. T. Z. Öztürk, V. C. van Rees Vellinga, J. Koning, P. Rodriguez and M. T. M. Koper, "Effects of electrolyte pH and composition on the ethanol electro-oxidation reaction" *Catalysis Today* **2010**, 154, 92-104.

[86] P. A. Christensen, S. W. M. Jones and A. Hamnett, "In Situ FTIR Studies of Ethanol Oxidation at Polycrystalline Pt in Alkaline Solution" *Journal of Physical Chemistry C* **2012**, 116, 24681-24689.

[87] A. J. Bard and L. R. Faulkner, "Electrochemical Methods. Fundamental and Applications", John Wiley & Sons, Inc., New York, **2001**.

[88] A. J. Bard and M. Stratmann, "Instrumentation and Electroanalytical Chemistry", *Encyclopedia of Electrochemistry vol. 3* P. R. Unwin (Ed.), Wiley, **2003**.

[89] P. Kissinger and W. R. Heineman, "Laboratory Techniques in Electroanalytical Chemistry, Second Edition, Revised and Expanded", Taylor & Francis, **1996**.

[90] M. Bergelin and M. Wasberg, "The impinging jet flow method in interfacial electrochemistry: an application to bead-type electrodes" *Journal of Electroanalytical Chemistry* **1998**, 449, 181-191.

[91] T. H. M. Housmans and M. T. M. Koper, "CO oxidation on stepped Rh [n(111) x (111)] single crystal electrodes: a chronoamperometric study" *Journal of Electroanalytical Chemistry* **2005**, 575, 39-51.

[92] F. J. Vidal-Iglesias, A. López-Cudero, J. Solla-Gullón and J. M. Feliu, "Towards More Active and Stable Electrocatalysts for Formic Acid Electrooxidation: Antimony-Decorated Octahedral Platinum Nanoparticles" *Angewandte Chemie-International Edition* **2013**, 52, 964-967.

[93] A. Kowal, M. Li, M. Shao, K. Sasaki, M. B. Vukmirovic, J. Zhang, N. S. Marinkovic, P. Liu, A. I. Frenkel and R. R. Adzic, "Ternary Pt/Rh/SnO_2 electrocatalysts for oxidizing ethanol to CO_2" *Nature Materials* **2009**, 8, 325-330.

[94] F. M. Hoffmann, "Infrared reflection-absorption spectroscopy of adsorbed molecules" *Surface Science Reports* **1983**, 3, 107-192.

[95] T. Iwasita and F. C. Nart, "In situ infrared spectroscopy at electrochemical interfaces" *Progress in Surface Science* **1997**, 55, 271-340.

[96] A. Berná, A. Rodes and J. M. Feliu, "In-situ FTIR Studies on the Acid-Base Equilibria of Adsorbed Species on Well-Defined Metal Electrode Surfaces", in *In-situ Spectroscopic Studies of Adsorption at the Electrode and Electrocatalysis*, S.-G. Sun, P. A. Christensen and A. Wieckowski (Eds.) Elsevier, Amsterdam, **2007**, pp. 1-32.

[97] G. Gauglitz and T. Vo-Dinh, "Handbook of Spectroscopy", Wiley, **2006**.

[98] T. Iwasita and F. C. Nart, "In-Situ Fourier Transform Infrared Spectroscopy: A Tool to Characterize the Metal-Electrolyte Interface at a Molecular Level", in *Advances in Electrochemical Science and Engineering, vol. 4,* Wiley, **2008**, pp. 123-216.

[99] R. G. Greenler, "Infrared Study of Adsorbed Molecules on Metal Surfaces by Reflection Techniques" *The Journal of Chemical Physics* **1966**, 44, 310-315.

[100] A. Rodes, J. M. Pérez and A. Aldaz, "Vibrational spectroscopy", in *Handbook of Fuel Cells - Fundamentals, Technology and Applications, vol. 2*, W. Vielstich, A. Lamm and H. A. Gasteiger (Eds.) Wiley, Chichester, **2003**, pp. 191-219.

[101] M. Osawa, "In-situ Surface-Enhanced Infrared Spectroscopy of the Electrode/Solution Interface", in *Advances in Electrochemical Science and Engineering, vol. 9,* Wiley, **2008**, pp. 269-314.

[102] Z. M. Khoshhesab, "Reflectance IR spectroscopy", INTECH Open Access Publisher, **2012**.

[103] M. Osawa, "Surface-Enhanced Infrared Absorption Spectroscopy", in *Handbook of Vibrational Spectroscopy, vol. 1,* Wiley, **2006**, pp. 785-799.

[104] H. Baltruschat, "Differential electrochemical mass spectrometry" *Journal of the American Society for Mass Spectrometry* **2004**, 15, 1693-1706.

[105] O. Wolter and J. Heitbaum, "Differential Electrochemical Mass-Spectroscopy (DEMS) - a New Method for the Study of Electrode Process" *Berichte Der Bunsen-Gesellschaft-Physical Chemistry Chemical Physics* **1984**, 88, 2-6.

[106] S. J. Ashton, "Design, Construction and Research Application of a Differential Electrochemical Mass Spectrometer (DEMS)", Springer, **2012**.

[107] M. Heinen, Y. X. Chen, Z. Jusys and R. J. Behm, "In situ ATR-FTIRS coupled with on-line DEMS under controlled mass transport conditions - A novel tool for electrocatalytic reaction studies" *Electrochimica Acta* **2007**, 52, 5634-5643.

[108] H. Miyake, S. Ye and M. Osawa, "Electroless deposition of gold thin films on silicon for surface-enhanced infrared spectroelectrochemistry" *Electrochemistry Communications* **2002**, 4, 973-977.

[109] Z. Jusys and R. J. Behm, "Methanol oxidation on a carbon-supported Pt fuel cell catalyst - A kinetic and mechanistic study by differential electrochemical mass spectrometry" *Journal of Physical Chemistry B* **2001**, 105, 10874-10883.

[110] V. Climent, "Nueva aproximación al estudio de los potenciales de carga cero de electrodos monocristalinos del grupo del platino: aplicación al estudio de la adsorción iónica y molecular", Tesis doctoral, Universidad de Alicante, **1999**.

[111] J. Clavilier, R. Faure, G. Guinet and R. Durand, "Preparation of monocrystalline Pt microelectrodes and electrochemical study of the plane surfaces cut in the direction of the {111} and {110} planes" *Journal of Electroanalytical Chemistry* **1980**, 107, 205-209.

[112] J. Clavilier, "The role of anion on the electrochemical behaviour of a {111} platinum surface; an unusual splitting of the voltammogram in the hydrogen region" *Journal of Electroanalytical Chemistry* **1980**, 107, 211-216.

[113] A. Hamelin, "Double layer properties at sp and sd Metal Single-Crystal electrodes", in *Modern Aspects of Electrochemistry, vol. 16,* Plenum, New York, **1985**, pp. 1-101.

[114] A. Hamelin, "Cyclic voltammetry at gold single-crystal surfaces: Part 1. Behaviour at low-index faces" *Journal of Electroanalytical Chemistry* **1996**, 407, 1-11.

[115] Q. Q. Xu, U. Linke, R. Bujak and T. Wandlowski, "Preparation and electrochemical characterization of low-index rhodium single crystal electrodes in sulfuric acid" *Electrochimica Acta* **2009**, 54, 5509-5521.

[116] R. Gómez, J. M. Orts, J. M. Feliu, J. Clavilier and L. H. Klein, "The role of surface crystalline heterogeneities in the electrooxidation of carbon monoxide adsorbed on Rh(111) electrodes in sulphuric acid solutions" *Journal of Electroanalytical Chemistry* **1997**, 432, 1-5.

[117] R. Gómez and M. J. Weaver, "Electrochemical Infrared Studies of Monocrystalline Iridium Surfaces Part I: Electrooxidation of Formic-Acid and Methanol" *Journal of Electroanalytical Chemistry* **1997**, 435, 205-215.

[118] R. Gómez and M. J. Weaver, "Electrochemical infrared studies of monocrystalline iridium surfaces. Part 2: Carbon monoxide and nitric oxide adsorption on Ir(110)" *Langmuir* **1998**, 14, 2525-2534.

[119] R. Gómez and M. J. Weaver, "Electrochemical infrared studies of monocrystalline iridium surfaces. 3. Adsorbed nitric oxide and carbon monoxide as probes of Ir(100) interfacial structure" *Journal of Physical Chemistry B* **1998**, 102, 3754-3764.

[120] N. Hoshi, K. Kagaya and Y. Hori, "Voltammograms of the single-crystal electrodes of palladium in aqueous sulfuric acid electrolyte: Pd(S)-[n(111)x(111)] and Pd(S)-[n(100)x(111)]" *Journal of Electroanalytical Chemistry* **2000**, 485, 55-60.

[121] N. Hoshi, M. Kuroda and Y. Hori, "Voltammograms of stepped and kinked stepped surfaces of palladium: Pd(S)-[n(111) x (100)] and Pd(S)-[n(100) x (110)]" *Journal of Electroanalytical Chemistry* **2002**, 521, 155-160.

[122] F. G. Will, "Hydrogen adsorption on platinum single crystal electrodes. I. Isotherms and heats of adsorption" *Journal of the Electrochemical Society* **1965**, 112, 451-455.

[123] A. T. Hubbard, R. M. Ishikawa and J. Katekaru, "Study of platinum electrodes by means of electrochemistry and low energy electron diffraction. 2. Comparison of electrochemical activity of Pt(100) and Pt(111) surfaces" *Journal of Electroanalytical Chemistry* **1978**, 86, 271-288.

[124] E. Yeager, W. E. O'Grady, M. Y. C. Woo and P. Hagans, "Hydrogen adsorption on single-crystal platinum" *Journal of the Electrochemical Society* **1978**, 125, 348-349.

[125] K. Yamamoto, D. M. Kolb, R. Koetz and G. Lehmpfuhl, "Hydrogen adsorption and oxide formation on platinum single crystal electrodes" *Journal of Electroanalytical Chemistry* **1978**, 96, 233-239.

[126] B. Lang, R. W. Joyner and G. A. Somorjai, "Low energy electron diffraction studies of high index crystal surfaces of platinum" *Surface Science* **1972**, 30, 440-453.

[127] C. Korzeniewski, V. Climent and J. M. Feliu, "Electrochemistry at Platinum Single Crystal Electrodes", in *Electroanalytical Chemistry: A Series of Advances, vol. 24*, A. J. Bard and C. Zoski (Eds.) CRC Press, Boca Ratón, **2012**, pp. 75-169.

[128] V. Climent and J. M. Feliu, "Thirty years of platinum single crystal electrochemistry" *Journal of Solid State Electrochemistry* **2011**, 15, 1297-1315.

[129] C. G. M. Hermse, A. P. van Bavel, M. T. M. Koper, J. J. Lukkien, R. A. van Santen and A. P. J. Jansen, "Modelling the butterfly: (√3 x √7) ordering on fcc(111) surfaces" *Surface Science* **2004**, 572, 247-260.

[130] J. M. Feliu, J. M. Orts, R. Gómez, A. Aldaz and J. Clavilier, "New information on the unusual adsorption states of Pt(111) in sulphuric acid solutions from potentiostatic adsorbate replacement by CO" *Journal of Electroanalytical Chemistry* **1994**, 372, 265-268.

[131] J. M. Orts, R. Gómez, J. M. Feliu, A. Aldaz and J. Clavilier, "Potentiostatic charge displacement by exchanging adsorbed species on Pt(111) electrodes—acidic electrolytes with specific anion adsorption" *Electrochimica Acta* **1994**, 39, 1519-1524.

[132] N. García-Aráez, V. Climent, P. Rodríguez and J. M. Feliu, "Thermodynamic analysis of (bi)sulphate adsorption on a Pt(111) electrode as a function of pH" *Electrochimica Acta* **2008**, 53, 6793-6806.

[133] N. García-Aráez, V. Climent, P. Rodríguez and J. M. Feliu, "Elucidation of the Chemical Nature of Adsorbed Species for Pt(111) in H_2SO_4 Solutions by Thermodynamic Analysis" *Langmuir* **2010**, 26, 12408-12417.

[134] A. Wieckowski, E. R. Savinova and C. G. Vayenas, "Catalysis and Electrocatalysis at Nanoparticle Surfaces", Taylor & Francis, **2003**.

[135] M. T. M. Koper, "Fuel Cell Catalysis: A Surface Science Approach", *Electrocatalysis and Electrochemistry* A. Wieckowski (Ed.), John Wiley & Sons, Hoboken, New Jersey, **2009**.

[136] H. S. Liu, C. J. Song, L. Zhang, J. J. Zhang, H. J. Wang and D. P. Wilkinson, "A review of anode catalysis in the direct methanol fuel cell" *Journal of Power Sources* **2006**, 155, 95-110.

[137] S. E. F. Kleijn, S. C. S. Lai, M. T. M. Koper and P. R. Unwin, "Electrochemistry of Nanoparticles" *Angewandte Chemie-International Edition* **2014**, 53, 3558-3586.

[138] R. Van Hardeveld and F. Hartog, "Statistics of surface atoms and surface sites on metal crystals" *Surface Science* **1969**, 15, 189-230.

[139] N. Tian, Z. Y. Zhou and S. G. Sun, "Platinum Metal Catalysts of High-Index Surfaces: From Single-Crystal Planes to Electrochemically Shape-Controlled Nanoparticles" *Journal of Physical Chemistry C* **2008**, 112, 19801-19817.

[140] J. Solla-Gullón, V. Montiel, A. Aldaz and J. Clavilier, "Synthesis and electrochemical decontamination of platinum-palladium nanoparticles prepared by water-in-oil microemulsion" *Journal of the Electrochemical Society* **2003**, 150, E104-E109.

[141] M.-C. Daniel and D. Astruc, "Gold Nanoparticles: Assembly, Supramolecular Chemistry, Quantum-Size-Related Properties, and Applications toward Biology, Catalysis, and Nanotechnology" *Chemical Reviews* **2003**, 104, 293-346.

[142] T. Nagaoka, T. Sakai, K. Ogura and T. Yoshino, "Oxygen Reduction at electrochemically treated glassy-carbon electrodes" *Analytical Chemistry* **1986**, 58, 1953-1955.

[143] M. Boutonnet, J. Kizling, P. Stenius and G. Maire, "The preparation of monodisperse colloidal metal particles from microemulsions" *Colloids and Surfaces* **1982**, 5, 209-225.

[144] T. S. Ahmadi, Z. L. Wang, A. Henglein and M. A. El-Sayed, ""Cubic" colloidal platinum nanoparticles" *Chemistry of Materials* **1996**, 8, 1161-1163.

[145] A. López-Cudero, J. Solla-Gullón, E. Herrero, A. Aldaz and J. M. Feliu, "CO electrooxidation on carbon supported platinum nanoparticles: Effect of aggregation" *Journal of Electroanalytical Chemistry* **2010**, 644, 117-126.

[146] J. Zhang and J. Fang, "A general strategy for preparation of Pt 3d-transition metal (Co, Fe, Ni) nanocubes" *Journal of the American Chemical Society* **2009**, 131, 18543-18547.

[147] D. Li, C. Wang, D. Tripkovic, S. Sun, N. M. Markovic and V. R. Stamenkovic, "Surfactant removal for colloidal nanoparticles from solution synthesis: The effect on catalytic performance" *ACS Catalysis* **2012**, 2, 1358-1362.

[148] S. I. Choi, S. Xie, M. Shao, J. H. Odell, N. Lu, H. C. Peng, L. Protsailo, S. Guerrero, J. Park, X. Xia, J. Wang, M. J. Kim and Y. Xia, "Synthesis and characterization of 9 nm Pt-Ni octahedra with a record high activity of 3.3 A/mg Pt for the oxygen reduction reaction" *Nano Letters* **2013**, 13, 3420-3425.

[149] J. Y. Park, C. Aliaga, J. R. Renzas, H. Lee and G. A. Somorjai, "The Role of Organic Capping Layers of Platinum Nanoparticles in Catalytic Activity of CO Oxidation" *Catalysis Letters* **2009**, 129, 1-6.

[150] J. Clavilier, R. Albalat, R. Gómez, J. M. Orts, J. M. Feliu and A. Aldaz, "Study of the charge displacement at constant potential during CO adsorption on Pt(110) and Pt(111) electrodes in contact with a perchloric acid solution" *Journal of Electroanalytical Chemistry* **1992**, 330, 489-497.

[151] V. Climent, R. Gómez and J. M. Feliu, "Effect of increasing amount of steps on the potential of zero total charge of Pt(111) electrodes" *Electrochimica Acta* **1999**, 45, 629-637.

[152] J. Solla-Gullón, V. Montiel, A. Aldaz and J. Clavilier, "Electrochemical characterization of platinum nanoparticles prepared by microemulsion: How to clean them without loss of crystalline surface structure" *Journal of Electroanalytical Chemistry* **2000**, 491, 69-77.

[153] E. Herrero, L. J. Buller and H. D. Abruña, "Underpotential deposition at single crystal surfaces of Au, Pt, Ag and other materials" *Chemical Reviews* **2001**, 101, 1897-1930.

[154] D. M. Kolb, "Physical and electrochemical properties of metal monolayers on metallic substrates", in *Advances in Electrochemistry and Electrochemical Engineering, vol. 11*, Wiley, New York, **1978**, pp. 125-271.

[155] V. Climent, N. García-Aráez and J. M. Feliu, "Clues for the Molecular-Level Understanding of Electrocatalysis on Single-Crystal Platinum Surfaces Modified by p-Block Adatoms", in *Fuel Cells*

Catalysis. A Surface Science Approach, M. T. M. Koper (Ed.) Wiley, Hoboken, New Jersey, **2009**, pp. 209-244.

[156] J. Clavilier, J. M. Feliu, A. Fernández-Vega and A. Aldaz, "Electrochemical behavior of Irreversibly Adsorbed Bismuth on Pt (100) with Different Degrees of Crystalline Surface Order" *Journal of Electroanalytical Chemistry* **1989**, 269, 175-189.

[157] F. J. Vidal-Iglesias, R. M. Arán-Ais, J. Solla-Gullón, E. Herrero and J. M. Feliu, "Electrochemical Characterization of Shape-Controlled Pt Nanoparticles in Different Supporting Electrolytes" *ACS Catalysis* **2012**, 2, 901-910.

[158] R. M. Arán-Ais, F. J. Vidal-Iglesias, J. Solla-Gullón, E. Herrero and J. M. Feliu, "Electrochemical characterization of clean shape-controlled Pt nanoparticles prepared in presence of oleylamine/oleic acid" *Electroanalysis* **2015**, 27, 945-956.

[159] J. Solla-Gullón, F. J. Vidal-Iglesias, E. Herrero, J. M. Feliu and A. Aldaz, "CO monolayer oxidation on semi-spherical and preferentially oriented (100) and (111) platinum nanoparticles" *Electrochemistry Communications* **2006**, 8, 189-194.

[160] J. Solla-Gullón, F. J. Vidal-Iglesias, A. López-Cudero, E. Garnier, J. M. Feliu and A. Aldaz, "Shape-dependent electrocatalysis: methanol and formic acid electrooxidation on preferentially oriented Pt nanoparticles" *Physical Chemistry Chemical Physics* **2008**, 10, 3689-3698.

[161] Z.-Y. Zhou, Q. Wang, J.-L. Lin, N. Tian and S.-G. Sun, "In situ FTIR spectroscopic studies of electrooxidation of ethanol on Pd electrode in alkaline media" *Electrochimica Acta* **2010**, 55, 7995-7999.

[162] M. López-Atalaya, E. Morallón, F. Cases, J. L. Vázquez and J. M. Pérez, "Electrochemical oxidation of ethanol on Pt(hkl) basal surfaces in NaOH and Na_2CO_3 media" *Journal of Power Sources* **1994**, 52, 109-117.

[163] S. C. S. Lai and M. T. M. Koper, "Ethanol electro-oxidation on platinum in alkaline media" *Physical Chemistry Chemical Physics* **2009**, 11, 10446-10456.

[164] S. Chumillas, C. Busó-Rogero, J. Solla-Gullón, F. J. Vidal-Iglesias, E. Herrero and J. M. Feliu, "Size and diffusion effects on the oxidation of formic acid and ethanol on platinum nanoparticles" *Electrochemistry Communications* **2011**, 13, 1194-1197.

[165] S. P. E. Smith, K. F. Ben-Dor and H. D. Abruña, "Structural effects on the oxidation of HCOOH by bismuth-modified Pt(111) electrodes with (100) monatomic steps" *Langmuir* **1999**, 15, 7325-7332.

[166] F. J. Vidal-Iglesias, A. López-Cudero, J. Solla-Gullón, A. Aldaz and J. M. Feliu, "Pd-Modified Shape-Controlled Pt Nanoparticles Towards Formic Acid Electrooxidation" *Electrocatalysis* **2012**, 3, 313-323.

[167] K. Bergamaski, E. R. Gonzalez and F. C. Nart, "Ethanol oxidation on carbon supported platinum-rhodium bimetallic catalysts" *Electrochimica Acta* **2008**, 53, 4396-4406.

[168] C. Lamy, S. Rousseau, E. M. Belgsir, C. Coutanceau and J. M. Léger, "Recent progress in the direct ethanol fuel cell: development of new platinum-tin electrocatalysts" *Electrochimica Acta* **2004**, 49, 3901-3908.

[169] M. E. Paulino, L. M. S. Nunes, E. R. Gonzalez and G. Tremiliosi-Filho, "In situ FTIR spectroscopic study of ethanol oxidation on Pt(111)/Rh/Sn surface. The anion effect" *Electrochemistry Communications* **2015**, 52, 85-88.

[170] A. O. Neto, R. R. Dias, M. M. Tusi, M. Linardi and E. V. Spinacé, "Electro-oxidation of methanol and ethanol using PtRu/C, PtSn/C and PtSnRu/C electrocatalysts prepared by an alcohol-reduction process" *Journal of Power Sources* **2007**, 166, 87-91.

[171] A. Crown, I. R. Moraes and A. Wieckowski, "Examination of Pt(111)/Ru and Pt(111)/Os surfaces: STM imaging and methanol oxidation activity" *Journal of Electroanalytical Chemistry* **2001**, 500, 333-343.

[172] V. Pacheco Santos and G. Tremiliosi-Filho, "Effect of osmium coverage on platinum single crystals in the ethanol electrooxidation" *Journal of Electroanalytical Chemistry* **2003**, 554–555, 395-405.

[173] Q. G. He, B. Shyam, K. Macounova, P. Krtil, D. Ramaker and S. Mukerjee, "Dramatically Enhanced Cleavage of the C-C Bond Using an Electrocatalytically Coupled Reaction" *Journal of the American Chemical Society* **2012**, 134, 8655-8661.

[174] P. A. Christensen, S. W. M. Jones and A. Hamnett, "An in situ FTIR spectroscopic study of the electrochemical oxidation of ethanol at a Pb-modified polycrystalline Pt electrode immersed in aqueous KOH" *Physical Chemistry Chemical Physics* **2013**, 15, 17268-17276.

Capítulo 2:

Efecto de la estructura superficial y del anión para la oxidación de etanol en nanopartículas de platino

<u>Capítulo 2</u>: Efecto de la estructura superficial y del anión para la oxidación de etanol en nanopartículas de platino

RESUMEN

Este trabajo busca comprobar si el efecto de la estructura superficial y el anión adsorbido en la oxidación de etanol, observados en electrodos monocristalinos de platino, son extrapolables a las nanopartículas de platino con orientación preferencial. Para ello, se analizan en primer lugar los perfiles voltamétricos para la oxidación de 0.2 M CH_3CH_2OH en disoluciones 0.5 M H_2SO_4 y 0.1 M $HClO_4$ en los planos base del platino, siendo el potencial al cual comienza la oxidación de etanol el indicador acerca de cuál es la superficie en la que se produce más CO procedente de la rotura del enlace C-C del etanol. Concretamente, el electrodo Pt(110) y, sobre todo, el Pt(100) se muestran activos para la formación de CO, lo cual concuerda con la histéresis observada entre el barrido positivo y negativo de potenciales después de oxidar el CO a CO_2 a potenciales elevados. Por el contrario, en el electrodo Pt(111) la histéresis es casi nula, mostrando la ausencia significativa de veneno y la preferencia por la ruta de la oxidación incompleta hasta ácido acético.

En cuanto al efecto de la adsorción del anión, se espera que cuando el anión sulfato esté presente en la disolución, las corrientes de oxidación sean menores que al utilizar ácido perclórico como electrolito soporte, debido a que la adsorción competitiva entre el reactivo y los aniones sulfato debe provocar una disminución en la actividad para la oxidación de etanol. Sin embargo, en los electrodos Pt(100) y Pt(110), la actividad es similar en ambos casos, asignándose dicho efecto a la adsorción de aniones acetato sobre platino. Como la adsorción de acetato tiene una fuerza similar a la de los aniones sulfato, esto resulta en corrientes similares en medio perclórico y sulfúrico. Únicamente en el caso del Pt(111), superficie donde la adsorción de los aniones sulfato es más estable debido a la formación de una estructura ordenada asociada a dominios bidimensionales muy extensos, las corrientes son menores empleando H_2SO_4 como electrolito soporte.

Al cambiar a las nanopartículas de platino con orientación preferencial, lo primero que se realiza es la caracterización electroquímica en 0.5 M H_2SO_4 para comprobar las formas predominantes en cada muestra mediante el perfil voltamétrico. Por otra parte, previo al análisis de las curvas, se comprueba que la oxidación de etanol no se ve afectada por problemas de aglomeración de nanopartículas, lo que impediría la correcta difusión del etanol hacia todo el depósito de las nanopartículas de platino. Por ello, se trabaja en todo momento con cantidades bajas de platino (entre 0.05 y 0.1 cm^2 de área superficial activa de Pt) y se comprueba siempre que la corriente de pico de oxidación de etanol es directamente proporcional a la cantidad total de nanopartículas tras realizar varios depósitos sucesivos de platino. Al estudiar la oxidación de etanol con las nanopartículas de platino en las mismas condiciones que en las superficies monocristalinas de platino, se confirman las tendencias observadas en cuanto a las corrientes de oxidación y los potenciales de inicio de la oxidación de etanol observados con los planos basales del platino. Se obtiene que las nanopartículas (100)Pt son más activas para la formación de CO mientras que las muestras (111)Pt favorecen la formación de ácido acético. Además, no se observa efecto relacionado con la adsorción del sulfato en la oxidación de etanol debido a la alta cantidad de ácido acético formado, incluso para las nanopartículas (111)Pt. Esto es debido a que los dominios con orientación cristalográfica {111} en estas muestras son pequeños, provocando que el efecto de la adsorción del sulfato sea menor que en el caso de los electrodos monocristalinos.

Por último, se realizaron experimentos de IR en configuración de reflexión externa para confirmar las suposiciones realizadas a partir de las corrientes de oxidación y del potencial al cual se inicia la oxidación en las voltametrías. Los experimentos se realizaron en una disolución 0.2 M CH_3CH_2OH pero con una menor concentración de electrolito soporte, 0.1 M H_2SO_4, para impedir posibles daños en el prisma de CaF_2. Las bandas detectadas se asignaron de acuerdo con lo establecido en la Tabla 2.1, viéndose claramente las bandas asociadas a la reacción de oxidación de etanol, como son las del CO adsorbido, la de formación de CO_2 y la de producción de acetato. La comparación directa entre los distintos experimentos IR no es sencilla debido a las diferentes condiciones de trabajo del espectrómetro en cada experimento. Por este motivo, la comparación se realiza normalizando las bandas de CO lineal y de CO_2 respecto a una de las bandas del producto ácido acético a 0.9 V. Como era de esperar, las superficies (100)Pt son las más favorables a

la formación de CO, mientras que las superficies (111)Pt son muy inactivas para la rotura del enlace C-C. En cuanto a la oxidación completa hasta CO_2, la muestra que exhibe un mejor comportamiento es la de las nanopartículas (poly)Pt, ya que las muestras (100)Pt presentan un exceso de formación de CO.

Chapter 2

Journal of
Materials Chemistry A

RSC Publishing

PAPER

Surface structure and anion effects in the oxidation of ethanol on platinum nanoparticles

Cite this: *J. Mater. Chem. A*, 2013, **1**, 7068

Carlos Busó-Rogero, Vitali Grozovski, Francisco J. Vidal-Iglesias, José Solla-Gullón, Enrique Herrero* and Juan M. Feliu

Ethanol oxidation on platinum nanoparticles with well-characterized surfaces is studied using cyclic voltammetry and FTIR techniques. Their behavior is compared with that obtained for platinum single crystal electrodes, in order to rationalize their performance and to understand the effects of the surface structure and anion adsorption on the reactivity. The results clearly demonstrate that there are strong effects of anion adsorption and surface structure on the measured current and oxidation mechanism. Thus, the main product of ethanol oxidation on (111) preferentially oriented Pt nanoparticles is acetic acid, and the amount of CO_2 produced can be considered negligible. On the other hand, (100) preferentially oriented Pt nanoparticles are effective for the cleavage of the C–C bond yielding adsorbed CO, which eventually is oxidized to CO_2. This nanoparticles electrode has the highest catalytic activity at high potentials, whereas (111) preferentially oriented Pt nanoparticles are more active at low potentials. In addition, no significant differences in the activity are reported by using different supporting electrolytes, which indicates that adsorbed acetate, which results from the adsorption of acetic acid, hinders ethanol oxidation.

Received 9th March 2013
Accepted 11th April 2013

DOI: 10.1039/c3ta10996h

www.rsc.org/MaterialsA

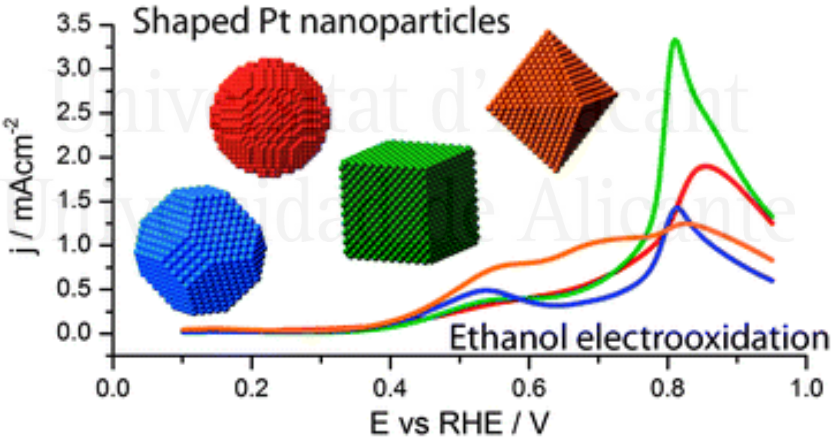

This chapter has been adapted and formatted from Journal of Materials Chemistry A, **2013,** 1, 7068-7076.

Corresponding author: herrero@ua.es

2.1 Introduction

Many electrochemical reactions are structure sensitive, that is to say, depending on how the atoms are arranged at the catalyst surface, the catalytic activity changes. In this way, by studying a given reaction with the different basal planes, the effect of the surface structure can be analyzed and understood. Unfortunately, from an applied point of view, single crystals cannot be used and real catalysts are normally dispersed in the form of nanoparticles. However, the effect of the arrangement of the atoms at the surface is still valid for nanoparticles catalysts, and therefore, the fact that many electrocatalytic reactions are structure sensitive or site demanding [1-6] makes the control over the surface structure of the nanoparticle an issue of paramount importance. In this sense, we have extensively studied the influence of the nanoparticles' surface structure in relevant reactions such as oxygen reduction, or oxidation of different molecules such as carbon monoxide, ammonia, methanol or formic acid [7-15]. However the effect of the surface structure with nanoparticles towards ethanol oxidation still remains unexplored.

Ethanol oxidation has received wide attention because of its possible use in fuel cells, since it can be easily produced from biomass and has a high energy density (12 electrons are exchanged in a complete oxidation to CO_2). However, incomplete oxidation and the high overpotentials required for the reaction reduce its potential applicability. On platinum electrodes, ethanol oxidation occurs in a dual path mechanism [16, 17]:

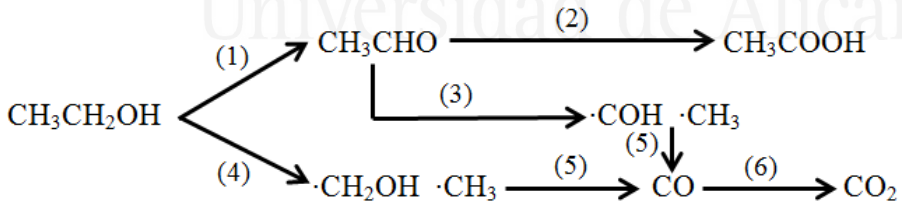

(2.1)

Pathway (1)-(2) shows the incomplete ethanol oxidation to yield first acetaldehyde with two electrons transferred and secondly, acetic acid, transferring two additional electrons. This incomplete oxidation route is not propitious because it yields lower energy density and the formation at the electrode of a stable product (acetic acid) which is very difficult to oxidize to CO_2 [18]. The preferred paths for the oxidation are those leading to the formation of CO_2, which requires the cleavage of the C-C bond. This cleavage can occur either in the ethanol molecule (reaction (4)) or in the acetaldehyde molecule

(reaction (3)) and leads to the formation of different fragments that eventually evolve to form adsorbed CO. By means of IR experiments, the different reaction intermediates and products can be identified. Due to the strong adsorbing properties of CO on platinum and the large overpotential required for its oxidation, it has been considered as a poison by some authors [19-21]. However, it can be argued that CO is not a poisoning specie but a true active intermediate, the formation of which is required for the complete oxidation of the molecule to CO_2 [16, 22, 23]. With the aim of achieving the complete oxidation of ethanol, by facilitating the cleavage of the C-C bond and the oxidation of adsorbed CO, different strategies have been used. Thus, different adatoms such as Ru, Sn or Rh have been used to decorate the platinum surface of the catalyst [24-29]. In addition, a further improvement of the activity can be obtained with the use of ternary catalysts [30-34].

Regarding the importance of the surface structure, it is well known that the ethanol oxidation mechanism depends on this parameter. The low reactivity of the Pt(100) electrode in the positive going scan at lower potentials is mainly a consequence of CO adsorption on the electrode surface. On the other hand, CO formation on the Pt(111) electrode is almost negligible being acetaldehyde and acetic acid the main products of its oxidation. Finally, Pt(110) has an intermediate behavior between that of Pt(100) and Pt(111). Additionally, the presence of adsorbed anions can decrease current densities due to a competitive adsorption of anions and reactants [19].

In the present paper, we report the influence of the surface structure/shape of well characterized bare Pt nanoparticles on ethanol electrooxidation reaction. The aim is to establish links between the activity reported for well-defined surface structures (basal planes) and that of preferentially oriented Pt nanoparticles. In addition, we also study the effect of anion adsorption on ethanol oxidation.

2.2 Experimental

Platinum single crystal electrode surfaces were prepared from small single crystal beads, *ca.* 2 mm in diameter following the method developed by Clavilier *et al.* [35]. Before any experiment, working electrodes were annealed for around 30 s in a gas-oxygen flame, cooled down in a reductive atmosphere (H_2 + Ar) and quenched in ultrapure water in equilibrium with this atmosphere [36]. Then, the electrodes were transferred to a cell under the protection of a droplet of deoxygenated water for further characterization.

Four different types of nanoparticles were used. The synthetic details of the different Pt nanoparticles as well as the characterization of their shape and particle size distribution have been previously reported [7, 11, 12, 37-39]. In brief, the quasi spherical polyoriented nanoparticles, denoted as (poly)Pt, were synthesized by the water-in-oil microemulsion method [40, 41] (water (3%) / polyethylene glycol dodecyl ether (Brij®30) (16.5%) / n-heptane (80.5%)), using sodium borohydride as the reducing agent. The concentration of H_2PtCl_6 in the water phase was 0.1 M. Reduction was performed by directly adding $NaBH_4$ (10 times the stoichiometric amount) to the micellar solution. After reduction was complete, nanoparticles were cleaned using acetone and ultrapure water [41]. With this cleaning procedure, nanoparticles were cleaned while the initial surface structure of the nanoparticles remained.

On the other hand, the terms (100)Pt, (111)Pt and (100)-(111)Pt nanoparticles correspond to the samples prepared using a colloidal method [37, 42]. These nanoparticles have a preferential surface orientation, for which the predominant ordered domain at surface corresponds to {100}, {111} and a mixture of {100} and {111} domains, respectively. For their synthesis 0.5 ml of 0.1 M sodium polyacrylate solution (M_w = 2100) was added to 100 ml of an aged 10^{-4} M solution containing the desired Pt precursor. As the Pt source, K_2PtCl_4 was employed for the synthesis of (100)Pt nanoparticles, whereas H_2PtCl_6 was used for the (100)-(111)Pt and (111)Pt nanoparticles. The concentration ratio of K_2PtCl_4 or H_2PtCl_6 to polyacrylate was 1:5. In addition, in the case of (100)-(111)Pt and (111)Pt nanoparticles, the pH of the solution was adjusted to 7 with 0.1 M HCl, whereas in the case of (100)Pt the pH was not adjusted. Finally, the solutions were purged with Ar for 20 min and Pt ions were reduced by bubbling H_2 for 5 min, except in the case of (111)Pt

where only 5 min of Ar bubbling and 1 min of H_2 bubbling were used. Then, the reaction vessel was sealed and the solution was left overnight. Once reduction was complete (12–14 h) two NaOH pellets were added to produce the precipitation of the nanoparticles. After complete precipitation, the nanoparticles were washed 3–4 times with ultrapure water. The predominant size of the nanoparticles was 4 nm for the (poly)Pt and 8-10 nm for the colloidal nanoparticles.

The Pt nanoparticles electrodes were prepared by depositing the dispersed Pt nanoparticles on a hemispherical polycrystalline gold substrate (*ca.* 3 mm^2) from a solution droplet ranging from 0.5 to 1.5 µL and drying under Ar atmosphere. The procedures used for the electrochemical cleaning of the different Pt nanoparticles have been described previously [37, 40, 41]. They involve, in the final step, a CO adsorption and stripping treatment, a process that does not perturb significantly the platinum surface order.

Voltammetric curves were first recorded in a 0.5 M H_2SO_4 or 0.1 M $HClO_4$ solution, in order to measure the active surface area of the Pt nanoparticles. The charge involved in the hydrogen and anion adsorption/desorption region, after the subtraction of apparent double layer contribution, was used assuming that the charge density for this region is 230 µC cm^{-2} in sulfuric acid solution and 200 µC cm^{-2} in perchloric acid solution [43]. Depending on the supporting electrolyte used, experiments for ethanol oxidation were carried out in 0.5 M H_2SO_4 + 0.2 M CH_3CH_2OH or in 0.1 M $HClO_4$ + 0.2 M CH_3CH_2OH.

Spectroelectrochemical experiments were performed with a Nicolet Magna 850 spectrometer equipped with a narrow-band mercury cadmium telluride (MCT) detector. The spectroelectrochemical cell had a prismatic CaF_2 window beveled at 60º [44, 45]. The IR spectra were collected with p-polarized light with a resolution of 8 cm^{-1}. For each spectrum, 100 interferograms were added to increase the signal-to-noise ratio. The spectra are presented as the value $(R_1-R_2)/R_1$, where R_2 and R_1 are the reflectance values corresponding to the single beam spectra recorded at the sample and reference potentials, respectively. The reference spectrum was acquired at 0.1 V whereas the sample spectra were recorded after applying successive potential steps of 100 mV in the positive direction from 0.1 to 0.9 V *vs.* the reversible hydrogen electrode (RHE). Positive bands in the spectra correspond to species that have been formed at the sampling potential (or with an

increase in concentration) whereas negatives bands are associated with a diminution of the concentration of the species. The experimental protocol for performing FTIR experiments with the Pt nanoparticle electrodes was identical to that used in the voltammetric experiments.

All experiments were carried out at room temperature in a typical three-electrode electrochemical cell. A gold wire was used as a counter-electrode and a reversible hydrogen (N50, Air Liquide) electrode (RHE) was used as a reference. Solutions were prepared from sulfuric acid (Merck 95-97% GR for analysis), perchloric acid (Merck 60% for analysis), ethanol (Merck p.a.) and ultra-pure water (Elga-Purelab Ultra 18.2 MΩ cm). Argon (N50, Air Liquide) was used for deoxygenating all the solutions and CO (N47, Air Liquide) for the aforementioned final cleaning step of the nanoparticles.

2.3 Results and discussion

2.3.1 Ethanol oxidation on single crystal electrodes

The voltammetric profiles of ethanol oxidation for Pt single crystal electrodes are presented in Fig. 2.1, using sulfuric acid and perchloric acid as a supporting electrolytes in the same concentration that will be used for the voltammetric experiments with platinum nanoparticles. The upper limit potential has thoughtfully been adjusted to 0.95 V to avoid significant changes in the surface structure of the electrodes due to oxide formation and its subsequent reduction while allowing the removal of all the CO adsorbed on the surface. In the presence of ethanol, the voltammetric profiles are stable, with only minor changes in the oxidation currents upon cycling, mainly in the positive going scan. For that reason, the first cycle is reported in the figure. In general, CO is formed at low potentials in the positive going scan as a result of the cleavage of the C-C bond of the ethanol molecule [46]. The adsorption of CO blocks the surface and causes a low activity for the ethanol oxidation at low potentials. At higher potentials (above 0.7 V), CO is oxidized and the surface regains its activity for the oxidation of ethanol. For the Pt(100) electrode, this behavior is very clear, since the current below 0.7 V in the positive going scan is negligible and a sharp increase is observed at 0.7 V.

On the other hand, the Pt(111) electrode shows the opposite behavior. Currents in the positive and negative going scans are very similar, due to the very low CO formation rate on this surface. In fact, the CO formation on Pt(111) has been linked to the presence of defects [20, 46]. Finally, the Pt(110) electrode shows an intermediate behavior between that of Pt(111) and Pt(100) regarding the amount of CO formed. Taking into account the currents measured at low potentials, *i.e.*, below 0.5 V, the trend observed for the activity of the electrodes is the following: Pt(100) < Pt(110) < Pt(111). However, when maximum currents are taken into account the order becomes Pt(111) < Pt(110) < Pt(100), as has been reported in the past [47]. Regarding the final product in the oxidation process, acetic acid is the major product for the three basal planes [19]. However, the yield of CO_2 is the highest for the Pt(100) while the Pt(111) electrode produces acetic acid almost exclusively.

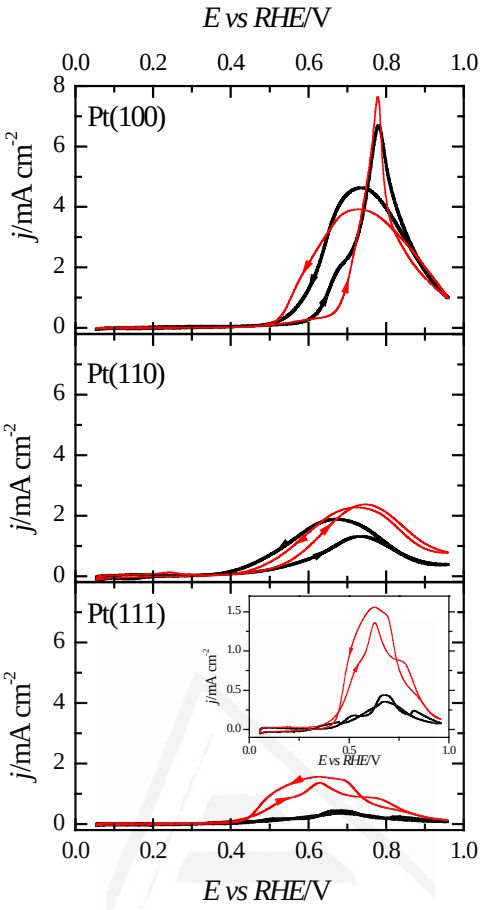

Fig. 2.1. Voltammetric profiles for ethanol oxidation (1st cycle) on Pt(100), Pt(110) and Pt(111) electrodes in 0.5 M H_2SO_4 + 0.2 CH_3CH_2OH (black line) and 0.1 M $HClO_4$ + 0.2 M CH_3CH_2OH (red line). Sweep rate: 50 mV s^{-1}.

The effect of the sulfate anion adsorption in the voltammetric profile is also shown in Fig. 2.1. In general, it is expected that currents in perchloric acid solutions are higher than those measured in sulfuric acid solutions, owing to the specific adsorption of sulfate. This is mainly due to a competitive adsorption of the reactant and sulfate anions at the surface of the electrode. However, previous results comparing 0.1 M H_2SO_4 and 0.1 M $HClO_4$ showed similar currents in both media [19]. Previous contributions ascribed this lower than expected activity in perchloric acid to the adsorption of acetate [19, 48]. In fact, when the comparison is made between 0.1 M $HClO_4$ and 0.5 M H_2SO_4 (Fig. 2.1), similar current densities are also obtained for the Pt(110) and Pt(100) electrodes, which indicates that the higher sulfate concentration in comparison with that of the previous contribution [19] has no major effect in the currents for those electrodes.

On the other hand, the currents in sulfuric acid for the Pt(111) electrode are significantly lower than those in 0.1 M $HClO_4$ or 0.1 M H_2SO_4, which implies a significant effect of the sulfate concentration for this electrode. It should be borne in mind that the adsorption of sulfate on the Pt(111) electrode is significantly stronger than that on the Pt(100) electrode [49] and that sulfate forms an ordered adlayer. The stronger sulfate adsorption and the increase in stability of the adlayer, due to the formation of the ordered structure, results in a significant effect of the anion on the oxidation currents. Similar effects have been observed, for example, for oxygen reduction [50]. In the absence of such an ordered adlayer, it would be expected that the currents in sulfuric and perchloric acid were similar, as for the other studied electrodes. In short, the formation of acetic acid, which adsorbs as acetate on the electrode surface above 0.3-0.4 V, implies that the electrode surface at the potentials where ethanol oxidation takes place is always covered with a layer of adsorbed anions. In perchloric acid solutions, the adsorbed adlayer is made of acetate anions, whereas in sulfuric acid, the adlayer is formed by a mixture of acetate and sulfate anions. In this way, ethanol always competes with an adlayer of the similar strength, regardless of the supporting electrolyte (sulfuric or perchloric acid) and then, oxidation currents are similar.

2.3.2 Electrochemical characterization of Pt nanoparticles

Fig. 2.2 shows the voltammetric profiles of the different nanoparticles in 0.5 M sulfuric acid solution. A detailed analysis of the relationship between the voltammetric profile and the surface structure of the nanoparticles has been carried out previously [37, 39]. A brief summary of the main characteristics is reported here. A typical polycrystalline platinum electrode presents two main peaks at 0.125 and 0.265 V. The peak at 0.125 V is linked to the presence of {110} sites, whereas that at 0.265 is due to the presence of {100} defects on {111} domains and {100} short domains. This typical shape is observed for the (poly)Pt sample (Fig. 2.2A), which has no preferential orientation on the surface.

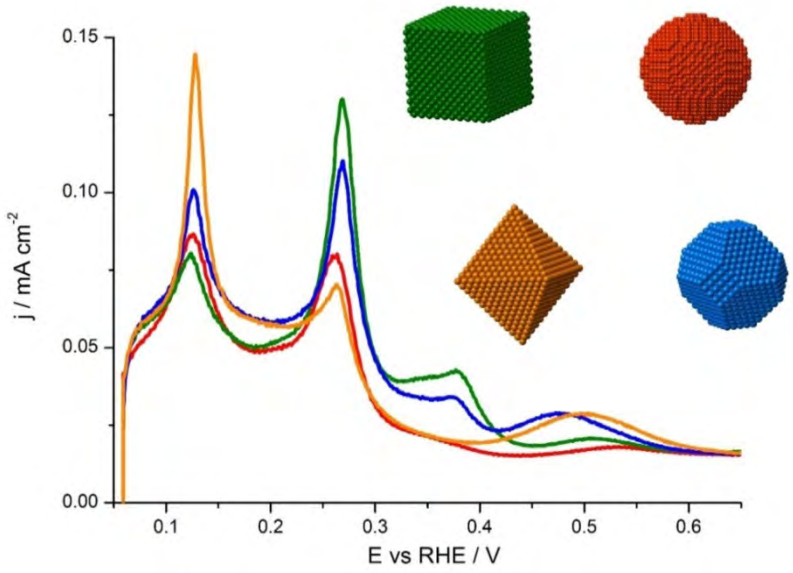

Fig. 2.2. Cyclic voltammetry for the (poly)Pt (red line), (100)Pt (green line), (100)-(111)Pt (blue line) and (111)Pt (orange line) nanoparticles used in this work in 0.5 M H_2SO_4. Scan rate: 50 mV s^{-1}.

When the surface structure presents a preferential orientation, additional features in the voltammogram can be observed. Large {100} ordered domains give rise to a peak at 0.37 V, as it is observed for (100)-(111)Pt and specially for the (100)Pt nanoparticles. Besides, adsorption of sulfate on {111} ordered domains gives rise to a wide signal around 0.5 V, which can be observed on the (111)Pt and on the (100)-(111)Pt nanoparticles. In addition, voltammetric peaks are sharp and reversible, showing the cleanliness of the nanoparticles' surface and indicating that chemicals from the synthesis process have been successfully removed. A similar analysis can also be made in $HClO_4$ (results not shown), although as it is known the adsorption desorption peaks are not as well resolved as in sulfuric acid. Different voltammetric profiles can also be obtained from the distinct shape of the nanoparticles [39, 43].

2.3.3 Ethanol oxidation on Pt nanoparticles.

Previous studies have demonstrated that the electrocatalytic results measured for a given nanoparticle sample can be erroneously interpreted depending on the nanoparticle

loading [51]. Large loadings may display a lower electrocatalytic activity than that expected. In this situation, a large amount of the reactant arriving from the solution to the electrode is consumed in the outermost part of the nanoparticle deposit, so that the inner part remains inactive (or nearly) due to the lack of reactants. However, when the active area is measured using the hydrogen adsorption/desorption process by cyclic voltammetry, those diffusion problems are negligible and therefore the whole sample contributes to the total area. Under these circumstances, the calculation of the current density uses an incorrect area, because part of the measured area is not taking part in the reaction. As a result, the reported current densities for the studied reaction are, erroneously, significantly lower than those that would have been obtained in absence of diffusion problems through the nanoparticle deposit, and possible catalytic enhancements can remain hidden because of this situation [51].

Thus, if the electrocatalytic activity of the nanoparticles has to be assessed, the experiments have to be designed in such a way that there are no diffusion problems in the nanoparticles deposit. In order to check it, the active surface area of a deposit was determined in a sulfuric acid solution and the current for ethanol oxidation was measured. After that, a second deposit was made on top of the first one, and the active area and currents for ethanol oxidation were once again measured.

For the experimental conditions used in this work, it was found that the current for ethanol oxidation was directly proportional to the active area of the electrode (Fig. 2.3), that is to say, the current density for ethanol oxidation is the same for the two different nanoparticles loadings. This proportionality ensures, while working for areas below that of the second deposit, the correct calculation of the current densities for ethanol oxidation experiments. This proportionality was obtained for the different samples used in this study in order to be sure of working inside the limits to obtain correct current density values. In addition, it should be mentioned that this proportionality disappears when larger deposits are made.

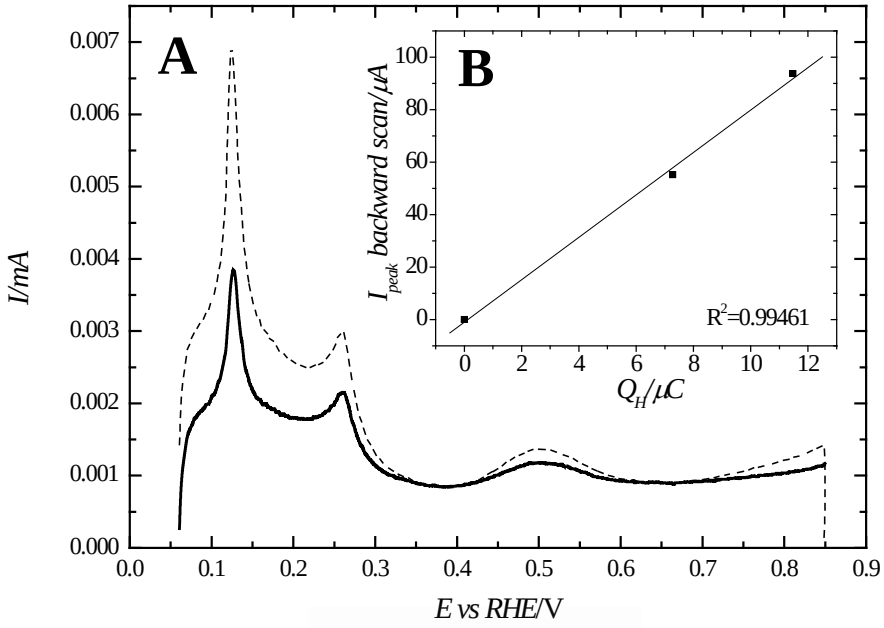

Fig. 2.3. (A) Voltammograms corresponding to two successive deposits of (111)Pt nanoparticles in H_2SO_4. Sweep rate: 50 mV s^{-1}. (B) Ethanol oxidation peak current plot *vs* hydrogen charge plot.

The voltammetric profiles for ethanol oxidation (first cycle) for the different types of Pt nanoparticles in 0.2 M CH_3CH_2OH both in 0.5 M H_2SO_4 and 0.1 M $HClO_4$ are shown in Fig. 2.4. As aforementioned, the upper potential limit was set at 0.95 V in order to avoid structural modifications due to oxide formation/reduction cycles. In all cases, the voltammetric profiles show an oxidation peak at 0.8-0.85 V in the positive going scan and higher oxidation currents in the negative going scan. For the (100)Pt nanoparticles, a prominent peak in the positive going scan at 0.8-0.85 V is obtained and is associated with the oxidation of the CO layer formed from the cleavage of the C-C bond at low potentials and the re-activation of the surface for the oxidation of ethanol [19], in a similar way to that observed for the Pt(100) single crystal in Fig. 2.1. This type of contribution is absent in the other two basal planes. Therefore, the peak observed for the nanoparticles at this potential is then clearly related to the presence of {100} domains on the nanoparticles. As expected, the current density is maximum for the (100)Pt nanoparticles, whereas (111)Pt nanoparticles, which have a very low amount of {100} ordered domains on the surface, show the lowest current density in this potential region. In addition, (poly)Pt and (100-111)Pt nanoparticles, which have an intermediate amount of {100} ordered domains, have intermediate current values in this potential region.

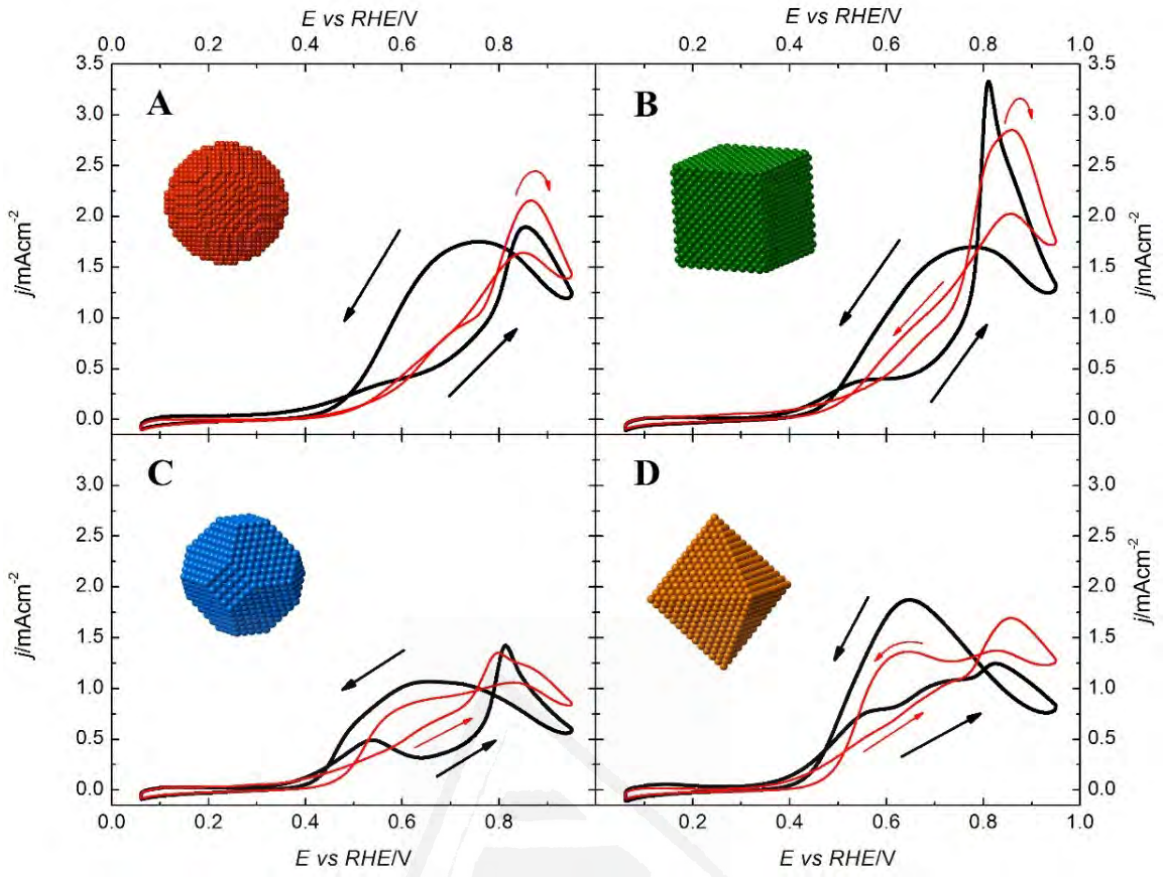

Fig. 2.4. Ethanol oxidation (1st cycle) on (A) (poly)Pt, (B) (100)Pt, (C) (100)-(111)Pt and (D) (111)Pt nanoparticles in 0.5 M H_2SO_4 + 0.2 M CH_3CH_2OH (black line) and 0.1 M $HClO_4$ + 0.2 M CH_3CH_2OH (red line). Sweep rate: 50 mV s^{-1}.

Another trend observed for the platinum basal planes which is also replicated by the nanoparticles is the dependence of the onset potential for the oxidation of ethanol with the surface structure. In this sense, Pt(111) shows the lowest value, and the difference in the currents between the negative and positive-going scans is also the lowest for this basal plane. In this way, current densities for nanoparticles electrodes at 0.4 V, in the positive-going sweep, are 109.8, 76.8, 125.5 and 139.6 μA cm^{-2} corresponding to (poly), (100), (100)-(111) and (111)Pt nanoparticles respectively. As it is observed, the higher the amount of (111) sites, the higher the current density recorded at this potential. The lower current density is evidently obtained for the (100)Pt nanoparticles, as the {100} sites are, as formerly explained, covered by CO. As in the previous case, this contribution can give qualitative information about the amount of {111} sites at the nanoparticles surface.

In order to get insight into the role played by the competitive adsorption of sulfate anions in ethanol oxidation with Pt nanoparticles, the same voltammetric experiments were repeated with the same ethanol concentration but in 0.1 M $HClO_4$. The resulting voltammograms are compared to those obtained in sulfuric acid solutions in Fig. 2.4. The results agree with the experiments performed by Colmati *et al.* [19], where the adsorption of anions has nearly no effect on the oxidation reaction. This fact implies that the amount of acetic acid formed is significantly high, so that acetate can adsorb on the surface and compete with ethanol for the adsorption sites. It is worth mentioning that the currents measured for the (111)Pt nanoparticles in 0.1 M $HClO_4$ and in 0.5 M H_2SO_4 are almost identical, unlike the behavior observed for the Pt(111) electrode. As previously mentioned, the difference arises from the fact that sulfate on very long range ordered {111} domains forms an ordered structure, which increases the stability of the adlayer [52, 53], and significantly diminishes the currents for the oxidation of ethanol and other organic molecules on the Pt(111) electrode. Nevertheless, such order structure is not observed for small {111} domains [52], such as those present on the surface of the nanoparticles and, thus, currents in both media are similar.

2.3.4 FTIR experiments of ethanol oxidation.

With the aim of determining the final products of the ethanol oxidation reaction and their relative ratio, FTIR experiments were carried out. In this case, 0.1 M H_2SO_4 solution was used as the supporting electrolyte as because of higher acid concentrations can damage the prism. Despite the different anion concentration, no differences in the results are expected due to the effective insensitivity of the oxidation currents to the presence of perchlorate or sulfate anions in the solution. On the other hand, the ethanol concentration was the same as in the previous experiments. Table 2.1 summarizes the frequencies of the observed bands in the different spectra and the vibrational modes of the molecules associated with these bands [18, 20, 54].

υ_{H2O}/cm^{-1}	Functional group	Mode
2340	CO_2	O-C-O asymmetric stretching
2030-2070	Adsorbed CO	Linearly bonded
1715	COOH or CHO	C=O stretching
1400	Adsorbed $-COO^-$	C-O symmetric stretching
1280	COOH	Coupling C-O stretching + OH deformation
1210	Adsorbed (bi)sulfate	

Table 2.1. Observed IR frequencies in the spectra for ethanol oxidation in H_2O.

Fig. 2.5 and 2.6 show the IR spectra for the ethanol oxidation reaction on the different platinum nanoparticles. In general, there are no qualitative differences in the spectra for the different nanoparticles. The small band around 2050 cm^{-1}, which is clearly observed above 0.3 V, indicates the presence of adsorbed linear CO. This band grows as the potential increases up to *ca.* 0.7 V, where CO is oxidized and then bands at 2340 cm^{-1}, corresponding to the formation of CO_2, start to appear. At 0.9 V, the band corresponding to CO is negative, in particular for the (100)Pt nanoparticles, demonstrating that adsorbed linear CO is present at the reference potential, that is, at 0.1 V. The presence of adsorbed CO at 0.1 V shows that the cleavage of the C-C bond of the ethanol molecule takes place at low potentials, as in the case of single crystal electrodes [46]. At potentials above the onset of oxidation of CO to CO_2, the bands associated with the formation of acetic acid are clearly visible at 1400 and 1280 cm^{-1}. Although no bands can be observed due to the presence of acetaldehyde, its formation cannot be discarded. It should be highlighted that bands associated with acetaldehyde are less intense and appear in the same frequency region as those corresponding to acetic acid, and for that reason, are difficult to resolve. Additionally, the band corresponding to the stretching of the C=O group at 1715 cm^{-1} is

masked by the changes in the band corresponding to the bending modes of water at *ca.* 1650 cm^1.

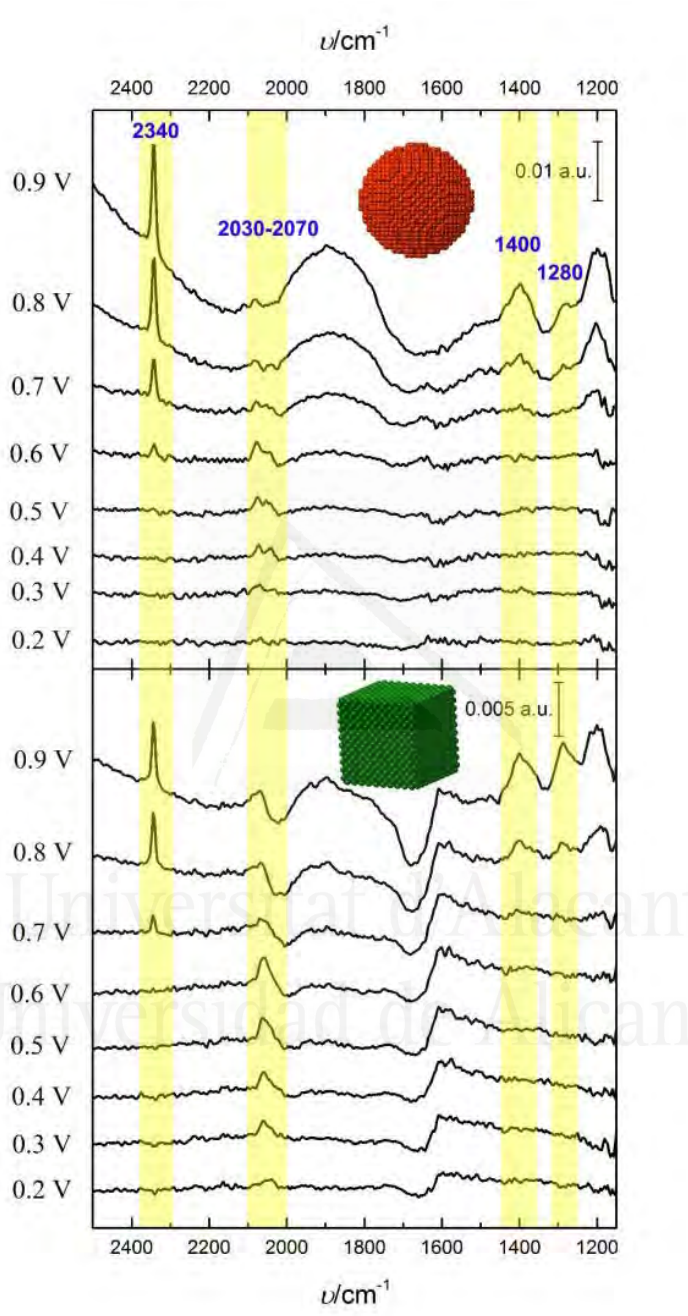

Fig. 2.5. SPAIR spectra obtained in 0.1 M H_2SO_4 + 0.2 M CH_3CH_2OH for the (poly)Pt (top) and (100)Pt (bottom) nanoparticles.

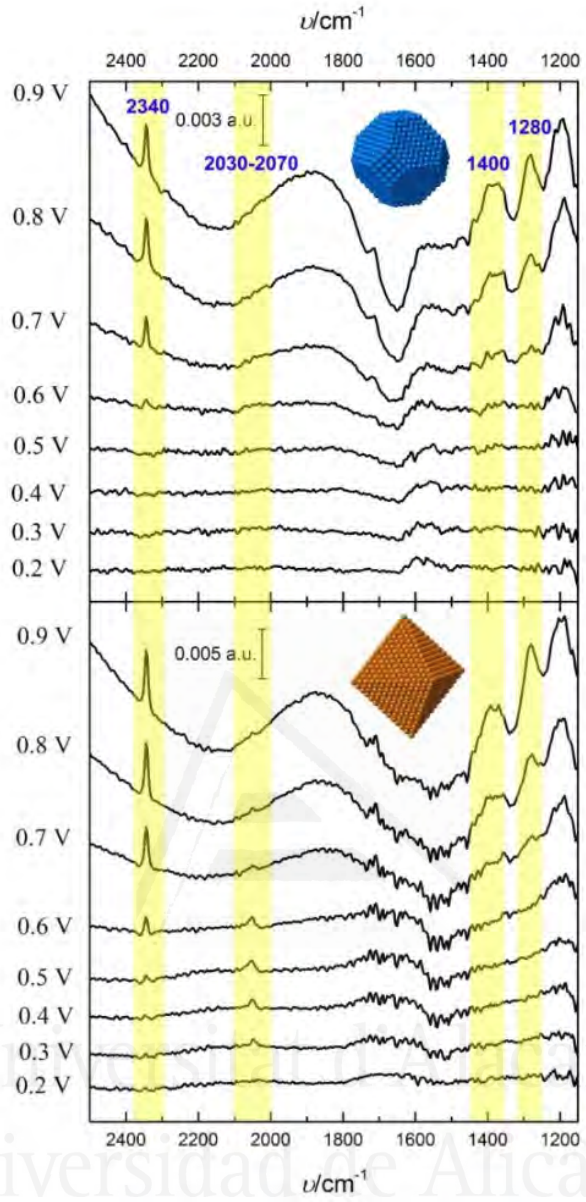

Fig. 2.6. SPAIR spectra obtained in 0.1 M H_2SO_4 + 0.2 M CH_3CH_2OH for the (100)-(111)Pt (top) and (111)Pt (bottom) nanoparticles.

In order to observe differences between the different nanoparticles, a quantitative analysis should be made, using the integrated intensity of each band. However, the absolute intensity for the bands depends on two experimental parameters that cannot be easily controlled. The same electrode can yield different band intensities depending on the thin layer gap between the electrode and the window and on the exact nanoparticle concentration in the spot where the IR beam hits the sample. Although the absolute intensity bands cannot be used, the relative band intensity can always be used, because all

the bands are affected in the same way by the experimental conditions. In this case, the integrated intensity band at 1400 cm^{-1} at 0.9 V, which corresponds to acetic acid, the main product of the reaction, has been used to normalize the other adsorption bands. In addition, for the CO bands, because of the presence of CO at the reference potential, spectra were recalculated so that the reference spectrum for this signal is that taken at 0.90 V. At this potential value, the CO band in Fig. 2.5 and Fig. 2.6 is always negative, indicating that adsorbed CO is probably no longer on the electrode surface.

Fig. 2.7 shows the ratio of the normalized integrated bands of CO and CO_2 with respect to that of acetic acid. As can be seen these ratios are strongly dependent on the used nanoparticles, revealing that the final product distribution is very sensitive to the arrangement of the atoms at the nanoparticles surface. First, concerning the relative amount of CO (Fig. 2.7A), two different trends can be observed. On the one hand, the nanoparticles having a large ratio of {111} domains, that is, (111)Pt and (100)-(111)Pt show a very low CO formation at low potentials. This fact means that the rate of cleavage of the C-C bond is very low, which is a typical behavior of the single crystal electrodes with {111} terraces. In fact, it has been reported that for those electrodes, the formation of CO occurs on the defects or steps [20, 25, 55], so that this process would not occur on a perfect (defect-free) Pt(111) electrode.

On the other hand, the most active basal plane for the formation of CO is the Pt(100) electrode. Thus, the nanoparticles having a large fraction of {100} sites display the largest activity for the cleavage of the C-C bond at low potentials. For the (poly)Pt nanoparticles, although they do not have a large fraction of ordered domains, they possess a large fraction of low coordinated atoms on the surface. This type of sites is also effective to cleave the C-C bond, and a significant amount of adsorbed CO is obtained. For these two nanoparticle samples, the amount of CO is almost constant between 0.1 and 0.5 V (the onset potential of CO oxidation) which implies that the cleavage of the C-C bond has occurred at low potentials and adsorbed CO blocks the surface almost completely.

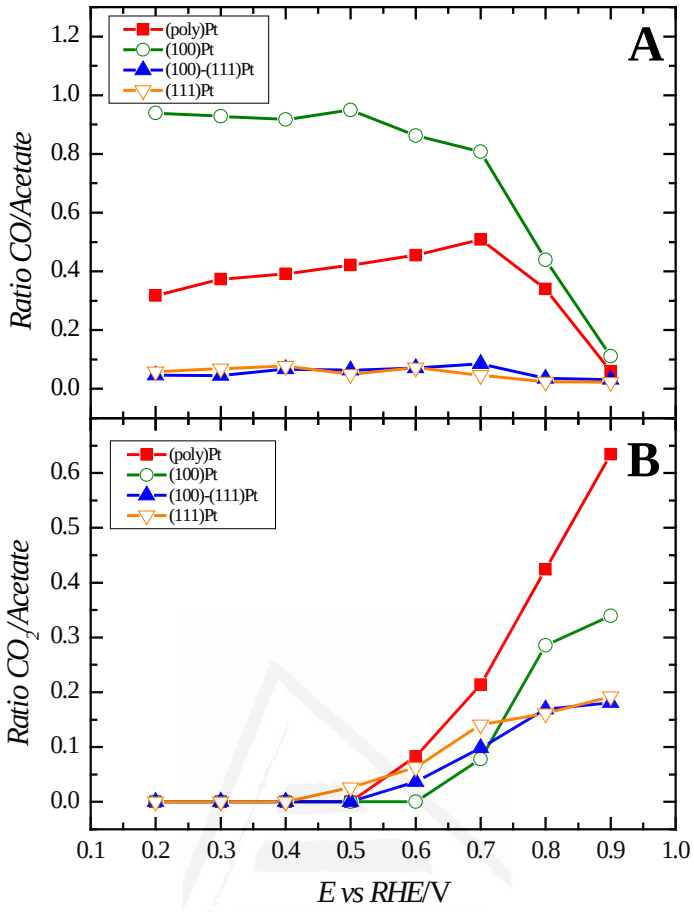

Fig. 2.7. Ratio between integrated intensity of the bands for (A) CO at 2030-2070 cm^{-1} and (B) CO_2 at 2340 cm^{-1} at different potentials and the integrated intensity for acetate at 1400 cm^{-1} at 0.9 V.

A similar situation is observed for CO_2 formation. CO_2 is detected above 0.6-0.7 V, which is the onset potential of CO oxidation. For the (100)Pt nanoparticles, the onset is the highest of all the samples, probably as a consequence of the formation of a CO layer with a higher coverage. From that point, the amount of CO_2 increases with the potential, a clear indication that the cleavage of the C-C bond is taking place at those potentials. Above 0.6 V, the cleavage of the ethanol C-C bond produces two adsorbed CO molecules that can be readily oxidized. Thus, the actual CO coverage on the surface at those potentials depends on the relative ratio of the rates for CO formation and CO oxidation. In this particular situation, (poly)Pt nanoparticles are the most active for CO_2 production. Although the (100)Pt nanoparticles are clearly more active for the cleavage of the C-C bond, the large CO coverage formed on the platinum nanoparticles surface makes its oxidation more difficult. Thus, the nanoparticles with an intermediate activity for the C-C bond cleavage

are those having the highest activity for CO_2 production. In this case, nanoparticles are active for breaking the C-C bond, but the activity is not very high so that dense CO layers are not formed and as a result the oxidation of CO to CO_2 is easier. On the other hand, nanoparticles with a large fraction of {111} sites produce a low amount of CO_2.

2.4 Conclusions

Ethanol oxidation has been studied on polyoriented and (100), (111) and (100)-(111) preferentially oriented Pt nanoparticles using electrochemical and IR experiments. The results point out that the surface structure of nanoparticles plays an important role in the reactivity, and that the activity of the nanoparticles can be predicted from the results obtained for the single crystal electrodes, which can be taken as model surfaces. In addition, the electrocatalytic properties are directly related to the surface structure/shape of the nanoparticles. In all the platinum nanoparticles samples, the incomplete oxidation of ethanol to acetaldehyde/acetic acid and the cleavage of the C-C bond to form CO and finally its complete oxidation to CO_2 are observed. However, the ratio of both paths is different for the different catalysts. On the one hand, nanoparticles with a large fraction of {111} domains form acetic acid almost exclusively. On the other hand, (100)-rich Pt nanoparticles are the best choice for the splitting of the C-C bond. Thus, polyoriented platinum nanoparticles, which have an intermediate behavior between the (100)Pt and the (111)Pt nanoparticles, show the highest activity for CO_2 production.

Finally, it should be highlighted that, as previously stated in the Introduction section, the ethanol electrooxidation activity can be modulated if a surface modifier such as Ru or Sn is added onto the surface of the nanoparticles. So far, however, the used Pt nanoparticles have not been preferentially oriented. In this sense, we have previously shown that the use of adatom decorated shape-controlled Pt nanoparticles is a very relevant approach to enhance the electrocatalytic properties of the bare samples [56-58]. We are currently working on this approach towards ethanol electrooxidation electrocatalysis and the results obtained will be reported in forthcoming contributions.

2.5 References

[1] R. R. Adzic, "Reaction kinetics and Mechanism on Metal Single Crystal Electrode surfaces", in *Modern aspects of electrochemistry, vol. 21*, R. E. White, J. O. M. Bockris and B. E. Conway (Eds.) Plenum Press, New York, **1990**, pp. 163-236.

[2] N. M. Markovic and P. N. Ross, "Electrocatalysis at Well-Defined Surfaces: Kinetics of Oxygen Reduction and Hydrogen Oxidation/Evolution on Pt(hkl) Electrodes", in *Interfacial Electrochemistry: Theory, Experiments and Applications*, A. Wieckowski (Ed.) Marcel Dekker, New York, **1998**, pp. 821-842.

[3] N. M. Markovic and P. N. Ross, "Surface science studies of model fuel cell electrocatalysts" *Surface Science Reports* **2002**, 45, 117-229.

[4] S. Sriramulu, T. D. Javi and E. M. Stuve, "Kinetic Modeling of Electrocatalytic Reactions: Methanol Oxidation on Platinum Electrodes", in *Interfacial Electrochemistry: Theory, Experiments and Applications*, A. Wieckowski (Ed.) Marcel Dekker, New York, **1998**, pp. 793-804.

[5] E. Herrero, J. M. Feliu and A. Aldaz, "Electrocatalysis", in *Encyclopedia of Electrochemistry - Interfacial Kinetics and Mass Transport, vol. 2*, A. J. Bard and M. Stratmann (Eds.) Wiley, Weinheim, Germany, **2003**, pp. 443-465.

[6] M. T. M. Koper, R. A. van Santen and M. Neurock, "Theory and Modeling of Catalytic and Electrocatalytic Reactions", in *Catalysis and Electrocatalysis at Nanoparticle Surfaces*, A. Wieckowski, E. R. Savinova and C. G. Vayenas (Eds.) Marcel Dekker, New York, **2003**, pp. 1-34.

[7] F. J. Vidal-Iglesias, J. Solla-Gullón, P. Rodríguez, E. Herrero, V. Montiel, J. M. Feliu and A. Aldaz, "Shape-dependent electrocatalysis: ammonia oxidation on platinum nanoparticles with preferential (100) surfaces" *Electrochemistry Communications* **2004**, 6, 1080-1084.

[8] J. Hernández, J. Solla-Gullón and E. Herrero, "Gold nanoparticles synthesized in a water-in-oil microemulsion: electrochemical characterization and effect of the surface structure on the oxygen reduction reaction" *Journal of Electroanalytical Chemistry* **2004**, 574, 185-196.

[9] J. Hernández, J. Solla-Gullón, E. Herrero, A. Aldaz and J. M. Feliu, "Characterization of the surface structure of gold nanoparticles and nanorods using structure sensitive reactions" *Journal of Physical Chemistry B* **2005**, 109, 12651-12654.

[10] J. Hernández, J. Solla-Gullón, E. Herrero, A. Aldaz and J. M. Feliu, "Electrochemistry of shape-controlled catalysts: Oxygen reduction reaction on cubic gold nanoparticles" *Journal of Physical Chemistry C* **2007**, 111, 14078-14083.

[11] J. Solla-Gullón, F. J. Vidal-Iglesias, E. Herrero, J. M. Feliu and A. Aldaz, "CO monolayer oxidation on semi-spherical and preferentially oriented (100) and (111) platinum nanoparticles" *Electrochemistry Communications* **2006**, 8, 189-194.

[12] J. Solla-Gullón, F. J. Vidal-Iglesias, A. López-Cudero, E. Garnier, J. M. Feliu and A. Aldaz, "Shape-dependent electrocatalysis: methanol and formic acid electrooxidation on preferentially oriented Pt nanoparticles" *Physical Chemistry Chemical Physics* **2008**, 10, 3689-3698.

[13] V. Grozovski, J. Solla-Gullón, V. Climent, E. Herrero and J. M. Feliu, "Formic Acid Oxidation on Shape-Controlled Pt Nanoparticles Studied by Pulsed Voltammetry" *Journal of Physical Chemistry C* **2010**, 114, 13802-13812.

[14] J. Solla-Gullón, F. J. Vidal-Iglesias and J. M. Feliu, "Shape dependent electrocatalysis" *Annual Reports on the Progress of Chemistry, Section C: Physical Chemistry* **2011**, 107, 263-297.

[15] Q. S. Chen, F. J. Vidal-Iglesias, J. Solla-Gullón, S. G. Sun and J. M. Feliu, "Role of surface defect sites: From Pt model surfaces to shape-controlled nanoparticles" *Chemical Science* **2012**, 3, 136-147.

[16] T. Iwasita and E. Pastor, "A DEMS and FTIR spectroscopic investigation of adsorbed ethanol on polycrystalline platinum" *Electrochimica Acta* **1994**, 39, 531-537.

[17] J. W. Shin, W. J. Tornquist, C. Korzeniewski and C. S. Hoaglund, "Elementary steps in the oxidation and dissociative chemisorption of ethanol on smooth and stepped surface planes of platinum electrodes" *Surface Science* **1996**, 364, 122-130.

[18] A. Rodes, E. Pastor and T. Iwasita, "An FTIR Study on the Adsorption of Acetate at the Basal Planes of Platinum Single-Crystal Electrodes" *Journal of Electroanalytical Chemistry* **1994**, 376, 109-118.

[19] F. Colmati, G. Tremiliosi-Filho, E. R. Gonzalez, A. Berná, E. Herrero and J. M. Feliu, "Surface structure effects on the electrochemical oxidation of ethanol on platinum single crystal electrodes" *Faraday Discussions* **2008**, 140, 379-397.

[20] F. Colmati, G. Tremiliosi-Filho, E. R. Gonzalez, A. Berná, E. Herrero and J. M. Feliu, "The role of the steps in the cleavage of the C-C bond during ethanol oxidation on platinum electrodes" *Physical Chemistry Chemical Physics* **2009**, 11, 9114-9123.

[21] G. A. Camara and T. Iwasita, "Parallel pathways of ethanol oxidation: The effect of ethanol concentration" *Journal of Electroanalytical Chemistry* **2005**, 578, 315-321.

[22] S. C. S. Lai, S. E. F. Kleyn, V. Rosca and M. T. M. Koper, "Mechanism of the Dissociation and Electrooxidation of Ethanol and Acetaldehyde on Platinum As Studied by SERS" *Journal of Physical Chemistry C* **2008**, 112, 19080-19087.

[23] J. F. E. Gootzen, W. Visscher and J. A. R. van Veen, "Characterization of ethanol and 1,2-ethanediol adsorbates on platinize d platinum with Fourier transform infrared spectroscopy and differential electrochemical mass spectrometry" *Langmuir* **1996**, 12, 5076-5082.

[24] G. A. Camara, R. B. de Lima and T. Iwasita, "Catalysis of ethanol electro oxidation by PtRu: the influence of catalyst composition" *Electrochemistry Communications* **2004**, 6, 812-815.

[25] V. Del Colle, A. Berná, G. Tremiliosi-Filho, E. Herrero and J. M. Feliu, "Ethanol electrooxidation onto stepped surfaces modified by Ru deposition: electrochemical and spectroscopic studies" *Physical Chemistry Chemical Physics* **2008**, 10, 3766-3773.

[26] C. Lamy, S. Rousseau, E. M. Belgsir, C. Coutanceau and J. M. Léger, "Recent progress in the direct ethanol fuel cell: development of new platinum-tin electrocatalysts" *Electrochimica Acta* **2004**, 49, 3901-3908.

[27] Q. W. Zheng, C. H. Fan, C. H. Zhen, Z. Y. Zhou and S. G. Sun, "Irreversible adsorption of Sn adatoms on basal planes of Pt single crystal and its impact on electrooxidation of ethanol" *Electrochimica Acta* **2008**, 53, 6081-6088.

[28] W. J. Zhou, S. Q. Song, W. Z. Li, Z. H. Zhou, G. Q. Sun, Q. Xin, S. Douvartzides and P. Tsiakaras, "Direct ethanol fuel cells based on PtSn anodes: the effect of Sn content on the fuel cell performance" *Journal of Power Sources* **2005**, 140, 50-58.

[29] J. P. I. de Souza, S. L. Queiroz, K. Bergamaski, E. R. Gonzalez and F. C. Nart, "Electro-oxidation of ethanol on Pt, Rh, and PtRh electrodes. A study using DEMS and in-situ FTIR techniques" *Journal of Physical Chemistry B* **2002**, 106, 9825-9830.

[30] A. Kowal, M. Li, M. Shao, K. Sasaki, M. B. Vukmirovic, J. Zhang, N. S. Marinkovic, P. Liu, A. I. Frenkel and R. R. Adzic, "Ternary Pt/Rh/SnO_2 electrocatalysts for oxidizing ethanol to CO_2" *Nature Materials* **2009**, 8, 325-330.

[31] W. P. Zhou, M. Li, C. Koenigsmann, C. Ma, S. S. Wong and R. R. Adzic, "Morphology-dependent activity of Pt nanocatalysts for ethanol oxidation in acidic media: Nanowires versus nanoparticles" *Electrochimica Acta* **2011**, 56, 9824-9830.

[32] J. Barroso, A. R. Pierna, T. C. Blanco, E. Morallón and F. Huerta, "Homolytic cleavage C-C bond in the electrooxidation of ethanol and bioethanol" *Journal of Power Sources* **2011**, 196, 4193-4199.

[33] C. Z. Zhu, S. J. Guo and S. J. Dong, "PdM (M = Pt, Au) Bimetallic Alloy Nanowires with Enhanced Electrocatalytic Activity for Electro-oxidation of Small Molecules" *Advanced Materials* **2012**, 24, 2326-2331.

[34] J. M. Sieben and M. M. E. Duarte, "Nanostructured Pt and Pt-Sn catalysts supported on oxidized carbon nanotubes for ethanol and ethylene glycol electro-oxidation" *International Journal of Hydrogen Energy* **2011**, 36, 3313-3321.

[35] J. Clavilier, D. Armand, S. G. Sun and M. Petit, "Electrochemical adsorption behaviour of platinum stepped surfaces in sulphuric acid solutions" *Journal of Electroanalytical Chemistry* **1986**, 205, 267-277.

[36] J. Clavilier, K. El Achi, M. Petit, A. Rodes and M. A. Zamakhchari, "Electrochemical Monitoring of the Thermal Reordering of Platinum Single-Crystal Surfaces after Metallographic Polishing from the Early Stage to the Equilibrium Surfaces" *Journal of Electroanalytical Chemistry* **1990**, 295, 333-356.

[37] J. Solla-Gullón, P. Rodríguez, E. Herrero, A. Aldaz and J. M. Feliu, "Surface characterization of platinum electrodes" *Physical Chemistry Chemical Physics* **2008**, 10, 1359-1373.

[38] A. López-Cudero, F. J. Vidal-Iglesias, J. Solla-Gullón, E. Herrero, A. Aldaz and J. M. Feliu, "Formic acid electrooxidation on Bi-modified polyoriented and preferential (111) Pt nanoparticles" *Physical Chemistry Chemical Physics* **2009**, 11, 416-424.

[39] F. J. Vidal-Iglesias, R. M. Arán-Ais, J. Solla-Gullón, E. Herrero and J. M. Feliu, "Electrochemical Characterization of Shape-Controlled Pt Nanoparticles in Different Supporting Electrolytes" *ACS Catalysis* **2012**, 2, 901-910.

[40] J. Solla-Gullón, V. Montiel, A. Aldaz and J. Clavilier, "Electrochemical characterization of platinum nanoparticles prepared by microemulsion: How to clean them without loss of crystalline surface structure" *Journal of Electroanalytical Chemistry* **2000**, 491, 69-77.

[41] J. Solla-Gullón, V. Montiel, A. Aldaz and J. Clavilier, "Synthesis and electrochemical decontamination of platinum-palladium nanoparticles prepared by water-in-oil microemulsion" *Journal of the Electrochemical Society* **2003**, 150, E104-E109.

[42] T. S. Ahmadi, Z. L. Wang, T. C. Green, A. Henglein and M. A. El-Sayed, "Shape-controlled synthesis of colloidal platinum nanoparticles" *Science* **1996**, 272, 1924-1926.

[43] Q. S. Chen, J. Solla-Gullón, S. G. Sun and J. M. Feliu, "The potential of zero total charge of Pt nanoparticles and polycrystalline electrodes with different surface structure: The role of anion adsorption in fundamental electrocatalysis" *Electrochimica Acta* **2010**, 55, 7982-7994.

[44] T. Iwasita, F. C. Nart and W. Vielstich, "An FTIR study of the catalytic activity of a 85:15 Pt:Ru alloy for methanol oxidation" *Berichte der Bunsen-Gesellschaft fuer Physikalische Chemie* **1990**, 94, 1030-1034.

[45] A. Rodes, J. M. Pérez and A. Aldaz, "Vibrational spectroscopy", in *Handbook of Fuel Cells - Fundamentals, Technology and Applications, vol. 2*, W. Vielstich, A. Lamm and H. A. Gasteiger (Eds.) Wiley, Chichester, **2003**, pp. 191-219.

[46] J. Souza-Garcia, E. Herrero and J. M. Feliu, "Breaking the C-C Bond in the Ethanol Oxidation Reaction on Platinum Electrodes: Effect of Steps and Ruthenium Adatoms" *ChemPhysChem* **2010**, 11, 1391-1394.

[47] M. C. Morin, C. Lamy, J. M. Léger, J. L. Vázquez and A. Aldaz, "Structural effects in electrocatalysis: Oxidation of ethanol on platinum single crystal electrodes. Effect of pH" *Journal of Electroanalytical Chemistry* **1990**, 283, 287-302.

[48] M. J. Prieto and G. Tremiliosi-Filho, "The influence of acetic acid on the ethanol electrooxidation on a platinum electrode" *Electrochemistry Communications* **2011**, 13, 527-529.

[49] M. E. Gamboa-Aldeco, E. Herrero, P. S. Zelenay and A. Wieckowski, "Adsorption of Bisulfate Anion on a Pt(100) Electrode - a Comparison with Pt(111) and Pt(Poly)" *Journal of Electroanalytical Chemistry* **1993**, 348, 451-457.

[50] M. D. Maciá, J. M. Campiña, E. Herrero and J. M. Feliu, "On the kinetics of oxygen reduction on platinum stepped surfaces in acidic media" *Journal of Electroanalytical Chemistry* **2004**, 564, 141-150.

[51] S. Chumillas, C. Busó-Rogero, J. Solla-Gullón, F. J. Vidal-Iglesias, E. Herrero and J. M. Feliu, "Size and diffusion effects on the oxidation of formic acid and ethanol on platinum nanoparticles" *Electrochemistry Communications* **2011**, 13, 1194-1197.

[52] J. Mostany, E. Herrero, J. M. Feliu and J. Lipkowski, "Thermodynamic studies of anion adsorption at stepped platinum(hkl) electrode surfaces in sulfuric acid solutions" *Journal of Physical Chemistry B* **2002**, 106, 12787-12796.

[53] E. Herrero, J. Mostany, J. M. Feliu and J. Lipkowski, "Thermodynamic studies of anion adsorption at the Pt(111) electrode surface in sulfuric acid solutions" *Journal of Electroanalytical Chemistry* **2002**, 534, 79-89.

[54] X. H. Xia, H. D. Liess and T. Iwasita, "Early stages in the oxidation of ethanol at low index single crystal platinum electrodes" *Journal of Electroanalytical Chemistry* **1997**, 437, 233-240.

[55] V. Del Colle, J. Souza-Garcia, G. Tremiliosi-Filho, E. Herrero and J. M. Feliu, "Electrochemical and spectroscopic studies of ethanol oxidation on Pt stepped surfaces modified by tin adatoms" *Physical Chemistry Chemical Physics* **2011**, 13, 12163-12172.

[56] F. J. Vidal-Iglesias, J. Solla-Gullón, E. Herrero, A. Aldaz and J. M. Feliu, "Pd Adatom Decorated (100) Preferentially Oriented Pt Nanoparticles for Formic Acid Electrooxidation" *Angewandte Chemie-International Edition* **2010**, 49, 6998-7001.

[57] F. J. Vidal-Iglesias, A. López-Cudero, J. Solla-Gullón and J. M. Feliu, "Towards More Active and Stable Electrocatalysts for Formic Acid Electrooxidation: Antimony-Decorated Octahedral Platinum Nanoparticles" *Angewandte Chemie-International Edition* **2013**, 52, 964-967.

[58] Q. S. Chen, Z. Y. Zhou, F. J. Vidal-Iglesias, J. Solla-Gullón, J. M. Feliu and S. G. Sun, "Significantly Enhancing Catalytic Activity of Tetrahexahedral Pt Nanocrystals by Bi Adatom Decoration" *Journal of the American Chemical Society* **2011**, 133, 12930-12933.

Capítulo 3:

Oxidación de etanol en nanopartículas de platino con forma controlada a diferentes pHs: estudio combinado de espectroscopía IR in situ y espectrometría de masas en línea

<u>Capítulo 3</u>: Oxidación de etanol en nanopartículas de platino con forma controlada a diferentes pHs: estudio combinado de espectroscopía IR *in situ* y espectrometría de masas en línea

RESUMEN

El cambio del pH en el electrolito soporte modifica la reactividad del etanol sobre las superficies de platino, alterando la proporción de ácido acético/acetato formado respecto al CO/CO_2 producido tras su oxidación. En este capítulo, se aborda el efecto del pH sobre dos superficies diferentes, concretamente las dos muestras principales que muestran más diferencias entre sí de los casos estudiados en el capítulo 2, las nanopartículas (100)Pt y las nanopartículas (111)Pt. La investigación se realizará a valores de pH ácidos menores a 4, ya que a valores superiores, el CO_2 comienza a reaccionar para dar carbonato, lo que impide su correcta cuantificación por DEMS. Además, en todo momento se utiliza una concentración 0.5 M SO_4^{2-} de electrolito soporte para minimizar la adsorción del anión acetato. El estudio se lleva a cabo con la combinación de las técnicas ATR y DEMS, permitiendo a la vez un seguimiento espectroscópico de las especies formadas, junto a información cuantitativa de las mismas especies con la espectrometría de masas en el caso de que los productos sean gases volátiles. En este capítulo, la concentración de etanol es en todo momento 0.05 M, menor de lo habitual, para evitar problemas de saturación en la membrana del DEMS.

Después de la caracterización electroquímica, se registran los perfiles voltamétricos para la oxidación de etanol en las dos muestras de nanopartículas empleadas. En ambas muestras se observan corrientes despreciables a potenciales bajos e histéresis entre el ciclo positivo y negativo del barrido de potenciales, características presentes cuando hay envenenamiento por formación de CO. Al aumentar el pH la histéresis disminuye, probablemente debido a la menor formación de CO, a pesar de que las corrientes obtenidas

difieren dependiendo de la muestra empleada: en la muestra (100)Pt la corriente de pico se mantiene, indicando que a pesar de la menor cantidad de veneno producida, la actividad total en la oxidación de etanol se conserva. En cambio, en la muestra (111)Pt, las corrientes y la forma de la voltametría cíclica varían totalmente, revelando un posible cambio en cuanto al mecanismo de reacción en los sitios {111}, lo cual se tratará de explicar con experimentos DEMS.

A continuación se inicia el estudio espectroscópico con los experimentos de ATR obtenidos a 0.4 V para las dos muestras estudiadas y a diferentes pHs, usando como referencia el espectro a 0.9 V. En todos los casos, la banda observada entre 2030 y 2070 cm^{-1} se corresponde con la adsorción del CO lineal sobre las nanopartículas de platino, observándose una pequeña disminución de la banda al aumentar el pH, confirmando la menor formación de CO. A diferencia de los espectros del capítulo 2, la banda asociada a la adsorción de acetato no se observa en este caso, ya que los experimentos son realizados en configuración de célula de flujo, que elimina el ácido acético formado en las proximidades del electrodo de trabajo, impidiendo su adsorción sobre la superficie de platino.

En cuanto a los experimentos DEMS, se comparan en primer lugar las corrientes de espectrometría de masas junto a las corrientes faradaicas correspondientes a una velocidad de barrido de 5 mVs^{-1}. Las corrientes de masas registradas en esta primera tanda de experimentos son la m/z=29 y la m/z=44. La corriente de m/z=44 presenta contribuciones del acetaldehído (CH_3CHO^+) y del CO_2, mientras que la corriente m/z=29 solamente se debe a la contribución del acetaldehído (CHO^+). A partir de estas corrientes, y siguiendo las Ec. (3.2), y (3.3), se obtiene la corriente faradaica producto de la formación de CO_2. La forma de esta corriente es similar a la de la oxidación de una monocapa de CO, esto es, a potenciales de 0.7 V la corriente empieza a crecer debido a la oxidación del CO hasta CO_2. Además, en el barrido negativo de potenciales, la ausencia de corriente indica que la rotura del enlace C-C sólo sucede a bajos potenciales, demostrando que toda la corriente de oxidación de etanol en el barrido negativo se debe a la formación de acetaldehído/ácido acético. La Fig. 3.7 muestra las eficiencias de formación de CO_2 para un valor de pH de 0.3 para las dos muestras estudiadas, de acuerdo con la Ec. (3.4). Comparando los resultados, queda claro que las nanopartículas (100)Pt tienen una mayor eficiencia para la

formación de CO_2 que las nanopartículas (111)Pt (10% vs 5%). Fijándose en el potencial al cual se obtiene la máxima eficiencia, en ambos casos el valor está sobre 0.65 V, más pequeño que el potencial de pico que muestran las curvas de corriente faradaica de CO_2. Esto es debido a la competición entre el proceso de oxidación incompleta de etanol hasta acetaldehído/acético y el de la oxidación del CO adsorbido.

A partir de los resultados previos y como era de esperar, se corrobora que la rotura del enlace C-C es la clave para la oxidación completa del etanol. Con el objetivo de conocer los fragmentos adsorbidos en el electrodo tras la oxidación de etanol, se realizan unos experimentos conocidos como 'stripping' de etanol para las diferentes muestras de nanopartículas de platino. El experimento consiste en hacer pasar por la célula de flujo a 0.4 V la disolución de etanol y luego registrar la corriente cuando se realiza un barrido de potenciales a 5 mVs^{-1} en la disolución sin etanol. Los resultados se muestran en la Fig. 3.8 y la Fig. 3.9. Las voltametrías cíclicas de los apartados a) de ambas figuras muestran la corriente faradaica, cuyo pico a altos potenciales se corresponde con la oxidación del CO (formado a 0.4 V) a CO_2. Resultados de la bibliografía muestran que la rotura de la molécula produce siempre 2 fragmentos. El fragmento CH_2OH evoluciona de forma casi instantánea para dar CO adsorbido, mientras que el CH_x no reacciona de forma rápida con la superficie. Los apartados b) y c) muestran las corrientes de espectrometría de masa para m/z=15, con la reducción de los fragmentos CH_x a CH_4 a bajos potenciales, y para m/z=44, con la oxidación del CO a CO_2.

Los resultados son bastante diferentes, dependiendo de la muestra. Las nanopartículas (100)Pt muestran una cantidad creciente del fragmento CH_x formado a bajos potenciales conforme avanza el pH, como demuestra el aumento de la cantidad de CH_4 registrada, mientras que la formación de CO se mantiene constante, como indican las corrientes de espectrometría de masa m/z=44 del apartado c) en la Fig. 3.8. En cambio, para las nanopartículas (111)Pt de la Fig. 3.9, las cantidades de CH_4 y CO_2 disminuyen con el pH. Este comportamiento se puede explicar por la distinta evolución de las reacciones de rotura del enlace C-C y de reducción de los fragmentos de CH_x a CH_4. Para las nanopartículas (100)Pt, la velocidad de rotura del enlace C-C es elevada, y aunque disminuye con el pH, es capaz de saturar la superficie con CO durante el tiempo de contacto a 0.4 V con la disolución de etanol. De esta forma, la cantidad de CO_2 medida tras

la oxidación se mantiene constante. Sin embargo, el proceso de reducción del fragmento de CH_x se ve favorecido al aumentar el pH, lo que lleva a mayores cantidades de CH_4. Por otra parte, para las nanopartículas de (111)Pt, la rotura del enlace C-C es mucho menos eficiente y en el tiempo de la experiencia nunca se llega a saturar la superficie con CO. De esta forma, al aumentar el pH disminuye la velocidad de rotura del enlace C-C, lo que lleva a menores cantidades de CO_2 y CH_4 detectadas.

Chapter 3

Journal of Electroanalytical Chemistry 763 (2016) 116–124

Contents lists available at ScienceDirect

Journal of Electroanalytical Chemistry

journal homepage: www.elsevier.com/locate/jelechem

Ethanol oxidation on shape-controlled platinum nanoparticles at different pHs: A combined in situ IR spectroscopy and online mass spectrometry study

Carlos Busó-Rogero [a], Sylvain Brimaud [b], Jose Solla-Gullon [a], Francisco J. Vidal-Iglesias [a], Enrique Herrero [a,*], R. Jürgen Behm [b], Juan M. Feliu [a]

[a] Instituto de Electroquímica, Universidad de Alicante, Apartado 99, E-03080 Alicante, Spain
[b] Institut für Oberflächenchemie und Katalyse, Universität Ulm, Albert-Einstein-Allee 47, D-89081 Ulm, Germany

ARTICLE INFO

Article history:
Received 3 October 2015
Received in revised form 19 December 2015
Accepted 22 December 2015
Available online 29 December 2015

Keywords:
Ethanol oxidation
pH effect
Platinum
Nanoparticles
DEMS

ABSTRACT

Ethanol oxidation on different shape-controlled platinum nanoparticles at different pHs was studied using electrochemical, Attenuated Total Reflection-Fourier Transform Infrared Spectroscopy (ATR-FTIR) and, especially, Differential Electrochemical Mass Spectrometry (DEMS) techniques, the latter giving interesting quantitative information about the products of ethanol oxidation. Two Pt nanoparticle samples were used for this purpose: (100) and (111) preferentially oriented Pt nanoparticles. The results are in agreement with previous findings that the preferred decomposition product depends on surface structure, with CO_{ads} formation on (100) domains and acetaldehyde/acetic acid formation on (111) domains. However, new information has been obtained about the changes in CH_x and CO formation at lower potentials when the pH is changed, showing that CH_x formation is favored against the decrease in CO adsorption on (100) domains. At higher potentials, complete oxidation to CO_2 occurs from both CH_x and CO fragments. In (111) Pt nanoparticles, the splitting of C—C bond is hindered, favoring acetaldehyde and acetate formation even in 0.5 M H_2SO_4. C1 fragments become even less when the pH increases, being nearly negligible in the highest pH studied.

This chapter has been adapted and formatted from Journal of Electroanalytical Chemistry **2016,** 763, 116-124.

Corresponding author: herrero@ua.es

3.1 Introduction

During the last years, the search for new energy sources has been intensified due to the depletion of fossil fuels. In this sense, fuel cell technology has gained momentum for obtaining electric energy from the oxidation of a chemical fuel [1]. In the quest for possible new fuels, several options have been considered and particularly the oxidation of some small organic molecules such as formic acid, methanol or ethanol has been extensively evaluated. The oxidation of these molecules normally requires the use of platinum as catalyst [2-4]. Among these fuels, ethanol presents some relevant advantages to other fuels as i) it can be obtained directly from biomass and ii) it does not present problems for its storage. Unfortunately, and despite its high density energy for the complete oxidation to CO_2, with 12 electrons exchanged, problems dealing with a classical CO poisoning as well as to an incomplete oxidation to undesired products such as acetic acid, limit its potentialities for practical purposes.

Ethanol oxidation is also known to be a surface structure sensitive reaction, that is, the resulting catalytic activity depends on the particular/specific arrangement of the surface atoms. This surface structure sensitivity has been clearly evidenced by the use of Pt single crystal electrodes [5-7]. However, single crystal electrodes are ideal model surfaces which cannot be used in real electrocatalytic systems. For this reason, these results have to be extended to nanoparticles, which can be effectively applied to such systems. As previously demonstrated, the effect of the particular arrangement of the atoms at the surface on the resulting ethanol oxidation activity is valid also for nanoparticles [8], thus highlighting the importance of gaining control of the surface structure of the nanoparticles to increase their electrocatalytic activity. Similar results on the effect of the surface structure of the nanoparticles for other important reactions such as oxygen reduction or other small organic molecule oxidations have been already reported [9-15]. In this sense, it is also worth noting that these shape/surface structure controlled Pt nanoparticles are usually about 8-10 nm in size which, from a practical point of view, may be insufficient to fulfill the requirement of a high surface-to-volume ratio for practical applications.

From a mechanistic point of view, it is known that, in acidic solutions the reaction occurs via a complex reaction network. Scheme (3.1) illustrates a simplified mechanism

where some additional steps such as desorption and re-adsorption of acetaldehyde have not been included for the sake of clarity.

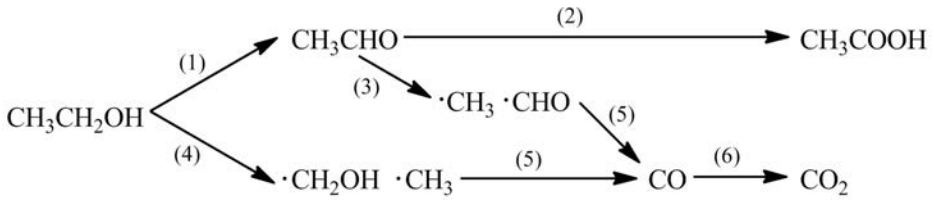

(3.1)

Reaction steps (1) and (2) give rise to the incomplete oxidation of ethanol, forming acetaldehyde and acetic acid as final products. To obtain this latter product, which is very difficult to oxidize, only four electrons are exchanged, thus wasting 2/3 of the formal energy density for ethanol. On Pt(111) electrodes and at room temperature, the reaction only takes places almost exclusively through this undesirable route [5]. On the other hand, the splitting of the C-C bond occurs in steps (3) and (4), which produce different carbon fragments that are subsequently transformed to CO_{ads} (step (5)) [5]. Finally, in step (6), CO_{ads} is oxidized to CO_2, thus completing the 12 electron exchange route. This reaction route presents two difficult steps, i) the splitting of the C-C bond and ii) the oxidation of adsorbed CO. Pt(110) and especially Pt(100) electrodes favor the C-C bond scission, but suffer from surface poisoning. The enhancement of the C-C bond breaking rate needs to be accompanied by a higher rate for CO_{ads} oxidation to avoid poisoning. In fact, the stronger the metal-adsorbate bond, the more C-C bond breaking is favored, while CO_{ads} oxidation is disfavored. This is likely to result in a Sabatier type behavior with an optimum bond strength. In order to overcome this CO_{ads} poisoning problem, the incorporation of different foreign atoms has been used to facilitate CO_{ads} oxidation to CO_2 [16-18]. In addition, the breakage of C-C bond is known to be improved on Pt surfaces containing {100} and {110} steps on {111} terraces [6, 19]. Consequently, a combination of these two approaches, that is, using stepped Pt electrodes and foreign adatoms, gave rise to significant improvements in the oxidation reaction [20-22].

On the other hand, the research of alkaline fuel cells (AFC) has currently grown due to the higher activity obtained at these pHs and also due to the their less corrosive properties, which favor the use of cheaper catalysts. In fact, the problems resulting from the carbonation of the system due to CO_2 retention as well as from the limited number of membranes capable of operating over long periods of time in alkaline media seem to be

solved with the development of new anion-exchange membranes [23, 24]. According to fundamental studies performed in alkaline solutions [7, 25, 26], acetate is presented as the main product for ethanol oxidation regardless the surface structure of the Pt electrode, with negligible amounts of CO_{ads} being formed. Consequently, a better understanding of the changes in the oxidation mechanism as a function of the pH and in particular, how the ratio between the products (incomplete oxidation to acetate or complete oxidation towards CO_2) is modified for increasing pHs, would be of utmost interest.

To access this information, we have performed a combined *in situ* infrared (IR) spectroscopy and online mass spectrometry study on different shape controlled Pt nanoparticles of the ethanol oxidation reaction (EOR) at different pHs. These experiments will be performed under well-defined mass transport conditions and with control of the surface structure, in contrast to infrared reflection-absorption spectroscopy (IRRAS) measurements, where by-product accumulation, e.g. adsorbed acetate, is common. Such experimental conditions are more convenient for mechanistic investigations. On the other hand, it is also worth noting that only pHs lower than 4 have been explored in order to avoid problems due to carbonate formation. This combined approach allows us to not only perform a quantitative analysis of the volatile products formed during the reaction and to calculate the efficiencies for the complete oxidation to CO_2, but also to follow the nature and potential window in which the adsorbed intermediate species are formed during the reaction.

3.2 Experimental

Two different kinds of Pt nanoparticles were used in this work. They were both synthesized using a colloidal method [27, 28], and displayed preferential {100} or {111} surface orientations. These nanoparticles were denoted as (100)Pt nanoparticles and (111)Pt nanoparticles, depending on their dominant surface structure. Experimental details about the synthesis, also including Transmission Electron Microscopy (TEM) characterization to determine their particle size and characterize their preferential shape, were previously described [29]. Very briefly, the predominant shape was cubic for (100)Pt nanoparticles and octahedral for (111)Pt ones. The particle size of both nanoparticle batches was estimated to be about 8-10 nm. The electrodes were prepared by depositing a droplet (4 μL) of the aqueous solution containing the nanoparticles on a hemispherical gold substrate, after which the electrode was protected under an Ar stream until complete solvent evaporation. Before the measurements, Pt nanoparticles were carefully cleaned by CO adsorption and subsequent stripping at potentials below 0.95 V to preserve the surface structure of the samples. The electrochemically active area of Pt nanoparticles was measured using the charge involved in the so-called hydrogen/anion adsorption/desorption region (between 0.05 V and 0.6 V) from the cyclic voltammograms recorded in 0.5 M H_2SO_4, assuming that the charge density for this region is 230 μC cm^{-2} in sulfuric acid solutions [30].

IR spectroelectrochemical probing of adsorbates and online detection of volatile reaction products were performed simultaneously using a dual thin-layer spectroelectrochemical flow-cell in which ATR-FTIR and DEMS measurements can be carried put. A more detailed description of this flow-cell configuration was previously given in [31]. In brief, the central cell is a double thin-layer flow cell, equipped with two Pt counter electrodes (a Pt gauge and a Pt wire) at the inlet and the outlet of flow cell. For electrolyte changing, two electrolyte reservoirs are available, one with the supporting electrolyte alone and one with ethanol + supporting electrolyte. The working electrode is prepared by depositing the nanoparticles on a Au film covering a Si wafer, which in turn is coupled with the flat side of a hemispherical Si prism. The Au film was prepared by electroless deposition following the procedure reported previously [32-34]. It has to be thin

enough to allow the IR radiation to pass to the nanoparticles, but thick enough to be sufficiently conductive for obtaining a good electrochemical response.

In the first thin-layer compartment, the flat side of the prism was pressed via a circular tightening gasket and a Cu foil current collector against the Kel-F body of the cell, forming a thin electrolyte layer with a volume of *ca.* 10 μL. The electrolyte flows to the second thin-layer compartment through six capillaries. The second thin-layer compartment is connected via a porous Teflon membrane to a mass spectrometer, such that gaseous species can pass through and be detected on-line.

The *in situ* ATR-FTIRS experiments were performed in a BioRad FTS-6000 spectrometer equipped with a homemade reflection accessory (incident angle of 70º) and mercury cadmium telluride (MCT) detector. The resolution and the acquisition time per spectra were 4 cm^{-1} and 10 s, respectively. The spectra are presented in absorbance values, as the ratio $-\log R/R_0$, where R and R_0 are the reflectance values corresponding with the single beam spectra measured at the sample or reference potential, respectively. Negative bands in the spectra correspond with species formed at the sampling potential, whereas positive bands indicate a consumption of the species with respect to reference potential.

The DEMS setup is explained in detail in ref. [35]. Briefly, it is based on a differentially pumped two-chamber system coupled with a Balzers QMS 12 quadrople mass spectrometer, a Pine Instruments potentiostat and a computerized data acquisition system. In all the mass spectrometry experiments, large Pt loadings were used to favor the performance of DEMS experiments.

The calibration constant for CO_2 was determined by passing a CO saturated solution at 0.1 V until the Pt surface is completely blocked. Then, the electrolyte is changed to CO-free supporting electrolyte for 15 min, to assure the complete removal of dissolved CO in the thin-layer cell. After that, a CO_{ads} stripping experiment was carried out. The calibration constant K* was calculated by comparison of the Faradaic oxidation current and the CO_2 mass signal, using the following equation [36]:

$$K^* = z\frac{Q_{MS}}{Q_F} \tag{3.2}$$

where z is the number of electrons exchanged in the CO oxidation reaction to CO_2, Q_{MS} is the integrated charge of the mass current for the CO_2 spectrometric signal (*m/z*=44) and Q_F is the integrated Faradaic current charge in the CO_{ad} stripping peak.

To eliminate contributions from acetaldehyde species to the mass signal *m/z*=44 for calculating the CO_2 current efficiency in the ethanol oxidation reaction, the following equation was used:

$$I_{MS}(CO_2) = I(m/z = 44) - n \times I(m/z = 29) \tag{3.3}$$

where *n* is a parameter determined from the ratio between the stable I_{44} and I_{29} currents in the oxidation transients at 0.9 V at each pH, and assuming that the efficiency for acetaldehyde production at this potential is 100%, as has been observed previously [36]. The values obtained for *n* are always between 0.60 and 0.65. To convert this CO_2 mass current to the Faradaic current, the calibration constant K^* was used:

$$I_F(CO_2) = z\frac{I_{MS}(CO_2)}{K^*} \tag{3.4}$$

For this expression, *z* is equal to 6, the number of electrons exchanged per C atom for completing CO_2 oxidation. Finally, the CO_2 current efficiency is the ratio between CO_2 and total Faradaic currents:

$$A_{CO_2} = \frac{I_F(CO_2)}{I_F} \tag{3.5}$$

All experiments were carried out at room temperature. Millipore Milli Q water (18.2 MΩ cm), H_2SO_4 (Suprapur, Merck), Na_2SO_4 (HiPerSolv, Prolabo) and ethanol absolute (Merck p.a.) were used to prepare the solutions. Solutions of different pH were obtained by adding some droplets of H_2SO_4 to 0.5 M SO_4^{2-} solutions until the desired pH value was reached. The sulfate concentration was kept at approximately 0.5 M for all experiments. Solutions were deaerated with N_2/Ar, and CO (Messer-Griesheim, N 4.7) was used to saturate the supporting electrolyte solution used for cleaning the nanoparticles and for calibrating the DEMS signals. A Saturated Calomel Electrode (SCE) served as a reference

during the simultaneous ATR-FTIRS/DEMS experiments, but all the potentials presented in this paper are referred to that of the reversible hydrogen electrode (RHE).

3.3 Results and discussion

3.3.1 Electrochemical characterization

Fig. 3.1 shows the characteristic cyclic voltammetric profiles in 0.5 M H_2SO_4 for the Pt nanoparticles used in this work. Both cyclic voltammograms (CVs) show symmetric voltammetric peaks, which is an indication of the surface cleanness. The resulting voltammetric profiles can be considered as a fingerprint of each Pt nanoparticle sample and allow a detailed evaluation of the specific surface structure [29].

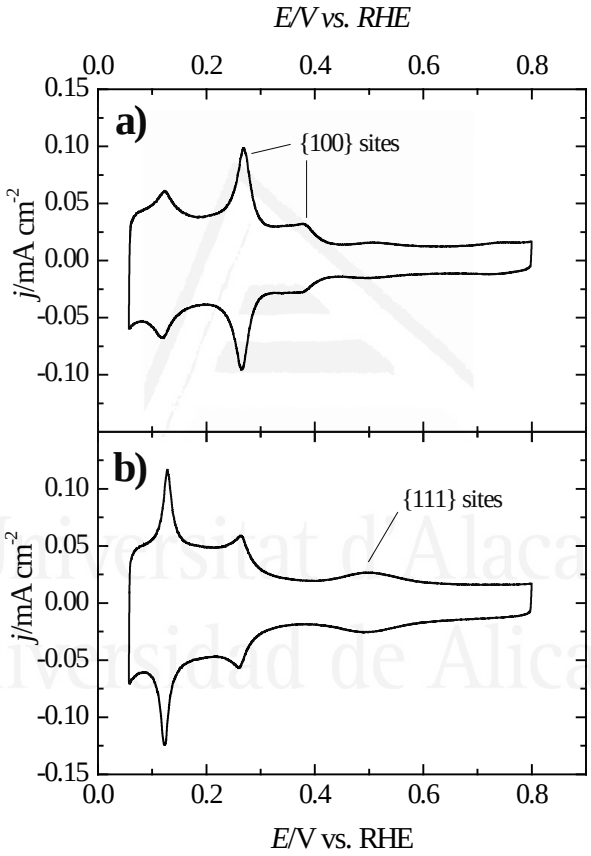

Fig. 3.1. Voltammetric profiles corresponding to a) (100)Pt and b) (111)Pt nanoparticles in 0.5 M H_2SO_4. Scan rate: 0.05 V s^{-1}.

As previously shown, the main features are those related to the presence of large {100} ordered domains (signal at about 0.37 V) due to the hydrogen adsorption/desorption process and those associated with the sulfate adsorption on {111} ordered domains (signal about 0.5 V) [29]. As expected, cubic Pt nanoparticles displayed the characteristic feature

of the wide {100} domains while for octahedral ones the CV was dominated by the characteristic features coming from the {111} ordered domains. A more detailed analysis about the correlations between shape, surface structure and resulting voltammetric profiles has been done previously in our group [12, 29, 30].

3.3.2 Ethanol oxidation at low pHs

The voltammetric responses for ethanol oxidation (1st scan) obtained with the different Pt nanoparticles in 0.05 M EtOH + 0.5 M SO_4^{2-} at two different pH values are displayed in Fig. 3.2. As previously mentioned, the upper potential limit is limited to 0.95 V in order to avoid significant changes of the Pt surfaces due to oxide formation/reduction processes. Also, and in comparison with previous works [7, 8], the ethanol concentration is lowered to prevent problems with membrane saturation in the DEMS experiments.

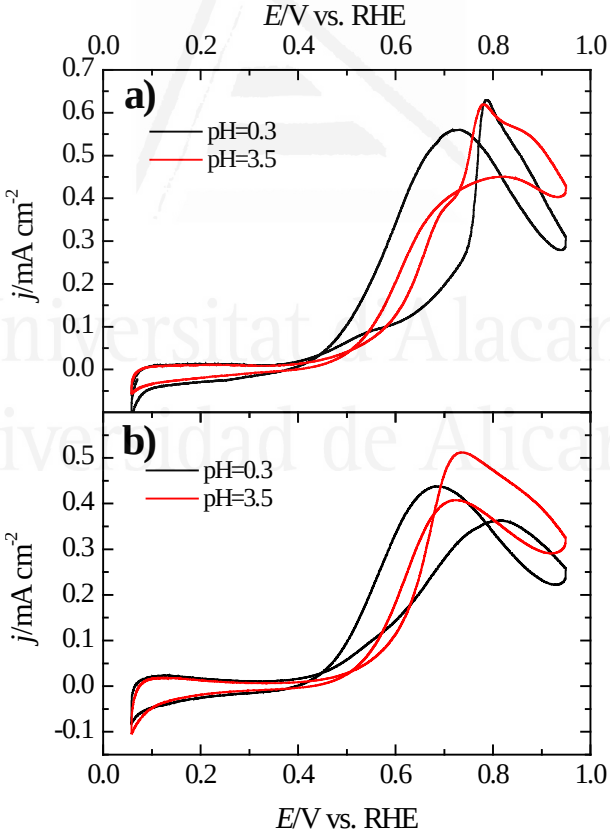

Fig. 3.2. Voltammetric profiles for a) (100)Pt and b) (111)Pt nanoparticles in 0.05 M CH_3CH_2OH + 0.5 M SO_4^{2-} at different pHs. Scan rate: 0.02 V s^{-1}.

As mentioned before, experiments were carried out at pH values below 4 to avoid carbonate formation from the reaction of CO_2 with water, which can mask the CO_2 efficiency. On the other hand, the surface area of the nanoparticles was kept relatively low (0.03-0.05 cm^2 of active area) to ensure that the entire deposit is contributing to the oxidation reaction. In this sense, it is worth noting that the use of high metal loadings and consequently high surface areas creates nanostructured electrodes in which only the outer part of the deposit is effectively working, due to a poor diffusion of ethanol to the inner parts, giving rise to lower than expected current densities [37].

In the positive-going sweep and at potentials below *ca.* 0.4 V, the voltammetric profiles present low currents due to the formation of CO_{ads}, which blocks the active surface. As has been shown, this process takes place even at potentials as low as 0.1 V [20, 21], and CO_{ads} is accumulated on the surface since it is not effectively oxidized at room temperature at E<0.6 V. As the potential is increased, CO_{ads} is oxidized and the current increases until an oxidation peak at around 0.8 V is observed. From this point, ethanol oxidation is hindered by adsorbed species (anions present in solution or OH^-) and/or by the incipient oxide formation.

In the negative-going sweep and after the reactivation of the surface, currents are higher than those measured in the positive-going scan, since the surface is now free from CO_{ads} and for E>0.6 V, the possible CO_{ads} formed in the process is immediately oxidized. This fact leads to a hysteresis between both scan directions, which is proportional to the amount of CO_{ads} formed at low potentials. The decrease at E<0.6 V is a consequence of the CO_{ads} re-poisoning of the surface and the diminution of oxidation rates as the electrode potential diminishes [38, 39]. However, this process depends on the surface structure and on the pH of the electrolyte.

At pH=0.3, (100)Pt nanoparticles (Fig. 3.2a) present a more prominent peak at 0.8 V, which is a characteristic of {100} surfaces. As it has been previously shown in single crystal electrode studies, Pt(100) is more active for the formation of CO than the Pt(111) electrode, leading to a complete blockage of the surface at low potentials [5]. The subsequent oxidation of CO with the concomitant reactivation of the surface gives rise to the peak at 0.8 V on the Pt(100) electrode [5, 8]. This preference for CO formation at low

potentials is also the cause of a more pronounced hysteresis between positive and negative-going sweeps for the (100)Pt nanoparticles than for the (111)Pt ones. However, by increasing the pH, this hysteresis decreases for both nanoparticle samples, probably due to a lower CO_{ads} formation rate, as will be shown later.

In terms of maximum current densities, (100)Pt nanoparticles (Fig. 3.2a) display a similar peak current density for the two pH values, which means that, despite different CO formation and probably different CO_2 current efficiencies, the overall activity for the reaction, under non-stationary conditions, is maintained. On the other hand, (111)Pt nanoparticles (Fig. 3.2b) show a lower hysteresis and higher peak current as the pH increases, suggesting that cleavage of the C-C bond is disfavored and acetaldehyde/acetic acid products are preferred instead of CO_2 formation. This fact seems to be in good agreement with what was observed for surfaces with large {111} ordered domains in strongly alkaline solutions [7, 40], where only the incomplete oxidation is achieved and no adsorbed CO is detected in the whole potential range. This discussion will be continued in the next sections with data obtained from DEMS experiments.

To evaluate the adsorbed species present on the Pt surface during ethanol oxidation at these pHs, FTIR experiments were carried out. Fig. 3.3 displays ATR measurements at 0.4 V vs RHE, using spectra taken at 0.9 V, where CO is completely oxidized to CO_2, as reference spectra. All spectra were recorded under almost stationary conditions. At 0.4 V, the fragments formed from ethanol oxidation poison the active surface.

In the IR experiments, the main band observed corresponds to linearly adsorbed CO in the spectral range between 2030 and 2070 cm^{-1}. In the two samples studied, (100)Pt and (111)Pt nanoparticles (Fig. 3.3a and 3.3b respectively), the CO bands diminish with increasing pH, as it was predicted from the hysteresis in the voltammetric experiments. Comparing the two experiments, it seems that the CO bands are higher for {100} domains than for {111} sites in agreement with our previous findings [8]. Unfortunately, the direct comparison done in this paper cannot be done due to the different experimental conditions for each electrode and the no appearance of the adsorbed acetate band, which is used for normalize the amount of CO formed.

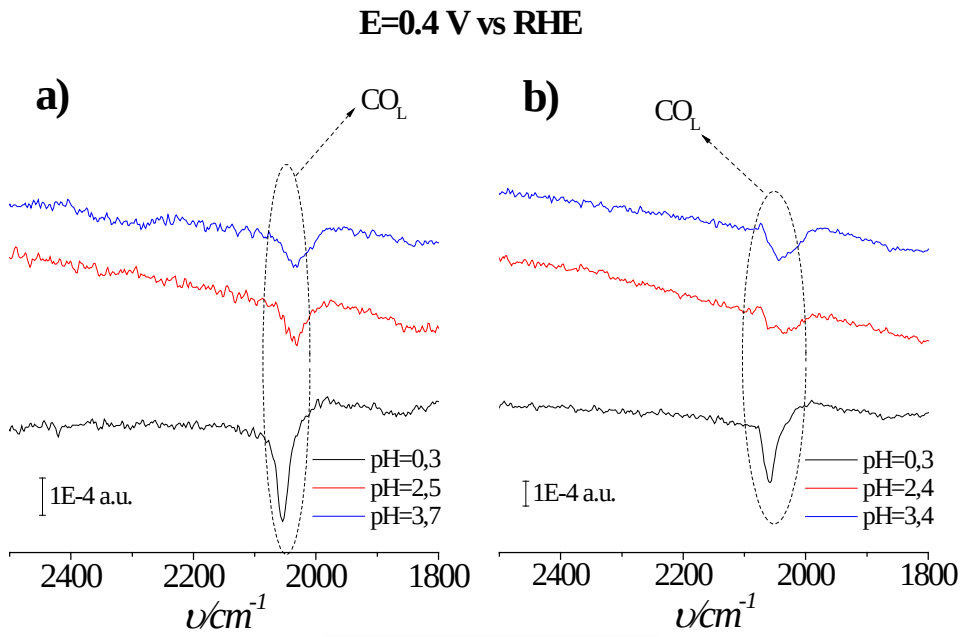

Fig. 3.3. ATR spectra obtained at E=0.4 V vs RHE for (a) (100)Pt and (b) (111)Pt nanoparticles in 0.05 M CH_3CH_2OH + 0.5 M SO_4^{2-} at different pHs (reference spectra at 0.9 V).

This absence of the adsorbed acetate band is due to the fact that these experiments are performed under flow cell conditions, where the acetic acid formed in the reaction is readily removed from the vicinity of the electrode, thus preventing its adsorption as weakly bound acetate. Thus, in this way, its accumulation on the surface is minimized, thus allowing a better approach to the understanding of the reaction mechanism.

3.3.3 DEMS experiments

For obtaining new quantitative data about the formation of acetate, CO_2, CH_x or other intermediates or products during ethanol oxidation, DEMS experiments were carried out. Fig. 3.4 and Fig. 3.5 display cyclic voltammetric experiments and the corresponding mass spectrometric currents (m/z=44 and m/z=29) obtained at different pH values using (100)Pt and (111)Pt nanoparticles, respectively.

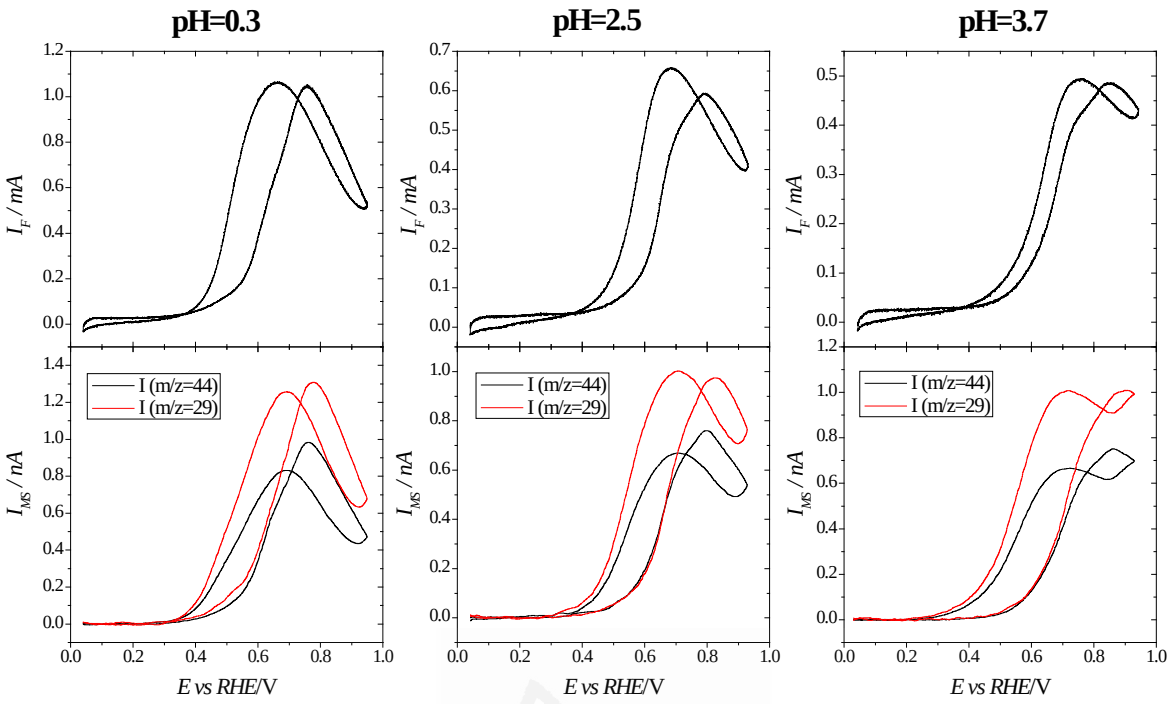

Fig. 3.4. Cyclic voltammetry (top) and mass spectrometric cyclic voltammograms for m/z=44 and m/z=29 (bottom) for the 2nd cycle during ethanol electroxidation in 0.05 M CH_3CH_2OH + 0.5 M SO_4^{2-} on (100)Pt nanoparticles. Scan rate: 0.005 V s^{-1}.

The scan rate used during the experiments was 5 mV s^{-1} and the flow rate was around 10 μL s^{-1}. In the figures, the 2nd cycle in DEMS experiments is presented, because this profile is a very good approximation to the steady-state behavior. As described in the experimental section, the m/z=44 current includes contributions from acetaldehyde (CH_3CHO^+) and CO_2, whereas the m/z=29 signal only includes contributions from the acetaldehyde (CHO^+) fragment.

In the case of (100)Pt nanoparticles (Fig. 3.4), the shape of the mass spectrometric voltammogram for I_{29} is similar to that observed for the Faradaic current, which suggests that ethanol oxidation proceeds mainly via acetaldehyde formation. However, the I_{44} mass spectrometric voltammogram shows some slight differences in the region at 0.7-0.8 V, probably due to the formation of CO_2 from the oxidation of CO_{ads} generated at lower potentials. On the other hand, for (111)Pt nanoparticles (Fig. 3.5), the shape of the I_{29} and I_{44} mass spectrometric voltammograms are almost identical, confirming that CO_{ads} formation/CO_{ads} oxidation is less than in the previous case. For both nanoparticle samples,

I_{29} and I_{44} come only from acetaldehyde formation at higher potentials than 0.9 V, where CO_{ads} formed at lower potentials has been completely oxidized to CO_2 [36].

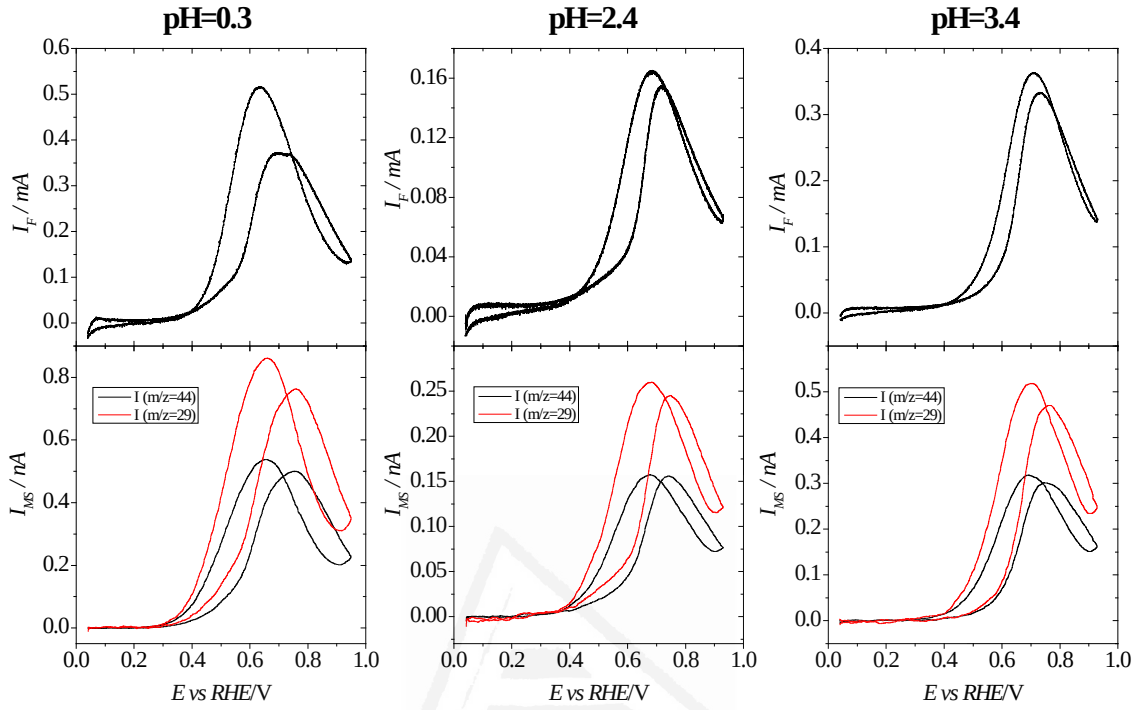

Fig. 3.5. Cyclic voltammetry (top) and mass spectrometric cyclic voltammograms for m/z=44 and m/z=29 (bottom) for the 2nd cycle during ethanol electroxidation in 0.05 M CH_3CH_2OH + 0.5 M SO_4^{2-} on (111)Pt nanoparticles. Scan rate: 0.005 V s^{-1}.

Considering the current peaks in the mass spectrometric signals for the negative-going potential scan, the ratio between I_{44} and I_{29} is around 60%, independent of the pH or the Pt sample. This is the same relative intensity as obtained in the steady-state oxidation process at 0.9 V. This ratio will be used later for calculating the CO_2 efficiency. Comparing the peak potentials measured for the three different pH values studied, the peak potential is shifted positively with increasing pH for (100)Pt nanoparticles, while for the (111)Pt nanoparticles no significant change is observed. Since the peak for the (100)Pt nanoparticles is mainly related to the oxidation of the adsorbed CO, this would mean that CO_{ads} oxidation is shifted toward more positive values as the pH increases due to the different CO_{ads} coverages observed in this sample. This effect is not observed for (111)Pt nanoparticles, presumably due to the lower amount of CO_{ads} formed at low potentials [5, 19].

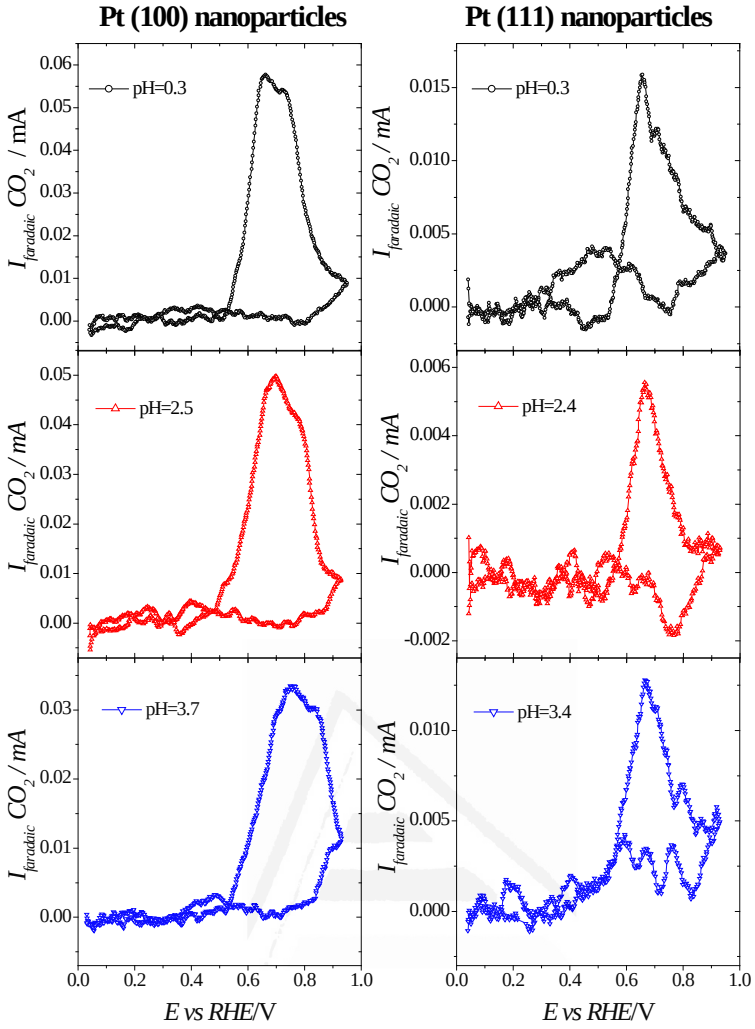

Fig. 3.6. CO_2 formation currents using data from Fig. 3.4 and Fig. 3.5 for 0.05 M CH_3CH_2OH + 0.5 M SO_4^{2-} (see text for more details).

Fig. 3.6 displays CO_2 Faradaic currents for the two samples studied during this work, calculated using Eqs. (3.3) and (3.4). The data used to calculate these currents were obtained from Fig. 3.4 and Fig. 3.5. These experiments were done to clarify the preference of {100} sites for complete oxidation as compared to {111} domains.

The shape of the CO_2 Faradaic current vs. E curve is similar to the voltammogram measured during a CO_{ads} stripping experiment, showing a peak at around 0.7 V vs RHE, which corresponds to the oxidation of adsorbed CO to CO_2. The shape of this CO_2 current trace agrees well with previous findings [41]. Also, the peak potential for the CO_2 Faradaic current shifts toward higher values with increasing pH, especially for the (100)Pt

nanoparticles, corroborating that the peak potential shift in the voltammogram is mainly related to the oxidation of adsorbed CO. The absence of currents in the negative scan direction clearly indicates that the cleavage of the C-C bond occurs only at low potentials, below 0.5 V. At those potentials, the cleavage produces adsorbed CO, which is only oxidized in the subsequent positive-going scan at higher potentials. If the cleavage of the C-C bond had taken place at high potentials, some Faradaic current for CO_2 formation would have been detected in the negative scan direction.

In order to better compare the CO_2 efficiency of the two samples, the current efficiencies for CO_2 at pH=0.3 calculated using Eq. (3.5) are displayed in Fig. 3.7 for the positive scan direction.

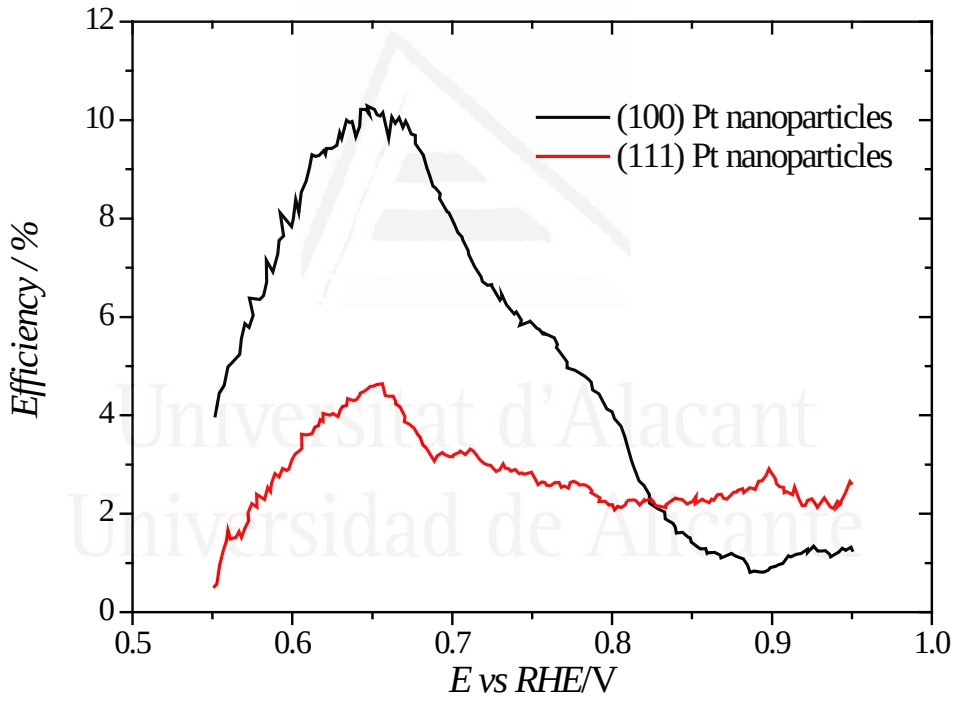

Fig. 3.7. CO_2 current **e**fficiency vs potential for (100)Pt nanoparticles and (111)Pt nanoparticles in the ethanol oxidation reaction (0.05 M) in 0.5 M H_2SO_4 (pH=0.3).

Maximum efficiencies are obtained at *ca.* 0.65 V for both samples. This potential is lower than the peak potential for the Faradaic CO_2 current, due to the competition between the oxidation of ethanol to acetaldehyde and acetic acid and that of adsorbed CO. As the CO_{ads} stripping process takes place, ethanol oxidation current becomes higher due to the

potential increase and also due to the rise in the number of free sites on the surface, where the partial oxidation of ethanol can occur. It should be highlighted that both curves have a very similar shape, indicating that the same type of sites are active for the C-C bond cleavage on both samples. The only difference between them is their relative number on the samples.

3.3.4 Ethanol stripping experiments

From the FTIR-DEMS results it is clear that the cleavage of the C-C bond is the key process to achieve the complete oxidation of ethanol. This process takes place at potentials below 0.4 V [42]. Results with single crystal electrodes have shown that once the C-C bond is broken, the carbon containing the alcohol group immediately evolves to give adsorbed CO, whereas the CH_x fragment only yields adsorbed CO at E>0.4-0.5 V [43]. To obtain additional information on this process, ethanol stripping experiments were done. In this experiment, an ethanol solution is flown through the cell at 0.4 V for two minutes, to allow the cleavage of ethanol molecules and adsorption of fragments. After that, the solution is changed to a solution containing only the supporting electrolyte at the same pH and then the electrode is cycled between 0.04 and 0.95 V vs RHE at v=5 mVs^{-1}, registering simultaneously the Faradic and mass spectrometric ion currents [39, 44].

Fig. 3.8 displays ethanol stripping experiments for the (100)Pt nanoparticles, studying ion currents m/z=15 and m/z=44. I_{15} provides information about the CH_x fragment in its reduction to CH_4 at low potentials [36, 45] whereas I_{44} in this particular case only gives information about CO_2 formed, since ethanol has been removed from the solution. Some authors have also evaluated the mass current m/z=61, which corresponds to a fragment of ethyl acetate ($CH_3COOH_2^+$), to follow the acetic acid formation, whose volatility is low and cannot be detected in DEMS experiments [46, 47]. However, as shown in these papers, the intensity of this mass current signal is very low and, consequently, it was not measured in the present contribution.

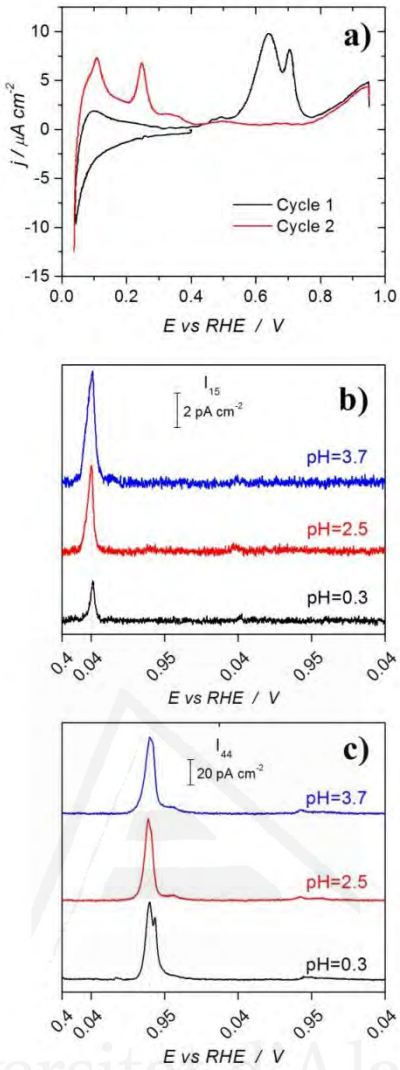

Fig. 3.8. Ethanol stripping experiments after adsorption for 2 minutes in 0.05 M ethanol + 0.5 M SO_4^{2-} at 0.4 V vs RHE on (100)Pt nanoparticles: Voltammetric response at 0.005 V s^{-1} (a) and mass spectrometric current densities of m/z=15 (b) and m/z=44 (c).

Fig. 3.8a shows the voltammetric profile after ethanol adsorption for (100)Pt nanoparticles. As expected, in the 1st cycle, active sites of platinum nanoparticles are blocked due to CO_{ads} formation. At higher potentials, CO_{ads} is oxidized to CO_2 and the voltammogram recovers the characteristic features of the (100)Pt nanoparticles in the so-called hydrogen region. Fig. 3.8b shows mass currents at m/z=15 simultaneously recorded with the voltammogram. At low potentials (around 0.1 V), a small peak is detected due to CH_4 formation from the reduction of the CH_x fragment. This signal increases with the pH. At higher potentials, adsorbed CO is oxidized to CO_2, as it can be seen in Fig. 3.8c. For this type of nanoparticles, I_{44} peak does not significantly change with the pH.

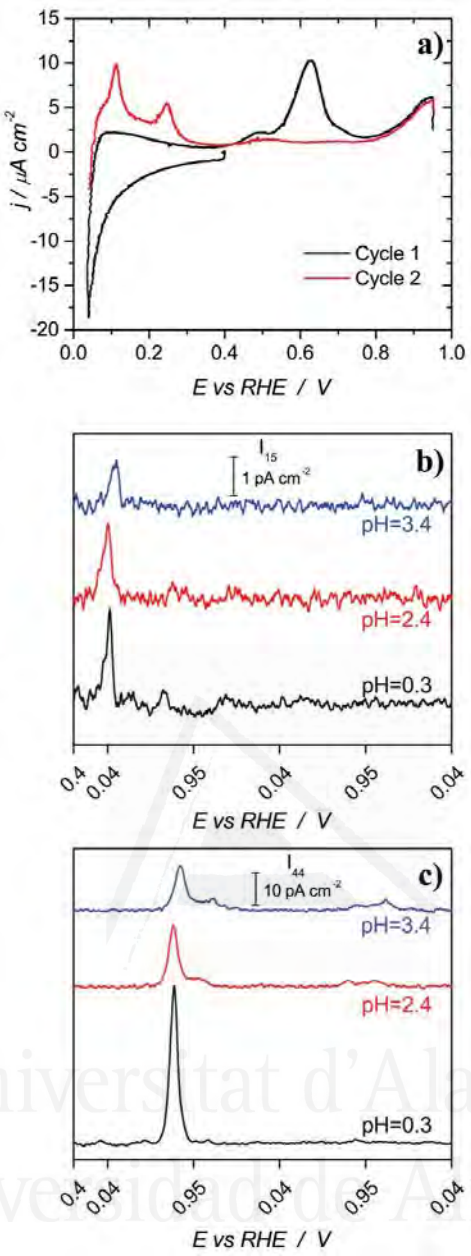

Fig. 3.9. Ethanol stripping experiments after adsorption for 2 minutes in 0.05 M ethanol + 0.5 M SO_4^{2-} at 0.4 V vs RHE on (111)Pt nanoparticles: Voltammetric response at 0.005 V s^{-1} (a) and mass spectrometric current densities of m/z=15 (b) and m/z=44 (c).

Fig. 3.9 shows the same experiments as done in Fig. 3.8, but using (111)Pt nanoparticles. From the evolution of the I_{15} and I_{44} currents with the pH it can be seen that both signals decrease significantly with pH. In order to quantitatively analyze the results of both samples, the normalized charges under mass signals m/z=15 and m/z=44 have been calculated (Fig. 3.10).

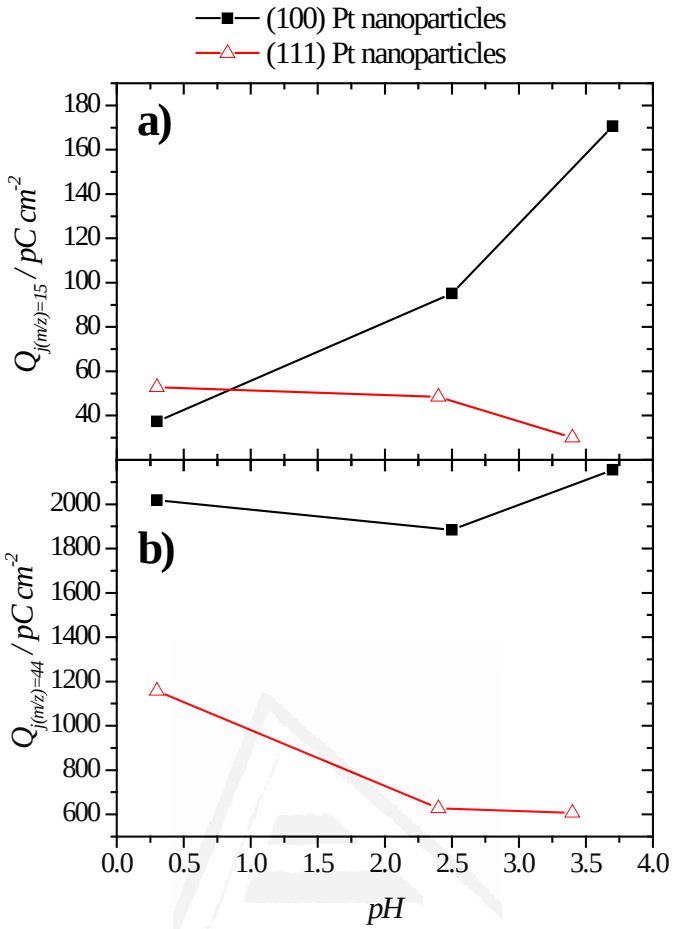

Fig. 3.10. a) CH_x and b) CO_2 charge vs pH. Data obtained from Fig. 3.8 and 3.9.

As stated before, at 0.4 V, ethanol molecules can dissociate, giving rise to two single carbon containing fragments, the one containing the oxygen group, which immediately reacts to adsorbed CO, and the CH_x fragment, which is more difficult to oxidize to form adsorbed CO. The CH_x fragment can also interact with the surface and be reduced at low potentials. Depending on the cleavage rate and the rate for the oxidation of the CH_x fragment to CO_{ads}. and how these rates evolve with the pH, several situations can be found. For the (100)Pt nanoparticles, the amount of CO_{ads} is independent of the pH, which indicates that the CO_{ads} coverage has reached a value where further C-C bond cleavage is fully inhibited. Probably only isolated sites remain free and, on those sites, this process cannot take place. This means that the C-C bond cleavage is fast enough to produce a saturated adlayer of CO during the time (2 min.) at 0.4 V. Since the oxidation of the CH_x fragment is very slow at 0.4 V, the increase of the signal for CH_4 production as the pH increases indicates that the oxidation of this fragment to yield adsorbed CO is even slower.

At lower pHs, the saturated CO adlayer formed contains a higher fraction of CO_{ads} molecules coming from the CH_x fragment and for this reason the signal is small. As the pH increases, the oxidation rate of this fragment to CO_{ads} diminishes at a higher rate than that of the C-C bond cleavage, resulting in a higher number of unreacted CH_x fragments on the electrode surface, thus producing a higher current for CH_4 production.

On the other hand, for the (111)Pt nanoparticles, the rate for the C-C cleavage is slower, because of the lower fraction of {100} sites on the sample. Thus, lower CO coverages are obtained as revealed in Fig. 3.10. These coverages are below the saturation value. On the other hand, the charge for CH_4 production at pH=0.3 is similar to that measured for the (100)Pt nanoparticles, which indicates that also the oxidation rate of CH_x to CO is low for these nanoparticles. As the pH increases, C-C bond cleavage rate diminishes, resulting in lower CO_{ads} coverages and lower CH_4 formation. The diminution in the CH_4 signal is proportionally smaller than that of the CO_2 due to a two effects. The C-C bond cleavage rate is slower but also the transformation of the CH_x fragment to CO, resulting in a compensating effect in which the diminution of unreacted CH_x fragments is smaller. The lower reactivity of surfaces for the cleavage of the C-C bond as the pH increases is in agreement with the results obtained in alkaline medium. In the latter environment, only acetate bands are detected in FTIR experiments for ethanol oxidation [7]. Bands related to $CH_{x,ads}$ have only been seen in wide {111} ordered domains by SERS in these media [25], whereas these bands were not detected in the case of Pt polyoriented surfaces [43], in agreement with our results.

3.4 Conclusions

Ethanol oxidation experiments with Pt nanoparticles were performed using voltammetric, ATR and DEMS experiments, studying the acidic pH range below 4 to avoid carbonate formation and using always 0.5 M SO_4^{2-} to discard anion effects. As a summary of the data obtained, the next scheme shows the preferred path for each site taking into account the pH effect in acidic solutions:

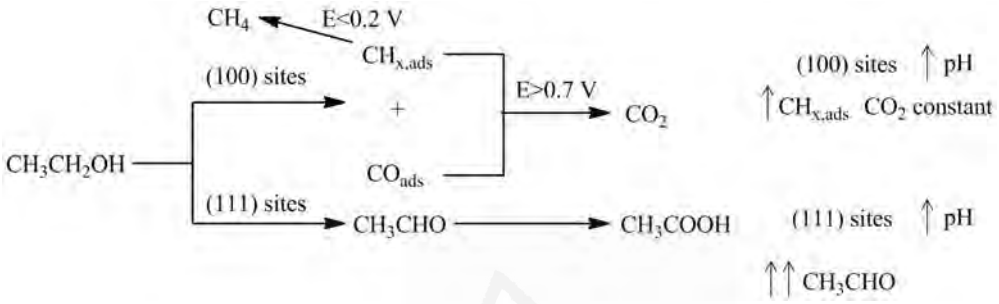

(3.6)

The results presented clearly show structure effects related to the {100} and {111} domains, in agreement with studies done with single crystal electrodes. In spite of the fact that the incomplete ethanol oxidation was established as the preferred route for both samples, a higher activity for the formation of C1-fragments (CO_{ads}, $CH_{x,ads}$) as intermediates was observed for {100} domains. The maximum CO_2 efficiency calculated from DEMS data corroborated this behavior, as it is higher for (100)Pt nanoparticles (around 10%) than for (111)Pt nanoparticles (around 5%). When the pH is increased, $CH_{x,ads}$ was also detected, in addition to CO_{ads}. $CH_{x,ads}$ formation is favored at lower potentials on preferentially oriented (100)Pt nanoparticles and decreasing CO formation. For (111)Pt nanoparticles, CO_{ads} formation is hindered and also the splitting of the C-C bond, promoting acetaldehyde/acetic acid formation up to quasi-negligible CO_2 formation at higher pHs.

3.5 References

[1] M. T. M. Koper, "Fuel Cell Catalysis: A Surface Science Approach", *Electrocatalysis and Electrochemistry* A. Wieckowski (Ed.), John Wiley & Sons, Hoboken, New Jersey, **2009**.

[2] C. Rice, R. I. Ha, R. I. Masel, P. Waszczuk, A. Wieckowski and T. Barnard, "Direct formic acid fuel cells" *Journal of Power Sources* **2002**, 111, 83-89.

[3] T. Iwasita, "Electrocatalysis of methanol oxidation" *Electrochimica Acta* **2002**, 47, 3663-3674.

[4] E. Antolini, "Catalysts for direct ethanol fuel cells" *Journal of Power Sources* **2007**, 170, 1-12.

[5] F. Colmati, G. Tremiliosi-Filho, E. R. Gonzalez, A. Berná, E. Herrero and J. M. Feliu, "Surface structure effects on the electrochemical oxidation of ethanol on platinum single crystal electrodes" *Faraday Discussions* **2008**, 140, 379-397.

[6] F. Colmati, G. Tremiliosi-Filho, E. R. Gonzalez, A. Berná, E. Herrero and J. M. Feliu, "The role of the steps in the cleavage of the C-C bond during ethanol oxidation on platinum electrodes" *Physical Chemistry Chemical Physics* **2009**, 11, 9114-9123.

[7] C. Busó-Rogero, E. Herrero and J. M. Feliu, "Ethanol Oxidation on Pt Single-Crystal Electrodes: Surface-Structure Effects in Alkaline Medium" *ChemPhysChem* **2014**, 15, 2019-2028.

[8] C. Busó-Rogero, V. Grozovski, F. J. Vidal-Iglesias, J. Solla-Gullón, E. Herrero and J. M. Feliu, "Surface structure and anion effects in the oxidation of ethanol on platinum nanoparticles" *Journal of Materials Chemistry A* **2013**, 1, 7068-7076.

[9] J. Hernández, J. Solla-Gullón and E. Herrero, "Gold nanoparticles synthesized in a water-in-oil microemulsion: electrochemical characterization and effect of the surface structure on the oxygen reduction reaction" *Journal of Electroanalytical Chemistry* **2004**, 574, 185-196.

[10] J. Solla-Gullón, F. J. Vidal-Iglesias, A. López-Cudero, E. Garnier, J. M. Feliu and A. Aldaz, "Shape-dependent electrocatalysis: methanol and formic acid electrooxidation on preferentially oriented Pt nanoparticles" *Physical Chemistry Chemical Physics* **2008**, 10, 3689-3698.

[11] F. J. Vidal-Iglesias, J. Solla-Gullón, V. Montiel, J. M. Feliu and A. Aldaz, "Ammonia selective oxidation on Pt(100) sites in an alkaline medium" *Journal of Physical Chemistry B* **2005**, 109, 12914-12919.

[12] V. Grozovski, J. Solla-Gullón, V. Climent, E. Herrero and J. M. Feliu, "Formic Acid Oxidation on Shape-Controlled Pt Nanoparticles Studied by Pulsed Voltammetry" *Journal of Physical Chemistry C* **2010**, 114, 13802-13812.

[13] F. J. Vidal-Iglesias, R. M. Arán-Ais, J. Solla-Gullón, E. Garnier, E. Herrero, A. Aldaz and J. M. Feliu, "Shape-dependent electrocatalysis: formic acid electrooxidation on cubic Pd nanoparticles" *Physical Chemistry Chemical Physics* **2012**, 14, 10258-10265.

[14] F. J. Vidal-Iglesias, J. Solla-Gullón, E. Herrero, A. Aldaz and J. M. Feliu, "Pd Adatom Decorated (100) Preferentially Oriented Pt Nanoparticles for Formic Acid Electrooxidation" *Angewandte Chemie-International Edition* **2010**, 49, 6998-7001.

[15] C. Busó-Rogero, J. V. Perales-Rondón, M. J. S. Farias, F. J. Vidal-Iglesias, J. Solla-Gullón, E. Herrero and J. M. Feliu, "Formic acid electrooxidation on thallium-decorated shape-controlled platinum nanoparticles: an improvement in electrocatalytic activity" *Physical Chemistry Chemical Physics* **2014**, 16, 13616-13624.

[16] C. Lamy, S. Rousseau, E. M. Belgsir, C. Coutanceau and J. M. Léger, "Recent progress in the direct ethanol fuel cell: development of new platinum-tin electrocatalysts" *Electrochimica Acta* **2004**, 49, 3901-3908.

[17] A. O. Neto, R. R. Dias, M. M. Tusi, M. Linardi and E. V. Spinacé, "Electro-oxidation of methanol and ethanol using PtRu/C, PtSn/C and PtSnRu/C electrocatalysts prepared by an alcohol-reduction process" *Journal of Power Sources* **2007**, 166, 87-91.

[18] J. P. I. de Souza, S. L. Queiroz, K. Bergamaski, E. R. Gonzalez and F. C. Nart, "Electro-oxidation of ethanol on Pt, Rh, and PtRh electrodes. A study using DEMS and in-situ FTIR techniques" *Journal of Physical Chemistry B* **2002**, 106, 9825-9830.

[19] S. C. S. Lai and M. T. M. Koper, "Electro-oxidation of ethanol and acetaldehyde on platinum single-crystal electrodes" *Faraday Discussions* **2008**, 140, 399-416.

[20] V. Del Colle, J. Souza-Garcia, G. Tremiliosi-Filho, E. Herrero and J. M. Feliu, "Electrochemical and spectroscopic studies of ethanol oxidation on Pt stepped surfaces modified by tin adatoms" *Physical Chemistry Chemical Physics* **2011**, 13, 12163-12172.

[21] J. Souza-Garcia, E. Herrero and J. M. Feliu, "Breaking the C-C Bond in the Ethanol Oxidation Reaction on Platinum Electrodes: Effect of Steps and Ruthenium Adatoms" *ChemPhysChem* **2010**, 11, 1391-1394.

[22] V. Del Colle, A. Berná, G. Tremiliosi-Filho, E. Herrero and J. M. Feliu, "Ethanol electrooxidation onto stepped surfaces modified by Ru deposition: electrochemical and spectroscopic studies" *Physical Chemistry Chemical Physics* **2008**, 10, 3766-3773.

[23] J. R. Varcoe, R. C. T. Slade, E. L. H. Yee, S. D. Poynton, D. J. Driscoll and D. C. Apperley, "Poly(ethylene-co-tetrafluoroethylene)-derived radiation-grafted anion-exchange membrane with properties specifically tailored for application in metal-cation-free alkaline polymer electrolyte fuel cells" *Chemistry of Materials* **2007**, 19, 2686-2693.

[24] C. Coutanceau, L. Demarconnay, C. Lamy and J. M. Léger, "Development of electrocatalysts for solid alkaline fuel cell (SAFC)" *Journal of Power Sources* **2006**, 156, 14-19.

[25] S. C. S. Lai and M. T. M. Koper, "Ethanol electro-oxidation on platinum in alkaline media" *Physical Chemistry Chemical Physics* **2009**, 11, 10446-10456.

[26] P. A. Christensen, S. W. M. Jones and A. Hamnett, "In Situ FTIR Studies of Ethanol Oxidation at Polycrystalline Pt in Alkaline Solution" *Journal of Physical Chemistry C* **2012**, 116, 24681-24689.

[27] T. S. Ahmadi, Z. L. Wang, T. C. Green, A. Henglein and M. A. El-Sayed, "Shape-controlled synthesis of colloidal platinum nanoparticles" *Science* **1996**, 272, 1924-1926.

[28] T. S. Ahmadi, Z. L. Wang, A. Henglein and M. A. El-Sayed, ""Cubic" colloidal platinum nanoparticles" *Chemistry of Materials* **1996**, 8, 1161-1163.

[29] J. Solla-Gullón, P. Rodríguez, E. Herrero, A. Aldaz and J. M. Feliu, "Surface characterization of platinum electrodes" *Physical Chemistry Chemical Physics* **2008**, 10, 1359-1373.

[30] Q. S. Chen, J. Solla-Gullón, S. G. Sun and J. M. Feliu, "The potential of zero total charge of Pt nanoparticles and polycrystalline electrodes with different surface structure: The role of anion adsorption in fundamental electrocatalysis" *Electrochimica Acta* **2010**, 55, 7982-7994.

[31] M. Heinen, Y. X. Chen, Z. Jusys and R. J. Behm, "In situ ATR-FTIRS coupled with on-line DEMS under controlled mass transport conditions - A novel tool for electrocatalytic reaction studies" *Electrochimica Acta* **2007**, 52, 5634-5643.

[32] S. Brimaud, Z. Jusys and R. J. Behm, "Shape-selected nanocrystals for in situ spectro-electrochemistry studies on structurally well defined surfaces under controlled electrolyte transport: A combined in situ ATR-FTIR/online DEMS investigation of CO electrooxidation on Pt" *Beilstein Journal of Nanotechnology* **2014**, 5, 735-746.

[33] H. Miyake, S. Ye and M. Osawa, "Electroless deposition of gold thin films on silicon for surface-enhanced infrared spectroelectrochemistry" *Electrochemistry Communications* **2002**, 4, 973-977.

[34] S. Brimaud, Z. Jusys and R. J. Behm, "Controlled Surface Structure for In Situ ATR-FTIRS Studies Using Preferentially Shaped Pt Nanocrystals" *Electrocatalysis* **2011**, 2, 69-74.

[35] Z. Jusys and R. J. Behm, "Methanol oxidation on a carbon-supported Pt fuel cell catalyst - A kinetic and mechanistic study by differential electrochemical mass spectrometry" *Journal of Physical Chemistry B* **2001**, 105, 10874-10883.

[36] A. A. Abd-El-Latif, E. Mostafa, S. Huxter, G. Attard and H. Baltruschat, "Electrooxidation of ethanol at polycrystalline and platinum stepped single crystals A study by differential electrochemical mass spectrometry" *Electrochimica Acta* **2010**, 55, 7951-7960.

[37] S. Chumillas, C. Busó-Rogero, J. Solla-Gullón, F. J. Vidal-Iglesias, E. Herrero and J. M. Feliu, "Size and diffusion effects on the oxidation of formic acid and ethanol on platinum nanoparticles" *Electrochemistry Communications* **2011**, 13, 1194-1197.

[38] H. Wang, Z. Jusys and R. J. Behm, "Ethanol electrooxidation on a carbon-supported Pt catalyst: Reaction kinetics and product yields" *Journal of Physical Chemistry B* **2004**, 108, 19413-19424.

[39] E. Mostafa, A. A. Abd-El-Latif, R. Ilsley, G. Attard and H. Baltruschat, "Quantitative DEMS study of ethanol oxidation: effect of surface structure and Sn surface modification" *Physical Chemistry Chemical Physics* **2012**, 14, 16115-16129.

[40] C. Busó-Rogero, J. Solla-Gullón, F. J. Vidal-Iglesias, E. Herrero and J. M. Feliu, "Oxidation of ethanol on platinum nanoparticles: surface structure and aggregation effects in alkaline medium" *Journal of Solid State Electrochemistry* **2016**, 20, 1095-1106.

[41] J. F. Gomes, D. Profeti and L. J. Deiner, "Influence of the Particle Size Distribution on the Activity and Selectivity of Carbon-Supported Platinum Nanoparticle Catalysts for Ethanol Electrooxidation" *ChemElectroChem* **2014**, 1, 655-662.

[42] C. Lamy and C. Coutanceau, "Electrocatalysis of Alcohol Oxidation Reactions at Platinum Group Metals", in *Catalysts for Alcohol-Fuelled Direct Oxidation Fuel Cells, vol. 6*, Z.-X. Liang and T. S. Zhao (Eds.) RSC Energy and Enviroment Series **2012**.

[43] S. C. S. Lai, S. E. F. Kleijn, F. T. Z. Öztürk, V. C. van Rees Vellinga, J. Koning, P. Rodriguez and M. T. M. Koper, "Effects of electrolyte pH and composition on the ethanol electro-oxidation reaction" *Catalysis Today* **2010**, 154, 92-104.

[44] M. Heinen, Z. Jusys and R. J. Behm, "Ethanol, Acetaldehyde and Acetic Acid Adsorption/Electrooxidation on a Pt Thin Film Electrode under Continuous Electrolyte Flow: An in Situ ATR-FTIRS Flow Cell Study" *Journal of Physical Chemistry C* **2010**, 114, 9850-9864.

[45] T. Iwasita and E. Pastor, "A DEMS and FTIR spectroscopic investigation of adsorbed ethanol on polycrystalline platinum" *Electrochimica Acta* **1994**, 39, 531-537.

[46] T. Herranz, M. Ibañez, J. L. G. de la Fuente, F. J. Pérez-Alonso, M. A. Pena, A. Cabot and S. Rojas, "In Situ Study of Ethanol Electrooxidation on Monodispersed Pt_3Sn Nanoparticles" *ChemElectroChem* **2014**, 1, 885-895.

[47] S. C. S. Lai and M. T. M. Koper, "The Influence of Surface Structure on Selectivity in the Ethanol Electro-oxidation Reaction on Platinum" *Journal of Physical Chemistry Letters* **2010**, 1, 1122-1125.

Capítulo 4:

Oxidación de etanol en electrodos monocristalinos de Pt: efecto de la estructura superficial en medio alcalino

Capítulo 4: Oxidación de etanol en electrodos monocristalinos de Pt: efecto de la estructura superficial en medio alcalino

RESUMEN

La investigación sobre la oxidación de pequeñas moléculas orgánicas a pHs básicos tiene un gran interés en la actualidad debido al desarrollo de las membranas aniónicas. Sobre el platino, la oxidación de etanol en estas condiciones tiene mayor actividad que en medio ácido. Sin embargo, no existen demasiados estudios acerca del efecto de la estructura superficial en medio alcalino, el principal objetivo de este capítulo. Para su estudio, se usan electrodos monocristalinos de platino con estructura superficial perfectamente conocida, empleando técnicas de voltametría cíclica y espectroscópicas.

En primer lugar, se muestra la caracterización electroquímica para los planos de base del platino en medio 0.1 M NaOH, las cuales muestran algunas diferencias con respecto a la caracterización habitual en medio ácido, sobre todo en los potenciales en los que aparece la adsorción del OH, que en medio alcalino se solapa con la adsorción de hidrógeno en los electrodos de Pt(100) y Pt(110).

La reacción de oxidación de etanol en electrodos de platino presenta una gran actividad que, en algunas ocasiones, como en el estudio de la oxidación de etanol en Pt(111), requiere una corrección de caída óhmica para la correcta realización de la voltametría, como se indica en la Fig. 4.2. A continuación se muestran las voltametrías cíclicas con la correspondiente desactivación para cada plano basal del Pt conforme pasan los ciclos de oxidación-reducción. La dependencia del orden de actividad total con la reactividad en los planes base del platino es Pt(111) > Pt(110) > Pt(100), la misma tendencia que sigue el umbral de potencial necesario para iniciar la oxidación de etanol. La histéresis entre el barrido positivo y negativo de potenciales es menor en el caso del

electrodo de Pt(111) y un poco mayor para el electrodo de Pt(100), aunque ésta no es asignada a la presencia de CO adsorbido sobre el electrodo, debido a que la histéresis es mucho menor que en los casos descritos en los capítulos anteriores. En cuanto a la desactivación, cuanta más corriente de oxidación se observa, mayor es la desactivación, como se observa en el electrodo de Pt(111), donde en el ciclo 25 la corriente es un 5% de la inicial. Las cronoamperometrías a 0.6 V muestran la variación de la actividad con el tiempo. Las corrientes a tiempos largos concuerdan con las voltametrías cíclicas anteriores, siendo el Pt(110) el electrodo más activo y menos inhibido, y, por tanto, el que menos potencial requiere para el inicio de oxidación de etanol.

Por otra parte, se estudia el efecto de introducir escalones de simetría {100} y {110} sobre terrazas {111} en la oxidación de etanol en medio alcalino. Al contrario que en medio ácido, las voltametrías cíclicas indican una única mejora en el potencial de inicio de la oxidación, decreciendo cada vez más la actividad total y aumentando la histéresis entre el barrido positivo y el barrido negativo de potenciales, observándose más corriente para las superficies con escalones {100} que las que presentan escalones {111}. Al realizar cronoamperometrías a 0.6 V, similares a las realizadas con los planos basales, se corrobora la mayor reactividad inducida por la presencia de sitios {100} vista en la voltametría cíclica, al contrario que en medio ácido, donde los escalones {110} son mucho más activos.

Previamente a los experimentos espectroelectroquímicos con electrodos de platino, se registraron los espectros de transmisión de los posibles productos en la oxidación de etanol, para conocer sus bandas características. Concretamente, se asigna que las bandas observadas a 1550 y 1415 cm^{-1} pertenecen al acetato, mientras que una banda a 1390 cm^{-1} es debida al carbonato, como se muestra en la Fig. 4.7, que contiene los espectros de transmisión y su comparación con espectros de IRRAS realizados con el Pt(111). Dichos espectros, realizados para los tres planos base del platino, muestran bandas de acetato como producto mayoritario, independientemente del electrodo utilizado. Sin embargo, no es descartable la formación de carbonato, cuya banda se puede solapar con la señal de acetato, debido a que aparecen a frecuencias similares. Para intentar aclarar la proporción entre el acetato y el carbonato formado, se ajustaron los espectros experimentales a 0.8 V con los espectros de transmisión del carbonato y el acetato, buscando averiguar la

contribución de cada especie al espectro en cada electrodo. En todos los casos la cantidad de carbonato estimada resulta ser muy baja.

Retornando a las voltametrías de los planos base del platino observados en la Fig. 4.3 y comparándolas con las obtenidas en medio ácido, la principal diferencia es la mayor actividad obtenida para el electrodo de Pt(111). La oxidación de etanol en este electrodo únicamente tiene lugar a través de la ruta de oxidación incompleta hasta ácido acético (acetato a pHs más elevados), por lo que la razón de estas altas corrientes es la de la no adsorción de acetato, debido a que el potencial al cual se trabaja (en torno a 0.7 V frente a RHE) es más negativo en la escala absoluta. En cuanto al potencial de inicio de la oxidación de etanol, éste se desplaza hacia valores más positivos (sobre 0.6 V en escala RHE), sugiriendo que es necesaria la adsorción de OH para iniciar la oxidación en medio alcalino, al contrario que en medio ácido donde la especie dadora de oxígeno puede variar debido al potencial absoluto más positivo. En los electrodos de Pt(100) y Pt(110), la oxidación de etanol en 0.1 M NaOH también es desencadenada por la adsorción del OH, que hace que el potencial al cual se inicia la oxidación de etanol sea menor.

En cuanto a la razón por la cual se produce la histéresis entre el barrido positivo y negativo de la voltametría cíclica, sobre todo en el caso del Pt(100) y el Pt(110), no se debe a la adsorción de CO, como en medio ácido. Es difícil asegurar cual es el intermedio que se adsorbe e inhibe la reacción de oxidación de etanol. En la bibliografía se propone la especie CH_x como causante de la inhibición, aunque este hecho no puede asegurarse a partir de los resultados espectroscópicos de la literatura. Otra posibilidad es la del incremento en la irreversibilidad en la adsorción de OH al realizar la oxidación de etanol.

La fuerte desactivación de la superficie de platino es muy elevada y probablemente es también causada por la misma especie inhibidora. La Fig. 4.9 muestra el efecto en la voltametría registrada en 0.1 M NaOH, de las especies inhibidoras sobre un electrodo de Pt(111) tras realizar 5 ciclos de oxidación-reducción de etanol. Como se ve, la carga de adsorción de hidrógeno es menor que en el blanco original. Al volver a la oxidación de etanol, la actividad sigue mostrándose pequeña debido a la desactivación de la superficie. Por el contrario, un simple enjuague del electrodo con agua destilada provoca una recuperación de la actividad inicial (Fig. 4.10), mostrando como la especie inhibidora es

estable a pHs alcalinos pero no en medio neutro. Si se realiza el mismo experimento con acetaldehído, se observa que esta especie no se oxida en medio alcalino y produce un bloqueo prácticamente instantáneo de la superficie. Por tanto, se puede pensar que la especie inhibidora está relacionada con la producción de acetaldehído y a su posible dimerización, que probablemente pueda dar lugar a la presencia de especies CH_x en superficie, como se propone en otros trabajos relacionados. El grado de desactivación entre los tres planos bases es Pt(111) > Pt(110) > Pt(100), relacionado directamente con la cantidad de acetaldehído formado en cada electrodo.

Chapter 4

CHEMPHYSCHEM
ARTICLES

ChemPubSoc Europe

DOI: 10.1002/cphc.201402044

VIP

Ethanol Oxidation on Pt Single-Crystal Electrodes: Surface-Structure Effects in Alkaline Medium

Carlos Busó-Rogero, Enrique Herrero,* and Juan M. Feliu[a]

Ethanol oxidation in 0.1 M NaOH on single-crystal electrodes has been studied using electrochemical and FTIR techniques. The results show that the activity order is the opposite of that found in acidic solutions. The Pt(111) electrode displays the highest currents and also the highest onset potential of all the electrodes. The onset potential for the oxidation of ethanol is linked to the adsorption of OH on the electrode surface. However, small (or even negligible) amounts of CO_{ads} and carbonate are detected by FTIR, which implies that cleavage of the C–C bond is not favored in this medium. The activity of the electrodes diminishes quickly upon cycling. The diminution of the activity is proportional to the measured currents and is linked to the formation and polymerization of acetaldehyde, which adsorbs onto the electrode surface and prevents further oxidation.

This chapter has been adapted and formatted from ChemPhysChem **2014**, 15, 2019-2028.

Corresponding author: herrero@ua.es

4.1 Introduction

In the research of possible new fuels for developing fuel cell technology, the oxidation of small organic molecules on pure platinum and alloys has been widely examined in recent years [1]. In particular, ethanol is one of the most studied molecules due to its advantages [2-5]. It is considered to be a 'green' chemical because it can be obtained directly from biomass after distillation, it can be easily introduced in the current fuel distribution system and it has a high energy density in the complete oxidation to CO_2. In this process 12 electrons are exchanged:

$$CH_3CH_2OH + 3H_2O \longrightarrow 2CO_2 + 12H^+ + 12e^- \quad (4.1)$$

The thermodynamic standard potential of this reaction is 0.085 V, which yields a standard cell potential for an ethanol/oxygen fuel cell of 1.145 V. However, there are some problems which should be solved prior to practical use. These problems are related with the slow kinetics of ethanol oxidation reaction that produce large overpotentials and diminish the operational potential, and to the incomplete oxidation to acetic acid.

With platinum as a catalyst, studies clearly show that the surface structure is an important parameter that significantly changes the reactivity for the oxidation of small molecules [6-8]. This is the case of ethanol [5, 9]. In acid solutions, the proposed oxidation mechanism has a dual route:

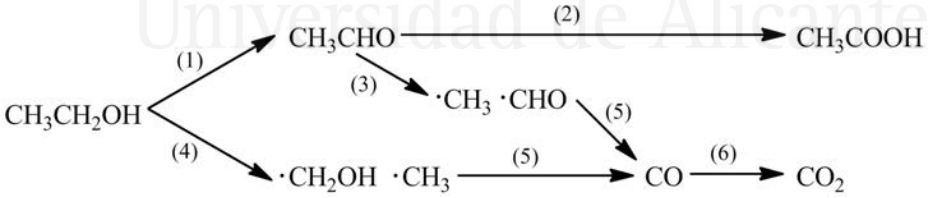

(4.2)

Reaction steps (1) and (2) represent the route for the incomplete oxidation of ethanol, which produces acetaldehyde with two electrons transferred, and acetic acid by transferring two additional electrons. This route should be avoided because acetic acid cannot be oxidized at room temperature. Thus, only four electrons are exchanged and 2/3 of the formal energy density of ethanol is not used. To give CO_2 as the final product, it is necessary to break the C-C bond through steps (3) and (4). The cleavage is followed by the transformation of the fragments into adsorbed CO in step (5). CO is considered to be a poison intermediate in many reactions because it is adsorbed strongly on the catalyst

surface and is difficult to oxidize. For that reason, it inhibits further reactions. However, for ethanol oxidation, it can be considered as a previous step in the complete oxidation to CO_2. In acid media and on Pt(111) electrodes, the reaction proceeds exclusively through the route that gives acetic acid, whereas Pt(100) electrodes and the stepped surfaces with {110} steps and {111} terraces favor cleavage of C-C bond and the formation of CO [5, 9, 10]. In addition, foreign adatoms are used to promote complete oxidation to CO_2, for example, ruthenium, rhodium or tin [11-13].

Nowadays, research into alkaline fuel cells (AFCs) has regained momentum and the alkaline environment has some advantages. Higher electrocatalytic currents are obtained in comparison with acidic media and it has lower corrosive properties, which opens up the possibility of using less expensive electrocatalysts [14]. However, the technology of AFCs has to overcome two main problems: the carbonation of the system due to CO_2 retention and the difficulty of finding membranes that can sustain operation in alkaline conditions over long periods of time. Nevertheless, new anion-exchange membranes have been developed in recent years to solve these problems [15-17].

To understand the behavior of the possible electrocatalysts, fundamental studies are required. However, there are few studies of ethanol oxidation in alkaline media on platinum electrodes. In only a small number of papers, single-crystal electrodes [18, 19] and polycrystalline surfaces [20, 21] have been used. In these investigations, it is clearly stated that the preferred route for the oxidation is the one that leads to acetaldehyde-acetate production. Additionally, there are some controversies with the oxidation mechanism presented. Koper and Lai [19] observed the presence of CO_{ads} on the platinum surface by using Raman spectroscopy. Conversely, Christensen *et.al* [21] state that no CO_{ads} occurs during ethanol oxidation in this environment and they propose that the observed signals for CO_{ads} in FTIR are due to a pH changes in the thin layer, which shifts to neutral or acidic values.

Herein, we report the influence of the surface structure of Pt single crystals for ethanol oxidation in alkaline media. We used voltammetric and chronoamperometric techniques to study the reactivity of the system and FTIR experiments to find intermediate

and final species formed during ethanol oxidation. These results were used to understand the oxidation mechanism on the Pt surfaces.

4.2 Experimental Section

Platinum single-crystal electrodes were oriented, cut and polished from small single crystal beads (≈2 mm in diameter for the voltammetric experiments and ≈4.5 mm for the spectroelectrochemical measurements) by following the procedure described by Clavilier and co-workers [22, 23]. The electrodes were cleaned by flame annealing for 30 s in an oxygen/gas flame, cooled in a H_2/Ar atmosphere and protected with water in equilibrium with this gas mixture to prevent contamination before immersion in the electrochemical cell, as described in detail elsewhere [23, 24]. The voltammetric profiles and, therefore, the surface structure of the electrodes is stable upon cycling provided that oxide formation is avoided.

Voltammetric and chronoamperometric measurements were carried out by using a waveform generator (EG&EG PARC 175), together with a potentiostat (Amel Model 2053) equipped with ohmic drop compensation and a digital recorder (eDAQ ED401). For the spectroelectrochemical measurements, a Nicolet 8700 spectrometer equipped with a mercury cadmium telluride (MCT) detector was used. The spetroelectrochemical cell was equipped with a CaF_2 prism beveled at 60º [25, 26]. IR spectra were collected with a resolution of 8 cm^{-1} and 100 interferograms for increasing the signal-to-noise ratio. A p-polarized light was used in all FTIR experiments. The spectra are presented as absorbance measurements ($A=-\log (R_1-R_2)/R_1$), where R_2 and R_1 are the reflectance values for the single-beam spectra recorded at the sample and the reference potential, respectively. Positive bands in the spectra correspond to species formed at the sample potential, whereas negative bands are assigned to species consumed. The sample spectra were collected after applying successive potential steps of 100 mV between 0.10 and 0.95 V. A reference spectrum was always recorded at 0.10 V.

Ethanol oxidation experiments were performed in a 0.1 M NaOH + 0.2 M CH_3CH_2OH solution, prepared by using ethanol absolute (Merck p.a.), NaOH (NaOH monohydrate 99.99% Merck Suprapur) and ultrapure water (Elga Purelab Ultra 18.2 MΩ cm). Ar (N50, Air Liquide) was used for deoxygenating the solutions. All the experiments were carried out at RT in a three-electrode electrochemical cell. A platinum wire was used

as a counter-electrode and a reversible hydrogen (N50, Air Liquide) electrode was used as the reference electrode (RHE).

4.3 Results

4.3.1 Ethanol oxidation on Pt basal planes

Fig. 4.1 shows cyclic voltammetric profiles of Pt single-crystal electrodes with basal orientation in alkaline medium, which are in agreement with previous results [27-32]. For these surfaces, the signals appearing in the voltammograms are related to the hydrogen and OH adsorption/desorption processes, in addition to double-layer contributions. These processes are well separated for the Pt(111) electrode and the signals that correspond to hydrogen adsorption can be found at potentials below 0.4 V, whereas OH adsorption occurs at potentials above 0.6 V.

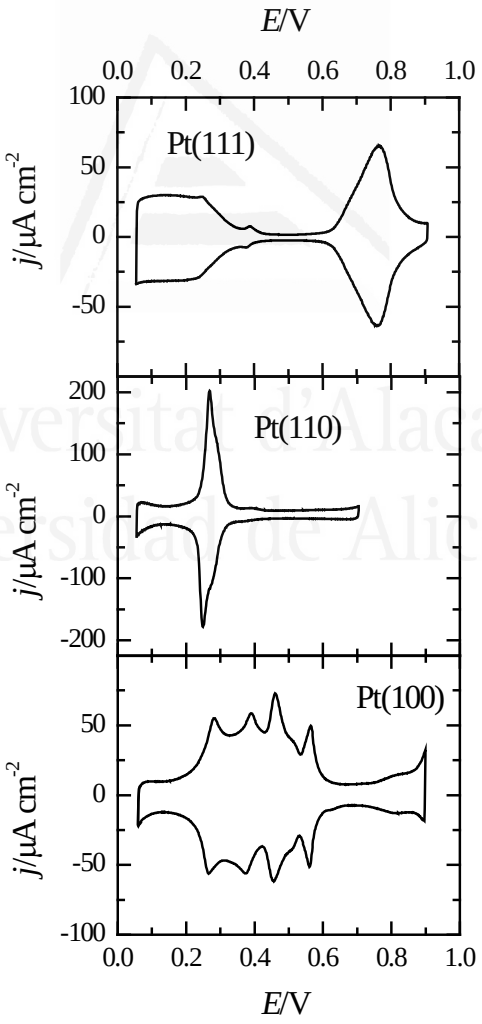

Fig. 4.1. Voltammetric profiles of the Pt(111), Pt(110) and Pt(100) electrodes in 0.1 M NaOH. Scan rate: 0.05 V s^{-1}.

For the other two basal planes, both processes overlap and competitive adsorption between hydrogen and OH takes place. For the Pt(100) electrode, signals at potentials below 0.4 V correspond mainly to the hydrogen adsorption processes, whereas OH adsorption occurs mainly above this potential [29]. For the Pt(110) electrode, the peak at 0.27 V in the positive scan direction corresponds to the desorption of a monolayer of hydrogen and the simultaneous adsorption of OH. Of course, the peak in the negative scan direction at 0.25 V corresponds to the opposite process. When compared with acidic solutions in absence of specific adsorption, that is, in perchloric acid solutions, OH and hydrogen adsorption processes appear in a similar potential range in the RHE scale. However, the detailed shape of the votammograms is markedly affected by the pH.

With ethanol oxidation in 0.1 M NaOH was studied, the measured oxidation currents for the Pt(111) electrode were much higher than those recorded in acidic media (Fig 4.2). The upper potential limit was adjusted to 0.95 V to avoid significant changes in the surface structure due to oxide formation [33, 34].

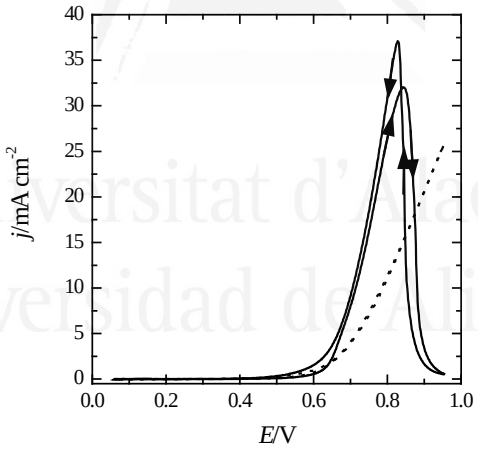

Fig. 4.2. Voltammetric profiles of the Pt(111) electrode (1st cycle) in 0.1 M NaOH + 0.2 M EtOH with (solid line) and without (dotted line) ohmic drop correction at 0.05 V s^{-1}

When the initial voltammogram recorded without ohmic drop compensation (Fig. 4.2, dotted line) was compared with those presented in the literature, some differences were found [18, 19]. Maximum currents and peak potentials were different depending on the data source. Due to the large currents and the lower conductivity of the alkaline solutions in comparison with acidic solutions, the ohmic drop in the electrolyte can affect

the results. The total resistance of the present cell configuration is approximately 200 Ω and the maximum current is around 1 mA. Thus, it is clear that the IR should be corrected to obtain the right voltammogram [35]. It should be noted that resistance in the meniscus can account for more than 80 % of the total resistance due to the small section of liquid in this part. The resistance in the meniscus depends on the electrode area and the meniscus high. Fig. 4.2 clearly shows the effect of ohmic drop correction in the ethanol voltammetric profile on Pt(111) in alkaline medium. A well-defined peak at 0.82 V is observed and peak currents as high as 37 mA cm^{-2} were recorded, significantly higher than those previously reported in the literature [18, 19].

The voltammetric profile for the Pt(111) electrode presents two main characteristics: it has low hysteresis between the positive and negative scan directions and the activity diminishes drastically upon cycling (Fig. 4.3).

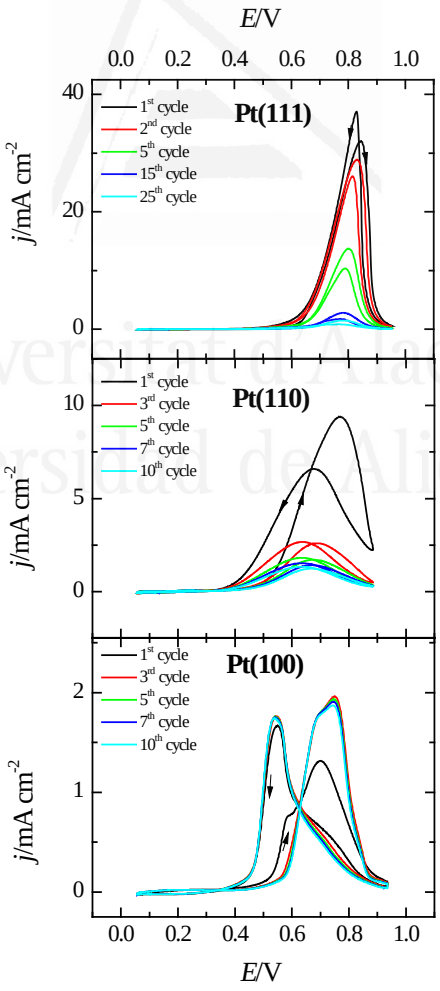

Fig. 4.3. Evolution of the voltammetric profile of the Pt(111), Pt(110) and Pt(100) electrodes upon cycling in 0.1 M NaOH + 0.2 M EtOH at a scan rate of 0.05 V s^{-1}.

In the oxidation of small organic molecules, the hysteresis is normally related to the formation and adsorption of CO at low potentials, which is only oxidized above 0.7 V [36]. The small hysteresis would then indicate that the total amount of CO formed and accumulated on the surface is very small. However, the deactivation is very significant and after 25 cycles the peak current is only a 20^{th} of that measured in the first cycle. It should be remarked that the deactivation depends on the upper potential limit. When the upper potential limit is set below 0.7 V, the activity remains almost constant upon cycling (not shown).

For the other two basal planes, the activity is much lower (Fig. 4.3). For the Pt(110) electrode, the maximum current is approximately 10 mA cm^{-2}, whereas only 2 mA cm^{-2} was measured for the Pt(100) electrode. In both cases, there is a clear hysteresis in the currents and peak potentials. However, this hysteresis is not the typical one associated with the formation and adsorption of CO at low potentials. When CO is accumulated on the surface, as occurs during the oxidation of ethanol or methanol in acid media [5, 37], the currents in the positive scan direction are significantly smaller than those measured in the negative scan direction. Here, peak currents in the positive scan direction are at least as high as those in the negative scan direction. Nevertheless, there is a significant shift in the region were currents are recorded. This is clearly the case for the Pt(100) electrode; in the positive scan direction, the activity for the oxidation of ethanol is obtained between 0.6 and 0.9 V and the peak current is located at 0.75 V, whereas currents for the negative scan direction are measured between 0.8 and 0.45 V with a peak potential at 0.53 V. Additionally, the deactivation upon cycling is negligible for the Pt(100) electrode. However, a significant deactivation is observed for the Pt(110) electrode, although to a lesser extent than that for the aforementioned Pt(111) electrode.

It should be highlighted that the activity order for the low index planes is just the opposite of that observed in acidic media. In this media, the order of peak currents is Pt(100) > Pt(110) > Pt(111) whereas in alkaline solutions the order is Pt(111) > Pt(110) > Pt(100). Another important difference is onset potential. In acid solution, the lower onset for the oxidation is observed for the Pt(111) electrode, whereas in alkaline media the lower onset is for the Pt(110) electrode.

To obtain more information the ethanol-oxidation reaction on those electrodes, chronoamperometric experiments were carried out. Fig. 4.4 shows the transients measured at 0.6 V for the basal planes for 10 minutes. This potential was chosen because it is a potential where ethanol oxidation has started but currents are low and are not controlled by the transport limitations of ethanol. The decay in the transients should be related to the presence of adsorbed species blocking the catalytic surface. The currents measured at 0.6 V follow the expected behavior from the currents measured in the voltammetric profiles at 0.6 V. Thus, the largest currents were measured for the Pt(110) electrode and the lowest for the Pt(111) electrode. For all the electrodes, a decrease in the currents was observed and is proportionally larger for the Pt(110) electrode. As aforementioned, this decay is not related to diffusion problems because the expected limiting diffusion current is more than 10 times larger than that measured here. Additionally, the transient for the Pt(100) electrode shows a small increase in the currents at short times. This process is related to the hysteresis observed in the voltammogram. At 0.6 V, currents in the negative scan direction are larger than those in the positive scan direction. Because the transients were recorded after stepping the electrode from 0.1 V, the initial currents are close to those measured in the positive scan direction at this potential. The current increase is then related to the difference with the negative scan direction. In fact, if the potential is halted at 0.6 V in the positive scan direction during the recording of a voltammogram, the currents increase to reach values close to those measured in the negative scan direction.

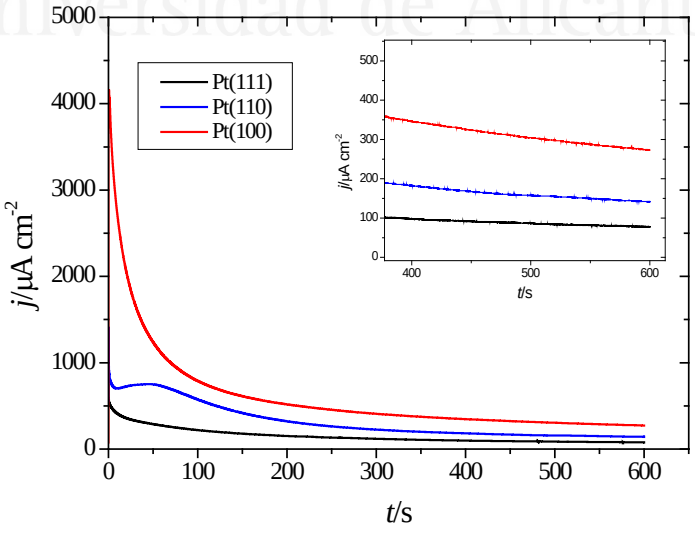

Fig. 4.4. Chronoamperometric transient at 0.6 V for ethanol oxidation on the Pt(111), Pt(110) and Pt(100) electrodes in 0.1 M NaOH + 0.2 M EtOH.

In acidic solutions, it has been found that the presence of steps in the {111} symmetry terrace catalyze the cleavage of the C-C bond [9-12], which is the key step in the mechanism for the oxidation of ethanol to CO_2 (or carbonate in alkaline solutions) and higher currents are measured for those electrodes. For that reason, it is interesting to study the effects of steps on the reactivity of the {111} terraces for ethanol oxidation. Fig. 4.5 shows voltammetric profiles for Pt stepped electrodes.

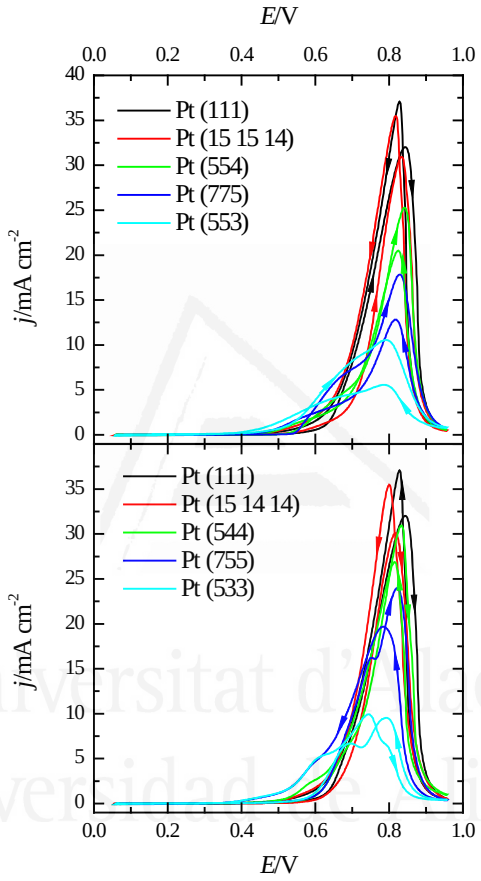

Fig. 4.5. Voltammetric profiles (1st cycle) for Pt stepped electrodes Pt(n,n,n-2) and Pt(n+1,n-1,n-1) in 0.1 M NaOH + 0.2 M EtOH at 0.05 V s^{-1}.

Two series of stepped surfaces that contained {111} terraces and {110} or {100} steps were studied. These surfaces are named Pt(s) [(n-1) (111)×(110)]= Pt(n,n,n-2) for the surfaces with (110) steps and Pt(s)[n(111)×(100)]= Pt(n+1, n-1, n-1), for the surfaces with {100} steps. In these notations, n represents the number of rows in the {111} terrace. For both series, the presence of steps on the {111} terrace does not improve peak current densities, as can be observed in Fig. 4.5. However, the onset potential for the oxidation is

displaced towards more negative potentials and the hysteresis between positive and negative scan directions increases. In fact, the behavior of the surfaces with high step density, namely, Pt(553) and Pt(533) electrodes, begin to resemble that of the {110} and {100} surfaces, respectively. In fact, the Pt(533) electrode shows, in the negative scan direction, significant currents up to 0.35 V.

From these results, it is clear that the activity of these stepped surfaces at high potentials (E>0.6 V) is dominated by the presence of the {111} terraces, whereas the activity at low potentials is dominated by the presence of the steps. In this sense, it can be said that the activity of the {100} step is higher than that of the {110} step because currents for comparable step densities in this region are larger in the negative scan direction. To demonstrate this effect, chronoamperometric transients for these series of surfaces were also recorded at 0.6 V (Fig. 4.6).

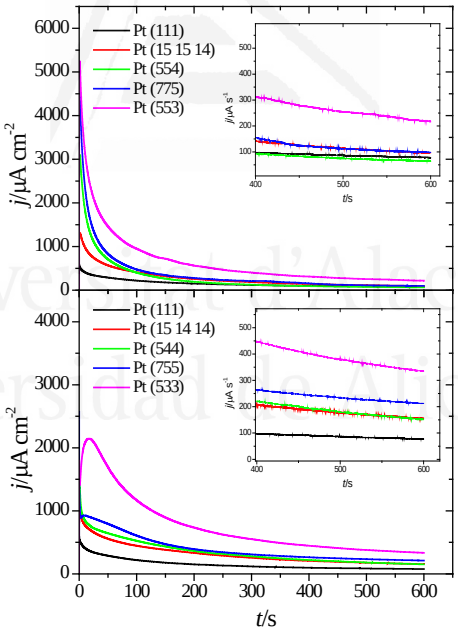

Fig. 4.6. Chronoamperometric transient at 0.6 V for Pt stepped electrodes Pt(n,n,n-2) and Pt(n+1,n-1,n-1) in 0.1 M NaOH + 0.2 M EtOH.

As can be seen, the initial current for the series with {110} steps is larger but the current density decays very fast. On the other hand, for the surfaces with {100} steps, the initial current is smaller but the decay is also smaller and, in some cases, an increase in the

currents is observed. This current increase is especially important for surfaces with a high {100} step density, that is, the Pt(533) surface. As in the case of the Pt(100) surface, the increase has the same origin as the hysteresis observed for the cyclic voltammogram between the positive and negative scan directions. When the activity of the {110} and {100} steps is compared with that of the low-index planes, it can be said that the activity of the (100) step is larger than that measured for the Pt(100) electrode at this potential, as Fig. 4.6 demonstrates. On the other hand, the activity of the {110} step is similar to that of the Pt(110) low-index plane. Thus, the activity order at long times at 0.6 V is the following {100} step > {110} terrace – {110} step > {100} terrace > {111} terrace. The order of reactivity for the steps is also the opposite to that found in acidic media because {110} steps are more reactive in this reaction than {100} steps [9].

4.3.2 FTIR experiments of ethanol oxidation

To find information about the adsorbates and final products formed during the ethanol-oxidation reaction in alkaline medium, FTIR experiments were carried out. Fig. 4.7 shows reference spectra in alkaline solutions for acetate and carbonate, two of the possible final products.

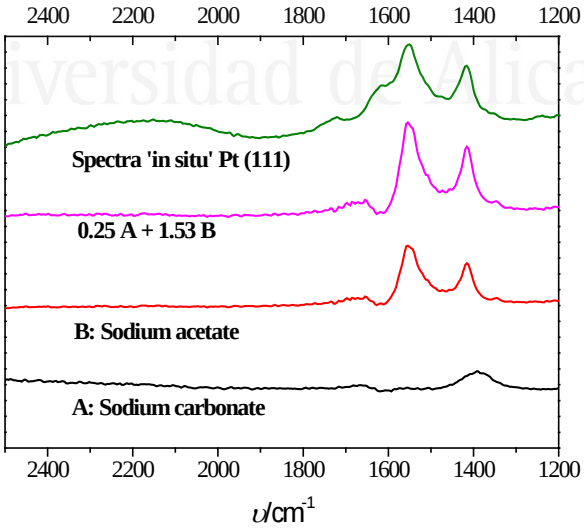

Fig. 4.7. Transmission spectra of 0.2 M acetate and 0.2 M carbonate in 0.1 M NaOH. The spectra of the Pt(111) electrode at 0.8 V in 0.2 M EtOH + 0.1 M NaOH is also shown with its adjusted spectra by using a linear combination of the carbonate and acetate spectra.

It should be mentioned that it is not possible to measure the spectra of acetaldehyde (another possible product) in alkaline solutions because acetaldehyde readily polymerizes through an aldol condensation in this medium. According to the literature [5, 21, 38], the bands at 1550 and 1415 cm^{-1} for acetate correspond to the O-C-O asymmetric and symmetric stretching vibrational modes, respectively. The band at 1390 cm^{-1} for carbonate is also related to the O-C-O vibrational mode.

For the different electrodes, the spectra at different electrode potentials are shown in Fig. 4.8.

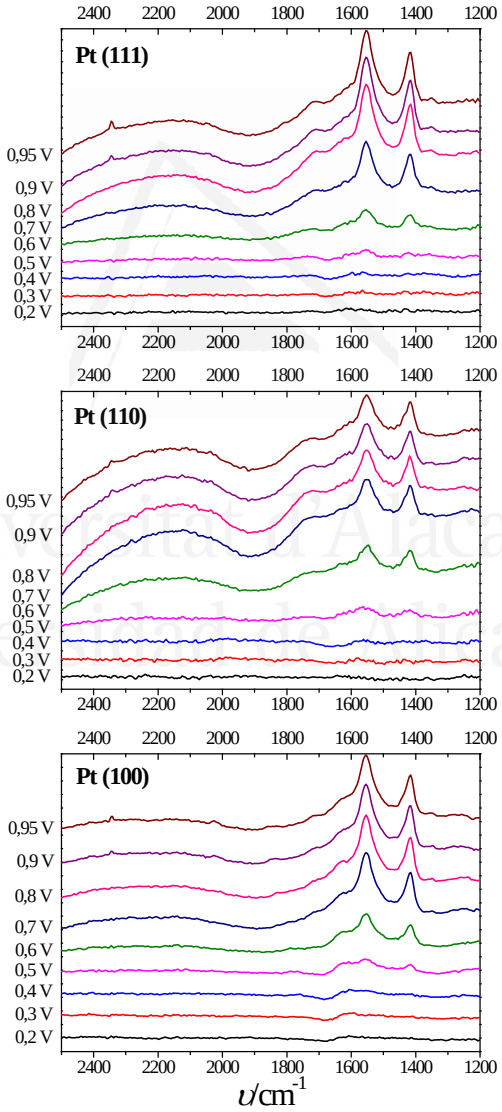

Fig. 4.8. FTIR spectra at different potentials for the Pt(111), Pt(110) and Pt(100) electrodes in 0,2 M EtOH + 0.1 M NaOH. Reference spectra taken at 0.1 V.

As can be seen, only acetate bands are visible. It should be highlighted that the band related to adsorbed CO at low potentials cannot be detected. Adsorbed CO on Pt electrodes in alkaline media shows strong bands at approximately 2030 cm^{-1} [39], and this band is not visible in the spectra of all the studied electrodes, even stepped electrodes. As mentioned, {110} steps are very active for the cleavage of the C-C bond at low potentials, which produces adsorbed CO in acid solutions [9, 10]. At high potentials, a very small band at 2340 cm^{-1} associated to CO_2 can be observed. The presence of this band is indicative of a large shift in the pH of the thin layer used for the spectra acquisition, due to the oxidation of ethanol trough the reactions of Eq. (4.2). Finally, the small band present at 1350 cm^{-1} is assigned to also the acetate group, in accordance with experiments by Zhou *et al.* [38].

In these spectra, the presence of carbonate cannot be discarded a priori because the carbonate band at 1390 cm^{-1} overlaps with the band of acetate at 1415 cm^{-1} [29, 40], which makes it difficult to correctly determine the CO_2/acetate ratio. For this reason, the reference spectra of carbonate and acetate (Fig. 4.7) were used to fit the measured spectra for the different electrodes [38]. The fitting was done in the spectral region between 1260 and 1615 cm^{-1} by using the spectra for acetate and carbonate as input functions and two adjustable parameters in the following expression:

$$f(\nu) = a \cdot g(\nu) + b \cdot h(\nu) \tag{4.3}$$

in which g(ν) and h(ν) are the spectra of acetate and carbonate, respectively, *a* and *b* two adjustable parameters and f(ν) is the fitting function, which is compared with the experimental spectra for the different electrodes. A least-squares method was used to determine the two adjustable parameters. The spectra for the Pt(111) at 0.8 V and the calculated fitting are also shown in Fig. 4.7. The results for the fittings are presented in Table 4.1. As can be seen, the amount of carbonate produced in all cases is low, even for the stepped surfaces that are quite active for the formation of CO_2 in acidic solutions. Only for the Pt(111) electrode can some carbonate be detected (≈14%). This carbonate has been formed above 0.6 V because no CO is detected below this potential. Thus, it can be concluded that the main products of the oxidation in this medium are acetate and acetaldehyde. These results are in agreement with the absence of CO adsorption bands at low potentials and the results obtained by Christensen *et. al.* [21] with polycrystalline electrodes, and suggest that the presence of CO and CO_2 bands are due to depletion of OH^-

in the thin layer, which causes a variation of pH. Thus the preferred route is the incomplete oxidation to acetate.

Electrode	Acetate	Carbonate
Pt(111)	1.53	0.25
Pt(110)	1.22	0.05
Pt(100)	1.39	0.00

Table 4.1. Adjust parameters for the acetate and carbonate spectra for the fitting of the spectra of the different electrodes at 0.8 V.

4.4 Discussion

From the results reported above, it is clear that the main product of ethanol oxidation in alkaline solutions is acetate (and possibly acetaldehyde), although the cleavage of the C-C bond to give CO and CO_2 cannot be completely discarded. Thus, it is important to understand the origin of the significant differences when the behavior of these electrodes is compared to that observed in acidic solutions. First, the high activity of the Pt(111) electrode in alkaline media is clearly associated with a large production of acetic acid. In perchloric acid solutions, chronoamperometric results also indicate that the activity for acetic acid production is very high at very short times [5]. However, the newly formed acetic acid molecules adsorb immediately on the electrode surface as acetate and inhibit the reaction. In fact, it can be considered a self-poisoned reaction [5]. In alkaline media, the activity is also very high, but acetate adsorption does not occur because the absolute potential is approximately 0.7 V more negative. Thus, the reaction can proceed at a high rate without any obstacle.

Although the reaction on the Pt(111) electrode follows the same mechanism in both media and gives mainly acetic acid (or acetate, depending on the pH) at a very high rate, there is an important difference in the onset potential on the RHE scale. In acidic media, the recorded onset for ethanol oxidation is as low as 0.4 V [5], but in alkaline solutions it is above 0.6 V, the region at which OH adsorption on the {111} terrace occurs. In the oxidation of ethanol to acetic acid, an oxygen group should be transferred to the ethanol molecule to give rise to the carboxylic group. This fact suggests that the oxidation process in alkaline solutions is triggered by the adsorption of OH on the surface, which is transferred to the ethanol molecule. However, in acidic solutions, adsorbed OH is not required because the onset for oxidation is at potentials below OH adsorption. In these later media, adsorbed water should then transfer the oxygen group to the ethanol molecule. These changes point to significant differences in the interfacial water properties (and/or adsorbed OH) between acidic and alkaline interfaces, which are probably related to the different absolute potential. Similar conclusions have been obtained when the reactivity of the single-crystal electrodes for the oxygen reduction reaction was studied in acidic and alkaline solutions [41]. For this reaction, the reactivity order in acidic and alkaline media are also completely different. Thus, it can be concluded that the different water structure at

different pH values and/or the absolute electrode potential significantly affect the reactivity of the species in the interfacial region.

With acetate as the major product, the effect of adsorbed OH can also explain the lower onset for ethanol oxidation for the other basal planes and stepped surfaces in 0.1 M NaOH. The onset for OH adsorption on the Pt(100) and Pt(110) is well below 0.6 V and, therefore, the effective transfer of OH to the ethanol molecule can occur at lower potentials. For Pt(100), the onset in the negative scan direction is at approximately 0.4 V, which coincides with the initial potential for OH adsorption on this plane. For the (110) surface, the onset is even lower in the negative scan direction and in this plane, OH adsorption occurs at potentials as low as 0.26 V.

Another important characteristic of the voltammetric profiles of all the electrodes studied here (except the Pt(111) electrode) is that the large hysteresis is not related to the formation of CO, as mentioned earlier. By using Raman spectra and polycrystalline electrodes Koper and co-worker proposed that CH_x species are adsorbed on the electrode surface [19] and these species could be the origin of the hysteresis. They are formed at low potential and partially block the surface, which inhibits the oxidation, and are oxidized at high potentials. However, spectroscopic signals for these adsorbed species are not accessible in infrared due to the interference of the window material in the spectral region of interest. For that reason, it is not possible to validate this hypothesis, although the possible origin of signals corresponding to CH_x species will be discussed below. However, if the oxidation is linked to the presence of OH on the surface, it is also possible that the hysteresis could be related to some irreversibility in the OH adsorption. In acid media, OH adsorption processes are completely reversible at 50 mV/s, which gives rise to a symmetrical voltammetric profile. In alkaline solutions, some irreversibility is observed because the peak potentials for OH adsorption on the Pt(100) and Pt(110) electrodes is not same in both scan directions. Thus, it is possible that the presence of ethanol increases the irreversibility of this process and gives rise to a large hysteresis.

Another problem in the oxidation of ethanol in alkaline media is the fast deactivation of the surface. This process cannot be linked to the formation of CO because it has not been detected on the surface and would have been completely oxidized at the upper

potential limit. Thus, another species, which could not be detected by IR, is responsible for the deactivation of the surface. It should be borne in mind that the spectrum for acetaldehyde could not be measured in alkaline solutions due to its reactivity, and for that reason acetaldehyde formation cannot be detected. However, during the oxidation of ethanol to acetic acid in acidic media, acetaldehyde is always formed. Therefore, in alkaline media, it can be proposed that acetaldehyde is also produced, and this molecule could be the cause of the deactivation after polymerization.

To determine the electrochemical properties of this blocking species, and the role of ethanol and acetaldehyde in this process, different voltammetric experiments with ethanol and acetaldehyde were carried out. In the first experiment, four voltammetric cycles for ethanol oxidation were recorded for the Pt(111) electrode (which has the highest deactivation rate) in 0.1 M NaOH + 0.2 M EtOH (Fig. 4.9A, dashed lines). After the fourth cycle, a clear deactivation of the surface was observed. Then the electrode was transferred to a cell containing only 0.1 M NaOH and the voltammetric profile was recorded and compared with that obtained for a newly prepared Pt(111) surface (Fig. 4.9B). As can be seen, after recording the ethanol oxidation curves, the surface is partially blocked by some species, because the hydrogen and OH adsorption charges are smaller than those measured for a clean Pt(111) electrode.

In the initial cycle, there is still some ethanol close to the interface and the extra current recorded at E>0.6 V in the first cycle is due to the oxidation of trace ethanol. However, the voltammogram is stable upon cycling and the blocking species cannot be removed if the electrode is cycled up to 0.9 V, even if the lower potential limit is set in the hydrogen evolution region (not shown). Once the profiles in the blank electrolyte were recorded, the electrode was transferred back to the solution that contained ethanol (Fig. 4.9A, solid line). As can be seen, the voltammetric profile corresponds to the one that would have been obtained without the transfer experiment, that is, the profile corresponds to the fifth cycle. Taking into account that the deactivation is linked to the oxidation of ethanol, the species responsible for this deactivation is stable on the surface and does not suffer any oxidation or reduction process at E < 0.95 V.

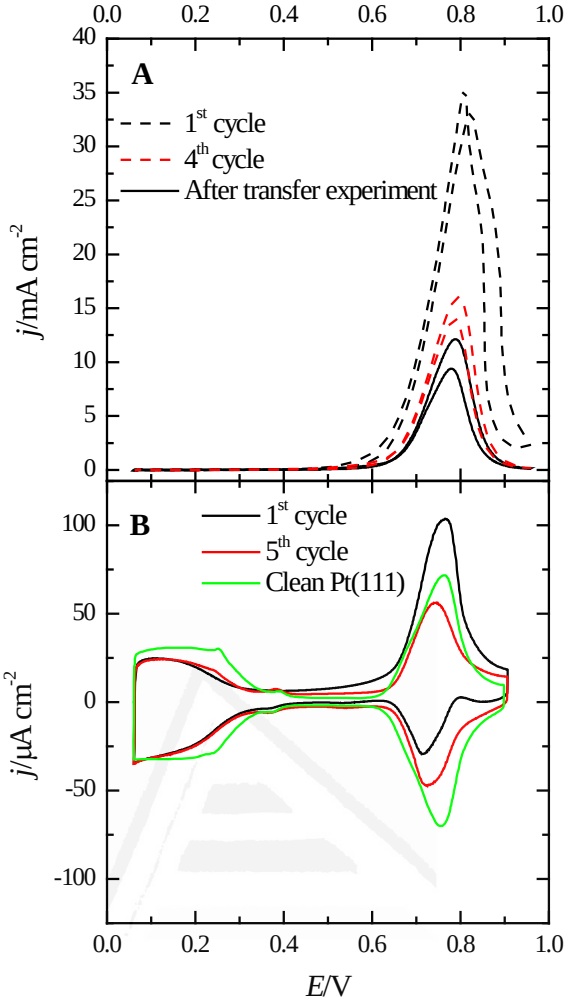

Fig. 4.9. A) Voltammetric profile of a Pt(111) electrode in 0.1 M NaOH + 0.2 M EtOH: Black and red dashed lines: 1st and 4th cycle. Solid line: initial cycle after recording experiment in panel B. B) Voltammetric profile of a Pt(111) electrode in 0.1 M NaOH after recording the 4th cycle in A). The voltammetric profile of a clean Pt(111) electrode is also shown for comparison (green line). Scan rate 0.05 V s^{-1}.

If the experiment is repeated but includes a rinsing step with water after recording the ethanol-oxidation cycles, the curves shown in Fig. 4.10 are obtained. As can be seen, after rinsing the electrode with water, the blocking species were completely removed and the voltammogram of a clean Pt(111) electrode is immediately recovered. Moreover, the initial activity of the electrode for ethanol oxidation is also recovered, as demonstrated by the voltammetric profile of the electrode after re-immersion of the electrode in the ethanol-containing solution. This experiment indicates that the blocking species does not survive at neutral pH values.

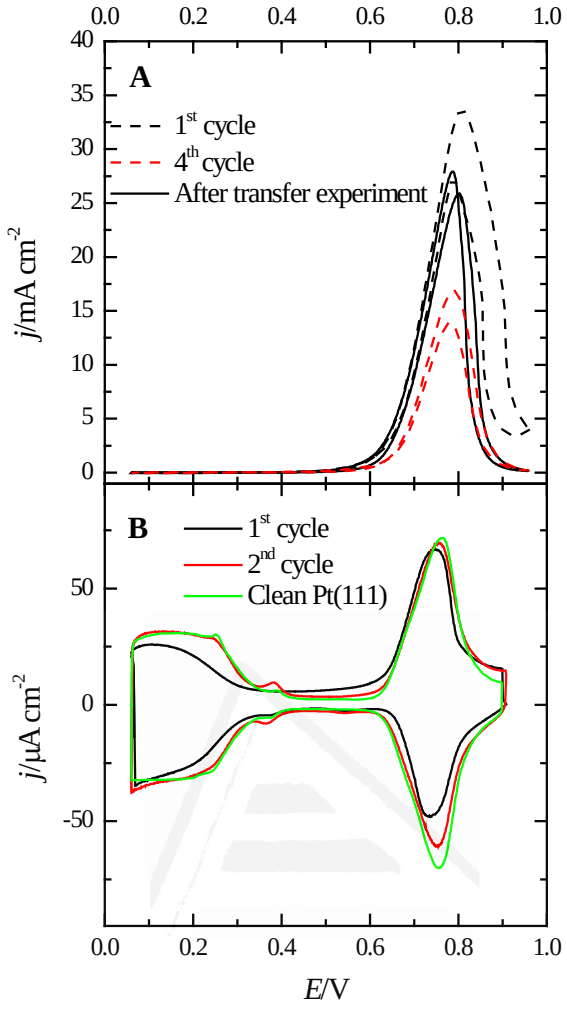

Fig. 4.10. A) Voltammetric profile of a Pt(111) electrode in 0.1 M NaOH + 0.2 M EtOH: Black and red dashed lines: 1st and 4th cycle. Full line, initial cycle after recording experiment in panel B. B) Voltammetric profile of a Pt(111) electrode in 0.1 M NaOH after recording the 4th cycle in A) and rinsing the electrode with water. The voltammetric profile of a clean Pt(111) electrode is also shown for comparison (green line). Scan rate 0.05 V s^{-1}.

To determine the role of acetaldehyde, the same experiments as in Fig. 4.9 and Fig. 4.10 were performed, but by using a 0.1 M NaOH + 0.2 M acetaldehyde solution. As can be seen in Fig. 4.11, acetaldehyde is not oxidized in this medium and the surface becomes instantly blocked by adsorbed species. When the electrode is transferred to the cell that contained 0.1 M NaOH, the surface was almost completely deactivated and the adsorbed species were not oxidized or reduced. Only rinsing the electrode with water removed the blocking species, in the same way as observed in Fig. 4.10. Thus, it is clear that the decrease in activity is linked to the production of acetaldehyde. Probably, as soon

acetaldehyde is produced, it readily dimerizes and adsorbs on the surface and hinders the ethanol-oxidation reaction.

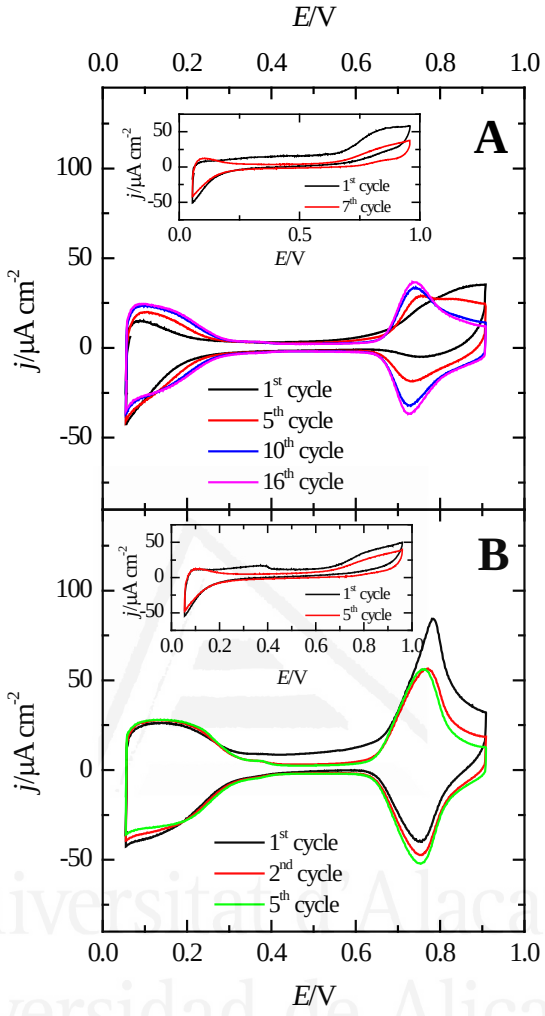

Fig. 4.11. A) Voltammetric profile of a Pt(111) electrode in 0.1 M NaOH after recording the voltammetric profiles in the inset. Inset: Voltammetric profile of a Pt(111) electrode in 0.1 M NaOH + 0.2 M acetaldehyde. B) As for A), but the electrode was rinsed prior to immersion in the cell that contained 0.1 M NaOH.

This blocking mechanism also explains why the decrease of current upon cycling follows the order Pt(111) > Pt(110) > Pt(100). This order is also the order of maximum currents. If the inhibition is linked to the formation of acetaldehyde, the higher the currents for the oxidation of ethanol are, the higher the amounts of acetaldehyde that are formed. Thus, when the Pt(111) electrode is cycled up to 0.65 V, with low oxidation currents, the poisoning of the electrode is very small and no poisoning is recorded. Also, it is in

agreement with the Raman experiments [19], from which adsorbed CH_x is proposed as the inhibiting species. The CH_x is clearly present in acetaldehyde or any polymerization product and can adsorb on the electrode surface. This fact also explains why it has been proposed that the adsorption of CH_x occurs particularly in the {111} domains, because that domain has higher oxidation currents. As has been shown by using both voltammetry and chronoamperometry, the higher the currents are, the faster the deactivation is observed.

4.5 Conclusions

The results presented here clearly show that the reactivity of platinum electrodes for ethanol oxidation is affected by the solution pH. The solution pH alters the water structure of the interfacial region and also the absolute potential range in which the oxidation occurs. Both factors clearly change the reactivity of platinum. In alkaline solutions, higher peak currents are measured, although the selectivity for CO_2 production is much lower. Additionally, the surfaces deactivate fast due to the production of acetaldehyde, which readily polymerizes in this medium, adsorbs on the electrode surface, and prevents further reaction.

4.6 References

[1] M. T. M. Koper, "Fuel Cell Catalysis: A Surface Science Approach", *Electrocatalysis and Electrochemistry* A. Wieckowski (Ed.), John Wiley & Sons, Hoboken, New Jersey, **2009**.

[2] E. Antolini, "Catalysts for direct ethanol fuel cells" *Journal of Power Sources* **2007**, 170, 1-12.

[3] W. Zhou, Z. Zhou, S. Song, W. Li, G. Sun, P. Tsiakaras and Q. Xin, "Pt based anode catalysts for direct ethanol fuel cells" *Applied Catalysis B: Environmental* **2003**, 46, 273-285.

[4] C. Lamy, S. Rousseau, E. M. Belgsir, C. Coutanceau and J. M. Léger, "Recent progress in the direct ethanol fuel cell: development of new platinum-tin electrocatalysts" *Electrochimica Acta* **2004**, 49, 3901-3908.

[5] F. Colmati, G. Tremiliosi-Filho, E. R. Gonzalez, A. Berná, E. Herrero and J. M. Feliu, "Surface structure effects on the electrochemical oxidation of ethanol on platinum single crystal electrodes" *Faraday Discussions* **2008**, 140, 379-397.

[6] N. M. Markovic and P. N. Ross, "Surface science studies of model fuel cell electrocatalysts" *Surface Science Reports* **2002**, 45, 117-229.

[7] V. Grozovski, V. Climent, E. Herrero and J. M. Feliu, "The role of the surface structure in the oxidation mechanism of methanol" *Journal of Electroanalytical Chemistry* **2011**, 662, 43-51.

[8] C. Lamy, J. M. Léger, J. Clavilier and R. Parsons, "Structural effects in electrocatalysis: A comparative study of the oxidation of CO, HCOOH and CH_3OH on single crystal Pt electrodes" *Journal of Electroanalytical Chemistry* **1983**, 150, 71-77.

[9] F. Colmati, G. Tremiliosi-Filho, E. R. Gonzalez, A. Berná, E. Herrero and J. M. Feliu, "The role of the steps in the cleavage of the C-C bond during ethanol oxidation on platinum electrodes" *Physical Chemistry Chemical Physics* **2009**, 11, 9114-9123.

[10] J. Souza-Garcia, E. Herrero and J. M. Feliu, "Breaking the C-C Bond in the Ethanol Oxidation Reaction on Platinum Electrodes: Effect of Steps and Ruthenium Adatoms" *ChemPhysChem* **2010**, 11, 1391-1394.

[11] V. Del Colle, A. Berná, G. Tremiliosi-Filho, E. Herrero and J. M. Feliu, "Ethanol electrooxidation onto stepped surfaces modified by Ru deposition: electrochemical and spectroscopic studies" *Physical Chemistry Chemical Physics* **2008**, 10, 3766-3773.

[12] V. Del Colle, J. Souza-Garcia, G. Tremiliosi-Filho, E. Herrero and J. M. Feliu, "Electrochemical and spectroscopic studies of ethanol oxidation on Pt stepped surfaces modified by tin adatoms" *Physical Chemistry Chemical Physics* **2011**, 13, 12163-12172.

[13] J. P. I. de Souza, S. L. Queiroz, K. Bergamaski, E. R. Gonzalez and F. C. Nart, "Electro-oxidation of ethanol on Pt, Rh, and PtRh electrodes. A study using DEMS and in-situ FTIR techniques" *Journal of Physical Chemistry B* **2002**, 106, 9825-9830.

[14] E. Antolini and E. R. Gonzalez, "Alkaline direct alcohol fuel cells" *Journal of Power Sources* **2010**, 195, 3431-3450.

[15] J. S. Spendelow and A. Wieckowski, "Electrocatalysis of oxygen reduction and small alcohol oxidation in alkaline media" *Physical Chemistry Chemical Physics* **2007**, 9, 2654-2675.

[16] J. R. Varcoe, R. C. T. Slade, E. L. H. Yee, S. D. Poynton, D. J. Driscoll and D. C. Apperley, "Poly(ethylene-co-tetrafluoroethylene)-derived radiation-grafted anion-exchange membrane with properties specifically tailored for application in metal-cation-free alkaline polymer electrolyte fuel cells" *Chemistry of Materials* **2007**, 19, 2686-2693.

[17] C. Coutanceau, L. Demarconnay, C. Lamy and J. M. Léger, "Development of electrocatalysts for solid alkaline fuel cell (SAFC)" *Journal of Power Sources* **2006**, 156, 14-19.

[18] M. López-Atalaya, E. Morallón, F. Cases, J. L. Vázquez and J. M. Pérez, "Electrochemical oxidation of ethanol on Pt(hkl) basal surfaces in NaOH and Na_2CO_3 media" *Journal of Power Sources* **1994**, 52, 109-117.

[19] S. C. S. Lai and M. T. M. Koper, "Ethanol electro-oxidation on platinum in alkaline media" *Physical Chemistry Chemical Physics* **2009**, 11, 10446-10456.

[20] B. Pierozynski, "On the Ethanol Electrooxidation Reaction on Catalytic Surfaces of Pt in 0.1 M NaOH" *International Journal of Electrochemical Science* **2012**, 7, 4261-4271.

[21] P. A. Christensen, S. W. M. Jones and A. Hamnett, "In Situ FTIR Studies of Ethanol Oxidation at Polycrystalline Pt in Alkaline Solution" *Journal of Physical Chemistry C* **2012**, 116, 24681-24689.

[22] J. Clavilier, D. Armand, S. G. Sun and M. Petit, "Electrochemical adsorption behaviour of platinum stepped surfaces in sulphuric acid solutions" *Journal of Electroanalytical Chemistry* **1986**, 205, 267-277.

[23] C. Korzeniewski, V. Climent and J. M. Feliu, "Electrochemistry at Platinum Single Crystal Electrodes", in *Electroanalytical Chemistry: A Series of Advances, vol. 24*, A. J. Bard and C. Zoski (Eds.) CRC Press, Boca Ratón, **2012**, pp. 75-169.

[24] A. Rodes, K. El Achi, M. A. Zamakhchari and J. Clavilier, "Hydrogen probing of step and terrace sites on Pt(S)-[n(111) × (100)]" *Journal of Electroanalytical Chemistry* **1990**, 284, 245-253.

[25] T. Iwasita, F. C. Nart and W. Vielstich, "An FTIR study of the catalytic activity of a 85:15 Pt:Ru alloy for methanol oxidation" *Berichte der Bunsen-Gesellschaft fuer Physikalische Chemie* **1990**, 94, 1030-1034.

[26] A. Rodes, J. M. Pérez and A. Aldaz, "Vibrational spectroscopy", in *Handbook of Fuel Cells - Fundamentals, Technology and Applications, vol. 2*, W. Vielstich, A. Lamm and H. A. Gasteiger (Eds.) Wiley, Chichester, **2003**, pp. 191-219.

[27] F. J. Vidal-Iglesias, N. García-Aráez, V. Montiel, J. M. Feliu and A. Aldaz, "Selective electrocatalysis of ammonia oxidation on Pt(100) sites in alkaline medium" *Electrochemistry Communications* **2003**, 5, 22-26.

[28] J. S. Spendelow, J. D. Goodpaster, P. J. A. Kenis and A. Wieckowski, "Mechanism of CO oxidation on Pt(111) in alkaline media" *Journal of Physical Chemistry B* **2006**, 110, 9545-9555.

[29] R. M. Arán-Ais, M. C. Figueiredo, F. J. Vidal-Iglesias, V. Climent, E. Herrero and J. M. Feliu, "On the behavior of the Pt(100) and vicinal surfaces in alkaline media" *Electrochimica Acta* **2011**, 58, 184-192.

[30] P. Rodríguez, G. García, E. Herrero, J. Feliu and M. Koper, "Effect of the Surface Structure of Pt(100) and Pt(110) on the Oxidation of Carbon Monoxide in Alkaline Solution: an FTIR and Electrochemical Study" *Electrocatalysis* **2011**, 2, 242-253.

[31] E. Morallón, J. L. Vázquez and A. Aldaz, "Electrochemical-Behavior of Basal Single-Crystal Pt Electrodes in Alkaline-Medium" *Journal of Electroanalytical Chemistry* **1990**, 288, 217-228.

[32] N. S. Marinkovic, N. M. Markovic and R. R. Adzic, "Hydrogen Adsorption on Single-Crystal Platinum-Electrodes in Alkaline-Solutions" *Journal of Electroanalytical Chemistry* **1992**, 330, 433-452.

[33] A. Björling, E. Herrero and J. M. Feliu, "Electrochemical Oxidation of Pt(111) Vicinal Surfaces: Effects of Surface Structure and Specific Anion Adsorption" *Journal of Physical Chemistry C* **2011**, 115, 15509-15515.

[34] A. Björling and J. M. Feliu, "Electrochemical surface reordering of Pt(111): A quantification of the place-exchange process" *Journal of Electroanalytical Chemistry* **2011**, 662, 17-24.

[35] I. Z. Kiss, E. Sitta and H. Varela, "On the Limit of Frequency of Electrochemical Oscillators and Its Relationship to Kinetic Parameters" *Journal of Physical Chemistry C* **2012**, 116, 9561-9567.

[36] M. T. M. Koper, S. C. S. Lai and E. Herrero, "Mechanisms of the Oxidation of Carbon Monoxide and Small Organic Molecules at Metal Electrodes", in *Fuel Cell Catalysis, A Surface Science Approach*, M. T. M. Koper (Ed.) John Wiley & Sons, Inc, Hoboken, NJ, **2009**, pp. 159-208.

[37] E. Herrero, K. Franaszczuk and A. Wieckowski, "Electrochemistry of Methanol at Low Index Crystal Planes of Platinum: An Integrated Voltammetric and Chronoamperometric Study" *Journal of Physical Chemistry* **1994**, 98, 5074-5083.

[38] Z.-Y. Zhou, Q. Wang, J.-L. Lin, N. Tian and S.-G. Sun, "In situ FTIR spectroscopic studies of electrooxidation of ethanol on Pd electrode in alkaline media" *Electrochimica Acta* **2010**, 55, 7995-7999.

[39] M. J. S. Farias, C. Busó-Rogero, R. Gisbert, E. Herrero and J. M. Feliu, "Influence of the CO Adsorption Environment on Its Reactivity with (111) Terrace Sites in Stepped Pt Electrodes under Alkaline Media" *The Journal of Physical Chemistry C* **2013**, 118, 1925-1934.

[40] T. Iwasita, A. Rodes and E. Pastor, "Vibrational Spectroscopy of Carbonate Adsorbed on Pt(111) and Pt(110) Single-Crystal Electrodes" *Journal of Electroanalytical Chemistry* **1995**, 383, 181-189.

[41] R. Rizo, E. Herrero and J. M. Feliu, "Oxygen reduction reaction on stepped platinum surfaces in alkaline media" *Physical Chemistry Chemical Physics* **2013**, 15, 15416-15425.

Capítulo 5:

Oxidación de etanol en nanopartículas de platino: efecto de la estructura superficial y de la agregación en medio alcalino

<u>Capítulo 5</u>: Oxidación de etanol en nanopartículas de platino: efecto de la estructura superficial y de la agregación en medio alcalino

RESUMEN

El objetivo de este capítulo es estudiar la oxidación de etanol en 0.1 M NaOH con nanopartículas de platino, un sistema más útil desde un punto de vista aplicado, incidiendo en el efecto de la estructura superficial (empleando las mismas muestras del capítulo 2), además de un estudio de la aglomeración de partículas esféricas soportadas en carbón, que provocan dificultades en la difusión del etanol sobre el catalizador.

Primero de todo, se realiza la habitual caracterización electroquímica *in-situ* con voltametría cíclica, además de una caracterización física *ex situ* mediante TEM, para obtener las formas predominantes en cada muestra de nanopartículas junto a su tamaño promedio. Posteriormente, se realizan las voltametrías cíclicas para la oxidación de 0.2 M CH_3CH_2OH + 0.1 M NaOH con las nanopartículas de platino de diferentes formas. Los resultados concuerdan con los obtenidos en el capítulo 4 con superficies monocristalinas de platino, siendo el orden de reactividad, determinado por la corriente de pico: (111)Pt > (100-111)Pt > (100)Pt > (poly)Pt. Los dominios con orientación {111} son los que presentan las mayores corrientes de oxidación, aunque el potencial de inicio de oxidación de etanol se desplaza a potenciales más positivos. La explicación a esta elevada actividad es la nula adsorción del anión acetato en medio alcalino, mientras que las diferencias en el potencial de inicio de la oxidación entre las distintas muestras de nanopartículas de platino se debe a que la adsorción del OH (necesaria para iniciar la oxidación de etanol) varía, dependiendo de la orientación cristalográfica de la superficie de platino.

Las cronoamperometrías realizadas con estas mismas muestras tienen como objetivo comprobar la estabilidad temporal del catalizador a un potencial de 0.6 V, donde la

oxidación de etanol ha comenzado pero las corrientes no son demasiado grandes como para tener dificultades en cuanto al transporte del etanol hacia la superficie del electrodo. Las corrientes medidas también siguen la tendencia esperada según las voltametrías cíclicas anteriores. La causa de la caída de corriente con el paso del tiempo se asocia con la formación de acetaldehído y su posterior dimerización. De los experimentos de FTIR, únicamente se puede corroborar la formación mayoritaria de acetato, independientemente de la muestra de nanopartículas empleada. Además, se confirman los menores potenciales necesarios para la aparición de las bandas en el caso de las muestras (100)Pt y (poly)Pt.

En cuanto al efecto de la aglomeración de nanopartículas, previo a su estudio en la oxidación de etanol, la misma caracterización realizada anteriormente se efectuó en las muestras de nanopartículas soportadas en carbón. La microscopía TEM muestra una mayor dispersión de partículas en la muestra de Pt(10%) y mayores aglomerados en muestras como la de Pt(50%), además de tamaños similares para todos los casos estudiados, descartando problemas de sinterización durante el depósito de mayor cantidad de nanopartículas. La caracterización electroquímica muestra picos de adsorción de hidrógeno parecidos a los de una superficie de platino poliorientada. Al normalizar al área electroactiva de platino, el aumento en la cantidad de Pt en las muestras provoca que la contribución aparente de la doble capa propia del carbón vaya disminuyendo. La relación lineal observada en el cociente entre las corrientes de pico debidos al platino y la de la doble capa asociada al carbón vítreo frente a la cantidad de platino presente en la muestra indica que todo el depósito de nanopartículas contribuye a la reacción electroquímica de adsorción de hidrógeno, además de confirmar que el área de la carga de adsorción de hidrógeno se puede utilizar para calcular el área activa del platino.

Posteriormente, se estudia el efecto de la aglomeración de estas nanopartículas esféricas para la oxidación de etanol en medio alcalino. Conforme aumenta la cantidad de Pt en las muestras, la densidad de corriente para la oxidación de etanol va decreciendo a causa del difícil acceso de las moléculas de etanol hacia el depósito entero de nanopartículas, siendo solamente activa la parte más externa del depósito de catalizador. Se considera la oxidación de etanol sobre la muestra de Pt(10%) como la corriente que se obtiene en ausencia de limitaciones de difusión, como se demuestra al comparar con un electrodo de Pt poliorientado ciclado, ya que se obtienen corrientes parecidas. Con el

propósito de evitar los problemas de aglomeración de nanopartículas de platino, se realiza el secado del depósito de las nanopartículas mientras se rota el depósito de carbón vítreo a una velocidad de 700 rpm. Con esto, es más uniforme la distribución de las partículas después de la rotación del soporte de carbón vítreo. El resultado positivo sobre la oxidación de etanol se demuestra en la Fig. 5.12: a bajos potenciales las densidades de corriente siguen siendo similares mientras que a altos potenciales las densidades de corriente son mayores cuando el depósito es uniforme, corroborando la mejora en la actividad después de preparar el depósito secando a la vez que se rota el electrodo y su mejor comportamiento para la electrooxidación de etanol.

Chapter 5

J Solid State Electrochem (2016) 20:1095–1106
DOI 10.1007/s10008-015-2970-0

ORIGINAL PAPER

Oxidation of ethanol on platinum nanoparticles: surface structure and aggregation effects in alkaline medium

Carlos Busó-Rogero[1] · Jose Solla-Gullón[1] · Francisco J. Vidal-Iglesias[1] · Enrique Herrero[1] · Juan M. Feliu[1]

Received: 16 May 2015 / Revised: 9 July 2015 / Accepted: 12 July 2015 / Published online: 23 July 2015

Abstract The ethanol oxidation reaction in 0.1 M NaOH on Pt nanoparticles with different shapes and loadings was investigated using electrochemical and spectroscopic techniques. The surface structure effect on this reaction was studied using well-characterized platinum nanoparticles. Regardless of the type of Pt nanoparticles used, results show that acetate is the main product with negligible CO_2 formation. From the different samples used, the nanoparticles with a large amount (111) of ordered domains have higher peak currents and a higher onset potential, in agreement with previous works with single crystal electrodes. In addition, spherical platinum nanoparticles supported on carbon with different loadings were used for studying possible diffusional problems of ethanol to the catalyst surface. The activity in these samples diminishes with the increase of Pt loading, due to diffusional problems of ethanol throughout the whole Pt nanoparticle layer, being the internal part of the catalyst layer inactive for the oxidation. To avoid this problem and prepare more dispersed nanoparticle catalyst layers, deposits were dried while the carbon support was rotated to favor the dispersion of the layer around the support. The improvement in the electrocatalytic activity for ethanol oxidation confirms the better performance of this procedure for depositing and drying.

This chapter has been adapted and formatted from Journal of Solid State Electrochemistry **2016,** 20, 1095-1106.

Corresponding authors: herrero@ua.es and juan.feliu@ua.es

5.1 Introduction

Platinum is one on the most studied materials for its use as anode and/or cathode in the fuel cell technology [1, 2]. Most of the electrochemical reactions occurring in fuel cells are structure sensitive, that is, depending on the crystallographic orientation of the atoms on the catalyst surface, the electrocatalytic activity changes. With the aim of understanding this effect, platinum single crystal electrodes with a well-known surface structure are used for fundamental studies of reactions with practical use in fuel cells [3-9]. However, single crystal electrodes are not very useful from an applied point of view, and electrocatalysts are usually presented in the form of nanoparticles. The effects of surface structure are still important in nanoparticles, so it is necessary to control the atom arrangement on the catalyst surface. With this aim, nanoparticles with different shapes, that is, with different distribution of well-ordered crystallographic domains, have been synthesized. These different nanoparticles have previously allowed extending the correlations between surface structure and reactivity observed with single crystal electrodes for several reactions such as the oxidations of formic acid, methanol, ethanol or ammonia [10-13] or the reduction of oxygen [14]. Additionally, in some cases, the behavior of the nanoparticle electrodes differs from that observed with single crystal electrodes [15, 16].

Among the molecules reacting in the anode of fuel cells, ethanol presents some advantages: it is possible to be obtained directly from biomass, it is easy to store and it has a higher energy density in the complete oxidation to CO_2. In this reaction, 12 e^- are exchanged:

$$CH_3CH_2OH + 3\,H_2O \longrightarrow 2\,CO_2 + 12\,H^+ + 12\,e^- \qquad (5.1)$$

The thermodynamic standard potential is 0.085 V vs SHE, giving a standard potential of 1.145 V for ethanol-oxygen fuel cell [17]. Nevertheless, the formation of many undesired products and by-products due to its complex oxidation process, in addition to the difficulty for breaking the C-C bond of ethanol at low temperatures, cause a decrease in the efficiency of the ethanol fuel cell.

As observed for other fuels, ethanol oxidation is a structure sensitive reaction on platinum electrodes [18]. The oxidation mechanism in acidic solutions has a dual-path mechanism:

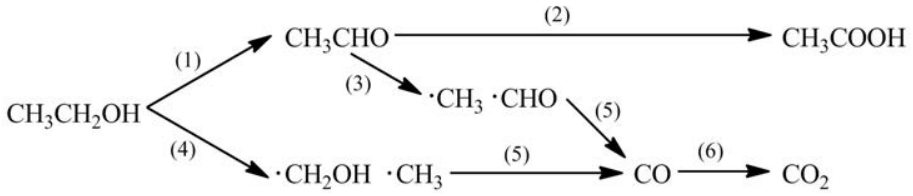

(5.2)

Steps (1) and (2) correspond to the incomplete oxidation route to acetic acid. Step (1) presents the formation of acetaldehyde, exchanging two electrons for this process, whereas step (2) displays the final acetic acid formation with the exchange of two additional electrons. Acetic acid is considered as a final product, because it is very difficult to oxidize at room temperature [19]. Steps (3) and (4) represent the reaction steps that lead to the C-C bond scission necessary for achieving the complete oxidation to CO_2, forming one-carbon fragments from ethanol or acetaldehyde [20, 21]. Behm's group [22, 23] have proposed acetyl species as the active intermediate for these CH_x and one carbon oxygenated fragments, which is quickly transformed in CO through the reaction step (5). CO is strongly adsorbed on the Pt surface and hinders the electrocatalytic response of the electrode. The final oxidation to CO_2 is presented in the step (6). On Pt(111) electrodes, only the incomplete oxidation to acetic acid is observed in acidic medium, whereas on Pt(110) and, mainly, on Pt(100), the breakage of the C-C bond and, consequently, CO formation is favored in the same medium [18]. The strategies to improve the electrocatalysis of this reaction seek electrode materials that increase the rate of the C-C bond cleavage and catalyze step (6) at lower potentials. Some alternatives for platinum are the use of {110} stepped surfaces on {111} terraces [24] or the presence of foreign atoms adsorbed on the Pt surface [25-29].

A change in the reactivity in the electrooxidation of small organic molecules such as C_1-C_2 alcohols is normally observed in alkaline solutions showing higher activities than in acidic solutions [30]. This fact, together with other advantages of the alkaline medium, such as the lower corrosive properties (allowing the use of cheaper catalysts) [31], have triggered fundamental studies in the electrocatalysis of these systems for alkaline fuel cells (AFCs). However, there are mainly two problems when working at higher pH values: the carbonation of the system due to the CO_2 trapping and the necessity of finding membranes capable of working in these pH values. Fortunately, new membranes have been developed recently [32, 33] for overcoming this problem. Some positive results have been obtained for the complete oxidation of ethanol working in alkaline solutions [34] with membrane

electrode assemblies (MEAs), obtaining efficiency values of 55% for CO_2 at 60ºC, improving the efficiency of 2% observed in the same conditions for acidic solutions.

Ethanol oxidation mechanism on platinum is also structure sensitive in alkaline medium, but the ratio between the products is different from that in acid medium. A previous work done by our group with single crystal electrodes using electrochemical and FTIR techniques at room temperature [35] showed the preference for the acetate formation independently of the surface structure of the electrodes. In this medium, CO_2 formation bands in FTIR were almost negligible and mainly related to pH changes in the thin layer configuration. These results agree with infrared experiments done by Christensen *et al.* with polycrystalline electrodes [36] or older results with single crystal electrodes [37]. However, Lai *et al.* proposed, according with Raman experiments, the adsorption of CO and CH_x species on {111} platinum sites during ethanol oxidation [38]. Finally, as in acidic solutions, some studies try to achieve the complete oxidation in alkaline media by adding foreign atoms adsorbed on the platinum surface, as for example, modifying Pt single crystal electrodes with Pb [39].

On the other hand, and in addition to the surface structure effect, the dispersion of the catalytic material on the supporting material is of paramount importance for the correct evaluation of the electrocatalyst properties. Nanoparticle agglomeration causes different effects on the studied reaction. A typical example of this is the CO electrooxidation reaction on platinum nanoparticles [15, 40]. These studies have shown that peak multiplicity and lower onset for CO oxidation are related to the nanoparticle agglomeration. In the case of formic acid or ethanol oxidation reactions, studies with different loadings of Pt nanoparticles supported on carbon in acidic medium show a decrease in current densities when the Pt loading is increased [16], due to diffusional problems of the reactant species in the platinum nanoparticle layer.

In the present manuscript, the effect of the surface structure/shape of platinum nanoparticles for ethanol oxidation has been studied in alkaline solutions, trying to establish a relationship with previous studies with Pt single crystal electrodes. In addition, agglomeration effects have also been examined in this medium, to determine the role of ethanol diffusion into the Pt nanoparticle catalyst layer by using disperse and non-disperse

deposits. For both objectives, voltammetric and chronoamperometric techniques were used for analyzing the reactivity of the Pt surfaces and spectroelectrochemical experiments were carried out for determining the species adsorbed and formed during ethanol oxidation on platinum nanoparticles.

5.2 Experimental

Four different Pt nanoparticle samples with different shapes were used. Polyoriented nanoparticles, denoted as (poly)Pt, were synthesized with the water-in-oil microemulsion method [41, 42] (water/polyethylene glycol dodecyl ether (Brij®30)/n-heptane) using 0.1 M H_2PtCl_6 as platinum precursor. Reduction was done directly by adding $NaBH_4$ (ten times the stoichiometric amount) to the micellar solution. After reduction, nanoparticles were precipitated by adding NaOH, and then cleaned using acetone and ultrapure water. Pt nanoparticles with preferential surface orientation were prepared using the colloidal method [43, 44]. They present predominant {100}, {111} and a mixture of {100} and {111} domains, denoted through the paper as (100)Pt, (111)Pt and (100-111)Pt nanoparticles, respectively. For synthesizing them, 0.5 mL of 0.1 M sodium polyacrilate solution (M_w = 2100) were added to 100 mL of an aged solution with the platinum precursor (10^{-4} M), K_2PtCl_4 for (100)Pt nanoparticles and H_2PtCl_6 for (111)Pt and (100-111)Pt nanoparticles. The ratio between the sodium polyacrilate and the Pt precursor was 5:1. The pH was adjusted to 7 with 0.1 M HCl for (100)-(111)Pt and (111)Pt nanoparticles, whereas for the (100)Pt nanoparticles, pH was not adjusted. After that, the solutions were deaerated with Ar for 20 min and Pt ions were reduced by bubbling H_2 during 5 minutes, except for the (111)Pt sample, which was purged for only 5 minutes whereas reduction time with H_2 was limited to 1 min. At this point, the reaction container was left overnight for complete the reduction (12-14 h). After this, two NaOH pellets were added to induce precipitation of nanoparticles. Finally, samples were cleaned three to four times with ultrapure water.

To analyze possible diffusional problems of ethanol to the catalyst surface during ethanol oxidation, polyoriented platinum nanoparticles supported on carbon were synthesized using the citrate method [15, 45] with different metal loadings. In brief, sodium citrate, which acts as stabilizer, and H_2PtCl_6 (the platinum precursor) were mixed in the same concentration (2.5×10^{-4} M) with ice-cold sodium borohydride, which is the reducing agent. Once the platinum was reduced, carbon vulcan XC-72R was added under stirring conditions. Magnetic and ultrasonic stirring was alternated for two hours with the aim of dispersing the carbon in the water solution and favoring the adsorption of the nanoparticles on the carbon surface. The different Pt loadings were obtained by varying the

ratio between the amount of Pt and carbon vulcan. After the adsorption of nanoparticles on carbon, two NaOH pellets were added to precipitate the catalysts overnight. Then, they were washed and filtered with ultrapure water-NaOH four to five times. These Pt nanoparticles supported on carbon are denoted as Pt(10%), Pt(20%), Pt(30%), Pt(40%) and Pt(50%) depending on the Pt loading of the sample, and Pt(100%) for the unsupported Pt nanoparticles.

For the studies with the preferentially oriented Pt nanoparticles, hemispherical polycrystalline gold was used as a support (*ca.* 3 mm^2) and the amount of nanoparticles was adjusted so that the platinum active area was between 0.05-0.1 cm^2, in order to avoid transport problems of the reactant species to the catalyst surface. This effect is studied with the nanoparticles supported in carbon. Therefore, for these nanoparticles, a fix amount of 4 μL was deposited on a commercial glassy carbon support with a 3 mm diameter. All the Pt nanoparticles were cleaned using CO adsorption and stripping in 0.5 M H_2SO_4, following the procedure of refs. [41, 46]. Before each experiment, a blank voltammogram was recorded in 0.5 M H_2SO_4. The active area was calculated using the charge of the hydrogen adsorption/desorption region after the apparent double layer subtraction, considering a charge density of 0.23 mC cm^{-2} up to 0.6 V [47]. The upper potential limit in all the voltammograms is set always below 0.95 V to assure the stability of the surface structure of the nanoparticles. Additionally, a blank voltammogram is also recorded after the ethanol oxidation experiments to verify that the nanoparticles samples have not suffered any modification.

In situ FTIR spectra were acquired using a Nicolet (Model 8700) spectrometer, equipped with a MCT (Mercury-Cadmium-Telluride) detector. The spectroelectrochemical cell was coupled in a CaF_2 window beveled at 60º as described previously [48]. The spectra were obtained from the average of 100 interferograms with a resolution of 8 cm^{-1} using p-polarized light and are presented with absorbance units, $A=-\log[(R_1-R_2)/R_1]$, where R_2 and R_1 are the reflectance values corresponding to the single-beam spectra recorded at the sample at any potential and at the reference potential, respectively. The reference spectra were taken at 0.1 V, whereas the sample spectra were acquired doing different steps between 0.1 V and 0.95 V vs. reversible hydrogen electrode (RHE). Positive bands

correspond to species that have increased their concentration with respect to the reference potential and negative bands indicate species consumed.

The experiments were performed at room temperature conditions and in a three-electrode electrochemical cell. A reversible hydrogen (N50, Air liquide) electrode was used as a reference and a gold or platinum wire was used as a counter-electrode depending on the support used (gold or glassy carbon respectively). Solutions were prepared with NaOH (NaOH monohydrate 99.99%, Merck Suprapur), ethanol absolute (Merck p.a.) and ultrapure water (Elga Purelab Ultra 18.2 MΩcm), whereas Ar (N50, Air Liquide) was used for deoxygenating the solutions. The electrode potential was controlled with a μAutolab type III. All the potentials presented in this paper are referred to the RHE. Finally, in order to study the agglomeration effect, different drying procedures were evaluated. To perform them, an EDI101 rotating disc electrode from Radiometer analytical with a commercial glassy carbon tip (*ca.* 3 mm) was used.

5.3 Results and discussion

5.3.1 Characterization of shape-controlled Pt nanoparticles

Fig. 5.1 shows some representative transmission electron microscopy (TEM) images of the four preferentially oriented Pt nanoparticles samples studied in this work to evaluate the surface structure effect of ethanol electrooxidation. As can be seen, each sample has different shape and size characteristics that are summarized in Table 5.1. In this table, the predominant are ordered domains on the surface are also given.

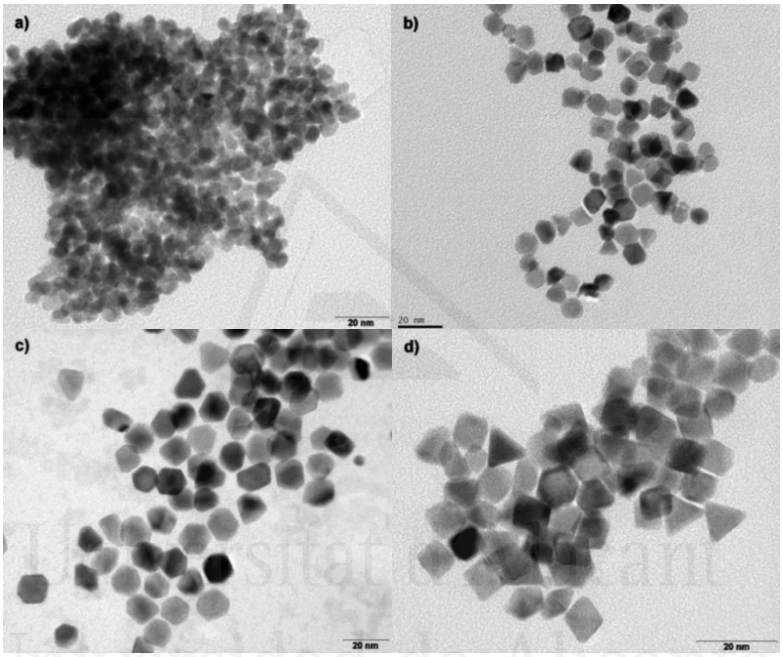

Fig. 5.1. TEM pictures for: a) (poly)Pt, b) (100)Pt, c) (100-111)Pt and d) (111)Pt nanoparticles.

	Average size/nm	Preferential shape	Preferential ordered domains
(poly)Pt	4.0 ± 0.6	Sphere	none
(100)Pt	8.2 ± 1.6	Cube	(100)
(100-111)Pt	11.5 ± 1.7	Truncated cube	(100) & (111)
(111)Pt	8.6 ± 1.4	Octahedron	(111)

Table 5.1. Physical characteristics of the preferentially ordered nanoparticles used in the work.

In addition to the TEM images of the nanoparticles, a voltammetric characterization is needed to corroborate the presence of the ordered Pt domains suggested with the TEM images. The voltammetric profile of a Pt sample in H_2SO_4 can be considered as a fingerprint of its surface structure, which allows assessing the type and ratio of the different domains present on the surface [46]. Fig. 5.2 displays the voltammograms obtained in 0.5 M H_2SO_4, highlighting the hydrogen adsorption region for the four samples studied.

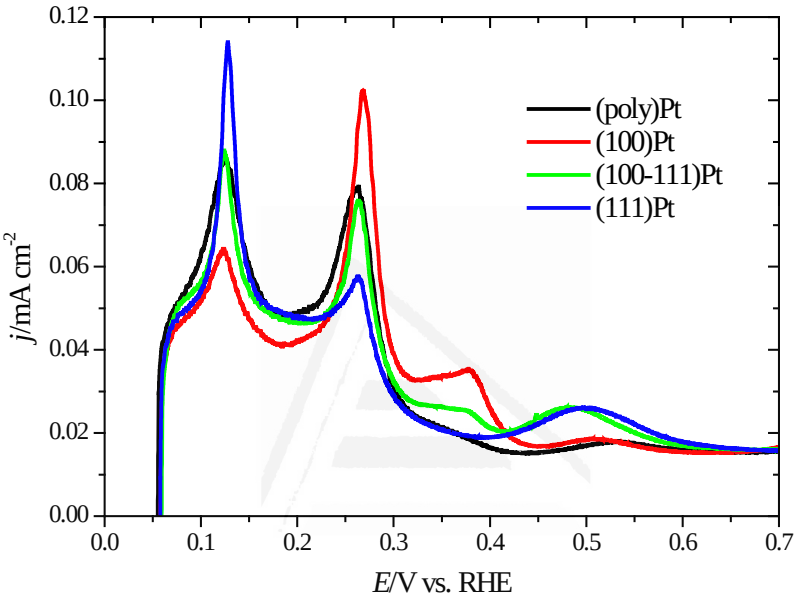

Fig. 5.2. Voltammetric profiles in 0.5 M H_2SO_4 for the different nanoparticle samples. Scan rate: 0.05 Vs^{-1}.

The (poly)Pt nanoparticles present the typical features of a polyoriented platinum electrode, with two main peaks at 0.125 and 0.265 V. The peak at 0.125 V is assigned to {110} sites, whereas the peak at 0.265 V corresponds to {100} defects on {111} domains or {100} short domains. In the other samples, characteristic peaks for ordered domains can be observed in addition to those present in a polyoriented sample. The (100)Pt nanoparticles present a peak at 0.370 V, related to the presence of long-range {100} ordered domains. This peak is also observed in the (100-111)Pt nanoparticles in addition to the wide signal around 0.500 V assigned to sulfate adsorption on {111} ordered domains. This latter signal is very prominent for the (100-111) and especially for the (111)Pt nanoparticles sample. The voltammetric profile of these samples is perfectly symmetrical,

corroborating the cleanliness of the surface of the nanoparticle and the success in the removal of the chemicals used during the synthesis. A more detailed study of the voltammetric profiles depending on the different preferential surface structure of the nanoparticles and the electrolyte has been previously published by our group [46, 47, 49].

5.3.2 Ethanol oxidation on preferentially shaped Pt nanoparticles

Ethanol oxidation experiments were carried out with the preferentially oriented Pt nanoparticles in alkaline medium (Fig. 5.3) to study the surface structure effect and to establish correlations with previous results with single crystal electrodes [35]. In addition, the behavior could be compared with that of the same Pt nanoparticles in acidic solutions [12]. In all the experiments, the upper potential limit was set to 0.95 V to avoid changes on the surface structure of the Pt nanoparticles due to oxide formation. The first cycle is presented in all the figures because a large deactivation process is observed in this medium upon cycling.

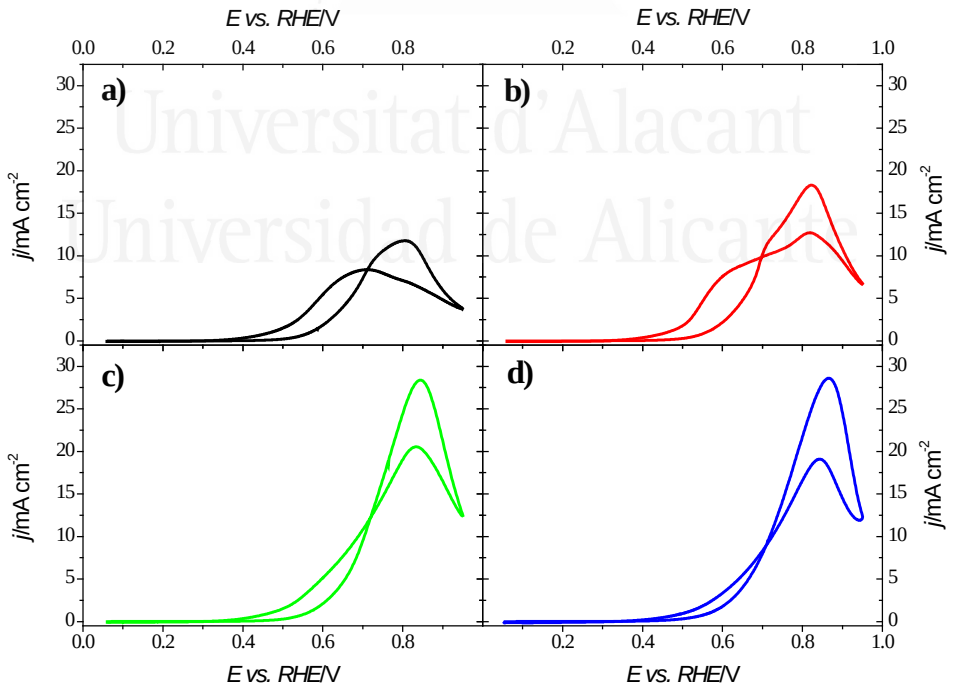

Fig. 5.3. Ethanol oxidation (1st cycle): a) (poly)Pt, b) (100)Pt, c) (100-111)Pt and d) (111)Pt nanoparticles. Test solution: 0.2 M CH_3CH_2OH + 0.1 M NaOH. Sweep rate: 0.02 Vs^{-1}.

The voltammetric profiles shown in Fig. 5.3 clearly illustrate the surface structure effect observed for this reaction in alkaline medium, and follow the same trends observed with single crystal electrodes [35]. Among the Pt basal planes, it is the Pt(111) electrode that exhibits the highest peak current density and also the highest onset potential. Thus, the nanoparticle sample with long range {111} domains, namely (111)Pt and (100-111)Pt nanoparticles, present higher currents and a higher onset potential, whereas the (100)Pt and (poly)Pt nanoparticles show a lower onset potential. The maximum activity (maximum peak current density) for the four prepared samples follows the expected order obtained from the reactivity of single crystal electrodes [35], that is, (111)Pt > (100-111)Pt > (100)Pt > (poly)Pt. On the other hand, the onset potential is associated with the adsorption of OH on the Pt surface, because it has been proposed that, in alkaline solutions, these species provides the oxygen group necessary for the oxidation of ethanol, in a different way to that taking place in acidic solutions, where water molecules act as the oxygen donor to the ethanol molecule. Thus, the OH adsorption is the key for triggering the ethanol oxidation, offering a lower onset potential in surfaces with {100} domains, as OH adsorption occurs at potentials more negative than those observed for the {111} domains [50].

When compared with the results obtained in acidic solutions, the voltammetric profile in alkaline medium is significantly different, showing higher currents and lower hysteresis, independently of the Pt nanoparticles sample used. In acidic conditions, anion adsorption plays a significant role in the process, since specific adsorption of anions hinder ethanol oxidation, giving rise to lower currents. In perchloric acid solutions, the adsorption of acetate coming from the acetic acid formed during the oxidation adsorbs strongly on the electrode surface and inhibits the oxidation [18]. When sulfuric acid solutions are employed, adsorbed sulfate is detected in the potential window where ethanol oxidation takes place. However, in alkaline medium, the absolute potential is more negative and acetate (or any other anion) adsorption does not take place, favoring the ethanol oxidation. This fact explains the high activity for platinum electrodes in alkaline solutions, especially in {111} domains, the most active electrode for acetate formation comparing with the other basal planes, as is also observed in perchloric acid solutions with the currents at very short times prior to the adsorption of acetate [18].

Regarding the different hysteresis observed depending on the nanoparticle sample used, this phenomenon is normally related in acidic pH values to the CO formation at low potentials and its posterior oxidation at potentials above 0.5-0.6 V. According with the low hysteresis observed in Fig. 5.3 and using previous results with Pt single crystal and Pt polyoriented electrodes [35, 36, 38], a change in the oxidation mechanism is proposed, with a low CO formation rate at low potentials and acetate formation as the main product of the oxidation. Another important difference for ethanol oxidation on Pt nanoparticles in alkaline solutions observed also in Pt single crystal electrodes [35] is the huge deactivation of the Pt surface (not shown) when the electrode is cycled several times, especially when {111} domains are present at the surface. This deactivation is due to acetaldehyde formation, the previous step before acetate formation. Acetaldehyde can dimerize and produce inhibiting species that adsorb on the surface through CH_x groups [38] and cause the deactivation.

In order to gain insight into the stability of the electrocatalytic process at low potentials and the importance of this deactivation process, chronoamperometric currents were recorded at 0.6 V. This potential was selected because ethanol oxidation has already started but currents are not very high so that there are no transport limitations of ethanol to the electrode surface.

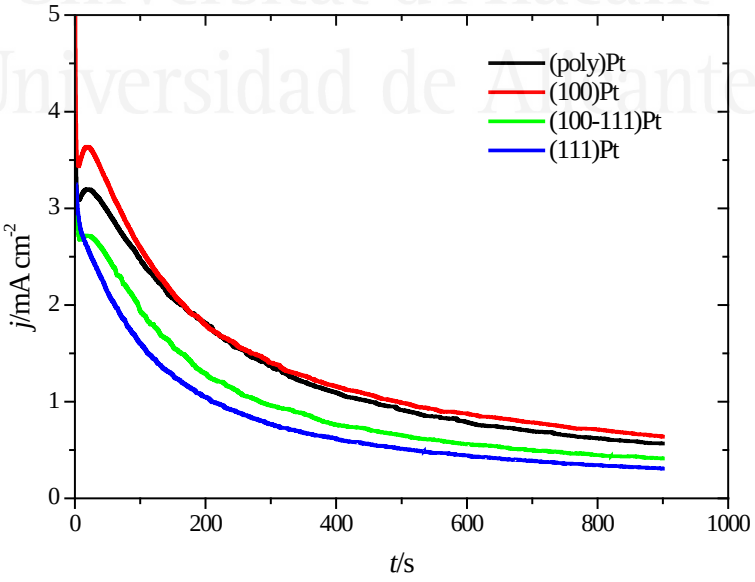

Fig. 5.4. Current transients recorded at 0.6 V for ethanol oxidation on the different Pt nanoparticles. Test solution: 0.2 M CH_3CH_2OH + 0.1 M NaOH.

Fig. 5.4 shows the transient currents registered for 15 min after two successive steps: first from 0.1 V to 0.9 V, for removing the possible poison species formed at lower potentials during 5 s, and then to 0.6 V for recording the transient. The measured currents follow the trend observed for the currents recorded in the voltammetric profile of Fig. 5.3 at 0.6 V, displaying the largest current for the (100)Pt nanoparticles, and lower activities for the nanoparticles with a larger amount of {111} domains, (100-111)Pt and (111)Pt nanoparticles.

Nevertheless, in similar experiments performed for single crystal electrodes in acidic medium [18], currents of the three platinum basal planes decay much faster at 0.6 V due to CO formed which poisons the surface in the case of Pt(100) and Pt(110) and to adsorbed anions as acetate or sulfate for Pt(111). However, in alkaline solutions, the effect of acetate adsorption can be discarded due to the displacement of the absolute potential towards negative values, and CO formation is negligible, suggesting that the differences in the transient currents come from the adsorption of the acetaldehyde and its polymerization [35]. In connection with this, a slight reactivation is observed at short times for all samples except for (111)Pt nanoparticles sample at 0.6 V. This feature is assigned to {100} domains [35], promoting a current increase due to the OH adsorption at the beginning of the transient measurements. At 0.6 V, OH adsorption occurs on these domains and favors the ethanol oxidation until the formation of the species coming from acetaldehyde, which inhibits the platinum surface.

5.3.3 FTIR experiments for ethanol oxidation

Fig. 5.5 and Fig. 5.6 show the FTIR experiments carried out with the four preferentially oriented Pt nanoparticles with the aim of finding out the species adsorbed or produced during ethanol oxidation. The spectra obtained are very similar to those obtained for single crystal electrodes [35], with two main bands at 1550 and 1415 cm^{-1} assigned to the O-C-O asymmetrical and symmetrical vibrational modes of acetate respectively, according to previous works [36, 51]. Acetate bands appear at around 0.3 V for the (100)Pt and 0.4 V for (poly)Pt nanoparticles, which are lower potentials in comparison with the

(111)Pt and (100-111)Pt nanoparticles, where the bands appear at 0.5 V, although small signals are observed for (111)Pt at 0.4 V. These data are in agreement with the onset potentials for ethanol oxidation, as it is shown in the voltammetric profiles of Fig. 5.3, that is, ethanol oxidation starts at lower potentials for (100)Pt and (poly)Pt nanoparticles.

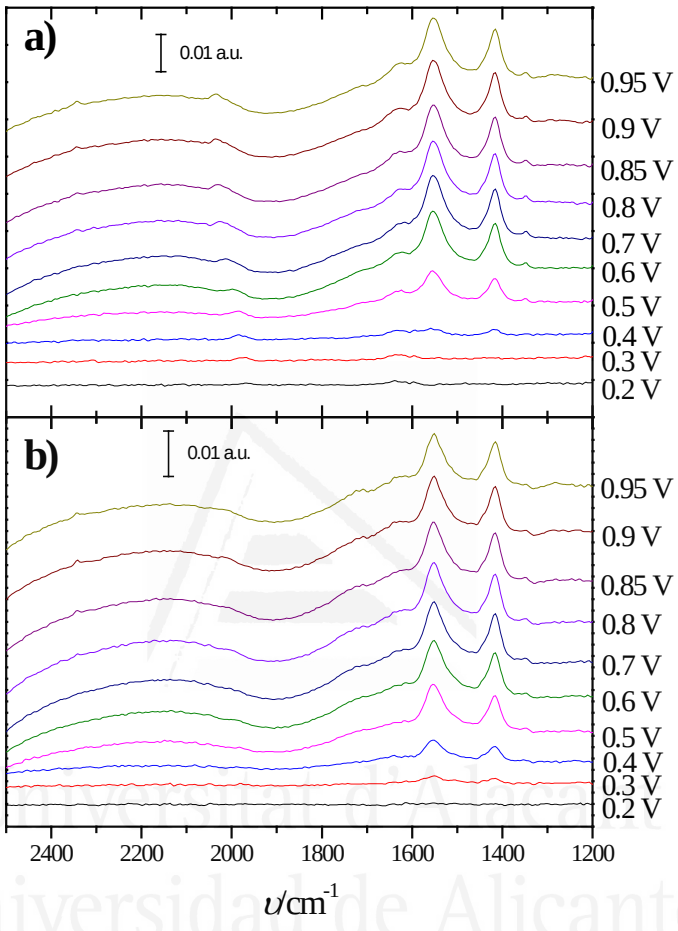

Fig. 5.5. *In situ* FTIR spectra for ethanol oxidation on a) (poly)Pt and b) (100)Pt nanoparticles, using spectra at 0.1 V as a reference. Test solution: 0.2 M CH_3CH_2OH + 0.1 M NaOH.

Additionally, a poor affinity of the nanoparticles for the C-C bond scission for ethanol oxidation at higher pHs is observed, with very weak bands of adsorbed CO at around 2030 cm^{-1} detected at low potentials [35] independently of the preferential surface structure of the Pt nanoparticles. These very weak bands support the proposed change in the oxidation mechanism with respect to acidic medium. The appearance of small CO_2 bands at 2340 cm^{-1}, atypical at these higher pHs, suggests a large shift in the interfacial pH, due to the depletion of the OH^- in the thin layer during ethanol oxidation [52, 53]. In this

sense, the presence of carbonate cannot be discarded, which shows a main band at 1390 cm^{-1}, which overlaps with the acetate bands. However, according to the negligible CO adsorption band, it can be confirmed that the main product in the ethanol oxidation is the incomplete oxidation to acetate in the same way that it is observed for the single crystal electrodes.

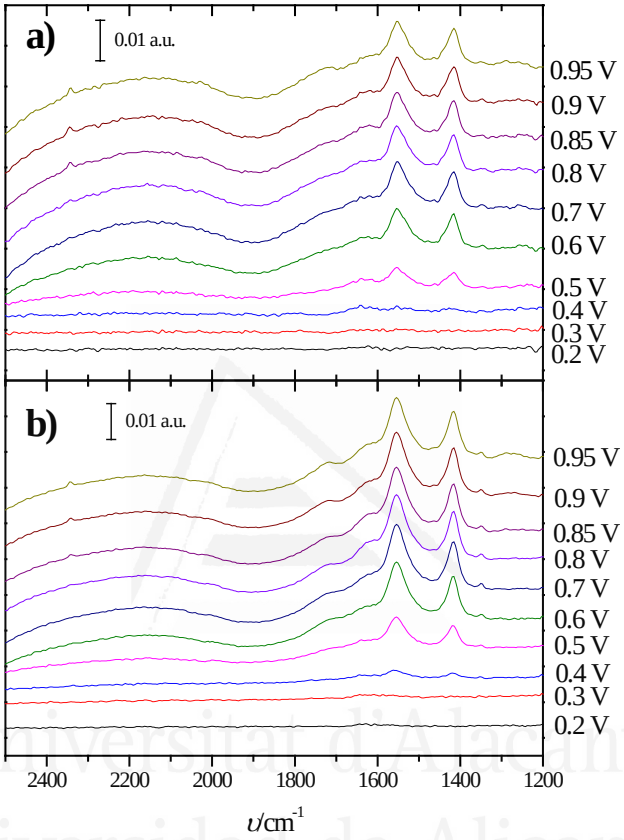

Fig. 5.6. *In situ* FTIR spectra for ethanol oxidation on a) (100-111)Pt and b) (111)Pt nanoparticles using spectra at 0.1 V as a reference. Test solution: 0.2 M CH_3CH_2OH + 0.1 M NaOH.

5.3.4 Characterization of Pt nanoparticles supported on carbon

To further characterize the behavior of Pt nanoparticles in alkaline solution and demonstrate the importance of a good dispersion of the catalyst in the reactive layer, additional experiments were carried out with polyoriented nanoparticles supported on carbon with different metal loadings. Fig. 5.7 displays the TEM images for these Pt samples. As can be seen, the degree of agglomeration increases with the metal loading. For the Pt(10%) sample, isolated nanoparticles can be distinguished throughout the carbon

support, whereas large agglomerates can be observed for the Pt(50%) sample. Nevertheless, it is important to highlight that the different samples are made with the same synthesis method and the average size of the nanoparticles is practically the same for all the samples (between 2.1 and 2.4 nm), implying that the individual nanoparticles are the same in all the samples, and discarding any sintering process during the deposition of the nanoparticles on the carbon support to produce larger nanoparticles.

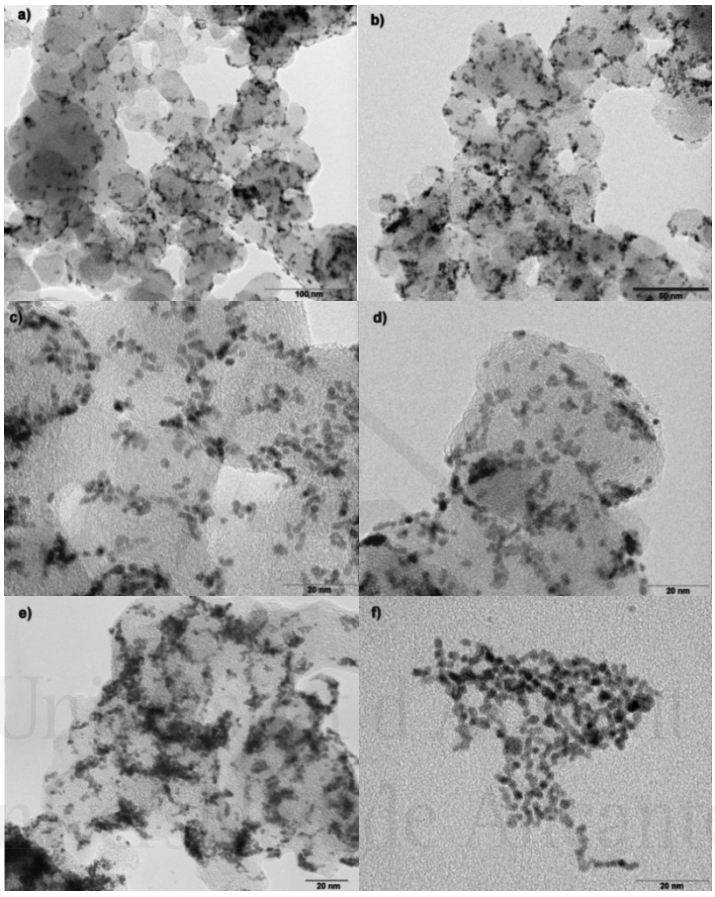

Fig. 5.7. TEM pictures for a) Pt(10%), b) Pt(20%), c) Pt(30%), d) Pt(40%) and e) Pt(50%) nanoparticles supported on carbon and f) Pt(100%), the unsupported Pt nanoparticles.

Following the same procedure observed in Fig. 5.2 for the electrochemical characterization in 0.5 M H_2SO_4, Fig. 5.8 presents the results of the voltammetric profiles for the Pt nanoparticles supported on carbon performed in the same electrolyte. Similarly to the (poly)Pt nanoparticles of Fig. 5.2 (black line), all the carbon-supported samples present the characteristic peaks in the hydrogen adsorption/desorption region of a polyoriented surface without showing signals coming from large {111} or {100} ordered

domains, which are absent on these small nanoparticles. The symmetry and sharpness of the hydrogen adsorption/desorption contributions prove the cleanliness of the surface. In addition, when the voltammetric profiles are normalized to the platinum electroactive area, the double layer contribution of the carbon in the voltammogram diminishes, leading to lower current densities in the so-called double layer region of Pt.

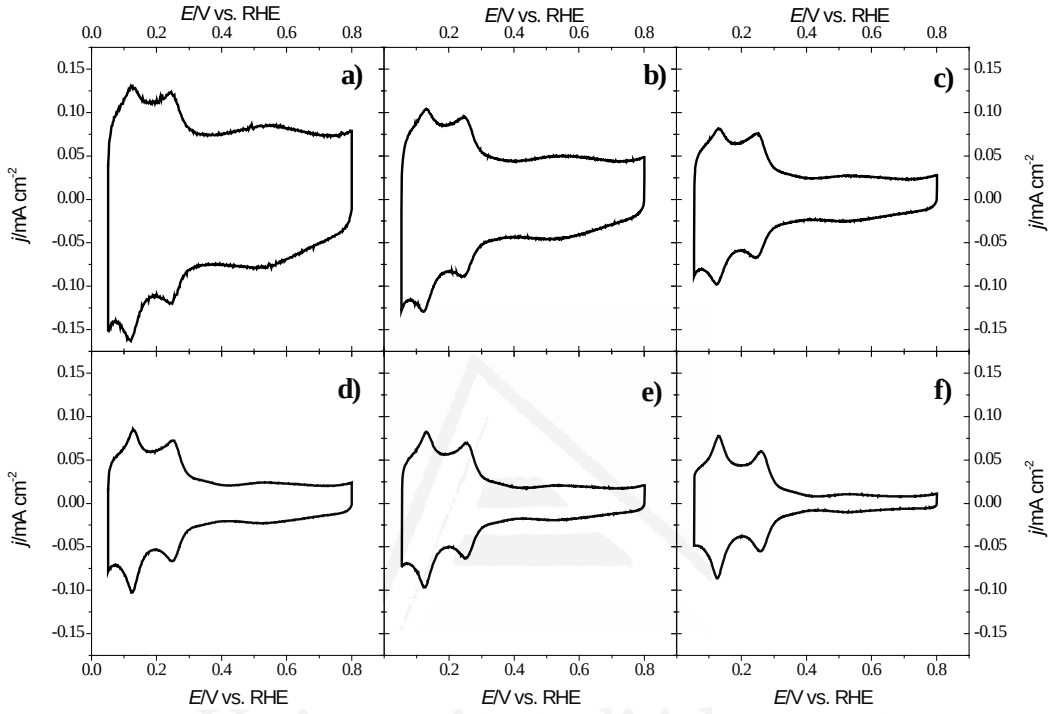

Fig. 5.8. Voltammetric profile for: a) Pt(10%), b) Pt(20%), c) Pt(30%), d) Pt(40%), e) Pt(50%) and f) Pt(100%) nanoparticles. Test solution: 0.5 M H_2SO_4. Scan rate: 0.05 V s^{-1}.

In order to confirm that the agglomeration observed by TEM in the samples with a high platinum loading does not affect their electrochemical activity, that is to say, that the whole sample is contributing to the electrochemical signal registered in the voltammograms, the ratio of the currents for hydrogen adsorption and for double layer was analyzed for the different samples. Fig. 5.9 shows the ratio between the currents at 0.12 V, which contains contributions from the platinum and carbon, and 0.42 V, where the current mainly comprises double-layer contributions from carbon. As can be seen, a clear linear dependence is observed, ensuring that the surface area of platinum is directly proportional to the total amount of platinum. In addition, the intercept of the linear fit is 1, which corroborates that the major contribution for the current at 0.42 V is the double layer current

from the carbon support. Thus, from the results show in Fig. 5.9, it can be confirmed that the entire surface of the platinum nanoparticles is available for the hydrogen adsorption-desorption process.

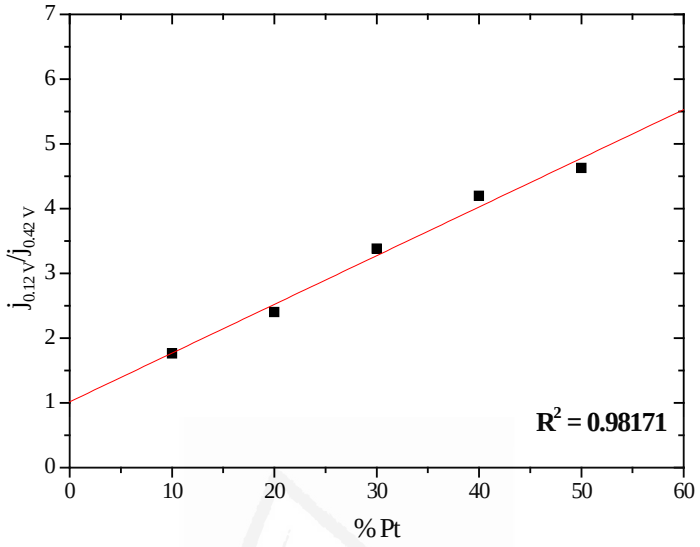

Fig. 5.9. Ratio between current densities at 0.12 V and 0.42 V vs Pt loading of the nanoparticle samples supported on carbon.

5.3.5 Aggregation effect in ethanol oxidation

The behavior for ethanol oxidation in alkaline medium was studied for these Pt samples. Fig. 5.10 shows the results using the same potential window and conditions as in Fig. 5.3. In spite of the different sizes and the presence of the vulcan support, the voltammetric shape and peak currents are the same as those recorded in Fig. 5.3 for the (poly)Pt nanoparticle sample, indicating that no significant size effects are observed for this reaction for polyoriented Pt nanoparticles. Additionally, as the platinum loading increases in the sample, current densities diminish. To calculate these current densities, the hydrogen adsorption charge has been used, because Fig. 5.9 indicates that the whole surface area is electrochemically active. However, the diminution of the current densities with the Pt loading indicates that the whole Pt surface area is not active in the same extent for ethanol oxidation. This diminution should be related to the increasing diffusional

problems of ethanol as the loading becomes higher, as happened also in sulfuric and perchloric acid solutions [16]. Surely, the most external part of the nanoparticle deposit is always contributing to the ethanol oxidation. However, the inner parts of this deposit for high loadings are not contributing in the same way because all the ethanol flux coming from the bulk solution is mainly consumed in the outer part of the layer.

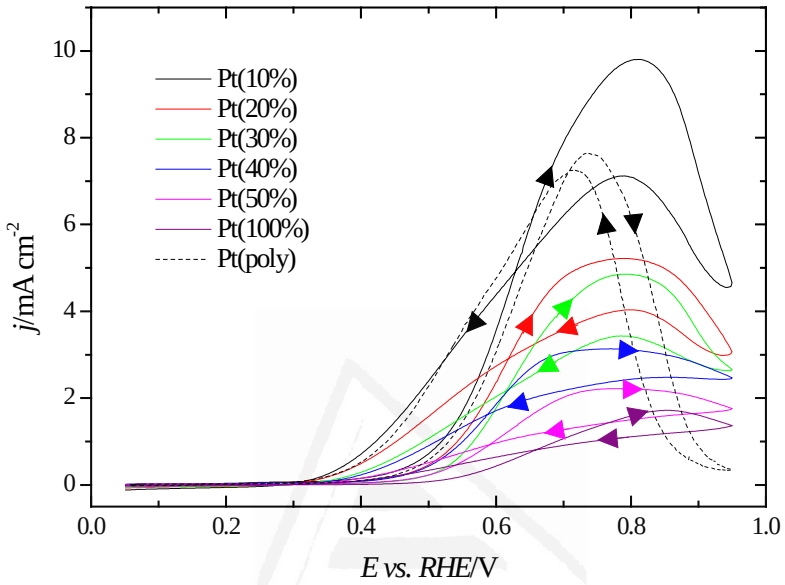

Fig. 5.10. Voltammetric profiles (1st cycle) in 0.2 M CH_3CH_2OH + 0.1 M NaOH for Pt nanoparticles supported on carbon with different metal loadings and for a cycled Pt poly electrode. Sweep rate: 0.02 V s^{-1}.

Thus, an apparent decrease in the activity is observed when the Pt loading increases due to diffusional problems of ethanol through the catalyst layer. It could be consider that the 10% loading represents the currents that could be obtained in absence of diffusional problems. To prove that, the voltammetric response of a bulk Pt electrode that has been previously cycled in the oxide region to remove all the {111} and {100} ordered domains [46], has been also incorporated in Fig. 5.10. This voltammogram represents the response of a typical polycrystalline Pt electrode with no preferential orientation in the same experimental conditions used in the nanoparticle tests. Due to the large limiting diffusion current that could be obtained for ethanol oxidation if the electrode kinetics for the reaction were fast (*ca*. 100 mA/cm^2 for the employed concentration), the measured currents for the bulk electrode are not affected by diffusion of ethanol and represent the intrinsic activity of the bulk Pt for the reaction. The measured currents for the Pt(10%) are slightly higher than

those for the Pt(poly), probably related to a small effect of the particular surface structure of the nanoparticles. Thus, these currents represent the behavior of the nanoparticles in absence of ethanol diffusion limitations.

From the results shown in Fig. 5.10, it can be said that the dispersion of Pt nanoparticles on the carbon support is the key parameter for obtaining the true activity of the nanoparticles. With the aim of avoiding the agglomeration of nanoparticles and improving the quality of the deposit with better dispersion of the nanoparticles, Garsany and co-workers [54-56] proposed a different procedure for preparing the Pt nanoparticle deposit that gives reproducible Pt thin films with an increase in activity for the oxygen reduction reaction. This method uses a RDE glassy carbon tip rotating at 700 rpm as support for the deposit of the different samples of nanoparticles. The same procedure to prepare the nanoparticles deposit was used here, using a commercial glassy carbon tip of a RDE, which was rotated at 700 rpm while the solution containing the supported nanoparticles was dried with Ar.

As expected, the dispersion of the layer is significantly improved when rotating conditions are used during the drying step. Fig. 5.11 shows the effect of the rotation in the dispersion of the catalyst layer. For improving the image contrast, a gold support was used instead of a glassy carbon. As can be seen from the optical microscope images, the deposit obtained with rotation (Fig. 5.11b) shows a uniform dispersion of the catalyst layer. However, in the normal deposit, that obtained without rotation (Fig. 5.11a), the deposit is non-uniform and a large fraction of the gold support is still visible.

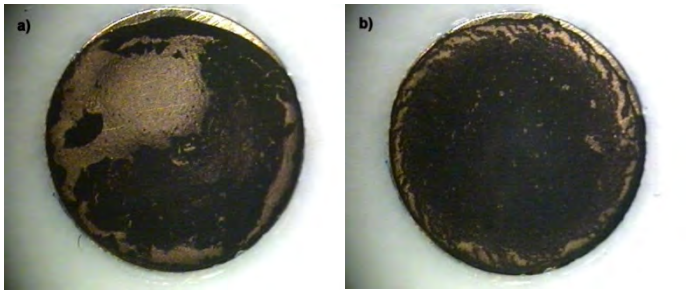

Fig. 5.11. Images of the Pt(40%) nanoparticles deposited on a gold support for a: a) non-rotating and b) rotating support (700 rpm) during the drying procedure.

The electrochemical response of two Pt(40%) nanoparticle layers prepared with and without rotation is shown in Fig. 5.12.

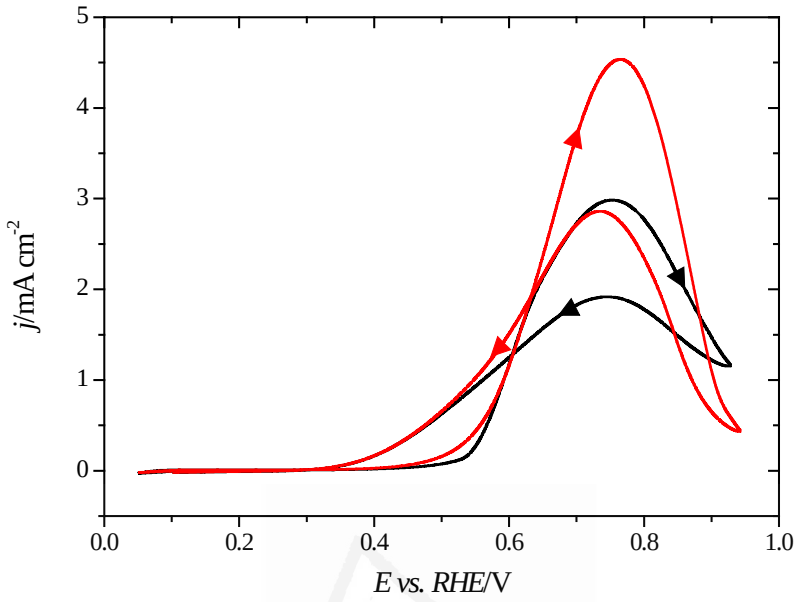

Fig. 5.12. Voltammetric profile (1st cycle) for ethanol oxidation for Pt(40%) nanoparticles supported on carbon with a static (*black line*) and rotating (*red line*) glassy carbon support (700 rpm) during the drying deposit procedure. Test solution: 0.2 M CH_3CH_2OH + 0.1 M NaOH. Sweep rate: 0.02 V s^{-1}. IR drop has been corrected.

A significant increase in the activity for the sample prepared using rotation is observed, which highlights the dependence of the electrocatalytic response with the film morphology. Comparing the measured currents for both experiments, it can be seen that the voltammograms almost overlap in the regions where small currents are recorded. In this current region, the only difference between both samples is a small displacement of the onset potential to lower values for the more dispersed sample, which can be related to some minor effect in the local conditions that affect the onset potential in agglomerated samples [15]. The almost constant currents in the low current regime is a clear indication that for those currents there are no diffusional problems, and the whole nanoparticles' surface is contributing in the same way to the ethanol electrooxidation. In the region where high current densities are obtained, larger currents are also recorded for the uniform deposit, corroborating its better performance for the ethanol electrooxidation.

5.4 Conclusions

The results presented here highlight the importance of controlling two parameters in the platinum electrocatalysts for ethanol oxidation in alkaline solutions: the surface structure and the dispersion of the nanoparticle electrocatalysts. The solution pH also affects the reactivity of ethanol in platinum, showing an increasing in the total activity when it becomes more alkaline and a change in potential range where the reaction occurs. For this purpose, two types of samples were used. For studying the surface structure effect, shape-controlled platinum nanoparticles were employed, whereas the effect of the dispersion of the catalyst was studied with different loadings of polyoriented nanoparticles supported on carbon.

Shape-controlled nanoparticles, namely, (poly)Pt, (100)Pt, (111)Pt and (100-111)Pt nanoparticles, were tested for ethanol oxidation in alkaline solution using electrochemical and IR techniques. The experiments show the preference for acetate formation independently of the preferential shape of the Pt nanoparticles, while the amount of CO_2 formed is always negligible. Additionally, (100) and (poly)Pt nanoparticles show lower currents and a lower onset than the nanoparticles that have a significant fraction of {111} ordered domains. The differences in the reactivity have been ascribed to the different OH adsorption potential of the different domains present on the surface.

The use of the polyoriented Pt nanoparticles supported on carbon has demonstrated that the dispersion of the catalyst is important for the optimum performance of the deposit. Lower activities have been reported in the case of more agglomerated and non-uniform deposits. With the aim of increasing the uniformity of the catalyst film, a previously reported methodology was used [54-56]. With this method the dispersion containing the nanoparticles was dried while the electrode was rotated at 700 rpm for improving the dispersion of the catalyst. A higher catalytic activity was obtained for the films obtained using this procedure, stressing the importance of the dispersion of the catalyst on the support for better performances.

5.5 References

[1] M. T. M. Koper, "Fuel Cell Catalysis: A Surface Science Approach", *Electrocatalysis and Electrochemistry* A. Wieckowski (Ed.), John Wiley & Sons, Hoboken, New Jersey, **2009**.

[2] R. Parsons and T. VanderNoot, "The oxidation of small organic molecules: A survey of recent fuel cell related research" *Journal of Electroanalytical Chemistry* **1988**, 257, 9-45.

[3] C. Lamy and J. M. Léger, "Electrocatalytic oxidation of small organic molecules at platinum single crystals" *Journal de Chimie Physique et de Physico-Chimie Biologique* **1991**, 88, 1649-1671.

[4] J. M. Feliu and E. Herrero, "Formic acid oxidation", in *Handbook of Fuel Cells - Fundamentals, Technology and Applications, vol. 2*, W. Vielstich, H. Gasteiger and A. Lamm (Eds.) Wiley, Chichester, **2003**, pp. 625-634.

[5] T. Iwasita, "Electrocatalysis of methanol oxidation" *Electrochimica Acta* **2002**, 47, 3663-3674.

[6] J. M. Orts, A. Fernández-Vega, J. M. Feliu, A. Aldaz and J. Clavilier, "Electrochemical Oxidation of Ethylene-Glycol on Pt Single-Crystal Electrodes with Basal Orientations in Acidic Medium" *Journal of Electroanalytical Chemistry* **1990**, 290, 119-133.

[7] N. M. Markovic, H. A. Gasteiger and P. N. Ross, "Oxygen Reduction on Platinum Low-Index Single-Crystal Surfaces in Sulfuric-Acid-Solution - Rotating Ring-Pt(Hkl) Disk Studies" *Journal of Physical Chemistry* **1995**, 99, 3411-3415.

[8] A. Kuzume, E. Herrero and J. M. Feliu, "Oxygen reduction on stepped platinum surfaces in acidic media" *Journal of Electroanalytical Chemistry* **2007**, 599, 333-343.

[9] R. Rizo, E. Herrero and J. M. Feliu, "Oxygen reduction reaction on stepped platinum surfaces in alkaline media" *Physical Chemistry Chemical Physics* **2013**, 15, 15416-15425.

[10] J. Solla-Gullón, F. J. Vidal-Iglesias, A. López-Cudero, E. Garnier, J. M. Feliu and A. Aldaz, "Shape-dependent electrocatalysis: methanol and formic acid electrooxidation on preferentially oriented Pt nanoparticles" *Physical Chemistry Chemical Physics* **2008**, 10, 3689-3698.

[11] V. Grozovski, J. Solla-Gullón, V. Climent, E. Herrero and J. M. Feliu, "Formic Acid Oxidation on Shape-Controlled Pt Nanoparticles Studied by Pulsed Voltammetry" *Journal of Physical Chemistry C* **2010**, 114, 13802-13812.

[12] C. Busó-Rogero, V. Grozovski, F. J. Vidal-Iglesias, J. Solla-Gullón, E. Herrero and J. M. Feliu, "Surface structure and anion effects in the oxidation of ethanol on platinum nanoparticles" *Journal of Materials Chemistry A* **2013**, 1, 7068-7076.

[13] F. J. Vidal-Iglesias, J. Solla-Gullón, P. Rodríguez, E. Herrero, V. Montiel, J. M. Feliu and A. Aldaz, "Shape-dependent electrocatalysis: ammonia oxidation on platinum nanoparticles with preferential (100) surfaces" *Electrochemistry Communications* **2004**, 6, 1080-1084.

[14] J. Hernández, J. Solla-Gullón, E. Herrero, A. Aldaz and J. M. Feliu, "Electrochemistry of shape-controlled catalysts: Oxygen reduction reaction on cubic gold nanoparticles" *Journal of Physical Chemistry C* **2007**, 111, 14078-14083.

[15] A. López-Cudero, J. Solla-Gullón, E. Herrero, A. Aldaz and J. M. Feliu, "CO electrooxidation on carbon supported platinum nanoparticles: Effect of aggregation" *Journal of Electroanalytical Chemistry* **2010**, 644, 117-126.

[16] S. Chumillas, C. Busó-Rogero, J. Solla-Gullón, F. J. Vidal-Iglesias, E. Herrero and J. M. Feliu, "Size and diffusion effects on the oxidation of formic acid and ethanol on platinum nanoparticles" *Electrochemistry Communications* **2011**, 13, 1194-1197.

[17] C. Lamy and C. Coutanceau, "Electrocatalysis of Alcohol Oxidation Reactions at Platinum Group Metals", in *Catalysts for Alcohol-Fuelled Direct Oxidation Fuel Cells, vol. 6*, Z.-X. Liang and T. S. Zhao (Eds.) RSC Energy and Enviroment Series **2012**.

[18] F. Colmati, G. Tremiliosi-Filho, E. R. Gonzalez, A. Berná, E. Herrero and J. M. Feliu, "Surface structure effects on the electrochemical oxidation of ethanol on platinum single crystal electrodes" *Faraday Discussions* **2008**, 140, 379-397.

[19] A. Rodes, E. Pastor and T. Iwasita, "An FTIR Study on the Adsorption of Acetate at the Basal Planes of Platinum Single-Crystal Electrodes" *Journal of Electroanalytical Chemistry* **1994**, 376, 109-118.

[20] T. Iwasita and E. Pastor, "A DEMS and FTIR spectroscopic investigation of adsorbed ethanol on polycrystalline platinum" *Electrochimica Acta* **1994**, 39, 531-537.

[21] U. Schmiemann, U. Müller and H. Baltruschat, "The Influence of the Surface-Structure on the Adsorption of Ethene, Ethanol and Cyclohexene as Studied by DEMS" *Electrochimica Acta* **1995**, 40, 99-107.

[22] H. Wang, Z. Jusys and R. J. Behm, "Ethanol electrooxidation on a carbon-supported Pt catalyst: Reaction kinetics and product yields" *Journal of Physical Chemistry B* **2004**, 108, 19413-19424.

[23] M. Heinen, Z. Jusys and R. J. Behm, "Ethanol, Acetaldehyde and Acetic Acid Adsorption/Electrooxidation on a Pt Thin Film Electrode under Continuous Electrolyte Flow: An in Situ ATR-FTIRS Flow Cell Study" *Journal of Physical Chemistry C* **2010**, 114, 9850-9864.

[24] F. Colmati, G. Tremiliosi-Filho, E. R. Gonzalez, A. Berná, E. Herrero and J. M. Feliu, "The role of the steps in the cleavage of the C-C bond during ethanol oxidation on platinum electrodes" *Physical Chemistry Chemical Physics* **2009**, 11, 9114-9123.

[25] V. Del Colle, A. Berná, G. Tremiliosi-Filho, E. Herrero and J. M. Feliu, "Ethanol electrooxidation onto stepped surfaces modified by Ru deposition: electrochemical and spectroscopic studies" *Physical Chemistry Chemical Physics* **2008**, 10, 3766-3773.

[26] V. Del Colle, V. Santos and G. Tremiliosi-Filho, "Comparative Electrochemical and Spectroscopic Studies of Ethanol Oxidation on Pt(h,k,l) Modified by Osmium Nanoislands" *Electrocatalysis* **2010**, 1, 144-158.

[27] V. Del Colle, J. Souza-Garcia, G. Tremiliosi-Filho, E. Herrero and J. M. Feliu, "Electrochemical and spectroscopic studies of ethanol oxidation on Pt stepped surfaces modified by tin adatoms" *Physical Chemistry Chemical Physics* **2011**, 13, 12163-12172.

[28] J. Souza-Garcia, E. Herrero and J. M. Feliu, "Breaking the C-C Bond in the Ethanol Oxidation Reaction on Platinum Electrodes: Effect of Steps and Ruthenium Adatoms" *ChemPhysChem* **2010**, 11, 1391-1394.

[29] G. A. B. Mello, M. J. S. Farias, M. J. Giz and G. A. Camara, "Oxidation of isotopically-labeled ethanol on platinum-tin-rhodium surfaces: Enhancing the production of CO_2 from methyl groups" *Electrochemistry Communications* **2014**, 48, 160-163.

[30] A. V. Tripkovic, K. D. Popovic and J. D. Lovic, "The influence of the oxygen-containing species on the electrooxidation of the C_1-C_4 alcohols at some platinum single crystal surfaces in alkaline solution" *Electrochimica Acta* **2001**, 46, 3163-3173.

[31] E. Antolini and E. R. Gonzalez, "Alkaline direct alcohol fuel cells" *Journal of Power Sources* **2010**, 195, 3431-3450.

[32] J. S. Spendelow and A. Wieckowski, "Electrocatalysis of oxygen reduction and small alcohol oxidation in alkaline media" *Physical Chemistry Chemical Physics* **2007**, 9, 2654-2675.

[33] C. Coutanceau, L. Demarconnay, C. Lamy and J. M. Léger, "Development of electrocatalysts for solid alkaline fuel cell (SAFC)" *Journal of Power Sources* **2006**, 156, 14-19.

[34] V. Rao, Hariyanto, C. Cremers and U. Stimming, "Investigation of the ethanol electro-oxidation in alkaline membrane electrode assembly by differential electrochemical mass spectrometry" *Fuel Cells* **2007**, 7, 417-423.

[35] C. Busó-Rogero, E. Herrero and J. M. Feliu, "Ethanol Oxidation on Pt Single-Crystal Electrodes: Surface-Structure Effects in Alkaline Medium" *ChemPhysChem* **2014**, 15, 2019-2028.

[36] P. A. Christensen, S. W. M. Jones and A. Hamnett, "In Situ FTIR Studies of Ethanol Oxidation at Polycrystalline Pt in Alkaline Solution" *Journal of Physical Chemistry C* **2012**, 116, 24681-24689.

[37] M. López-Atalaya, E. Morallón, F. Cases, J. L. Vázquez and J. M. Pérez, "Electrochemical oxidation of ethanol on Pt(hkl) basal surfaces in NaOH and Na_2CO_3 media" *Journal of Power Sources* **1994**, 52, 109-117.

[38] S. C. S. Lai and M. T. M. Koper, "Ethanol electro-oxidation on platinum in alkaline media" *Physical Chemistry Chemical Physics* **2009**, 11, 10446-10456.

[39] P. A. Christensen, S. W. M. Jones and A. Hamnett, "An in situ FTIR spectroscopic study of the electrochemical oxidation of ethanol at a Pb-modified polycrystalline Pt electrode immersed in aqueous KOH" *Physical Chemistry Chemical Physics* **2013**, 15, 17268-17276.

[40] O. V. Cherstiouk, P. A. Simonov, V. I. Zaikovskii and E. R. Savinova, "CO monolayer oxidation at Pt nanoparticles supported on glassy carbon electrodes" *Journal of Electroanalytical Chemistry* **2003**, 554, 241-251.

[41] J. Solla-Gullón, V. Montiel, A. Aldaz and J. Clavilier, "Electrochemical characterization of platinum nanoparticles prepared by microemulsion: How to clean them without loss of crystalline surface structure" *Journal of Electroanalytical Chemistry* **2000**, 491, 69-77.

[42] J. Solla-Gullón, V. Montiel, A. Aldaz and J. Clavilier, "Synthesis and electrochemical decontamination of platinum-palladium nanoparticles prepared by water-in-oil microemulsion" *Journal of the Electrochemical Society* **2003**, 150, E104-E109.

[43] T. S. Ahmadi, Z. L. Wang, T. C. Green, A. Henglein and M. A. El-Sayed, "Shape-controlled synthesis of colloidal platinum nanoparticles" *Science* **1996**, 272, 1924-1926.

[44] T. S. Ahmadi, Z. L. Wang, A. Henglein and M. A. El-Sayed, ""Cubic" colloidal platinum nanoparticles" *Chemistry of Materials* **1996**, 8, 1161-1163.

[45] M.-C. Daniel and D. Astruc, "Gold Nanoparticles: Assembly, Supramolecular Chemistry, Quantum-Size-Related Properties, and Applications toward Biology, Catalysis, and Nanotechnology" *Chemical Reviews* **2003**, 104, 293-346.

[46] J. Solla-Gullón, P. Rodríguez, E. Herrero, A. Aldaz and J. M. Feliu, "Surface characterization of platinum electrodes" *Physical Chemistry Chemical Physics* **2008**, 10, 1359-1373.

[47] Q. S. Chen, J. Solla-Gullón, S. G. Sun and J. M. Feliu, "The potential of zero total charge of Pt nanoparticles and polycrystalline electrodes with different surface structure: The role of anion adsorption in fundamental electrocatalysis" *Electrochimica Acta* **2010**, 55, 7982-7994.

[48] T. Iwasita and F. C. Nart, "In situ infrared spectroscopy at electrochemical interfaces" *Progress in Surface Science* **1997**, 55, 271-340.

[49] F. J. Vidal-Iglesias, R. M. Arán-Ais, J. Solla-Gullón, E. Herrero and J. M. Feliu, "Electrochemical Characterization of Shape-Controlled Pt Nanoparticles in Different Supporting Electrolytes" *ACS Catalysis* **2012**, 2, 901-910.

[50] R. M. Arán-Ais, M. C. Figueiredo, F. J. Vidal-Iglesias, V. Climent, E. Herrero and J. M. Feliu, "On the behavior of the Pt(100) and vicinal surfaces in alkaline media" *Electrochimica Acta* **2011**, 58, 184-192.

[51] Z.-Y. Zhou, Q. Wang, J.-L. Lin, N. Tian and S.-G. Sun, "In situ FTIR spectroscopic studies of electrooxidation of ethanol on Pd electrode in alkaline media" *Electrochimica Acta* **2010**, 55, 7995-7999.

[52] D. Z. Jeffery and G. A. Camara, "The formation of carbon dioxide during glycerol electrooxidation in alkaline media: First spectroscopic evidences" *Electrochemistry Communications* **2010**, 12, 1129-1132.

[53] J. F. Gomes and G. Tremiliosi-Filho, "Spectroscopic Studies of the Glycerol Electro-Oxidation on Polycrystalline Au and Pt Surfaces in Acidic and Alkaline Media" *Electrocatalysis* **2011**, 2, 96-105.

[54] Y. Garsany, I. L. Singer and K. E. Swider-Lyons, "Impact of film drying procedures on RDE characterization of Pt/VC electrocatalysts" *Journal of Electroanalytical Chemistry* **2011**, 662, 396-406.

[55] Y. Garsany, J. Ge, J. St-Pierre, R. Rocheleau and K. E. Swider-Lyons, "Standardizing thin-film Rotating disk electrode measurements of the oxygen reduction activity of Pt/C" *ECS Transactions* **2013**, 58, 3-14.

[56] Y. Garsany, O. A. Baturina, K. E. Swider-Lyons and S. S. Kocha, "Experimental methods for quantifying the activity of platinum electrocatalysts for the oxygen reduction reaction" *Analytical Chemistry* **2010**, 82, 6321-6328.

Capítulo 6:

Electrooxidación de ácido fórmico con nanopartículas de platino de forma controlada decoradas con talio: mejora en la actividad electrocatalítica

<u>Capítulo 6</u>: Electrooxidación de ácido fórmico con nanopartículas de platino de forma controlada decoradas con talio: mejora en la actividad electrocatalítica

RESUMEN

En este capítulo se estudia la mejora en la oxidación del ácido fórmico al adsorber talio sobre las superficies de las nanopartículas de platino con diferente forma, con el objetivo de evitar la formación de CO que envenene la superficie catalítica y facilitar la completa oxidación hasta CO_2, intentando imitar comportamientos similares a lo obtenido trabajando con superficies monocristalinas de platino y depositando adátomos como Bi o Sb.

En primer lugar, se muestra el efecto de la adsorción de Tl sobre superficies monocristalinas de Pt(100) y Pt(111) en 0.5 M H_2SO_4, resaltando la disminución de los picos característicos de cada electrodo y la presencia de nuevos picos después de adsorberse el Tl, 0.15 V en el caso del Pt(100) y 0.43 V en el del Pt(111). A continuación, se estudia la oxidación de 0.1 M HCOOH con los mismos electrodos de platino modificados con talio. El Pt(100), más favorable a la formación de veneno en forma de CO al disociar el ácido fórmico, muestra una clara mejora de la actividad a bajos potenciales. Sin embargo, en el Pt(111), no se ve un incremento de las corrientes de oxidación a ningún potencial. A partir de estos resultados, se admite que el Tl actúa como tercer cuerpo, impidiendo la formación de CO y favoreciendo la ruta directa en la reacción de oxidación de ácido fórmico. Esta mejora es despreciable en el Pt(111), donde la producción de veneno es nula.

En cuanto al uso de las nanopartículas de platino, en primer lugar se presenta la caracterización electroquímica habitual al trabajar con las mismas muestras que en anteriores capítulos, junto al efecto de la adsorción de Tl sobre ellas. Se observa una

disminución de la corriente en los picos de adsorción de hidrógeno conforme aumenta la cantidad de Tl, que al llegar a altos recubrimientos provoca que solamente sea visible una doble capa en los perfiles voltamétricos. En este caso, el recubrimiento es complicado de calcular, por lo que se le denomina durante todo el capítulo como *recubrimiento máximo*.

Al estudiar la oxidación del ácido fórmico en las nanopartículas de platino modificadas con talio, las voltametrías cíclicas corroboran el efecto positivo de la adsorción de talio sobre todo con la disminución del potencial de inicio de oxidación del ácido fórmico hasta valores tan bajos como 0.08 V vs RHE. Como era de esperar, la mejora electrocatalítica es mayor en las nanopartículas (100)Pt que en las (111)Pt, debido a la menor tendencia para la formación de CO en estas últimas superficies. Posteriormente se compara la actividad de ambas muestras al introducir el máximo recubrimiento de talio, confirmando el mayor *factor de mejora* para las nanopartículas de (100)Pt, que llega a ser hasta de 1.5 veces mayor.

De manera similar a los estudios anteriores con nanopartículas, las cronoamperometrías evalúan la estabilidad con el tiempo de los electrodos modificados con Tl a un potencial de 0.2 V, donde la actividad aumenta debido al impedimento en la formación de CO. Este mismo resultado se confirma con los experimentos de FTIR realizados con la muestra de nanopartículas de (100)Pt, donde las bandas de CO a bajos potenciales desaparecen cuando el electrodo es modificado con Tl hasta el recubrimiento máximo, al contrario que las bandas de CO_2, las cuales sí se observan a bajos potenciales. Para los experimentos FTIR se trabajó con una concentración 0.05 M de ácido fórmico y 0.1 M de H_2SO_4, para evitar elevadas formaciones de CO_2 que desestabilicen la configuración de doble capa e impedir también daños en el prisma de CaF_2.

En la parte final del capítulo, se estudia el efecto que tiene la concentración del ácido fórmico en su oxidación para las dos muestras modificadas con un recubrimiento máximo de Tl. En las voltametrías cíclicas se produce un aumento de la actividad con la concentración de ácido fórmico. Se esperaría que las corrientes de oxidación fueran directamente proporcionales a la concentración de ácido fórmico. Sin embargo, al realizar la representación logarítmica *log j vs log [HCOOH]*, la pendiente toma un valor de 0.75 en lugar del esperado valor de 1, revelando la influencia de especies adicionales en el

mecanismo de reacción. Las corrientes transitorias registradas a un potencial de 0.2 V, muestran una mayor actividad conforme aumenta la concentración, al igual que en el caso de las voltametrías cíclicas, sobre todo a partir de valores de 0.1 M. Por último, se resumen los datos de corrientes obtenidas en las cronoamperometrías después de 10 min, considerando que casi se ha alcanzado un estado estacionario y ratificando la mucha mayor actividad para las nanopartículas de (100)Pt en el rango de concentraciones estudiado.

Chapter 6

PCCP

PAPER

View Article Online
View Journal | View Issue

Cite this: *Phys. Chem. Chem. Phys.*, 2014, 16, 13616

Formic acid electrooxidation on thallium-decorated shape-controlled platinum nanoparticles: an improvement in electrocatalytic activity

Carlos Busó-Rogero, Juan V. Perales-Rondón, Manuel J. S. Farias, Francisco J. Vidal-Iglesias, Jose Solla-Gullon, Enrique Herrero and Juan M. Feliu*

Received 20th January 2014,
Accepted 27th February 2014

DOI: 10.1039/c4cp00304g

www.rsc.org/pccp

Thallium modified shape-controlled Pt nanoparticles were prepared and their electrocatalytic activity towards formic acid electrooxidation was evaluated in 0.5 M sulfuric acid. The electrochemical and *in situ* FTIR spectroscopic results show a remarkable improvement in the electrocatalytic activity, especially in the low potential region (around 0.1–0.2 V *vs.* RHE). Cubic Pt nanoparticles modified with Tl were found to be more active than the octahedral Pt ones in the entire range of Tl coverages and potential windows. *In situ* FTIR spectra indicate that the promotional effect produced by Tl results in the inhibition of the poisoning step leading to CO_{ads}, thus improving the onset potential for the complete formic acid oxidation to CO_2. Chronoamperometric experiments were also performed at 0.2 V to evaluate the stability of the electrocatalysts at constant potential. Finally, experiments with different concentrations of formic acid (0.05–1 M) were also carried out. In all cases, Tl-modified cubic Pt nanoparticles result to be the most active. All these facts reinforce the importance of controlling the surface structure of the electrocatalysts to optimize their electrocatalytic properties.

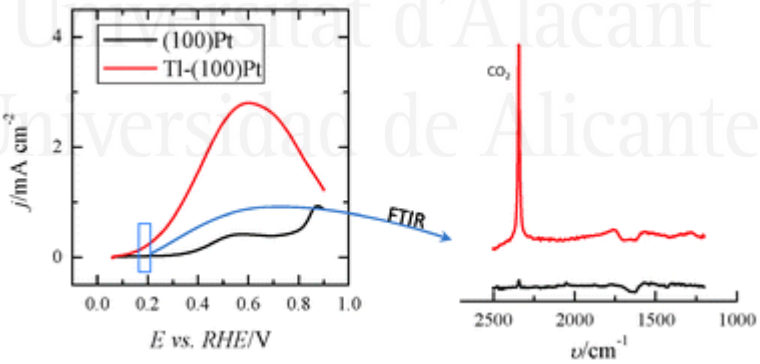

This chapter has been adapted and formatted from Phys. Chem. Chem. Phys. **2014**, 16, 13616-13624.

Corresponding author: juan.feliu@ua.es

6.1 Introduction

Formic acid is among the most promising fuels for anodic reactions in electrochemical energy conversion devices such as Polymer Electrolyte Membrane (PEM) fuel cells [1, 2]. Assuming that the change in the Gibbs free energy for the reaction in the fuel cell ($HCOOH + 1/2O_2 \rightarrow CO_2 + H_2O$) is $\Delta G^o \approx -285$ kJ mol^{-1} [3], the standard electrode potential for the formic acid/CO_2 redox couple is *ca.* −0.25 V. However, formic acid electro-oxidation takes place at potentials that are 0.6 V higher than the reversible thermodynamic potential on platinum electrodes [4, 5]. From an electrocatalytic point of view, this large overpotential is mainly due to the high resistance to the oxidation of intermediate products that diminish the performance of platinum as an anode catalyst by blocking surface sites [6]. In this sense, many studies on formic acid electro-oxidation reaction aim at developing new electrocatalytic materials which present higher selectivity than platinum electrodes for the formic acid dissociation. In this respect, the mechanism of formic acid electro-oxidation occurs through two parallel routes on platinum electrodes [7-11]. In one of these pathways, HCOOH is oxidized through an active intermediate, which decomposes to yield CO_2. In the other reaction pathway, *i.e.* the indirect one, the reaction mechanism occurs through the non-faradaic dehydration reaction of formic acid yielding CO_{ads} and water molecules. The latter reaction also takes place at open circuit potential on platinum [12] and requires more surface sites than the active intermediate reaction path [13]. Since the oxidation of CO_{ads} requires a large overpotential, this species is considered to be a poisoning intermediate.

It is also known that the formic acid electro-oxidation reaction is very sensitive to the local surface structure [5, 14, 15]. Concerning this point, it was shown that the Pt(100) electrode was the most active among platinum basal planes, while the activity was observed for Pt(111) for both routes [5]. To modify the electrocatalytic activity and/or selectivity of bare substrates for the different routes, the presence of other species such as foreign atoms is a powerful strategy. In fact, many studies on modified single crystal Pt electrodes with Sb [16], Bi [17], Pb [18], Pd [19] and Te [20] show an improvement in the catalytic performance of these materials towards formic acid oxidation. These electrocatalytic improvements by foreign atoms are possible due to: (i) a third-body effect, where adatoms block neighboring sites required for CO_{ads} formation [13]; (ii) electronic

effects, where the foreign adatoms modify the adsorption energy between the adsorbate and the substrate facilitating the oxidation reaction [12, 13, 21]; and (iii) a bifunctional mechanism, where, in this case, the presence of foreign atoms can reduce the overpotential for CO_{ads} oxidation providing easily activated oxygen-species at lower potentials than those on the corresponding bare substrate [22].

From an applied point of view, the use of single crystal surfaces is not feasible and nanomaterials with a much higher surface to volume ratio are required. Since the development of methods to synthesize shape-controlled Pt nanoparticles [23] and their first use in electrocatalysis [24], many studies have been focused on the evaluation of the electrocatalytic properties of these shaped Pt particles for oxidation reactions of promising fuels, such as formic acid [25, 26]. For this reaction, shape-controlled Pt nanoparticles have confirmed the structural electrocatalytic dependence related to the presence of facets with {100} and {111} symmetry. Thus, Pt nanoparticles rich in {100} facets are the most electroactive applicable system towards formic acid oxidation. Unfortunately, shaped Pt nanoparticles also show a high CO poisoning rate [26].

As has been done with platinum single crystals, in order to increase the activity and/or to overcome the poisoning effect, Pt nanoparticles have been decorated with adatoms such as Pd [27, 28], Bi [29, 30], or Sb [31]. In addition, Pt/Pd alloyed [32] and PtBi intermetallic nanoparticles [33] have also been tested. Based on the reported results in ref. [28] and [29] it can be proposed that the improvement in electrocatalytic activity seems to be mainly related to the geometry of the surface atoms of the shaped nanoparticles and the chemical nature of foreign adatoms.

Studies in the 1980s showed that thallium (Tl) UPD (under potential deposition) on both polycrystalline platinum and gold increases the rate of formaldehyde electro-oxidation [34, 35]. However, even considering these promising results, almost no studies have been devoted to the impact of Tl in the electrocatalysis of formic acid [36]. For that reason, we report in this paper an electrochemical and spectroscopic (in situ FTIR – Fourier Transform Infrared) study on the electrocatalytic properties of Tl-decorated shape-controlled Pt nanoparticles towards HCOOH electrooxidation.

6.2 Experimental

Platinum single crystal surfaces were prepared following the method developed by Clavilier et al. [37] from single crystal beads (*ca*. 2 mm in diameter). Before the experiments, working electrodes were flame annealed during 30 s, cooled down in a H_2/Ar atmosphere and quenched in ultrapure water in equilibrium with this atmosphere before they were transferred to the electrochemical cell [38]. Cubic and octahedral shape-controlled Pt nanoparticles, denoted as (100)Pt and (111)Pt respectively, were employed. The synthesis of these shape-controlled Pt nanoparticles was performed as previously described in detail [39]. Transmission Electron Microscopy (TEM) measurements were performed to estimate both particle size and morphology/shape [39].

For electrochemical and in situ FTIR measurements, the nanoparticles dispersed in water were deposited on a polished gold disk and dried under argon atmosphere. Thereafter, the nanoparticles were cleaned by CO (N47, Air Liquide) monolayer adsorption and stripping treatment before the experiments, avoiding high potential excursions to preserve surface order. The active area of platinum nanoparticles was calculated by measuring the charge involved in the so-called hydrogen UPD region after the subtraction of the conventional double-layer contribution in 0.5 M H_2SO_4 solution, using a reference value of 0.23 mC cm^{-2} [40]. A small quantity of nanoparticles (with an active area of ca. 0.05–0.1 cm^2) was deposited in all the experiments in order to avoid/minimize transport problems of the reactant species to the surface of the nanoparticles [41].

The deposition of Tl on Pt was performed using dilute concentrations of 10^{-4}–10^{-5} M Tl_2SO_4 (Aldrich® 99.995%) in 0.5 M H_2SO_4 solution, cycling the electrode potential between 0.06 V and 0.90 V at 0.05 V s^{-1}. The Tl coverage was monitored through the decrease of the hydrogen adsorption/desorption peaks, according to the equation:

$$\theta_{Tl} = 1 - \theta_H = \frac{q_H^0 - q_H^{Tl}}{q_H^0} \quad (6.1)$$

where q^0_H and q^{Tl}_H are the hydrogen adsorption charges of the clean and thallium modified electrodes respectively, which were also calculated after the subtraction of the double layer charging contribution. In the case of platinum single crystals, the electrodes were cycled in

specific potential ranges to preserve the surface order and to avoid problems of Tl desorption at higher potentials.

A platinum wire was used as a counter electrode, and a reversible hydrogen (N50, Air Liquide) electrode (RHE) was employed as a reference electrode. All potentials used in this paper are referenced to the RHE. Experiments were carried out in 0.5 M H_2SO_4 (Merck KGaA Suprapur® 96%), prepared in ultrapure water (Elga PureLab Ultra 18.2 MΩ cm), and deareated with Ar (N50, Air Liquide). Formic acid (Merck KGaG 98%) oxidation experiments were performed in 0.5 M H_2SO_4.

For electrochemical measurements, cyclic voltammetry and chronoamperometry were employed using a waveform generator (EG&G PARC 175) together with a potentiostat (eDAQ EA161) and a digital recorder (eDAQ ED401).

In situ FTIR spectra were acquired using a Nicolet (Model 8700) spectrometer, equipped with an MCT (Mercury–Cadmium–Telluride) detector. The spectroelectrochemical cell was fitted with a prismatic 60° CaF_2 window, as described previously [42]. The spectra, obtained from the average of 100 interferograms using a resolution of 8 cm^{-1}, were collected at intervals of 50 mV between 0.05 V to 0.90 V vs. RHE. For all experiments, p-polarized light was employed, which allows detecting changes in the concentration of active species on the electrode surface and electrolyte solution [42]. Spectra are presented in absorbance units $A=-\log[(R_1-R_2)/R_1]$ in which R_2 and R_1 are referred to as the reflectance values of the single beam spectra corresponding to the sample and the reference potentials, respectively. Positive bands in the spectra are related to species that have been formed at the sample potential whereas negative bands correspond to species consumed. All the experiments were performed at room temperature.

6.3 Results and discussion

6.3.1 Formic acid oxidation on Tl-modified Pt single crystal electrodes

Preliminary experiments with Pt(100) and Pt(111) single crystal electrodes were performed to evaluate the effects of the Tl adsorption on these Pt model surfaces both in the absence and presence of formic acid. Fig. 6.1 shows voltammetric results for Tl modified Pt(100) and Pt(111) single crystal electrodes in a 0.5 M H_2SO_4 solution. The effect of Tl deposition can be easily monitored by the changes in the cyclic voltammetric profile. In addition, in order to avoid possible Tl dissolution, the upper potential limits were set at 0.65 and 0.6 V for Pt(100) and Pt(111) electrodes, respectively.

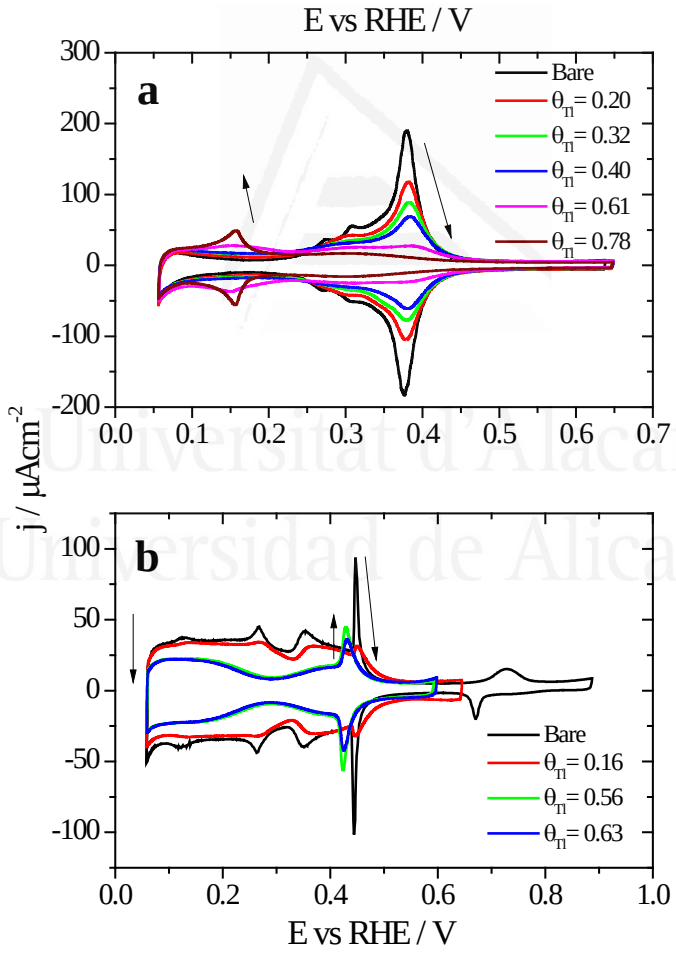

Fig. 6.1. Evolution of the voltammetric profiles in 0.5 M H_2SO_4 with increasing amounts of Tl on (a) Pt(100) and (b) Pt(111). Scan rate: 0.05 V s^{-1}. Arrows indicate changes associated with increasing Tl amounts at the surface.

For the Pt(100) electrode (Fig. 6.1a), the adsorption/desorption states between 0.2 and 0.5 V (which are associated with the competitive adsorption between hydrogen and anions) remarkably decrease during Tl deposition, whereas a small peak appears at about 0.15 V at Tl coverages close to the full blockage.

In the case of the Pt(111) electrode, Fig. 6.1b, similar effects are observed for the diminution of the charge in the hydrogen adsorption/desorption region (between 0.06 and 0.35 V) and the (bi)sulfate adsorption (between 0.35 and 0.65 V). Again, a new small peak for this electrode appears at about 0.43 V at high coverages of Tl. This peak is associated with the adsorption of sulfate on the modified electrode, because it is absent in perchloric acid solutions. Although it appears in the same potential region that the spike in sulfuric acid solutions for the Pt(111) electrode, the origin is not the same. The spike at 0.45 V diminishes upon Tl deposition and at a given Tl coverage the new peak appears. It is then probably related to structural changes in the adlayer that changes the interaction of sulfate with the electrode surface.

The positive going sweep voltammetric profiles of formic acid oxidation for the same Tl-modified Pt single crystal electrodes from Fig. 6.1 are presented in Fig. 6.2, using 0.1 M HCOOH in 0.5 M H_2SO_4 as test solution. As expected, very low currents are observed for the bare Pt(100) electrode as a consequence of the well-established CO poisoning process coming from the dehydration of formic acid, which is favored on Pt(100) [11]. With increasing amounts of Tl, the indirect path (through CO poisoning) is hindered. Then formic acid oxidation can take place through the direct path and oxidation currents increase very significantly. The results suggest an optimum Tl coverage at values close to 0.4. At higher coverages, the onset potential increases and the current diminishes.

However, in the case of the Pt(111) electrode (Fig. 6.2b), for which it is well-established that the CO poisoning is almost negligible [11], the addition of Tl does not provide significant changes in the electrooxidation process. These results seem to indicate that Tl acts as a third body preventing the dehydration reaction. For the Pt(111) electrode, owing to the almost negligible CO formation rate [5], the presence of Tl does not improve its catalytic activity. The current diminution for this electrode is just the result of the diminution of the Pt free sites.

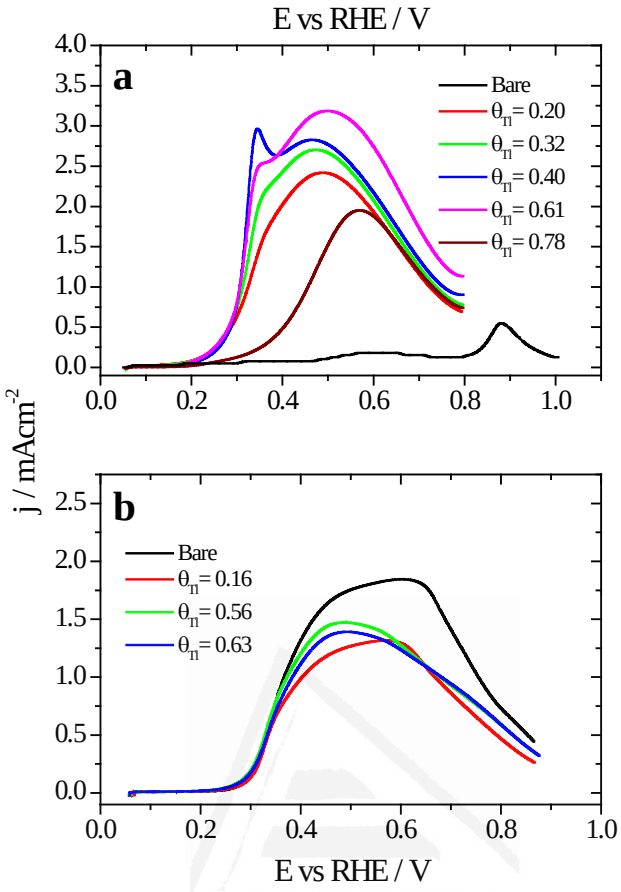

Fig. 6.2. Positive sweep voltammetric profiles for 0.1 M formic acid oxidation in 0.5 M H_2SO_4 with and without Tl for (a) Pt(100) and (b) Pt(111) single crystals. Scan rate: 0.02 V s^{-1}.

On the other hand, the increase of activity for the Pt(100) electrode can be related to the diminution of the CO_{ads} coverage which leads to an increase of the oxidation through the active intermediate reaction path. However, electronic effects cannot be discarded for this electrode. It should be noted that the onset for the direct oxidation reaction in the absence of poison on the Pt(100) electrode is 0.30 V (see ref. [43]), whereas in the presence of Tl the onset is *ca*. 0.20 V. This diminution of the onset potential at a Tl coverage of *ca*. 0.4 suggests the possible presence of an electronic effect. These results also point out the importance of controlling the surface structure of the Pt substrate, the Pt(100) square structure being much more convenient than the hexagonal Pt(111). Thus, in terms of the particle shape, it would be preferable to use cubic Pt nanoparticles in which the number of {100} surface sites is maximized [44].

6.3.2 Electrochemical characterization of Tl modified Pt nanoparticles

Fig. 6.3 displays the voltammetric profiles of the (100)Pt and (111)Pt nanoparticles before and after Tl incorporation. Before the Tl decoration, the voltammetric profiles of the cubic and octahedral Pt nanoparticles are those that are expected from their shape–surface structure relationship [45]. Thus, the cubic Pt nanoparticles show the main features related to a preferential {100} surface structure, that is, a sharp peak at ~0.27 V related to {100} edge/corner sites and a signal around 0.37 V associated with wide {100} terrace sites. In contrast, the octahedral nanoparticles show the characteristics of a preferential {111} surface structure, with a broad peak at about 0.52 V related to sulfate adsorption on relatively wide two-dimensional {111} terrace sites. A detailed analysis of the characteristic voltammetric features of similar shape-controlled Pt nanoparticles was described in previous contributions [44].

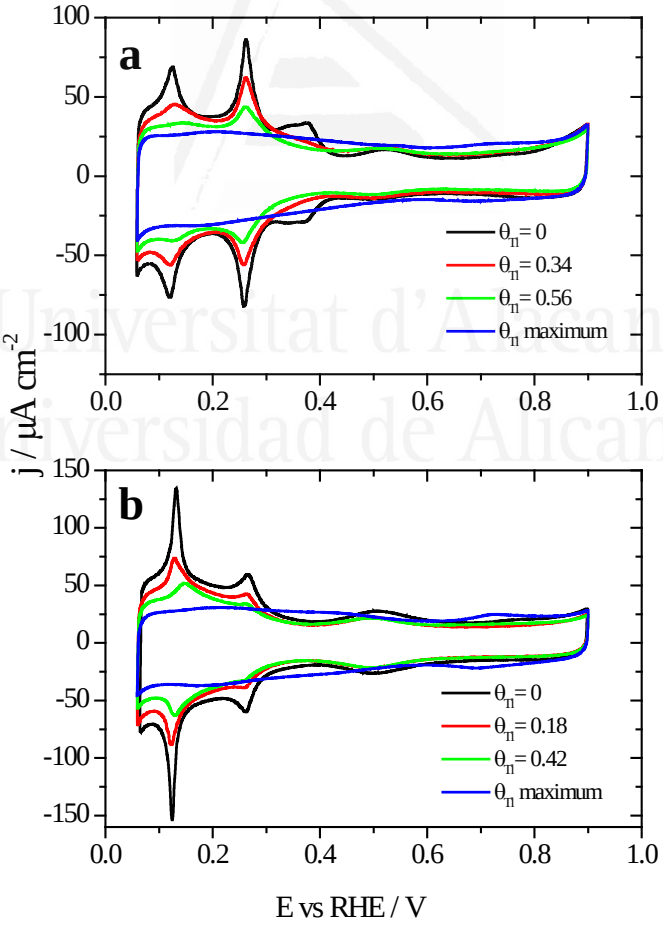

Fig. 6.3. Voltammetric profiles for increasing amounts of Tl coverages on (a) (100)Pt and (b) (111)Pt nanoparticles in 0.5 M H_2SO_4 + 10^{-4} ~ 10^{-5} M Tl_2SO_4. Scan rate: 0.05 Vs^{-1}.

Fig. 6.3 also shows the voltammetric responses of the (100)Pt and (111)Pt nanoparticles after partial and maximum deposition of Tl. The evolution of the voltammetric profiles is similar to those previously reported for Pd and Bi on shape-controlled Pt nanoparticles [28, 29] or after deposition of Bi(III), Te(IV) and Se(IV) on stepped Pt surfaces [46]. In addition, the Tl adsorption process does not produce appreciable changes in the charge density on the so-called double layer region until high thallium coverages are reached. As described in the experimental section, the Tl coverage can be calculated considering the expression $\theta_{Tl} = 1 - \theta_H$, where θ_{Tl} and θ_H are the thallium and hydrogen coverages, respectively. However, at the maximum thallium coverage on both Pt nanoparticles, Fig. 6.3, an important increase of the double layer region is observed. This fact prevents an accurate determination of the Tl coverage for highly covered surfaces that cannot be properly calculated. For that reason, the maximum coverage for each sample will be referred to as "maximum" and no numeric value will be given. In addition, it is important to note the absence of additional voltammetric features at high coverages and remark that only a small broad peak is visible at about 0.70 V, particularly in the preferential (111)Pt nanoparticles. This feature can be linked to the thallium desorption from (111) terrace sites, as pointed out for Tl UPD in Pt(111) reports [47, 48].

6.3.3 Formic acid oxidation on Tl modified shape controlled Pt nanoparticles

After each particular Tl adsorption, the modified Pt nanoparticles were transferred to a second electrochemical cell containing 0.1 M formic acid + 0.5 M H_2SO_4. Fig. 6.4 compares the positive going sweep voltammetric responses obtained for the bare and Tl modified shaped nanoparticles. For the bare cubic (100)Pt nanoparticles (Fig. 6.4a, black line), the positive going scan shows almost zero current density at potentials below 0.35 V, due to CO poisoning effects. The HCOOH oxidation starts at around 0.35 V, and the current density increases slowly until ~0.80 V. Above this potential, the current density starts to grow rapidly due to CO oxidation and therefore in the reverse scan the current density would be much higher as the surface is CO-free. As before, these negative-going results are not shown, because they are irrelevant in electrocatalytic studies [26, 39].

Interestingly, for Tl modified cubic (100)Pt nanoparticles with θ_{Tl} = 0.34 and 0.56, Fig. 6.4a (red and green lines, respectively), the onset potential of HCOOH oxidation remarkably decreases to about 0.1 V. Moreover, at the maximum coverage (blue line), the onset potential is even lower (about 0.08 V). This feature clearly evidences the positive impact of thallium on the electro-oxidation of formic acid in the low potential region.

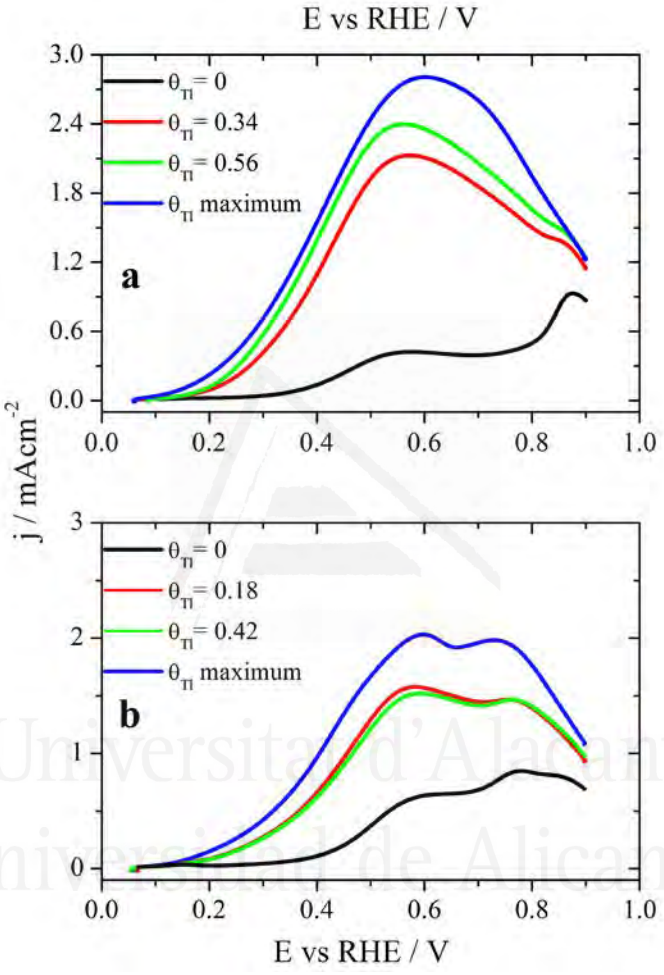

Fig. 6.4. Positive sweep voltammetric profiles for formic acid electro-oxidation with increasing amounts of Tl coverages for (a) (100)Pt and (b) (111)Pt nanoparticles. Scan rate: 0.02 Vs^{-1}. Test solution: 0.1 M formic acid in 0.5 M H_2SO_4.

For the (111)Pt nanoparticles, Fig. 6.4b, a similar effect on the onset potential is observed after surface decoration with Tl. Taking into account that (i) the {111} domains do not suffer the same strong CO poisoning effect as that observed with the {100} domains [11] (see Fig. 6.2) and (ii) the {111} domains have a low catalytic activity for the direct oxidation [5], the electrocatalytic enhancement observed is lower than that reported for the

(100)Pt nanoparticles. Anyhow, the onset potential diminishes when θ_{Tl} increases, decreasing to around 0.1 V at the maximum coverage (blue line). Also, the onset for the formic acid oxidation observed for the Tl modified nanoparticles at high coverages is *ca*. 0.2–0.3 V lower than the onset for the direct oxidation route in the unmodified nanoparticles [26].

Finally, with the aim of comparing the activity of both samples in the whole potential range, Fig. 6.5 displays the HCOOH activity ratio between the bare and Tl modified (maximum coverage) Pt nanoparticles. From Fig. 6.5, it is evident that the "improvement factor" due to the presence of Tl for the (100)Pt nanoparticles is larger than that obtained with the (111)Pt nanoparticles in the entire potential range. In fact, the highest ratio between both activities is observed at *ca*. 0.3 V, the potential at which the {100} domains have the greatest activity, in agreement with the large catalytic activity of Tl on the {100} domains (Fig. 6.2a). In addition, in terms of maximum currents, the electrooxidation activity of the Tl-modified (100)Pt nanoparticles is always higher (about 1.5 times) than that of the (111)Pt nanoparticles, Fig. 6.6.

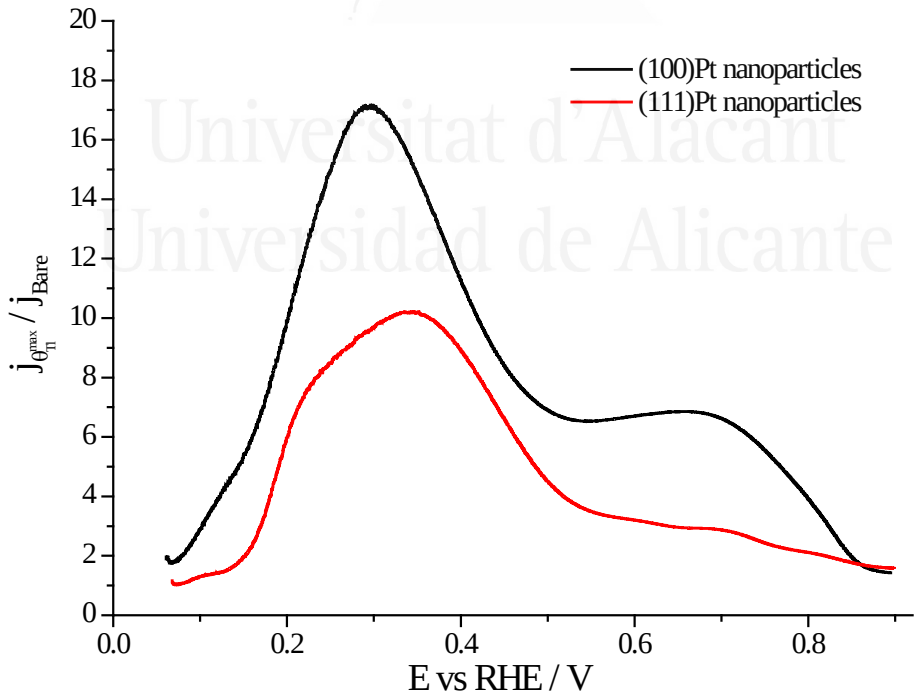

Fig. 6.5. Ratio between the HCOOH oxidation current densities obtained with the bare and Tl-decorated (maximum coverage) shape-controlled Pt nanoparticles. Data taken from Fig. 6.4.

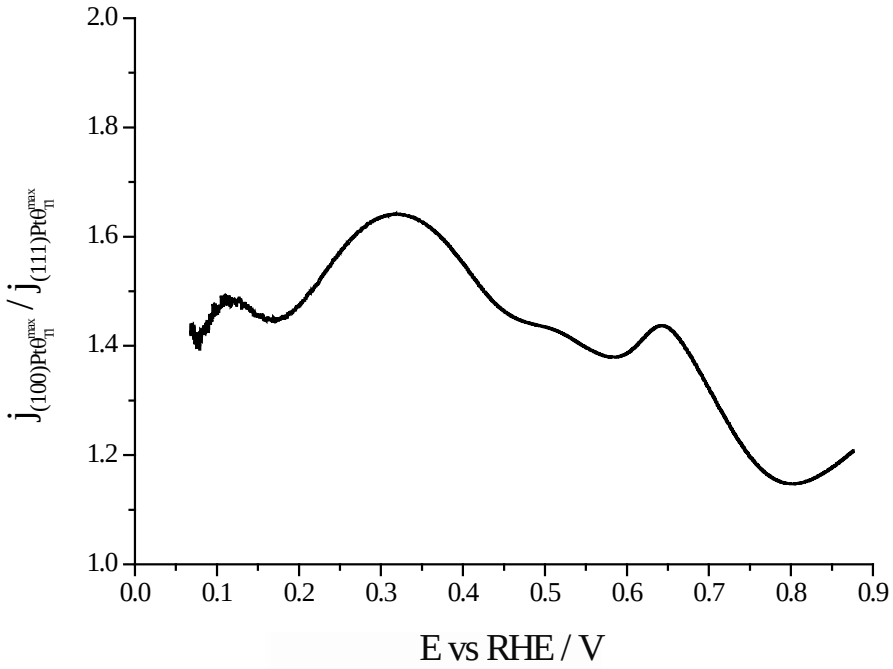

Fig. 6.6. Ratio between the HCOOH oxidation current densities obtained using Tl-modified (maximum coverage) (100) and (111)Pt nanoparticles. Data taken from Fig. 6.4.

In order to better evaluate the activity as well as the stability of the Tl-modified samples, current transient responses for each modified electrode were recorded at 0.2 V (Fig. 6.7), a reasonably low potential value. In these experiments, a pretreatment consisting of a potential step at 0.85 V for 10 s prior to the potential step at 0.2 V was performed in order to oxidize all the possible CO blocking surface sites [26]. Current transients for the bare nanoparticles are not reported, as current densities for both samples are almost zero. This is due to the fact that the CO formation rate is very high and the surface is immediately covered by CO after the cleaning step. For Tl modified (100)Pt nanoparticles (Fig. 6.7a) the current densities after 600 s are 0.002, 0.010 and 0.014 mA cm^{-2} at Tl coverages of 0.25, 0.48 and the maximum one, respectively. For Tl modified (111)Pt nanoparticles (Fig. 6.7b), reactivity is lower and current densities of 0.002, 0.004 and 0.006 mA cm^{-2} were obtained at coverages of 0.43, 0.57 and the maximum one, respectively. These results indicate that Tl adsorbed on the surface successfully hinders the CO adsorption through the poisoning pathway, and this effect increases with the Tl coverage.

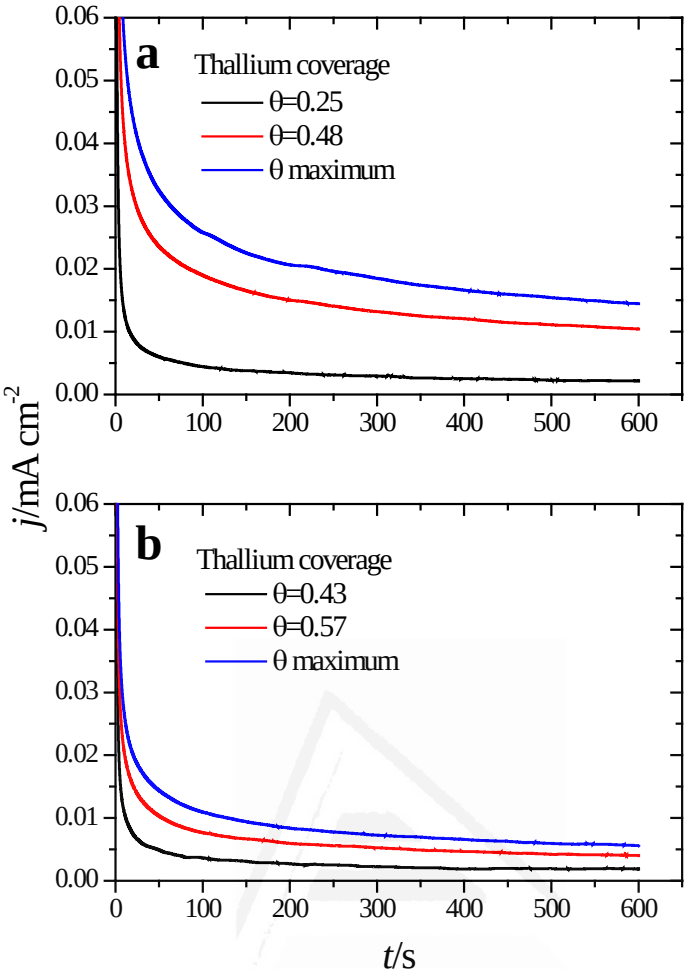

Fig. 6.7. Current transients recorded at 0.2 V for formic acid electrooxidation for (a) (100)Pt and (b) (111)Pt nanoparticles with different Tl coverages. Test solution: 0.1 M formic acid in 0.5 M H_2SO_4.

6.3.4 FTIR experiments of formic acid oxidation on Tl-decorated Pt nanoparticles

In situ FTIR spectra were measured in order to better understand the role of Tl in the enhancement of formic acid oxidation on the modified nanoparticles. Only the (100)Pt nanoparticles were studied because these nanoparticles present more CO_{ads} than the (111)Pt nanoparticles [39, 49], and then, it is easier to determine the electrocatalytic effects induced by the presence of Tl. Spectra were collected in 0.05 M formic acid in 0.1 M H_2SO_4 on non-modified and Tl-modified electrodes (at maximum thallium coverage).

Formic acid concentration was diminished with the aim of decreasing the huge amount of CO_2 formed during formic acid oxidation, which destabilizes the thin-layer configuration. Sulfuric acid concentration was also reduced in order to avoid possible damage in the CaF_2 prism. For all spectra presented, the spectrum acquired at 0.05 V was used as a reference.

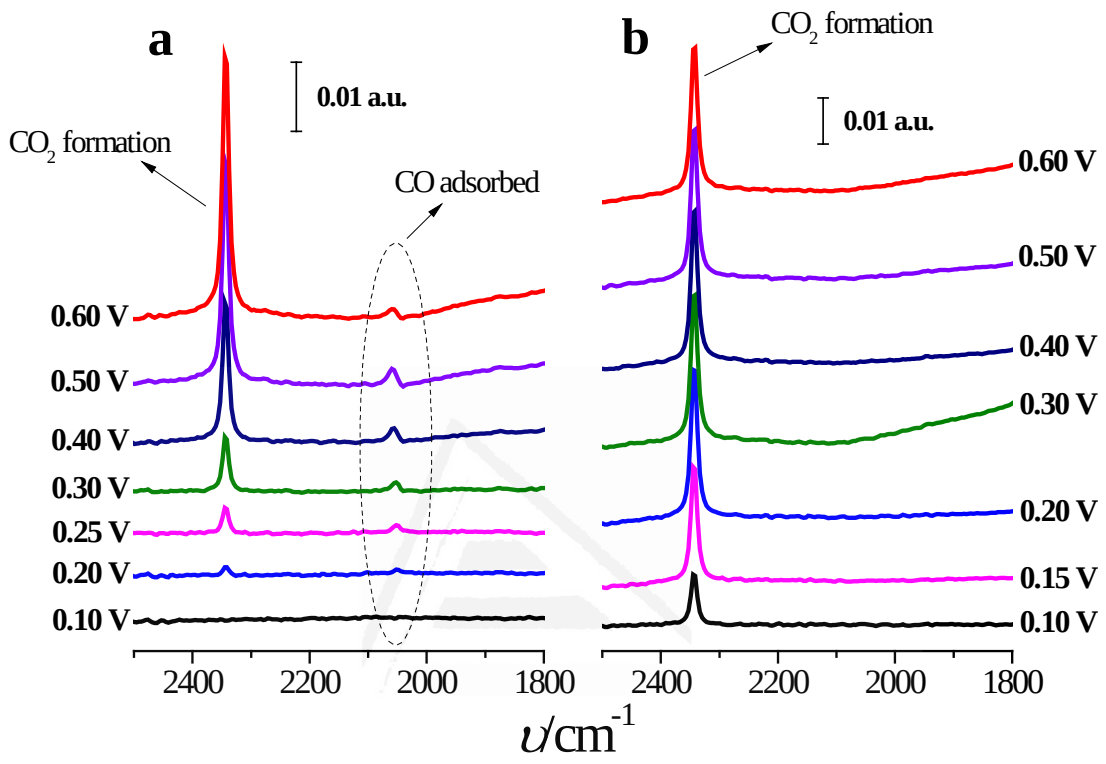

Fig. 6.8. *In situ* FTIR spectra for formic acid electro-oxidation on (100)Pt nanoparticles: (a) bare Pt and (b) maximum Tl coverage. Reference spectra were taken at 0.05 V. Test solution: 0.05 M formic acid in 0.1 M H_2SO_4.

Fig. 6.8a displays the spectra for formic acid oxidation on (100)Pt bare nanoparticles. From 0.2 V to 0.6 V, the spectra show the linearly adsorbed CO band between 2050 and 2060 cm^{-1} [42]. At 0.2 V, the band frequency is around 2052 cm^{-1}, whereas at 0.6 V the frequency shifts to 2060 cm^{-1}, likely due to the Stark effect [50]. Between 0.4 and 0.5 V, the band shows a slightly bipolar character, meaning that adsorbed CO was present in the reference potential (0.05 V) [42]. At around 0.2 V, a new band at 2343 cm^{-1} appears, which is associated with the start of CO_2 formation [42]. The spectra do not show any signal band that could be attributed to bridge adsorbed CO, which should appear at around 1820 cm^{-1} as was observed for formic acid oxidation in ATR-SEIRA (Attenuated Total

Reflection – Surface Enhanced Infra-Red Absorption) experiments on thin-film polycrystalline platinum electrodes at 0.35 V vs. RHE [9].

Fig. 6.8b shows the spectra for formic acid oxidation on Tl-modified (100)Pt nanoparticles. The band for CO_2 can be clearly observed at 0.1 V, and the CO_{ads} band is absent for all the spectra, pointing out that Tl enhances the electrocatalytic activity (Fig. 6.4a) by hindering the poisoning pathway thus allowing formic acid oxidation to proceed through the direct pathway, which also explains why CO_2 is formed at low potentials.

6.3.5 Effect of formic acid concentration

Once the catalytic effect of Tl over Pt nanoparticles for formic acid oxidation has been confirmed, experiments using different formic acid concentrations were also performed with the maximum Tl coverage to evaluate its possible effect on the electrocatalytic activity. The corresponding potentiodynamic responses are shown in Fig. 6.9, for both (100)Pt and (111)Pt nanoparticles. In the two cases, current densities increase with the concentration of formic acid, especially at low potentials. In principle, it would be expected that currents were directly proportional to the concentration of formic acid, that is, $j \propto C_o^*$. Thus, the representation of log(j) at a given potential vs. log(C_o^*) should be linear with a slope of 1, the expected reaction order for the formic acid concentration. The plots are linear in the range between 0.2 and 0.7 V in both scan directions (inset of Fig. 6.9b). However, the slope is 0.75 ± 0.03 in this potential range for both electrodes, which would indicate that the reaction order is 0.75. This fact clearly suggests that the reaction mechanism is complex. It could be argued that the complexity is due to the presence of the two routes for the reaction. However, it is known that the CO formation reaction occurs in the potential window lower than 0.5 V [26]. Thus, the oxidation reaction in the negative scan at E > 0.5 V would take place on a clean surface and only through the active intermediate. Moreover, the presence of Tl has suppressed the route through CO significantly. The constant value for the reaction order in the whole range, then, suggests that the complexity is not due to the CO route, but there is an intrinsic factor in the direct

oxidation route. This fact would indicate that an additional species (not only formic acid) is involved in the reaction mechanism.

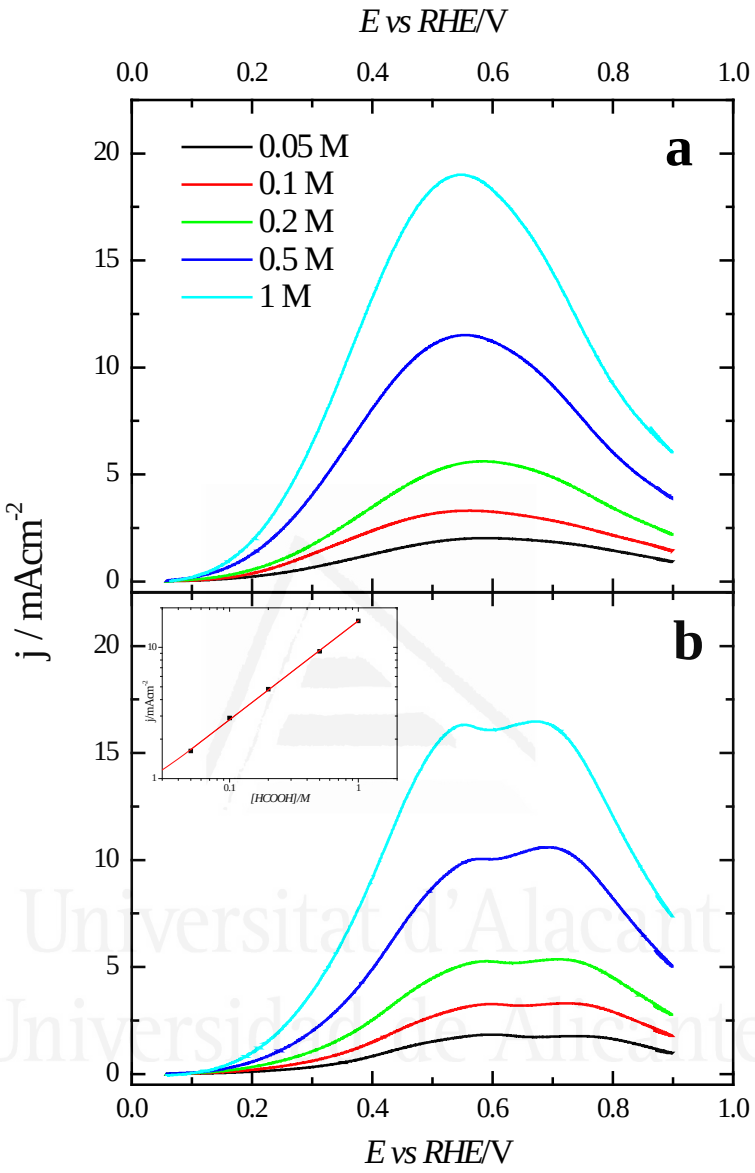

Fig. 6.9. Positive sweep voltammetric profiles for (a) (100)Pt and (b) (111)Pt nanoparticles with maximum Tl coverage in different concentrations of formic acid in 0.5 M H_2SO_4. Scan rate: 0.02 Vs^{-1}. Inset: double logarithmic plot of the current density at 0.5 V for the (111)Pt nanoparticles *vs.* formic acid concentration.

Additional evidence on that is found in the chronoamperometric responses after 600 s of reaction at 0.2 V for both nanoparticles at maximum Tl coverage at different formic acid concentrations (Fig. 6.10). In the case of (100)Pt nanoparticles (Fig. 6.10a), there is

nearly no clear difference between the final current density for 0.05 M and 0.1 M (around 0.015–0.020 mA cm^{-2}), but for the other concentrations, current density increases with the amount of formic acid in solution, increasing up to 0.145 mA cm^{-2} for 1 M formic acid concentration. A similar behavior was observed for (111)Pt nanoparticles in Fig. 6.10b, with a final current density of 0.049 mA cm^{-2} for 1 M formic acid. As for voltammetric curves, chronoamperometric currents become higher when the concentration of formic acid increases. Fig. 6.11 summarizes the differences observed for the final current density after 10 min at 0.2 V for both samples at maximum coverage, clearly indicating that the Tl-modified (100)Pt nanoparticles are much more active than the (111)Pt nanoparticles in the range of HCOOH concentration under study (0.05–1 M HCOOH). Currents recorded after 10 minutes reflect a nearly stationary situation. For the currents at 10 min the reaction order is similar to that measured by voltammetry, which reinforces the fact that the reaction mechanism through the active intermediate is complex.

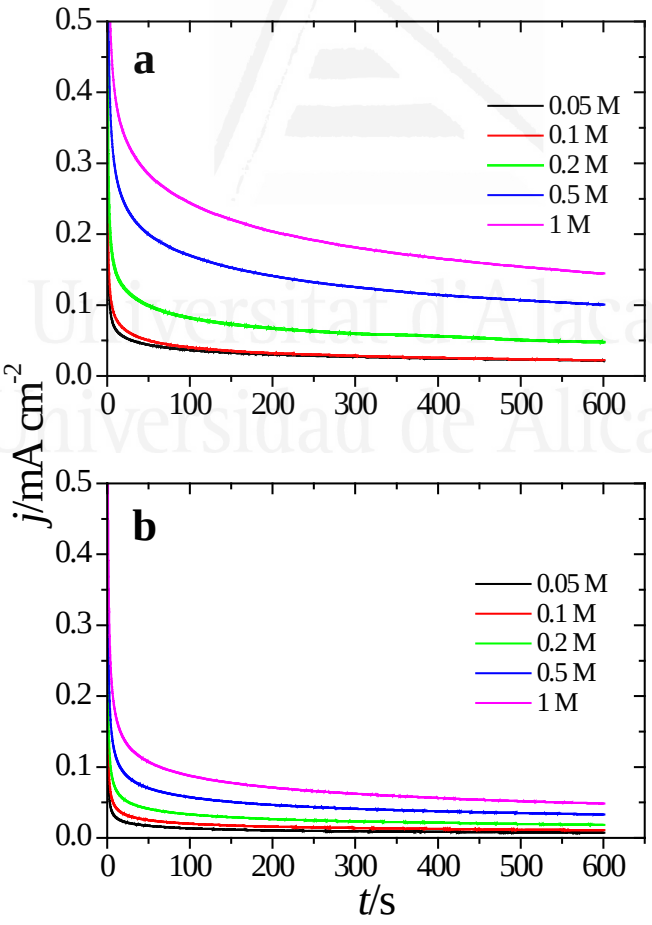

Fig. 6.10. Current transients for (a) (100)Pt and (b) (111)Pt nanoparticles with maximum Tl coverage recorded at 0.20 V for different formic acid concentrations in 0.5 M H_2SO_4.

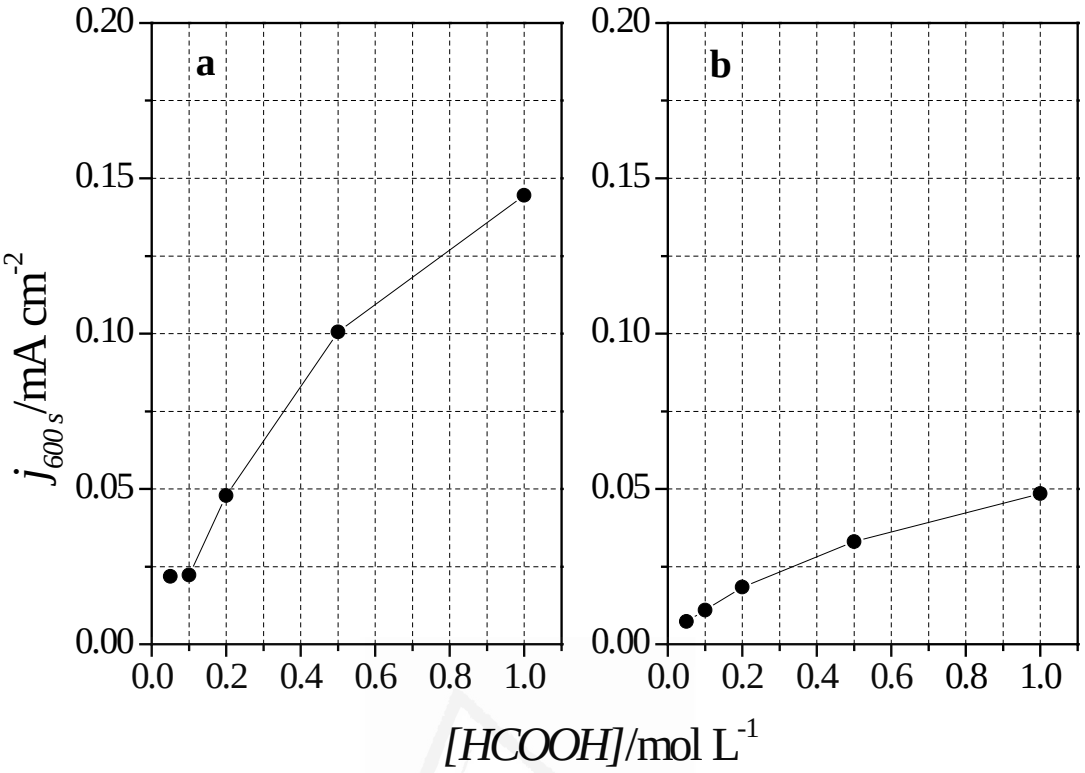

Fig. 6.11. Comparison between formic acid concentrations and current densities obtained after 10 minutes at 0.20 V Data extracted from Fig. 6.10 for (a) (100)Pt and (b) (111)Pt nanoparticles.

6.4 Conclusions

The deposition of Tl on (100)Pt and (111)Pt nanoparticles remarkably improves their electrocatalytic activity towards formic acid oxidation, especially in the low potential region. The activity enhancement is also dependent on the surface structure of the Pt substrate. In agreement with fundamental data from Pt single crystal studies, the use of (100)Pt nanoparticles is clearly more beneficial than the use of (111)Pt nanoparticles. Voltammetric and in situ FTIR data indicate that Tl decoration prevents the formation of adsorbed CO_{ads}. Consequently, it can be concluded that the enhancement of formic acid oxidation with Tl-decorated platinum nanoparticles (especially with (100)Pt nanoparticles) is due to the hindrance of the indirect pathway (third body effect). So, the reaction mainly takes place through the direct pathway (via non-CO_{ads}). However, electronic effects cannot be discarded, due to the diminution of the onset potential for the formic acid oxidation reaction.

6.5 References

[1] C. Rice, R. I. Ha, R. I. Masel, P. Waszczuk, A. Wieckowski and T. Barnard, "Direct formic acid fuel cells" *Journal of Power Sources* **2002**, 111, 83-89.

[2] N. V. Rees and R. G. Compton, "Sustainable energy: A review of formic acid electrochemical fuel cells" *Journal of Solid State Electrochemistry* **2011**, 15, 2095-2100.

[3] S. Uhm, H. J. Lee and J. Lee, "Understanding underlying processes in formic acid fuel cells" *Physical Chemistry Chemical Physics* **2009**, 11, 9326-9336.

[4] G. Q. Lu, A. Crown and A. Wieckowski, "Formic acid decomposition on polycrystalline platinum and palladized platinum electrodes" *Journal of Physical Chemistry B* **1999**, 103, 9700-9711.

[5] V. Grozovski, V. Climent, E. Herrero and J. M. Feliu, "Intrinsic activity and poisoning rate for HCOOH oxidation on platinum stepped surfaces" *Physical Chemistry Chemical Physics* **2010**, 12, 8822-8831.

[6] C. Rice, S. Ha, R. I. Masel and A. Wieckowski, "Catalysts for direct formic acid fuel cells" *Journal of Power Sources* **2003**, 115, 229-235.

[7] A. Capon and R. Parsons, "The oxidation of formic acid at noble metal electrodes Part III. Intermediates and mechanism on platinum electrodes" *Journal of Electroanalytical Chemistry* **1973**, 45, 205-231.

[8] M. Osawa, K. Komatsu, G. Samjeske, T. Uchida, T. Ikeshoji, A. Cuesta and C. Gutiérrez, "The Role of Bridge-Bonded Adsorbed Formate in the Electrocatalytic Oxidation of Formic Acid on Platinum" *Angewandte Chemie-International Edition* **2011**, 50, 1159-1163.

[9] A. Cuesta, G. Cabello, M. Osawa and C. Gutiérrez, "Mechanism of the Electrocatalytic Oxidation of Formic Acid on Metals" *ACS Catalysis* **2012**, 2, 728-738.

[10] Y. X. Chen, M. Heinen, Z. Jusys and R. J. Behm, "Bridge-bonded formate: Active intermediate or spectator species in formic acid oxidation on a Pt film electrode?" *Langmuir* **2006**, 22, 10399-10408.

[11] J. M. Feliu and E. Herrero, "Formic acid oxidation", in *Handbook of Fuel Cells - Fundamentals, Technology and Applications, vol. 2*, W. Vielstich, H. Gasteiger and A. Lamm (Eds.) Wiley, Chichester, **2003**, pp. 625-634.

[12] E. Herrero, A. Fernández-Vega, J. M. Feliu and A. Aldaz, "Poison formation reaction from formic acid and methanol on Pt(111) electrodes modified by irreversibly adsorbed Bi and As" *Journal of Electroanalytical Chemistry* **1993**, 350, 73-88.

[13] E. Leiva, T. Iwasita, E. Herrero and J. M. Feliu, "Effect of adatoms in the electrocatalysis of HCOOH oxidation. A theoretical model" *Langmuir* **1997**, 13, 6287-6293.

[14] S. G. Sun and Y. Y. Yang, "Studies of kinetics of HCOOH oxidation on Pt(100), Pt(110), Pt(111), Pt(510) and Pt(911) single crystal electrodes" *Journal of Electroanalytical Chemistry* **1999**, 467, 121-131.

[15] A. Cuesta, M. Escudero, B. Lanova and H. Baltruschat, "Cyclic Voltammetry, FTIRS, and DEMS Study of the Electrooxidation of Carbon Monoxide, Formic Acid, and Methanol on Cyanide-Modified Pt(111) Electrodes" *Langmuir* **2009**, 25, 6500-6507.

[16] Y.-Y. Yang, S.-G. Sun, Y.-J. Gu, Z.-Y. Zhou and C.-H. Zhen, "Surface modification and electrocatalytic properties of Pt(100), Pt(110), Pt(320) and Pt(331) electrodes with Sb towards HCOOH oxidation" *Electrochimica Acta* **2001**, 46, 4339-4348.

[17] S. P. E. Smith, K. F. Ben-Dor and H. D. Abruña, "Structural effects on the oxidation of HCOOH by bismuth-modified Pt(111) electrodes with (100) monatomic steps" *Langmuir* **1999**, 15, 7325-7332.

[18] H. W. Lei, H. Hattori and H. Kita, "Electrocatalysis by Pb adatoms of HCOOH oxidation at Pt(111) in acidic solution" *Electrochimica Acta* **1996**, 41, 1619-1628.

[19] F. J. Vidal-Iglesias, J. Solla-Gullón, E. Herrero, A. Aldaz and J. M. Feliu, "Formic acid oxidation on Pd-modified Pt(100) and Pt(111) electrodes: A DEMS study" *Journal of Applied Electrochemistry* **2006**, 36, 1207-1214.

[20] E. Herrero, M. J. Llorca, J. M. Feliu and A. Aldaz, "Oxidation of formic acid on Pt(100) electrodes modified by irreversibly adsorbed tellurium" *Journal of Electroanalytical Chemistry* **1995**, 383, 145-154.

[21] M. Shibata, N. Furuya, M. Watanabe and S. Motoo, "Electrocatalysis by ad-atoms. Part XXIV. Effect of arrangement of Bi ad-atoms on formic acid oxidation" *Journal of Electroanalytical Chemistry* **1989**, 263, 97-108.

[22] M. Watanabe and S. Motoo, "Electrocatalysis by ad-atoms: Part III. Enhancement of the oxidation of carbon monoxide on platinum by ruthenium ad-atoms" *Journal of Electroanalytical Chemistry* **1975**, 60, 275-283.

[23] T. S. Ahmadi, Z. L. Wang, T. C. Green, A. Henglein and M. A. El-Sayed, "Shape-controlled synthesis of colloidal platinum nanoparticles" *Science* **1996**, 272, 1924-1926.

[24] F. J. Vidal-Iglesias, J. Solla-Gullón, P. Rodríguez, E. Herrero, V. Montiel, J. M. Feliu and A. Aldaz, "Shape-dependent electrocatalysis: ammonia oxidation on platinum nanoparticles with preferential (100) surfaces" *Electrochemistry Communications* **2004**, 6, 1080-1084.

[25] N. Tian, Z.-Y. Zhou, S.-G. Sun, Y. Ding and Z. L. Wang, "Synthesis of Tetrahexahedral Platinum Nanocrystals with High-Index Facets and High Electro-Oxidation Activity" *Science* **2007**, 316, 732-735.

[26] V. Grozovski, J. Solla-Gullón, V. Climent, E. Herrero and J. M. Feliu, "Formic Acid Oxidation on Shape-Controlled Pt Nanoparticles Studied by Pulsed Voltammetry" *Journal of Physical Chemistry C* **2010**, 114, 13802-13812.

[27] P. Waszczuk, T. M. Barnard, C. Rice, R. I. Masel and A. Wieckowski, "A nanoparticle catalyst with superior activity for electrooxidation of formic acid" *Electrochemistry Communications* **2002**, 4, 599-603.

[28] F. J. Vidal-Iglesias, J. Solla-Gullón, E. Herrero, A. Aldaz and J. M. Feliu, "Pd Adatom Decorated (100) Preferentially Oriented Pt Nanoparticles for Formic Acid Electrooxidation" *Angewandte Chemie-International Edition* **2010**, 49, 6998-7001.

[29] Q. S. Chen, Z. Y. Zhou, F. J. Vidal-Iglesias, J. Solla-Gullón, J. M. Feliu and S. G. Sun, "Significantly Enhancing Catalytic Activity of Tetrahexahedral Pt Nanocrystals by Bi Adatom Decoration" *Journal of the American Chemical Society* **2011**, 133, 12930-12933.

[30] A. Sáez, E. Expósito, J. Solla-Gullón, V. Montiel and A. Aldaz, "Bismuth-modified carbon supported Pt nanoparticles as electrocatalysts for direct formic acid fuel cells" *Electrochimica Acta* **2012**, 63, 105-111.

[31] F. J. Vidal-Iglesias, A. López-Cudero, J. Solla-Gullón and J. M. Feliu, "Towards More Active and Stable Electrocatalysts for Formic Acid Electrooxidation: Antimony-Decorated Octahedral Platinum Nanoparticles" *Angewandte Chemie-International Edition* **2013**, 52, 964-967.

[32] H. Lee, S. E. Habas, G. A. Somorjai and P. Yang, "Localized Pd overgrowth on cubic Pt nanocrystals for enhanced electrocatalytic oxidation of formic acid" *Journal of the American Chemical Society* **2008**, 130, 5406-5407.

[33] E. Casado-Rivera, Z. Gal, A. C. D. Angelo, C. Lind, F. J. DiSalvo and H. D. Abruña, "Electrocatalytic oxidation of formic acid at an ordered intermetallic PtBi surface" *ChemPhysChem* **2003**, 4, 193-199.

[34] M. D. Spasojevic, R. R. Adzic and A. R. Despic, "Electrocatalysis on surfaces modified by foreign metal adatoms: Oxidation of formaldehyde on platinum" *Journal of Electroanalytical Chemistry* **1980**, 109, 261-269.

[35] R. R. Adzic and M. L. Avramovivic, "Improvements of the catalytic activity of gold by foreign metal ad-atoms: Oxidation of formaldehyde in alkaline solutions" *Journal of Electroanalytical Chemistry* **1982**, 134, 177-180.

[36] A. Kelaidopoulou, E. Abelidou and G. Kokkinidis, "Electrocatalytic oxidation of methanol and formic acid on dispersed electrodes: Pt, Pt-Sn and Pt/M(upd) in poly(2-hydroxy-3-aminophenazine)" *Journal of Applied Electrochemistry* **1999**, 29, 1255-1261.

[37] J. Clavilier, D. Armand, S. G. Sun and M. Petit, "Electrochemical adsorption behaviour of platinum stepped surfaces in sulphuric acid solutions" *Journal of Electroanalytical Chemistry* **1986**, 205, 267-277.

[38] J. Clavilier, K. El Achi, M. Petit, A. Rodes and M. A. Zamakhchari, "Electrochemical Monitoring of the Thermal Reordering of Platinum Single-Crystal Surfaces after Metallographic Polishing from the Early Stage to the Equilibrium Surfaces" *Journal of Electroanalytical Chemistry* **1990**, 295, 333-356.

[39] J. Solla-Gullón, F. J. Vidal-Iglesias, A. López-Cudero, E. Garnier, J. M. Feliu and A. Aldaz, "Shape-dependent electrocatalysis: methanol and formic acid electrooxidation on preferentially oriented Pt nanoparticles" *Physical Chemistry Chemical Physics* **2008**, 10, 3689-3698.

[40] Q. S. Chen, J. Solla-Gullón, S. G. Sun and J. M. Feliu, "The potential of zero total charge of Pt nanoparticles and polycrystalline electrodes with different surface structure: The role of anion adsorption in fundamental electrocatalysis" *Electrochimica Acta* **2010**, 55, 7982-7994.

[41] S. Chumillas, C. Busó-Rogero, J. Solla-Gullón, F. J. Vidal-Iglesias, E. Herrero and J. M. Feliu, "Size and diffusion effects on the oxidation of formic acid and ethanol on platinum nanoparticles" *Electrochemistry Communications* **2011**, 13, 1194-1197.

[42] T. Iwasita and F. C. Nart, "In situ infrared spectroscopy at electrochemical interfaces" *Progress in Surface Science* **1997**, 55, 271-340.

[43] V. Grozovski, V. Climent, E. Herrero and J. M. Feliu, "Intrinsic Activity and Poisoning Rate for HCOOH Oxidation at Pt(100) and Vicinal Surfaces Containing Monoatomic (111) Steps" *ChemPhysChem* **2009**, 10, 1922-1926.

[44] J. Solla-Gullón, P. Rodríguez, E. Herrero, A. Aldaz and J. M. Feliu, "Surface characterization of platinum electrodes" *Physical Chemistry Chemical Physics* **2008**, 10, 1359-1373.

[45] Z. Y. Zhou, N. Tian, Z. Z. Huang, D. J. Chen and S. G. Sun, "Nanoparticle catalysts with high energy surfaces and enhanced activity synthesized by electrochemical method" *Faraday Discussions* **2008**, 140, 81-92.

[46] E. Herrero, V. Climent and J. M. Feliu, "On the different adsorption behavior of bismuth, sulfur, selenium and tellurium on a Pt(775) stepped surface" *Electrochemistry Communications* **2000**, 2, 636-640.

[47] J. Clavilier, J. P. Ganon and M. Petit, "A comparative study of the underpotential deposition of two monovalent cations, Tl^+ and H^+, on Pt (111) as a way to the interpretation of the unusual adsorption states" *Journal of Electroanalytical Chemistry* **1989**, 265, 231-245.

[48] R. R. Adzic, J. X. Wang, O. M. Magnussen and B. M. Ocko, "Structure of Tl adlayers on the Pt(111) electrode surface: Effects of solution pH and bisulfate coadsorption" *Journal of Physical Chemistry* **1996**, 100, 14721-14725.

[49] C. Busó-Rogero, V. Grozovski, F. J. Vidal-Iglesias, J. Solla-Gullón, E. Herrero and J. M. Feliu, "Surface structure and anion effects in the oxidation of ethanol on platinum nanoparticles" *Journal of Materials Chemistry A* **2013**, 1, 7068-7076.

[50] D. K. Lambert, "Vibrational Stark effect of adsorbates at electrochemical interfaces" *Electrochimica Acta* **1996**, 41, 623-630.

Capítulo 7:

Nanopartículas de platino de forma controlada modificada con adátomos para la oxidación de etanol

<u>Capítulo 7</u>: Nanopartículas de platino de forma controlada modificada con adátomos para la oxidación de etanol

RESUMEN

El actual capítulo trata de encontrar algún catalizador bimetálico capaz de mejorar la actividad en la oxidación de etanol, intentando beneficiar la formación de CO_2 en detrimento de la producción de ácido acético. Estos catalizadores son preparados a partir de nanopartículas de platino a las cuales se le adsorbe algún átomo de un metal diferente (Sn, Rh, Ru o Pb). La reactividad de las superficies modificadas para la oxidación de etanol se estudia en medios ácido y alcalino, específicamente en 0.5 M H_2SO_4 y 0.1 M NaOH, empleando las mismas muestras que en el capítulo 6, esto es, la (100)Pt y la (111)Pt con el correspondiente átomo adsorbido.

La adsorción de los metales sobre las nanopartículas de platino se realiza utilizando disoluciones diluidas (10^{-5}-10^{-6} M) de los metales precursores, concretamente $SnSO_4$, $RhCl_3$, $RuCl_3$ y $Pb(NO_3)_2$ en 0.5 M H_2SO_4. Las bajas concentraciones de precursor metálico permiten un depósito lento sobre las superficies de platino, el cual se controla mediante una voltametría cíclica en H_2SO_4. El recubrimiento metálico se calcula mediante la disminución de la carga de adsorción de hidrógeno característica del platino en el caso del Sn, el Ru y el Pb, denotándose también como recubrimiento máximo cuando han desaparecido los picos de adsorción de hidrógeno del Pt al igual que en el caso del capítulo 6. Sin embargo, en el caso del Rh, esa zona de adsorción de hidrógeno se solapa con la del platino, por lo que no es adecuado usar este método para calcular el recubrimiento. En este caso, se indica únicamente el incremento de la cantidad de Rh.

Al estudiar la oxidación de 0.2 M CH_3CH_2OH en medio 0.5 M H_2SO_4, la adsorción de Rh sobre Pt ejerce un efecto negativo para la oxidación de etanol, mientras que las

superficies modificadas Pt-Ru y Pt-Pb muestran ligeras mejoras. El Ru provoca un avance en los potenciales a los cuales se inicia la reacción de oxidación, sobre todo en el caso de la muestra (100)Pt, revelando la catálisis para la oxidación del CO adsorbido hasta CO_2, pero mostrando también un decrecimiento de las corrientes totales de oxidación, indicativo de una disminución en la eficiencia respecto a las nanopartículas de platino sin modificar, sobre todo para la formación de ácido acético. El Pb mejora ligeramente la actividad en la oxidación de etanol, pero sin alterar drásticamente la distribución de productos, como se observa en la poca alteración en la forma de las voltametrías cíclicas.

No obstante, de todos los adátomos estudiados en medio ácido, el más efectivo es el Sn, como así indican las voltametrías cíclicas de la Fig. 7.3 y la Fig. 7.4. En este caso, el potencial al cual se inicia la oxidación de etanol se desplaza hacia valores más negativos independientemente de la muestra usada, ya sea (100)Pt o (111)Pt. Este comportamiento se puede explicar mediante el denominado mecanismo bifuncional, donde moléculas OH adsorbidas sobre los átomos de Sn favorecen la catálisis CO/CO_2. El efecto del Sn sobre las dos muestras es diferente dependiendo del potencial al cual se encuentre: a bajos potenciales (hasta 0.6 V), se produce la mencionada catálisis del CO hasta CO_2, mientras que a potenciales más elevados se mejora la oxidación incompleta hasta ácido acético. Además, resultados de cronoamperometría investigan la estabilidad con el tiempo de estas superficies modificadas, asignando la caída de corriente al CO adsorbido durante la reacción de oxidación de etanol. En el caso de la muestra (100)Pt, la actividad disminuye a recubrimientos más bajos que en el caso de la muestra (111)Pt, debido al efecto competitivo del Sn sobre las nanopartículas de platino para la oxidación del CO adsorbido o la formación de ácido acético dependiendo del potencial.

En el caso de las superficies modificadas en medio alcalino 0.1 M NaOH, se efectúan estudios exclusivamente de voltametría cíclica, prestando únicamente atención a los potenciales de inicio de la oxidación de etanol, más interesantes desde un punto de vista práctico como el de las pilas de combustible. Además, a potenciales elevados las corrientes observadas están fuertemente afectadas por la caída óhmica, otra razón por la que no es posible una correcta comparación entre los diferentes catalizadores. Como se deduce del capítulo 4 de la tesis, el mecanismo de reacción a este pH es totalmente diferente, formando casi exclusivamente acetato. Por ello, átomos como el Ru no ejercen ningún

efecto positivo ya que no catalizan la reacción del CO a CO_2, la cual necesita la rotura del enlace C-C. Sn, Rh y Pb favorecen mínimamente la oxidación de etanol en este medio, debido de nuevo a la adsorción de OH sobre estos átomos, siguiendo el mismo mecanismo bifuncional pero en este caso solo para la formación de ácido acético (acetato en condiciones de pHs alcalinos), al contrario de lo que ocurre en el medio ácido.

Chapter 7

Electrochimica Acta 196 (2016) 270–279

Contents lists available at ScienceDirect

Electrochimica Acta

journal homepage: www.elsevier.com/locate/electacta

Adatom modified shape-controlled platinum nanoparticles towards ethanol oxidation

Carlos Busó-Rogero, Jose Solla-Gullón, Francisco J. Vidal-Iglesias, Enrique Herrero*, Juan M. Feliu

Instituto de Electroquímica, Universidad de Alicante, Ap. 99 E-03080, Alicante, Spain

ARTICLE INFO

Article history:
Received 13 January 2016
Received in revised form 15 February 2016
Accepted 25 February 2016
Available online 27 February 2016

Keywords:
Ethanol oxidation
electrocatalysis
Pt-based electrodes
tin
rhodium
ruthenium
lead
shape-controlled nanoparticles

ABSTRACT

Different adatom modified shape-controlled Pt nanoparticles have been prepared and their electrocatalytic properties have been evaluated toward ethanol electrooxidation. Based on previous findings with Pt model surfaces, Sn, Rh, Ru and Pb adatoms have been selected as promising surface modifiers. The different adatoms have been gradually incorporated on the surface of the preferentially oriented (100) and (111) Pt nanoparticles under electrochemical conditions. The results obtained in 0.5 M H_2SO_4 indicated that, among the selected adatoms, Sn-modified nanoparticles displayed not only a significant shift to negative values on the onset potential of the ethanol oxidation, but also an important decrease on the hysteresis between the positive and negative sweeps. Interestingly, in chronoamperometic measurements at 0.6 V, the oxidation enhancement factors have been found to be dependent on the surface structure of the Pt nanoparticles. On the other hand, Ru and Pb-modified Pt nanoparticles only presented a rather small oxidation enhancement, whereas the activity of the Rh-modified Pt nanoparticles clearly diminished. In alkaline solutions, the oxidation mechanism changes, and the adsorption of Rh, Sn and Pb on the platinum surfaces just displays small catalytic effect at lower coverage for the potential onset in the voltammetric experiments. Ru adsorption does not present any positive effect over the reaction.

This chapter has been adapted and formatted from Electrochimica Acta **2016**, 196, 270-279.

Corresponding author: herrero@ua.es

7.1 Introduction

Nowadays, the studies about new energy sources are gaining momentum due to the depletion of fossil fuels. One of these alternative energy sources is the development of fuel cells, which can obtain energy simply from the reaction between a fuel and an oxidant species (usually oxygen). Fundamental research in fuel cells is usually centered in the material used for manufacturing the catalyst and its electrocatalytic response to the desired reaction on the cathode or on the anode [1]. As a catalyst, platinum is a good choice due to its well-known catalytic properties. Different chemicals have been selected as possible candidates for using as a fuel in the anode, from the most typical hydrogen to some small organic molecules such as formic acid, methanol or ethanol. Among these organic molecules, ethanol is one of the most studied fuels [2], because it presents some advantages as the easiness for obtaining it from biomass in addition to its low toxicity or its high energy density for the complete oxidation to CO_2, where 12 electrons are exchanged according with the reaction:

$$CH_3CH_2OH + 3H_2O \longrightarrow 2CO_2 + 12H^+ + 12e^- \quad (7.1)$$

Nevertheless, this reaction is not as simple as appears in the general equation presented above, because parallel reactions can occur, decreasing the efficiency of the complete oxidation, the desired route. When using platinum as catalyst, this reaction has shown to be structure sensitive [3], that is, depending on the arrangement of the platinum atoms on the surface of the electrode, the reactivity changes. On this electrode, ethanol oxidation mechanism has a dual-path mechanism:

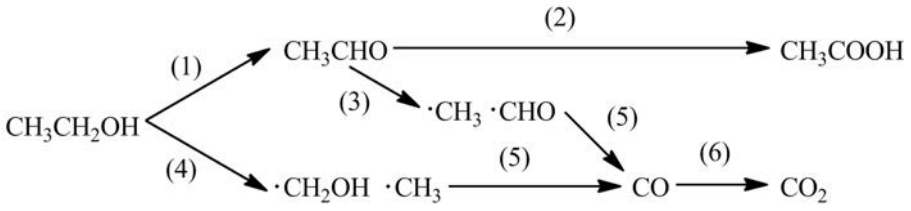

(7.2)

Step (1) of the scheme corresponds to the ethanol oxidation to acetaldehyde, whereas step (2) is the acetaldehyde oxidation to acetic acid. These two reactions compose the route known as ethanol incomplete oxidation. Step (3) and step (4) show the C-C bond scission from acetaldehyde and ethanol respectively, needed to achieve CO_2 formation. However,

previous to the complete oxidation, CO is formed and poisons the catalyst surface. At high potentials, this CO is finally oxidized to CO_2. On Pt(111) electrodes, only acetic acid is formed without poison formation. However, on Pt(100) and Pt(110) electrodes, C-C bond scission is observed and CO is formed, blocking the surface for further reaction at low potentials [3, 4]. On the other hand, the oxidation in alkaline solutions leads to the almost exclusive production of acetate and negligible amounts of CO and CO_2 (carbonate at higher pH values) [5].

The problem of using platinum is its high price. One option for reducing the cost of platinum is to use it in the form of nanoparticles, with high active area, thus allowing the use of lower amounts of platinum. In addition, most of the reactions in fuel cell applications are structure sensitive. Thus, a careful selection of the surface structure of the nanoparticle can lead to an increase in the electrocatalysis. This can be achieved by synthesizing shape-controlled platinum nanoparticles, as has been done for the oxidation of interesting molecules (formic acid, methanol, ethanol, glycerol and ammonia [6-9]) or oxygen reduction [10-12]. An additional increase in the catalytic activity of the Pt can be obtained by the modification of the electronic properties by forming alloys.

Focusing on ethanol oxidation, alloys composed of platinum and other metals, such as Sn, Ru, Rh, Mo or Cu, show improved selectivity to the C-C bond scission and/or enhanced activity for the oxidation of CO, so that the total electrocatalytic activity is increased [13-19]. However, for a better understanding of the actuation mechanism of the additional element in the Pt alloys, the controlled deposition of foreign adatoms on platinum with a well-known surface structure is considered as a suitable approach for this study. With this approach, a large amount of different modified platinum surfaces can be tested due to the easiness of preparation of electrodes with variable composition [20]. Additionally, the test of the different modifications can be carried out in similar conditions, which allows a better comparison between different modifiers.

The metals chosen for depositing on Pt surface and study their electrocatalytic effect towards ethanol oxidation were tin, rhodium, ruthenium and lead. In previous studies, Sn and Ru deposition on stepped surfaces showed some enhancement for the oxidation to CO_2 [21, 22], whereas Pt deposited on Rh electrodes also shows increased activity for the C-C

bond scission [23]. In addition, some works have demonstrated the improvement in the carbonate formation when Pb atoms are adsorbed on polycrystalline Pt surfaces in alkaline solutions [24, 25].

In this work, fundamental studies about the electroactivity of the Sn, Rh, Ru and Pb-modified platinum nanoparticles, specifically in (100) and (111)Pt nanoparticles, for ethanol oxidation are reported in two different pH values (acidic and alkaline solutions). These two types of nanoparticles have been selected because they represent two different paradigms for the ethanol oxidation reaction. As aforementioned, the (111) plane of Pt is inactive for the cleavage of the C-C bond, yielding acetic acid/acetate both in acid and alkaline solutions, whereas the (100) plane is active for this process in acidic conditions. Thus, the effect of the adatoms on both reaction paths can be analyzed. The studies will be carried out using voltammetric and chronoamperometric techniques, which will allow the best conditions to achieve the highest electrocatalytic activity (pH and composition) to be determined for the studied reaction.

7.2 Experimental

Preferential cubic and octahedral Pt nanoparticles were used in this study. According to the observed shape by TEM, these nanoparticles should contain a high fraction of (100) and (111) domains, respectively [6, 26]. For that reason, they have been named (100)Pt nanoparticles and (111)Pt nanoparticles. These Pt nanoparticles were prepared according to the colloidal method [27]. In brief, solutions containing K_2PtCl_4 for (100) nanoparticles and H_2PtCl_6 for (111)Pt nanoparticles were reduced using H_2 in controlled conditions to form nanoparticles. After that, nanoparticles were cleaned with NaOH pellets and dispersed in water. Additional details on the synthesis can be found in ref. [7, 26].

Pt nanoparticles were deposited on a glassy carbon support, and dried during 15-20 minutes in Ar atmosphere. After the drying, Pt nanoparticle samples were cleaned using CO adsorption and stripping, but avoiding the use of high potential values to preserve the surface structure order. Cyclic voltammetry was used to assure the correct cleaning of the platinum nanoparticles. The active area was measured from the hydrogen adsorption charge after double layer subtraction using the reported reference value of 0.23 mC cm^{-2} [28].

The deposition of Sn, Rh, Ru, and Pb on the nanoparticles was carried out from solutions containing $SnSO_4$ (Merck®), hydrated $RhCl_3$ (Aldrich®), hydrated $RuCl_3$ (Fluka®) and $Pb(NO_3)_2$ (Aldrich®), all of them with a purity higher than 99.8%. A very low concentration of the metal precursor was used (10^{-5}-10^{-6} M in 0.5 M H_2SO_4), so that the deposition of the metal is slow and diffusion controlled. This allows the change of the adatom coverage on the surface to be followed by using the cyclic voltammogram recorded between 0.06 and 0.8 V at 0.05 V s^{-1}. The increase in the adatom coverage leads to the decrease in the hydrogen adsorption charge, as shown in previous experiments with Pd, Sb, Bi or Tl [29-32]. Thus, the coverage can be determined using the following expression:

$$\theta_x = 1 - \theta_H = \frac{q_H^0 - q_H^x}{q_H^0} \tag{7.3}$$

where q_H^0 and q_H^x are the hydrogen adsorption charges for bare and adatom modified Pt nanoparticles. This method for measuring the adatom coverage is valid for all the metals used in this work except for Rh, where new peaks appear in the voltammetric profile in the hydrogen adsorption region, due to hydrogen adsorption on rhodium. This prevents an accurate determination of the Rh coverage and for that reason an increasing order of coverage is only indicated.

Once completed the preparation of the modified electrodes, a cyclic voltammogram or a chronoamperogram were recorded in 0.2 M CH_3CH_2OH in 0.5 M H_2SO_4 or 0.1 M NaOH as supporting electrolyte, depending on the desired pH conditions. Ethanol absolute (Merck® p.a.), H_2SO_4 (Merck® Suprapur 96%) and NaOH monohydrate (99.99%, Merck® Suprapur) were used for preparing the solutions together with ultrapure water (Elga Purelab Ultra 18.2 MΩ cm).

All the experiments were carried out at room temperature in a three-cell electrochemical cell, using a Pt wire as a counter-electrode, and reversible hydrogen (N50, Air Liquide) as reference electrode (RHE). Ar (N50, Air Liquide) was employed for deoxygenating the solutions. Cyclic voltammetry and chronoamperometric experiments were performed using a waveform generator (EG&EG PARC 175), together with a potentiostat (eDAQ EA161) and a digital recorder (eDAQ ED401).

7.3 Results and discussion

7.3.1 Electrochemical characterization of modified Pt nanoparticles

Previous to the ethanol oxidation studies, a cyclic voltammogram is recorded to characterize the Pt nanoparticles samples in 0.5 M H_2SO_4. This voltammogram is considered as a fingerprint of the Pt surfaces and allows the characterization of the different domains present on the nanoparticle samples. This electrochemical characterization is presented in Fig. 7.1 and Fig. 7.2 (Θ=0). Very briefly, the (111) nanoparticles show a wave due to the adsorption of sulfate on the (111) domains between 0.45 and 0.6 V, whereas the adsorption processes on the (100) ordered domains produces a defined signal at *ca.* 0.37 V. Additionally, monodimensional domains such as edges, steps or defects with (110) and (100) symmetry appear as peaks at 0.125 and 0.26 V, respectively. A more exhaustive description of the voltammetric profiles of these shape-controlled Pt nanoparticles can be found in references [26, 33].

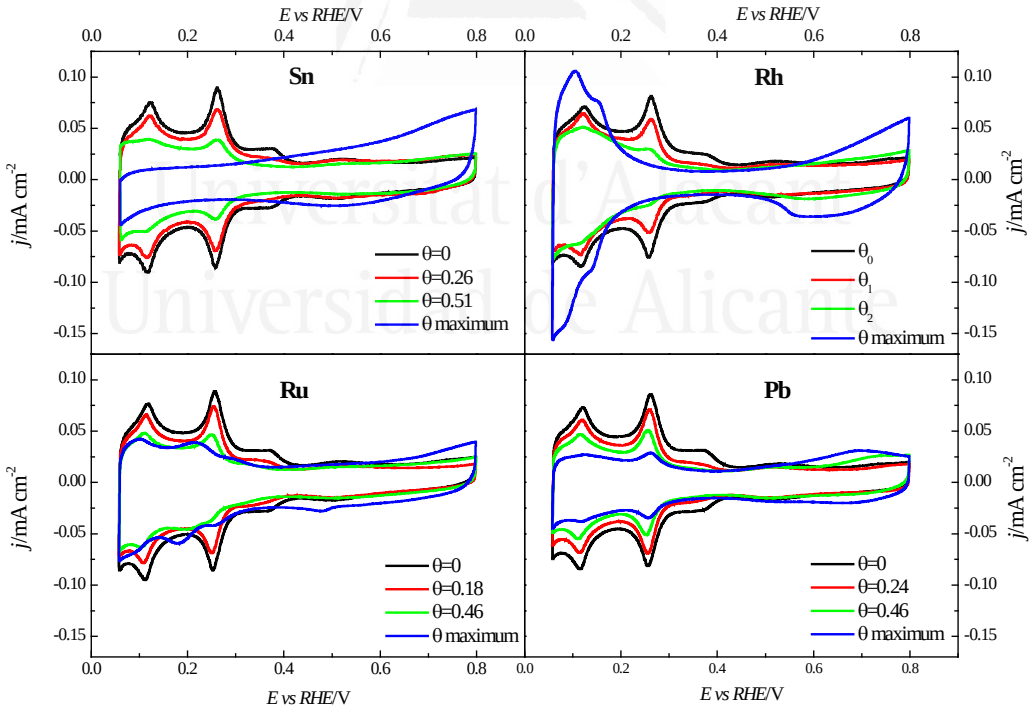

Fig. 7.1. Voltammetric profiles for different adatoms and coverages in (100)Pt nanoparticles. Test solution: 0.5 M H_2SO_4. Scan rate: 0.05 V s^{-1}.

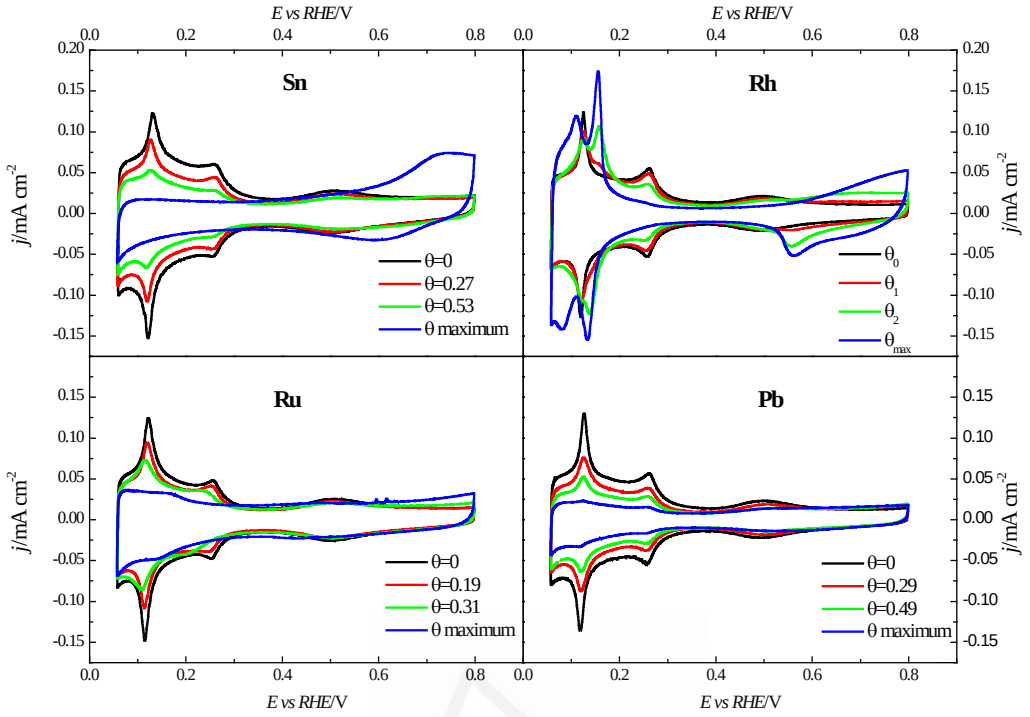

Fig. 7.2. Voltammetric profiles for (111)Pt nanoparticles modified by different adatoms in 0.5 M H_2SO_4 at 0.05 V s^{-1}.

The changes of the profiles upon the adsorption of the different adatoms have been also followed using voltammetry. Fig. 7.1 and Fig. 7.2 show the evolution of the voltammetric profile for both Pt nanoparticle samples after being modified by Sn, Rh, Ru and Pb in 0.5 M H_2SO_4. For Sn, the first stage in the deposition is the adsorption on monodimensional domains as can be observed by the diminution of the peaks associated with those sites, whereas the (111) ordered domains are only covered at high adatom coverages. This behavior is in agreement with previous experimental and theoretical results using stepped (111) surfaces for tin [21, 34-36] or for other adatoms with lower electronegativity values than Pt [37, 38]. In addition, an irreversible redox process was observed around 0.6-0.7 V, assigned to the surface oxidation at tin atoms. The same feature is clearly observed for Sn-modified Pt nanoparticles with high adatom coverage in this range of potential. No additional peaks due to the adsorption of tin can be observed between 0.1 and 0.4 V, which allow the coverage to be determined by the decrease of the hydrogen adsorption charge.

When Rh is adsorbed on the Pt surface, the voltammetric profiles progressively evolve until the typical features of Rh in this medium appear [39]. Thus, the hydrogen adsorption region shifts to negative potential values and the onset for oxide formation takes place at lower potential values. For the Rh-modified (111)Pt nanoparticles, Fig. 7.2, two irreversible peaks can be seen at 0.16 V and 0.13 V, also observed in Rh/Pt (111) [40, 41]. The Rh adsorption produces an overlapping between the two hydrogen adsorption regions in Pt and Rh, preventing an accurate determination of the Rh coverage. For this reason, as it is mentioned above, specific coverage values for these modified electrodes are not given, being simply ordered in increasing coverage values.

For Ru adsorption on the Pt nanoparticles, the behavior is similar to the Sn deposition, thus allowing an easy follow up of the Ru coverage with the decrease of hydrogen adsorption peaks [22, 42, 43]. Some additional Ru adsorption characteristics for sulfuric acid solutions appear in Fig. 7.1, as the small peak at 0.22 V assigned to the sulfate adsorption on large-ordered (100) domains close to Ru atoms, in addition to the current increase from 0.6 V due to the Ru oxidation, which takes place at high potentials.

Finally, Pb adsorption on Pt surfaces is not very stable, and the adatom can be desorbed only with a few cycles at relative low potentials [44]. Thus, high coverage values cannot be achieved. However, no additional peaks are observed due to Pb redox processes at lower potentials, so the usual method of the decrease in hydrogen adsorption charge can be used to follow the Pb coverage. The voltammetric curves are similar to others reported to Pb adsorption on polycrystalline surfaces [25], observing also an increase in the current around 0.6 V due to the OH adsorption on Pb atoms.

7.3.2 Ethanol oxidation in acidic medium

Fig. 7.3 shows the voltammetric profiles for ethanol oxidation on bare and adatom decorated (100)Pt nanoparticles. For the bare nanoparticles, the prominent peak at 0.8 V is due to the oxidation of CO layer from the C-C bond cleavage of ethanol, more favorable in (100) ordered domains, and the subsequent activation of the surface for the direct oxidation

to acetic acid and to CO_2 [7]. This fact leads to a large hysteresis between the positive and negative scan directions. Thus, in the negative scan direction, larger currents are observed, due to the absence of CO accumulation on the surface below 0.5 V, which allows the oxidation of ethanol on the surface. On the other hand, Fig. 7.4 displays the voltammetric response for (111)Pt nanoparticles. As can be seen, the hysteresis is very low, due to the preference of the (111) ordered domains for the incomplete oxidation of ethanol to acetic acid [3].

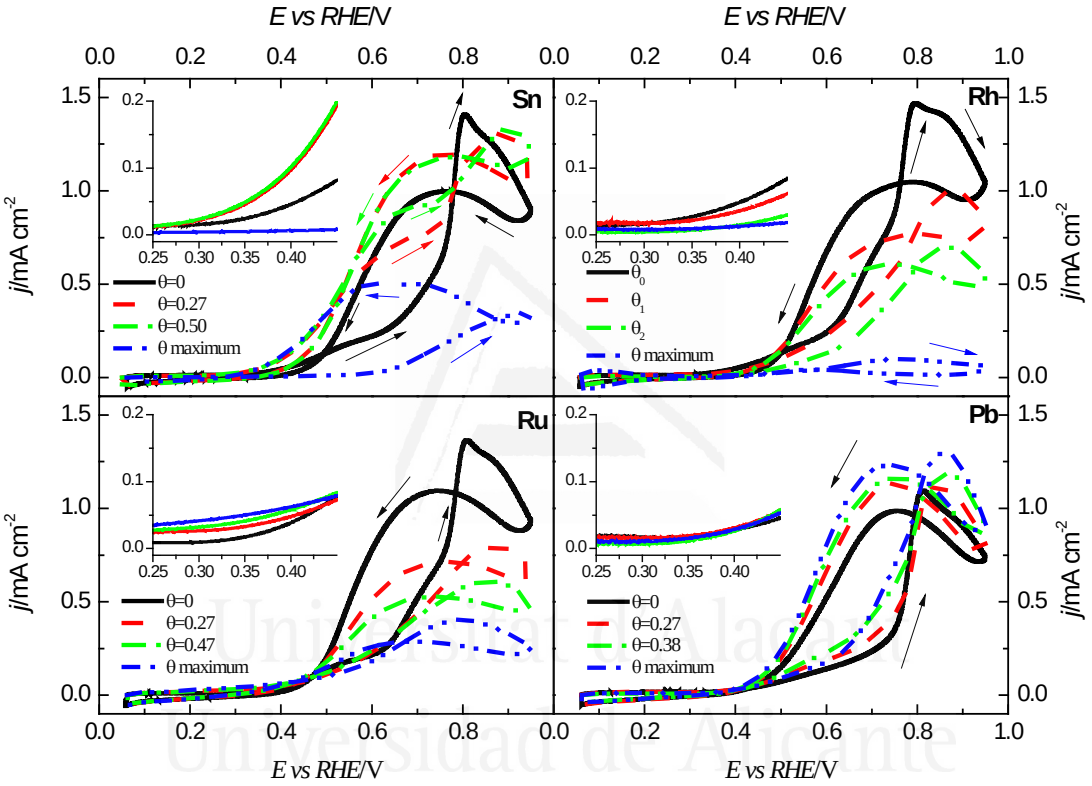

Fig. 7.3. Voltammetric profiles for (100)Pt nanoparticles modified by Sn, Rh, Ru and Pb in 0.2 M ethanol + 0.5 M H_2SO_4 at 0.02 V s^{-1}. Inset: Currents for positive scan direction in the onset potential region.

Small differences in the voltammograms recorded in the absence of the adatoms for the same type of nanoparticles are observed, especially regarding the maximum current density. These effects are due to changes in the spatial distribution of the deposit. Although the amount of nanoparticles is similar in all cases, some agglomeration of the nanoparticles may take place during the drying process. As has been shown [45], nanoparticle agglomeration leads to deposits in which some nanoparticles are not active for the oxidation since the incoming flux of ethanol is consumed in the outer layers of the deposit,

leading to lower current densities than the reported previously [7]. Since the main objective of the manuscript is to understand the role of the adatoms in the oxidation mechanism, the voltammograms for the different coverages for a given adatom were recorded with the same sample, so that currents can be compared and the different effects of the adatoms can be rationalized.

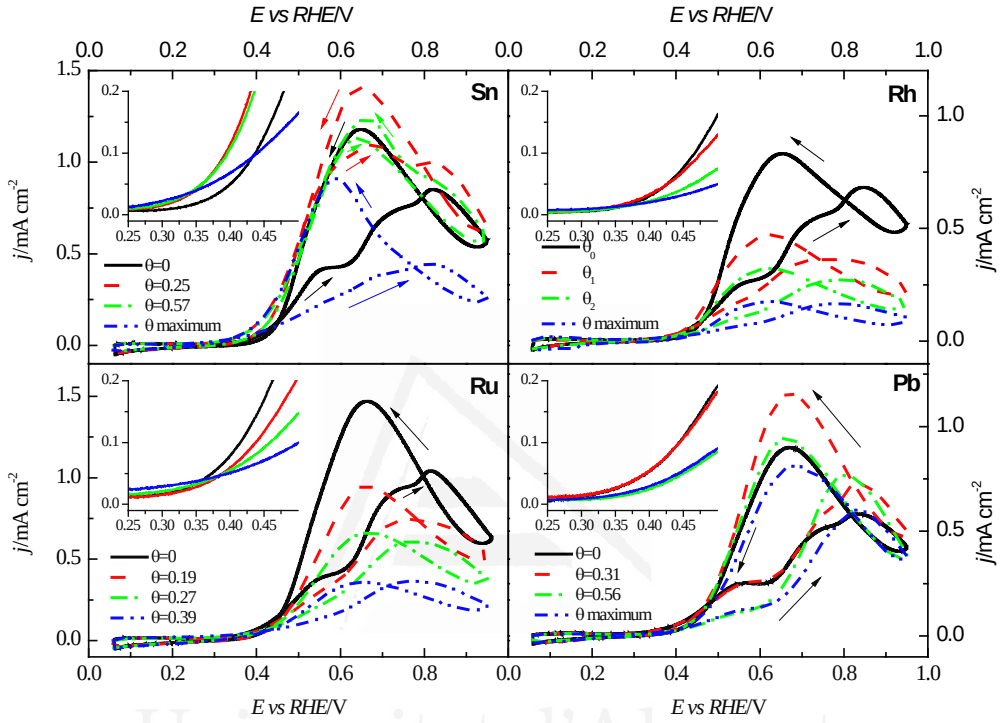

Fig. 7.4. Voltammetric profiles for ethanol oxidation on (111)Pt nanoparticles modified by Sn, Rh, Ru and Pb in 0.2 M ethanol + 0.5 M H_2SO_4. Scan rate: 0.02 V s^{-1}. Inset: Currents for positive scan direction in the onset potential region.

Among all the tested adatoms, the one that has a clear negative impact in the oxidation of ethanol is Rh. In all cases, the current diminishes significantly and no change in the onset potential can be detected. Although it has been reported that PtRh alloys increase the CO_2/acetaldehyde ratio in ethanol oxidation [15, 23], the net effect observed here is a diminution of the total current. At this respect, it is worth noting that Rh atoms are exclusively adsorbed at the surface of Pt nanoparticles, that is, Rh decorated Pt surface is formed, whose behavior can be different from that observed for a PtRh surface alloy. Although it has been proposed that RhPt alloys catalyze the C-C bond splitting [15], there is not a significant increase in the total currents. This is probably due to the low activity of

the Rh atoms for the dehydrogenation of small organic molecules. The net result of Rh is a diminution of the total current, because the increase in the C-C bond splitting rate does not compensate the diminution of the rate in the other steps of the reaction. Finally, for the highest coverage, the curves resemble those obtained in pure Rh electrodes [46], that are known to be much less active than Pt for ethanol electrooxidation.

Ruthenium on platinum surfaces is known to catalyze the oxidation of CO which appears as intermediate on oxidation processes of small organic molecules. For that reason, previous results for ethanol oxidation on Pt stepped surfaces [22, 47] and for methanol oxidation in platinum surfaces [43, 48] show the improvement of the electrocatalytic activity. In the case of ethanol, Ru is not affecting other steps in the reaction, that is, is not enhancing the C-C bond cleavage or the formation of acetic acid as has been shown with single crystal electrodes [22]. Thus, for the (100)Pt nanoparticles, a lower potential onset for ethanol oxidation is observed in Fig. 7.3, since Ru catalyzes the oxidation of CO formed at low potential values. For the (111)Pt nanoparticles, since the activity for the C-C bond cleavage is low, the onset does not change significantly. It should be stressed that the observed effects of Ru deposition for the nanoparticles are smaller than those recorded for the Ru decorated stepped surfaces. In this latter case, the Ru adatoms are deposited neighboring the sites active for the C-C bond cleavage, so that, their activity is maximized. For the nanoparticles, such control is not possible, and thus its effect is lower. Additionally, the progressive current decrease with increasing coverages indicates a negligible activity of the other steps in the reaction and the poor catalytic behavior for these surfaces.

The deposition of Pb on Pt surfaces in acidic solutions improves the onset potential for formic acid oxidation [49, 50]. In the case of ethanol, a small increase in the currents is observed for low and intermediate coverages. Additionally, the shape of the voltammogram remains almost unaffected by the presence of lead on the surface of the nanoparticles. This fact means that lead on the Pt surface catalyzes the oxidation of ethanol but it does not change significantly the product distribution. Additionally, the huge current decay with the other adatoms at the maximum coverage is not observed for lead because of the poor stability of these surfaces [44], that prevent higher coverages for the Pb-modified Pt nanoparticles.

Clearly, the most significant catalytic effects for ethanol oxidation are observed for the Sn modified nanoparticles. For low and medium Sn coverages, the onset potential for ethanol oxidation is shifted to negative values, independently of the platinum nanoparticle samples used. This current increase at low potentials is related to the catalysis of the CO adsorbed to CO_2, as it is confirmed with the disappearance of the prominent peak in the (100)Pt nanoparticles characteristic of the CO presence. This fact can be understood with the bifunctional mechanism [21, 51], where the catalysis CO/CO_2 is enhanced with OH adsorbed on Sn atoms. Nevertheless, for (100)Pt nanoparticles the onset potential seems to be unaltered for coverage values above 0.3, whereas in (111)Pt nanoparticles (Fig. 7.4) continuously decreases for increasing coverages. This effect can be explained by the competitive adsorption between CO and tin atoms, which produces a decrease in the free sites where ethanol oxidation occurs. For this reason, mainly for (100)Pt nanoparticles, the catalytic effect of Sn remains constant after coverages of 0.3, whereas in (111)Pt nanoparticles sample, where the CO formation rate is significantly lower, the onset potential for ethanol oxidation still diminishes for high adatom coverages. In addition, for this sample, the increase in the total currents and the diminution of the hysteresis confirms that the presence of tin adsorbed on (111) ordered domains catalyzed the incomplete ethanol oxidation to acetic acid [21]. At maximum coverage, activity decays drastically due to the absence of free sites necessary for catalyzing the ethanol oxidation reaction.

Since tin is the most active adatom in the catalysis, it is important to deepen in the understanding of its effects in the reaction. In Fig. 7.5, the ratio of the currents recorded in the positive going-sweep between the modified nanoparticles with the highest activity (coverage close to 0.5) and the unmodified nanoparticles is shown. Two regions can be observed in these curves, especially for the (111)Pt nanoparticles. At low potentials, the increase is due to the catalysis of CO oxidation. In this region, the improvement factor is slightly better in (111)Pt nanoparticles, probably due to a small increase in the production of CO or the catalysis of the oxidation for the CH_3 fragment on the free Pt sites. On the (100)Pt nanoparticles, this latter process is less possible because the CO coverage is higher. At higher potentials (above 0.75 V), when all the adsorbed CO molecules have been effectively oxidized to CO_2, the currents of the modified and unmodified samples become essentially similar independently of the Pt nanoparticles used.

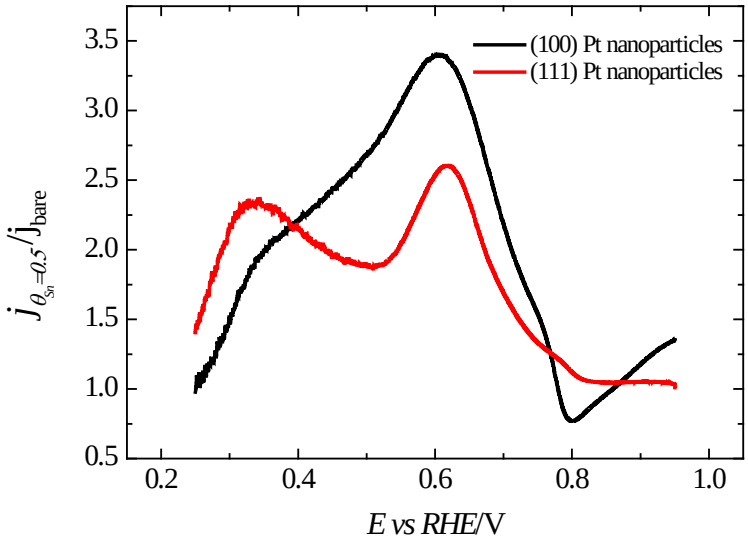

Fig. 7.5. Ratio between ethanol oxidation current densities obtained for the bare and Sn-decorated (coverage around 0.5) shape-controlled platinum nanoparticles in the positive scan direction. Data taken from the tin experiments of Figs. 7.3 and 7.4.

Chronoamperometric results are presented in Fig. 7.6 for evaluating the variance of the activity and assure the stability of the modified electrodes with time. In this experiment, after a step to 0.9 V for oxidizing the CO formed at low potentials, the potential is set at 0.6 V to record the evolution of the oxidation currents. In all cases, a significant decay in the currents is measured after 10 min. This decay should be due to the accumulation of CO on the surface, because the rate of the C-C bond cleavage step is higher than the CO oxidation rate.

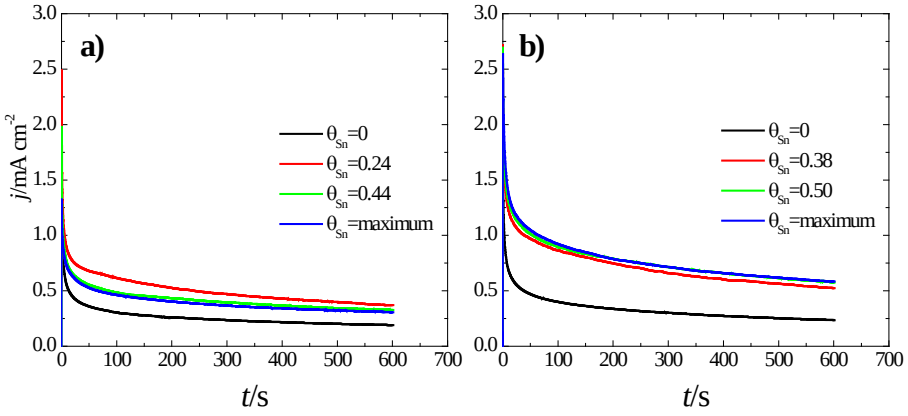

Fig. 7.6. Chronoamperometric response at 0.6 V for 0.2 M ethanol + 0.5 M H_2SO_4 in: a) (100)Pt and b) (111)Pt nanoparticles modified with different coverages of Sn.

Comparing (100) and (111)Pt nanoparticles, the increase of the currents after 10 min with respect to those recorded in absence of tin is higher for the (111)Pt nanoparticles. This effect can be easily explained by the higher activity for the C-C bond splitting of the (100)Pt nanoparticles. Thus, the stationary CO coverage will be higher, that is, there are less free Pt sites, and consequently lower currents are recorded at long times. For the (111)Pt nanoparticles, the higher number of free Pt available sites and the catalytic effect of tin for the oxidation of ethanol to acetic acid results in higher currents [21].

The currents at 600 s of the chronoamperometric curves vs. tin coverage are plotted in Fig. 7.7 for the two Pt nanoparticles samples used. Initially, currents increase with the addition of tin on the surface. For (100)Pt nanoparticles, at coverage values higher than 0.3, it diminishes, whereas for the (111)Pt nanoparticles, it reaches the maximum and stable value for coverages above 0.5. At higher tin coverages, currents increase but very slightly. Again, the competitive catalytic effect of tin for oxidation of CO and the oxidation of ethanol to acetic acid explains this behavior.

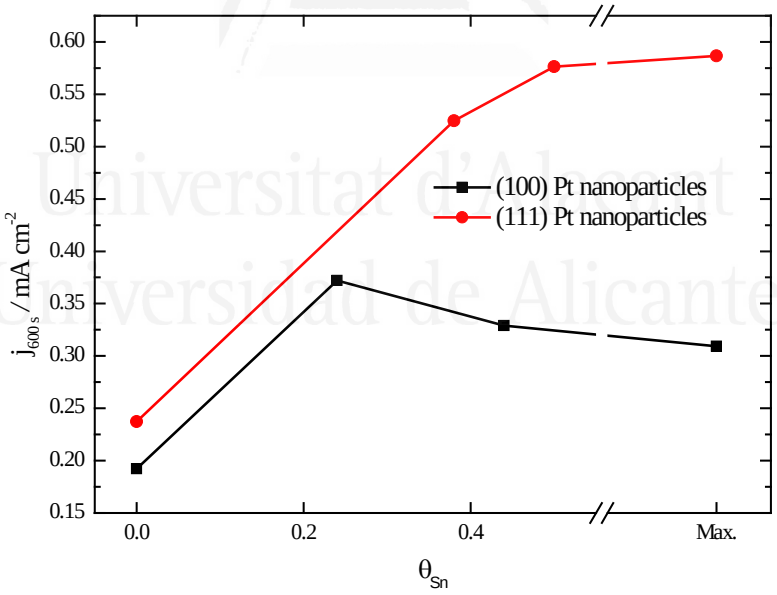

Fig. 7.7. Current densities measured after 600 s in Fig. 7.6 vs tin coverage for Sn-decorated shape-controlled Pt nanoparticles.

7.3.3 Ethanol oxidation in alkaline solutions.

Similarly to that shown in Fig. 7.3 and 7.4, the study of the effect of the adatoms towards the oxidation of ethanol in alkaline conditions is shown in Figs. 7.8 and 7.9. Due to the high activity above 0.7 V, the voltammograms are affected by the diffusion of the electroactive species through the catalyst layers and also by ohmic drop, due to the large currents and the lower conductivity of the alkaline solutions [5, 45]. However, for practical applications, currents above 0.7 V are not interesting, since the voltage obtained in a fuel cell would be negligible. For that reason, only onset potentials will be analyzed in this case.

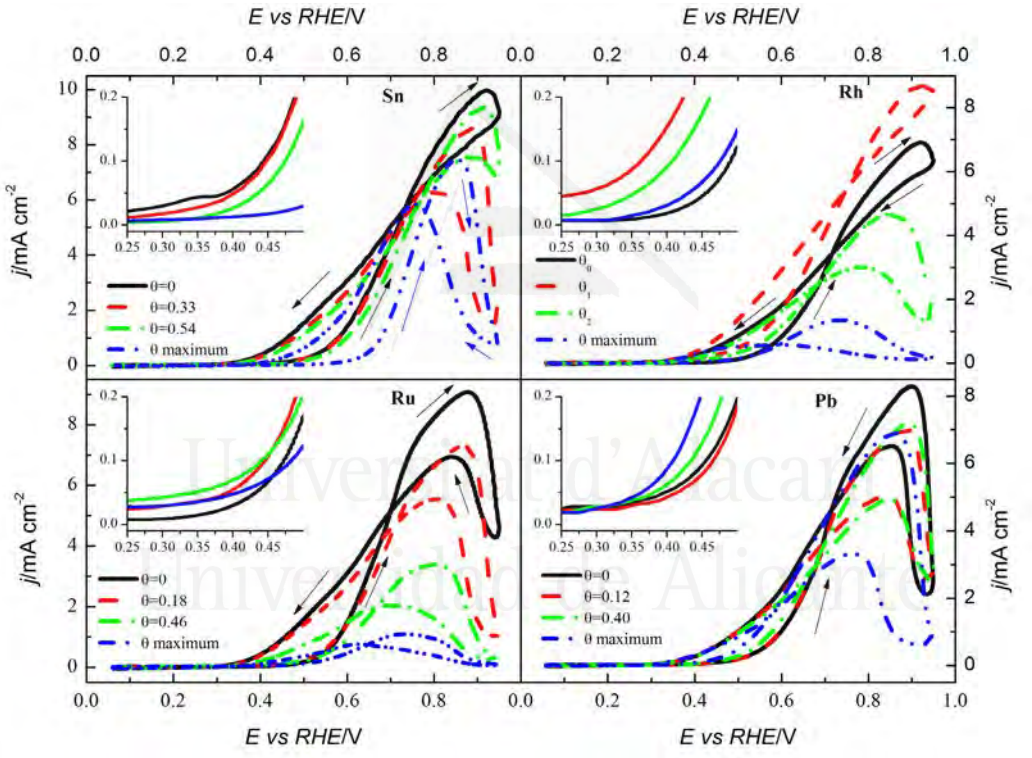

Fig. 7.8. Voltammetric profiles for ethanol oxidation on (100)Pt nanoparticles modified by Sn, Rh, Ru and Pb in 0.2 M ethanol + 0.1 M NaOH. Scan rate: 0.02 V s^{-1}. Inset: Currents for positive scan direction in the onset potential region.

It was shown before that the solution pH has a strong influence on the oxidation mechanism, considerably modifying the ratio between the products formed after changing from acidic to alkaline solutions [5, 52]. As previously mentioned, the main product in the oxidation for the different Pt single crystal electrodes and nanoparticles is acetate, whereas

the amount of carbonate detected can be considered negligible. This drastic change in the oxidation mechanism has been related to changes in the adsorption modes of ethanol. Thus, ethanol adsorption on platinum in alkaline media is proposed to occur through the oxygen atom and not through the C1 atom of ethanol [52, 53]. Since the cleavage of the C-C bond requires a bidentate adsorption mode with the C1 and C2 atoms bonded to the surface, the adsorption through the oxygen atom hinders this process.

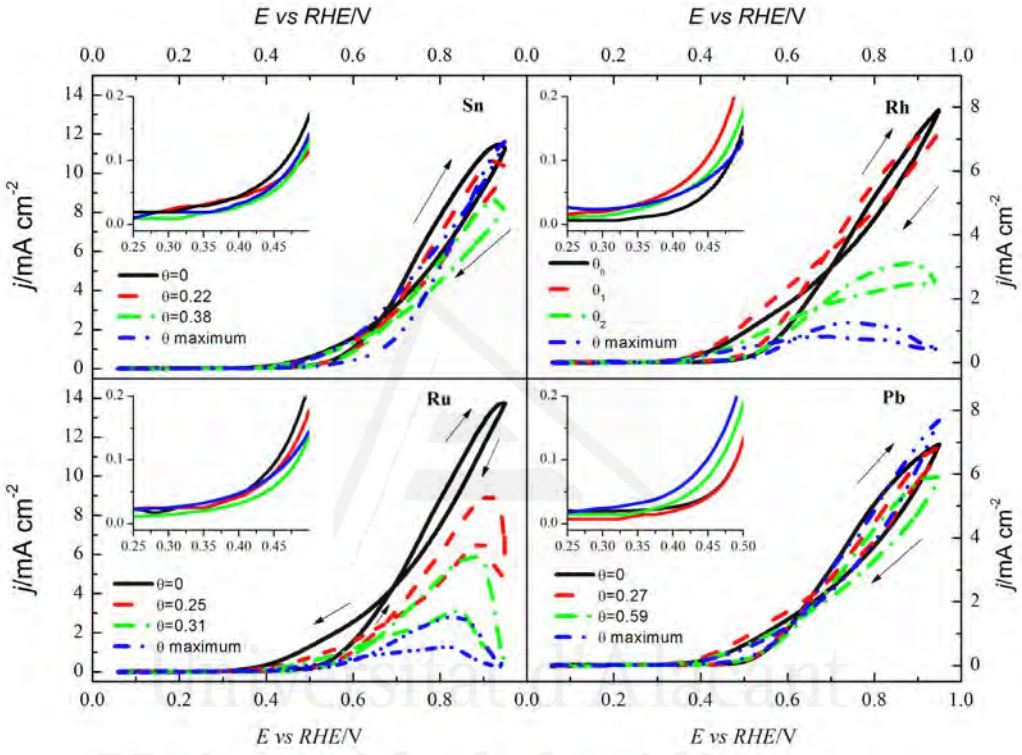

Fig. 7.9. Voltammetric profiles for ethanol oxidation on (111)Pt nanoparticles modified by Sn, Rh, Ru and Pb in 0.2 M ethanol + 0.1 M NaOH. Scan rate: 0.02 V s^{-1}. Inset: Currents for positive scan direction in the onset potential region.

On the other hand, the oxidation to acetate requires the transfer of an OH group to the C1 atom. In this medium, the results with single crystal electrodes show that ethanol oxidation to acetic acid takes place when OH is adsorbed on the Pt surface. Thus, the main product is acetate, and CO formation is quasi negligible in these conditions. This fact determines the effect of the adatoms. Ru, which has high oxophilicity, could have contributed to two different steps in the reaction mechanism: to the oxidation of CO to CO_2 and to the oxidation of acetaldehyde to acetic acid/acetate, since both steps require the

transfer of an oxygen group. As aforementioned, CO is not detected in alkaline solutions, and therefore, this step cannot be catalyzed by Ru.

The complex nature of the oxidation process of Ru, yielding a mixture of hydroxides and oxides, whose ratio depends on the electrode potential, prevents an effective catalytic effect on this second step (acetaldehyde to acetate). In the positive scan direction and at low potentials (inset of Fig. 7.8 and 7.9), the current is almost independent of the Ru coverage. However, as the potential is increased, a significant diminution is observed. This is probably due to a progressive transformation of Ru hydroxides to oxides, which are not active for the catalysis. Since this process is irreversible, in the negative scan direction, the currents at low potentials diminish with the Ru coverage. Consequently, Ru adatoms, the role of which is the catalysis of the CO oxidation to CO_2, do not show any enhancement for the oxidation in alkaline conditions, acting almost as a pure third body for the reaction.

On the other hand, low Rh, Pb or Sn coverages show very small effects on the oxidation of ethanol in this medium. As can be seen, the increase of the currents for low coverages is small and the only net effect is a lower onset for low adatom coverages. At higher coverages for those adatoms, total currents at any potential decrease. Previous results for Pb deposited on polycrystalline platinum electrodes showed a significant increase in the currents in alkaline solutions [24, 25]. In this case, a lower onset for the oxidation is observed mainly for the (100)Pt nanoparticles. According with the references cited, OH adsorption on Pb atoms takes place at potentials around 0.5-0.6 V, lower than on platinum, allowing ethanol to be oxidized at more negative potentials. Thus, it can be proposed that these adatoms act as a bifunctional catalyst by facilitating the transfer of the OH to the adsorbed ethanol molecule, which compensates the lower amount of Pt free sites due to the adatom coverage. However, the large increase previously observed with the Pt-Pb combined surfaces is not achieved in these conditions, probably related with differences in the deposition method and the low coverages reached due to the poor stability of Pb adsorbed on Pt surfaces [44]. At higher coverages, current decreases, since the small increase of the activity due to the deposition of the adatom does not compensate the loss of the activity due to the blockage of platinum sites by the adatom.

For Sn, which also has high oxophilicity, the observed behavior is better than that of Ru, probably related to the different electrochemistry of the oxides/hydroxides. In this case, the transfer of the OH takes place in the whole potential range, which results in currents that are almost independent of the Sn coverage. This suggests that there is no significant transformation of the hydroxides into oxides in this potential range, unlike what is observed for Ru.

7.4 Conclusions

The electrocatalytic properties of clean cubic and octahedral platinum nanoparticles modified with Sn, Rh, Ru and Pb adatoms have been evaluated for ethanol oxidation reaction in both acidic and alkaline media, using cyclic voltammetry and chronoamperometry. The results indicate that, for the Sn-modified Pt nanoparticles, a clear enhancement of both the onset potential and hysteresis is observed in acidic medium. In addition, this enhancement is also dependent on the surface structure of the Pt nanoparticles. The current increment at lower potentials for Sn-modified Pt nanoparticles in acidic solutions is assigned to the catalysis of CO adsorbed to CO_2 where Sn atoms provide the OH needed to complete the oxidation. Interestingly, the (111)Pt nanoparticles maintain the catalytic effect for higher coverages compared with (100)Pt nanoparticles because of the lower competition with Sn atoms for the Pt free sites where takes place the reaction. At higher coverages, both samples enhance the acetic acid formation. In similar conditions, Ru-modified Pt nanoparticles only favors the oxidation of CO to CO_2 at lower potentials, without any effect for the C-C bond split or the acetic acid formation. Finally, Pb-modified Pt modified surfaces improve slightly the ethanol oxidation but with the same product distribution, whereas Rh adsorbed on Pt nanoparticles has a negative effect over ethanol oxidation reaction.

In alkaline solutions, the main product in the oxidation is acetate, with negligible CO formation. Thus, Ru atoms adsorbed on platinum nanoparticles, which major effect is to catalyze the CO oxidation, does not affect ethanol oxidation in these conditions. However, Sn, Rh and Pb-modified platinum nanoparticles show a very small improvement of the potential onset. This effect is related to the OH adsorption on the adatom surfaces at lower potentials, favoring ethanol oxidation to acetate by a bifunctional mechanism.

7.5 References

[1] M. T. M. Koper, "Fuel Cell Catalysis: A Surface Science Approach", *Electrocatalysis and Electrochemistry* A. Wieckowski (Ed.), John Wiley & Sons, Hoboken, New Jersey, **2009**.

[2] E. Antolini, "Catalysts for direct ethanol fuel cells" *Journal of Power Sources* **2007**, 170, 1-12.

[3] F. Colmati, G. Tremiliosi-Filho, E. R. Gonzalez, A. Berná, E. Herrero and J. M. Feliu, "Surface structure effects on the electrochemical oxidation of ethanol on platinum single crystal electrodes" *Faraday Discussions* **2008**, 140, 379-397.

[4] F. Cases, M. López-Atalaya, J. L. Vázquez, A. Aldaz and J. Clavilier, "Dissociative adsorption of ethanol on Pt (h, k, l) basal surfaces" *Journal of Electroanalytical Chemistry and Interfacial Electrochemistry* **1990**, 278, 433-440.

[5] C. Busó-Rogero, E. Herrero and J. M. Feliu, "Ethanol Oxidation on Pt Single-Crystal Electrodes: Surface-Structure Effects in Alkaline Medium" *ChemPhysChem* **2014**, 15, 2019-2028.

[6] J. Solla-Gullón, F. J. Vidal-Iglesias, A. López-Cudero, E. Garnier, J. M. Feliu and A. Aldaz, "Shape-dependent electrocatalysis: methanol and formic acid electrooxidation on preferentially oriented Pt nanoparticles" *Physical Chemistry Chemical Physics* **2008**, 10, 3689-3698.

[7] C. Busó-Rogero, V. Grozovski, F. J. Vidal-Iglesias, J. Solla-Gullón, E. Herrero and J. M. Feliu, "Surface structure and anion effects in the oxidation of ethanol on platinum nanoparticles" *Journal of Materials Chemistry A* **2013**, 1, 7068-7076.

[8] J. Monzó, Y. Malewski, F. J. Vidal-Iglesias, J. Solla-Gullón and P. Rodríguez, "Electrochemical Oxidation of Small Organic Molecules on Au Nanoparticles with Preferential Surface Orientation" *ChemElectroChem* **2015**, 2, 958-962.

[9] F. J. Vidal-Iglesias, J. Solla-Gullón, P. Rodríguez, E. Herrero, V. Montiel, J. M. Feliu and A. Aldaz, "Shape-dependent electrocatalysis: ammonia oxidation on platinum nanoparticles with preferential (100) surfaces" *Electrochemistry Communications* **2004**, 6, 1080-1084.

[10] J. Hernández, J. Solla-Gullón, E. Herrero, J. M. Feliu and A. Aldaz, "In Situ Surface Characterization and Oxygen Reduction Reaction on Shape-Controlled Gold Nanoparticles" *Journal of Nanoscience and Nanotechnology* **2009**, 9, 2256-2273.

[11] C. M. Sánchez-Sánchez, J. Solla-Gullón and V. Montiel, "Electrocatalysis at nanoparticles", in *Electrochemistry: Volume 11 - Nanosystems Electrochemistry*, The Royal Society of Chemistry, **2013**, pp. 34-70.

[12] H. Erikson, A. Sarapuu, N. Alexeyeva, K. Tammeveski, J. Solla-Gullón and J. M. Feliu, "Electrochemical reduction of oxygen on palladium nanocubes in acid and alkaline solutions" *Electrochimica Acta* **2012**, 59, 329-335.

[13] C. Lamy, S. Rousseau, E. M. Belgsir, C. Coutanceau and J. M. Léger, "Recent progress in the direct ethanol fuel cell: development of new platinum-tin electrocatalysts" *Electrochimica Acta* **2004**, 49, 3901-3908.

[14] N. Fujiwara, K. A. Friedrich and U. Stimming, "Ethanol oxidation on PtRu electrodes studied by differential electrochemical mass spectrometry" *Journal of Electroanalytical Chemistry* **1999**, 472, 120-125.

[15] J. P. I. de Souza, S. L. Queiroz, K. Bergamaski, E. R. Gonzalez and F. C. Nart, "Electro-oxidation of ethanol on Pt, Rh, and PtRh electrodes. A study using DEMS and in-situ FTIR techniques" *Journal of Physical Chemistry B* **2002**, 106, 9825-9830.

[16] F. Colmati, E. Antolini and E. R. Gonzalez, "Preparation, structural characterization and activity for ethanol oxidation of carbon supported ternary Pt-Sn-Rh catalysts" *Journal of Alloys and Compounds* **2008**, 456, 264-270.

[17] A. O. Neto, M. J. Giz, J. Perez, E. A. Ticianelli and E. R. Gonzalez, "The electro-oxidation of ethanol on Pt-Ru and Pt-Mo particles supported on high-surface-area carbon" *Journal of the Electrochemical Society* **2002**, 149, A272-A279.

[18] M. Ammam and E. B. Easton, "PtCu/C and Pt(Cu)/C catalysts: Synthesis, characterization and catalytic activity towards ethanol electrooxidation" *Journal of Power Sources* **2013**, 222, 79-87.

[19] W. Zhou, Z. Zhou, S. Song, W. Li, G. Sun, P. Tsiakaras and Q. Xin, "Pt based anode catalysts for direct ethanol fuel cells" *Applied Catalysis B: Environmental* **2003**, 46, 273-285.

[20] V. Climent, N. García-Aráez and J. M. Feliu, "Clues for the Molecular-Level Understanding of Electrocatalysis on Single-Crystal Platinum Surfaces Modified by p-Block Adatoms", in *Fuel Cells Catalysis. A Surface Science Approach*, M. T. M. Koper (Ed.) Wiley, Hoboken, New Jersey, **2009**, pp. 209-244.

[21] V. Del Colle, J. Souza-Garcia, G. Tremiliosi-Filho, E. Herrero and J. M. Feliu, "Electrochemical and spectroscopic studies of ethanol oxidation on Pt stepped surfaces modified by tin adatoms" *Physical Chemistry Chemical Physics* **2011**, 13, 12163-12172.

[22] V. Del Colle, A. Berná, G. Tremiliosi-Filho, E. Herrero and J. M. Feliu, "Ethanol electrooxidation onto stepped surfaces modified by Ru deposition: electrochemical and spectroscopic studies" *Physical Chemistry Chemical Physics* **2008**, 10, 3766-3773.

[23] V. Del Colle, V. Grozovski, E. Herrero and J. M. Feliu, "Unusually High Activity of Pt Islands on Rh(111) Electrodes for Ethanol Oxidation" *ChemCatChem* **2013**, 5, 1350-1353.

[24] Q. G. He, B. Shyam, K. Macounova, P. Krtil, D. Ramaker and S. Mukerjee, "Dramatically Enhanced Cleavage of the C-C Bond Using an Electrocatalytically Coupled Reaction" *Journal of the American Chemical Society* **2012**, 134, 8655-8661.

[25] P. A. Christensen, S. W. M. Jones and A. Hamnett, "An in situ FTIR spectroscopic study of the electrochemical oxidation of ethanol at a Pb-modified polycrystalline Pt electrode immersed in aqueous KOH" *Physical Chemistry Chemical Physics* **2013**, 15, 17268-17276.

[26] J. Solla-Gullón, P. Rodríguez, E. Herrero, A. Aldaz and J. M. Feliu, "Surface characterization of platinum electrodes" *Physical Chemistry Chemical Physics* **2008**, 10, 1359-1373.

[27] T. S. Ahmadi, Z. L. Wang, T. C. Green, A. Henglein and M. A. El-Sayed, "Shape-controlled synthesis of colloidal platinum nanoparticles" *Science* **1996**, 272, 1924-1926.

[28] Q. S. Chen, J. Solla-Gullón, S. G. Sun and J. M. Feliu, "The potential of zero total charge of Pt nanoparticles and polycrystalline electrodes with different surface structure: The role of anion adsorption in fundamental electrocatalysis" *Electrochimica Acta* **2010**, 55, 7982-7994.

[29] F. J. Vidal-Iglesias, J. Solla-Gullón, E. Herrero, A. Aldaz and J. M. Feliu, "Pd Adatom Decorated (100) Preferentially Oriented Pt Nanoparticles for Formic Acid Electrooxidation" *Angewandte Chemie-International Edition* **2010**, 49, 6998-7001.

[30] F. J. Vidal-Iglesias, A. López-Cudero, J. Solla-Gullón and J. M. Feliu, "Towards More Active and Stable Electrocatalysts for Formic Acid Electrooxidation: Antimony-Decorated Octahedral Platinum Nanoparticles" *Angewandte Chemie-International Edition* **2013**, 52, 964-967.

[31] A. Sáez, E. Expósito, J. Solla-Gullón, V. Montiel and A. Aldaz, "Bismuth-modified carbon supported Pt nanoparticles as electrocatalysts for direct formic acid fuel cells" *Electrochimica Acta* **2012**, 63, 105-111.

[32] C. Busó-Rogero, J. V. Perales-Rondón, M. J. S. Farias, F. J. Vidal-Iglesias, J. Solla-Gullón, E. Herrero and J. M. Feliu, "Formic acid electrooxidation on thallium-decorated shape-controlled platinum nanoparticles: an improvement in electrocatalytic activity" *Physical Chemistry Chemical Physics* **2014**, 16, 13616-13624.

[33] F. J. Vidal-Iglesias, R. M. Arán-Ais, J. Solla-Gullón, E. Herrero and J. M. Feliu, "Electrochemical Characterization of Shape-Controlled Pt Nanoparticles in Different Supporting Electrolytes" *ACS Catalysis* **2012**, 2, 901-910.

[34] H. Massong, S. Tillmann, T. Langkau, E. A. A. Elmeguid and H. Baltruschat, "On the Influence of Tin and Bismuth UPD on Pt(111) and Pt(332) on the Oxidation of CO" *Electrochimica Acta* **1998**, 44, 1379-1388.

[35] E. Mostafa, A. A. Abd-El-Latif, R. Ilsley, G. Attard and H. Baltruschat, "Quantitative DEMS study of ethanol oxidation: effect of surface structure and Sn surface modification" *Physical Chemistry Chemical Physics* **2012**, 14, 16115-16129.

[36] G. Stalnionis, L. Tamasauskaite-Tamasiunaite, V. Pautieniene, A. Sudavicius and Z. Jusys, "Modification of a Pt surface by spontaneous Sn deposition for electrocatalytic applications - 1. Catalyst preparation and characterization" *Journal of Solid State Electrochemistry* **2004**, 8, 892-899.

[37] E. Herrero, V. Climent and J. M. Feliu, "On the different adsorption behavior of bismuth, sulfur, selenium and tellurium on a Pt(775) stepped surface" *Electrochemistry Communications* **2000**, 2, 636-640.

[38] A. Ferre-Vilaplana, R. Gisbert and E. Herrero, "On the electrochemical properties of platinum stepped surfaces vicinal to the (100) pole. A computational study" *Electrochimica Acta* **2014**, 125, 666-673.

[39] D. A. J. Rand and R. Woods, "A study of the dissolution of platinum, palladium, rhodium and gold electrodes in 1 M sulphuric acid by cyclic voltammetry" *Journal of Electroanalytical Chemistry and Interfacial Electrochemistry* **1972**, 35, 209-218.

[40] R. Gómez and J. M. Feliu, "Rhodium adlayers on Pt(111) monocrystalline surfaces. Electrochemical behavior and electrocatalysis" *Electrochimica Acta* **1998**, 44, 1191-1205.

[41] R. Gómez, F. J. Gutiérrez de Dios and J. M. Feliu, "Carbon monoxide oxidation and nitrous oxide reduction on Rh/Pt(111) electrodes" *Electrochimica Acta* **2004**, 49, 1195-1208.

[42] F. Maillard, G. Q. Lu, A. Wieckowski and U. Stimming, "Ru-decorated Pt surfaces as model fuel cell electrocatalysts for CO electrooxidation" *Journal of Physical Chemistry B* **2005**, 109, 16230-16243.

[43] Z. D. Wei, L. L. Li, Y. H. Luo, C. Yan, C. X. Sun, G. Z. Yin and P. K. Shen, "Electrooxidation of methanol on UPD-Ru and UPD-Sn modified Pt electrodes" *Journal of Physical Chemistry B* **2006**, 110, 26055-26061.

[44] J. Clavilier, J. M. Orts, J. M. Feliu and A. Aldaz, "Study of the conditions for irreversible adsorption of lead at Pt(h,k,l) electrodes" *Journal of Electroanalytical Chemistry* **1990**, 293, 197-208.

[45] S. Chumillas, C. Busó-Rogero, J. Solla-Gullón, F. J. Vidal-Iglesias, E. Herrero and J. M. Feliu, "Size and diffusion effects on the oxidation of formic acid and ethanol on platinum nanoparticles" *Electrochemistry Communications* **2011**, 13, 1194-1197.

[46] N. R. de Tacconi, R. O. Lezna, B. Beden, F. Hahn and C. Lamy, "In-situ FTIR study of the electrocatalytic oxidation of ethanol at iridium and rhodium electrodes" *Journal of Electroanalytical Chemistry* **1994**, 379, 329-337.

[47] J. Souza-Garcia, E. Herrero and J. M. Feliu, "Breaking the C-C Bond in the Ethanol Oxidation Reaction on Platinum Electrodes: Effect of Steps and Ruthenium Adatoms" *ChemPhysChem* **2010**, 11, 1391-1394.

[48] E. Herrero, K. Franaszczuk and A. Wieckowski, "A voltammetric identification of the surface redox couple effective in methanol oxidation on a ruthenium-covered platinum (110) electrode" *Journal of Electroanalytical Chemistry* **1993**, 361, 269-273.

[49] M. Bełtowska-Brzezinska, T. Łuczak, J. Stelmach and R. Holze, "The electrooxidation mechanism of formic acid on platinum and on lead ad-atoms modified platinum studied with the kinetic isotope effect" *Journal of Power Sources* **2014**, 251, 30-37.

[50] S. Uhm, S. T. Chung and J. Lee, "Activity of Pt anode catalyst modified by underpotential deposited Pb in a direct formic acid fuel cell" *Electrochemistry Communications* **2007**, 9, 2027-2031.

[51] M. Watanabe and S. Motoo, "Electrocatalysis by ad-atoms: Part II. Enhancement of oxidation of methanol on platinum by ruthenium ad-atoms" *Journal of Electroanalytical Chemistry* **1975**, 60, 267-273.

[52] P. A. Christensen, S. W. M. Jones and A. Hamnett, "In Situ FTIR Studies of Ethanol Oxidation at Polycrystalline Pt in Alkaline Solution" *Journal of Physical Chemistry C* **2012**, 116, 24681-24689.

[53] S. C. S. Lai, S. E. F. Kleijn, F. T. Z. Öztürk, V. C. van Rees Vellinga, J. Koning, P. Rodriguez and M. T. M. Koper, "Effects of electrolyte pH and composition on the ethanol electro-oxidation reaction" *Catalysis Today* **2010**, 154, 92-104.

Capítulo 8:

Conclusiones

Capítulo 8: Conclusiones

La presente tesis abarca estudios fundamentales para la oxidación de etanol y ácido fórmico en nanopartículas de platino orientadas preferencialmente y poliorientadas soportadas en carbón. El objetivo principal en estas investigaciones es el de completar la oxidación hasta dióxido de carbono evitando la formación de veneno durante el transcurso de la reacción. Partiendo del etanol, la molécula principalmente estudiada en la tesis, se han realizado multitud de trabajos investigando diferentes parámetros que pueden afectar a su reactividad, como es el caso de la estructura superficial del catalizador de platino, el efecto de cambiar el pH de trabajo hasta llegar a disoluciones alcalinas, la importancia de dispersar correctamente el depósito de nanopartículas en los soportes de carbón vítreo y, por último, el cambio en la electrocatálisis al modificar la superficie de las nanopartículas de platino con un átomo diferente. De acuerdo con estos estudios realizados con adátomos, también se probó la efectividad de un electrodo modificado parecido para la oxidación de ácido fórmico. Para el estudio de los mecanismos de oxidación implicados, se recurrieron a técnicas electroquímicas (voltametría cíclica y cronoamperometría), espectro-electroquímicas (FTIR de reflexión externa y ATR) y de espectrometría de masas (DEMS).

El primer trabajo presentado en la tesis (capítulo 2) corrobora, en nanopartículas de platino con diferentes formas (indicativo de diferentes orientaciones cristalográficas), la dependencia en la reactividad para la oxidación de etanol con la estructura superficial observada en superficies monocristalinas, mostrándose los dominios {100} como más apropiados para la rotura del enlace C-C del etanol (y también de CO formado) y los sitios {111} más adecuados para la formación de acetaldehído/ácido acético. Además, se estudia el efecto de la adsorción competitiva del anión sulfato sobre la oxidación de etanol, empleando para ello H_2SO_4 y $HClO_4$. En ambos electrolitos soportes, dicha adsorción no tiene efecto debido a la formación de ácido acético, cuyos aniones acetato formados pueden competir con el etanol por los sitios activos del platino.

Para una aproximación al estudio del efecto del pH, el capítulo 3 indaga sobre la reacción de oxidación de etanol en nanopartículas de platino con forma controlada,

siempre sin superar valores de pH=4 en la disolución de trabajo. Con ayuda de experimentos DEMS, se estudian las diferencias en cuanto al uso de las muestras con orientación preferencial {100} y {111}. La muestra con mayor presencia de dominios {100} se confirma como la mejor para la rotura del enlace C-C en la oxidación de etanol, ratificándose la mayor eficiencia para la formación de CO_2 en las nanopartículas (100)Pt respecto a las (111)Pt. Al incrementar ligeramente el pH de la disolución de trabajo, la formación de fragmentos $CH_{x,ads}$ a bajos potenciales aumenta respecto al veneno presente en forma de CO_{ads}. En la muestra de nanopartículas (111)Pt, al aumentar el pH la formación de CO es impedida y, por tanto, se favorece cada vez más la formación de acetaldehído/ácido acético.

El capítulo 4 se introduce de lleno en el estudio de la oxidación de etanol en medio alcalino. Como no se dispone de resultados previos en superficies con estructura superficial totalmente conocida, se realiza previamente el estudio con superficies monocristalinas de platino, concretamente planos base y superficies escalonadas en largas terrazas {111}. La actividad es mucho mayor en medio alcalino que en medio ácido, mostrándose el electrodo de Pt(111) como el que mayor corriente de oxidación presenta seguido del electrodo de Pt(110) y del Pt(100), orden inverso al observado en medio ácido. Sin embargo, la selectividad hasta la producción de CO_2 es mucho menor, casi despreciable en comparación con la cantidad de acetaldehído/acetato producida independientemente de la orientación cristalográfica del electrodo de trabajo. Asimismo, la desactivación de las superficies de platino es mucho mayor a causa de la polimerización del acetaldehído formado en el catalizador que inhibe sucesivamente la oxidación de etanol, principalmente en las superficies con mayor presencia de terrazas {111}.

A continuación, de manera análoga al capítulo 4, el capítulo 5 experimenta la oxidación de etanol en medio alcalino pero empleando las nanopartículas de platino con forma controlada, concretamente las mismas muestras del capítulo 2. Los resultados del capítulo 4 se corroboran con estas muestras de nanopartículas en cuanto al efecto de la estructura superficial, relacionando los diferentes potenciales de adsorción de los OH con el potencial observado para comenzar la oxidación de etanol en medio alcalino. Además, los experimentos FTIR revelan que el acetato se forma casi con total exclusividad independientemente de la muestra de nanopartículas de platino estudiada. Por otra parte, el

uso de nanopartículas de platino poliorientadas con cantidad de metal variable soportadas en carbón demuestra la importancia de la correcta dispersión del catalizador a lo largo del soporte para impedir la aglomeración. Para solucionar este problema, se realiza el depósito de las nanopartículas a la vez que se rota el soporte de carbón vítreo, lo cual favorece una mayor dispersión de catalizador y un mejor comportamiento de éste, como se confirma con la mayor actividad observada siguiendo un nuevo procedimiento de preparación que promueve un depósito con las partículas más dispersas.

Las investigaciones con electrodos modificados de nanopartículas de platino con átomos de un metal diferente se inician en el capítulo 6, empleando para ello las mismas muestras (100)Pt y (111)Pt de los capítulos anteriores. El primer estudio se refiere a la oxidación de ácido fórmico en las nanopartículas de platino con Tl adsorbido, el cual favorece la oxidación de CO hasta CO_2 a bajos potenciales, especialmente en la muestra (100)Pt como se ratifica en experimentos FTIR. Se estudia el efecto de la diferente concentración de ácido fórmico para los mismos electrodos modificados, mostrando como aumenta la actividad para la oxidación de ácido fórmico a pesar de que se demuestra que el mecanismo de oxidación no es tan sencillo como aparenta. A la vista de los resultados, se acepta que el Tl ejerce un efecto de tercer cuerpo sobre la superficie de platino, impidiendo la ruta indirecta de oxidación del ácido fórmico (por medio de la formación de CO) y favoreciendo la ruta directa de oxidación de ácido fórmico, sin descartar los efectos electrónicos.

Por último, el capítulo 7 trata de encontrar la combinación óptima entre las muestras (100)Pt y (111)Pt y diferentes metales con el objetivo de completar la oxidación de etanol. Se prueban todas las combinaciones posibles entre los adátomos Sn, Rh, Ru y Pb con las dos muestras de nanopartículas de platino tanto en medio ácido como en medio alcalino. Para las disoluciones 0.5 M H_2SO_4, los nanopartículas de platino modificadas con Sn son las que muestran mejor comportamiento, principalmente con la mejora del potencial de inicio de la oxidación de etanol en las dos muestras de nanopartículas estudiadas, e incluso, para el caso de la (111)Pt, un incremento de la actividad. La explicación de este comportamiento se asigna a la catálisis en la oxidación del CO hasta CO_2 a bajos recubrimientos, mientras que con grandes cantidades de estaño en la superficie de platino se favorece la formación de ácido acético. Para el resto de superficies, el Ru únicamente

mejora levemente las corrientes a bajos potenciales, indicando una catálisis en la formación del CO_2, mientras que el Pb también mejora ligeramente la actividad, aunque sin llegar a alterar la distribución de productos. El Rh adsorbido sobre la superficie de platino no ejerce ningún efecto positivo para la oxidación de etanol. En medio 0.1 M NaOH, el mecanismo de reacción se modifica totalmente como se prueba en el capítulo 4, así que las superficies combinadas más efectivas no son las mismas que en medio ácido. Así, las superficies combinadas Pt-Ru no muestran ningún efecto catalítico en medio alcalino, mientras que las superficies Pt-Sn, Pt-Rh y Pt-Pb enseñan pequeñas mejoras en el potencial de inicio de oxidación del etanol, sin exponer cambios significativos en las corrientes medidas, sobre todo en el caso de las muestras de nanopartículas (100)Pt.

Como conclusión general de toda la tesis, hay que resaltar que se han aportado estudios fundamentales que confirman la tendencia en cuanto al efecto de la estructura superficial en los mecanismos de la oxidación de etanol y ácido fórmico para las nanopartículas de platino, tanto en medio ácido como en medio alcalino, prestando especial atención a parámetros que pueden afectar la reactividad como la aglomeración de partículas. Además, se ensayaron electrodos útiles desde el punto de vista electrocatalítico para la oxidación de etanol en medio ácido, como es el caso de la combinación Pt-Sn para la oxidación de etanol y la combinación de Pt-Tl para la oxidación de ácido fórmico, aportando información valiosa para la posible elaboración de nuevos catalizadores a partir de aleaciones bimetálicas válidas para estas dos reacciones.

Chapter 8: Conclusions

The present thesis includes fundamental studies for ethanol and formic acid oxidation on shape-controlled and carbon supported platinum nanoparticles. The final aim of these studies is to understand the oxidation process to achieve the complete oxidation to CO_2, avoiding the formation of undesired species during the reaction. Starting with ethanol, the main molecule studied in this thesis, several investigations have been carried out on the effect of different parameters on the reactivity. These parameters include the surface structure of the platinum catalyst, the pH effect (containing alkaline solutions), the importance of the correct nanoparticle dispersion on the carbon support and, finally, the changes in the electrocatalysis after modifying the platinum nanoparticles surfaces with a different adatoms. Modified platinum nanoparticles have been also used in the study of the formic acid oxidation reaction. Electrochemical (cyclic voltammetry and chronoamperometry), spectro-electrochemical (FTIR with external reflection and ATR) and mass spectrometry techniques (DEMS) have been employed in the examination of the oxidation mechanisms.

The first work presented in the thesis (chapter 2) demonstrates that the surface structure trends observed with single crystal electrodes for the reactivity of ethanol oxidation are also valid for the reactivity of shape-controlled platinum nanoparticles. {100} domains are effective for promoting the C-C bond scission, whereas {111} sites favor acetaldehyde/acetic acid formation. On the other hand, the effect of the competitive adsorption of sulfate is also investigated, employing H_2SO_4 and $HClO_4$ solutions. In both supporting electrolytes, this adsorption has no effect on the currents due to the presence of acetate anions coming from the acetic acid production after ethanol oxidation, which can compete with ethanol for the platinum active sites.

As an approach for the pH effect studies, chapter 3 deals on the ethanol oxidation reaction in the same shape-controlled platinum nanoparticles, working always at pH values lower than 4. Employing DEMS, the differences in reactivity between nanoparticles with {100} and {111} preferential domains are investigated. (100)Pt is confirmed as the best

sample for the cleavage of the C-C bond, ratifying the higher efficiency compared with the (111)Pt nanoparticles. When the pH of the working solution is increased, $CH_{x,ads}$ formation is augmented at low potentials respect to the poison present in the form of CO_{ads}. For the (111)Pt nanoparticles sample, the formation of one-carbon fragments is prevented as pH increases, favoring the acetaldehyde/acetic acid formation.

Chapter 4 addresses the subject of ethanol oxidation in alkaline medium. Since there are no previous studies on the surface structure effect, experiments were carried out first with surfaces with a well-defined structure, *i.e.*, platinum single crystal electrodes, especially basal planes and stepped surfaces with {111} terraces. The activity is higher in alkaline media than in acidic media and the Pt(111) surface exhibits the largest oxidation currents followed by Pt(110) and Pt(100), which is the opposite order to that obtained in acidic solutions. However, selectivity for CO_2 production is very low, almost negligible when compared with the amount of acetaldehyde/acetate produced, regardless the crystallographic orientation of the working electrode. Also, the Pt surfaces show a large deactivation because of the polymerization of acetaldehyde formed on the catalyst, which inhibits ethanol oxidation, mainly in surfaces with large {111} terraces.

After the fundamental studies with single crystal electrodes, chapter 5 investigates ethanol oxidation in alkaline medium employing the same shape-controlled platinum nanoparticles of the previous chapters, using similar approach than that carried out in chapter 4. The results obtained there for the preferential acetate formation are confirmed with these Pt nanoparticles samples. Additionally the onset of ethanol oxidation in alkaline medium is related to the different potentials for the OH adsorption depending on the crystallographic orientation. Additionally, it is also corroborated using IR experiments that the almost only product formed in the oxidation is acetate, regardless of the shape-controlled platinum nanoparticle sample employed. On the other hand, the studies with spherical platinum nanoparticles supported on carbon with different metal loadings demonstrate the importance of the correct catalyst dispersion on the support for preventing the particle agglomeration. To solve this problem, the deposit is performed under rotation of the glassy carbon, which optimizes the catalyst dispersion and its behavior, as it is corroborated with the higher activity observed in ethanol oxidation observed after this new preparation procedure.

The studies with platinum nanoparticle electrodes modified by a foreign metal atom are conducted in chapter 6, using the previously used (100)Pt and (111)Pt samples. The first work refers to formic acid oxidation in platinum nanoparticles with adsorbed Tl, that promotes CO oxidation to CO_2 at low potentials, especially in the (100)Pt sample as it was verified with FTIR experiments. The observed effect of the formic acid concentration in the currents demonstrates that the oxidation mechanism is not as simple as it appears. From the obtained results, it is accepted that Tl exercises a three-body effect on the platinum surface, avoiding the indirect route of formic acid oxidation (after the CO formation) and favoring the direct route for formic acid oxidation, without discarding the presence of electronic effects.

At last, chapter 7 tries to find the optimal combination between (100)Pt and (111)Pt samples and the different adatoms, with the objective of achieving the complete oxidation of ethanol. All the possible combinations using Sn, Rh, Ru and Pb adatoms and the two platinum nanoparticle samples in both acidic and alkaline mediums were tested. For 0.5 M H_2SO_4 solutions, platinum nanoparticles modified by Sn present the better electrocatalytic behavior, mainly for the improvement of the onset potential for ethanol oxidation in both platinum nanoparticles studied. The explanation for this behavior is assigned to the catalysis of CO oxidation to CO_2 at lower coverages by a bifunctional mechanism, whereas with higher tin coverages on the platinum surface, acetic acid formation is favored. For the other surfaces, only Ru shows small improvements in the currents at low potentials (indicating the catalysis in the CO_2 production), whereas Pb also slightly enhances the activity, although without altering the products distribution. Rh adsorbed on platinum surface does not have any positive effect for ethanol oxidation. In 0.1 M NaOH, the oxidation mechanism is completely different as was proved in chapter 4, causing a change in the effectiveness of the mixed surfaces from that observed in acidic solutions. Thus, Pt-Ru surfaces do not show any catalytic effect in alkaline medium, whereas Pt-Sn, Pt-Rh and Pt-Pb display small improvements in the onset potential for ethanol oxidation, especially for the (100)Pt nanoparticles sample. However, the experimental results do not show significant changes in the measured currents.

As a general conclusion, this doctoral thesis provides fundamental studies which confirm the tendency in the surface structure effect for ethanol and formic acid oxidation

on the platinum nanoparticles in both acidic and alkaline medium, paying special attention to different parameters such as the particles agglomeration that can affect the reactivity. In addition, practical electrodes from the electrocatalytic viewpoint for ethanol (Pt-Sn) and formic acid oxidation (Pt-Tl) in acidic solutions have been tested, providing valuable information for the preparation of new catalysts using bimetallic alloys.

Lista de publicaciones

Lista de publicaciones

Publicaciones relacionadas con los trabajos realizados en la tesis:

1. Carlos Busó-Rogero; Vitali Grozovski; Francisco J. Vidal-Iglesias; José Solla-Gullón; Enrique Herrero; Juan M. Feliu; **Surface structure and anion effects in the oxidation of ethanol on platinum nanoparticles**, *Journal of Materials Chemistry A*, Volume 1, Issue 24, Pages 7068-7076 (2013).

2. Carlos Busó-Rogero; Enrique Herrero; Juan M. Feliu, **Ethanol Oxidation on Pt Single-Crystal Electrodes: Surface-Structure Effects in Alkaline Medium**, *ChemPhysChem*, Volume 15, Issue 10, Pages 2019-2028 (2014).

3. Carlos Busó-Rogero, Juan V. Perales-Rondón; Manuel J. S. Farias; Francisco J. Vidal-Iglesias; José Solla-Gullón; Enrique Herrero; Juan M. Feliu; **Formic acid electrooxidation on thallium-decorated shape-controlled platinum nanoparticles: an improvement in electrocatalytic activity**, *Physical Chemistry Chemical Physics*, Volume 16, Issue 27, Pages 13616-13624 (2014).

4. Carlos Busó-Rogero; José Solla-Gullón; Francisco J. Vidal-Iglesias; E. Herrero; Juan M. Feliu; **Oxidation of ethanol on platinum nanoparticles: surface structure and aggregation effects in alkaline medium**, *Journal of Solid State Electrochemistry*, Volume 20, Issue 4, Pages 1095-1106 (2016).

5. Carlos Busó-Rogero; Sylvain Brimaud; José Solla-Gullón; Francisco J. Vidal-Iglesias; Enrique Herrero; R. Jürgen Behm; Juan M. Feliu; **Ethanol oxidation on shape-controlled platinum nanoparticles at different pHs: A combined in situ IR spectroscopy and online mass spectrometry study**, *Journal of Electroanalytical Chemistry*, Volume 763, Pages 116-124 (2016).

6. Carlos Busó-Rogero; José Solla-Gullón; Francisco J. Vidal-Iglesias; Enrique Herrero; Juan M. Feliu; **Adatom modified shape-controlled platinum**

nanoparticles towards ethanol oxidation, *Electrochimica Acta*, Volume 196, Pages 270-279 (2016).

Otras publicaciones:

7. Sara Chumillas; Carlos Busó-Rogero; José Solla-Gullón; Francisco J. Vidal-Iglesias; Enrique Herrero; Juan M. Feliu; **Size and diffusion effects on the oxidation of formic acid and ethanol on platinum nanoparticles**, *Electrochemistry Communications*, Volume 13, Issue 11, Pages 1194-1197 (2011).

8. Carlos Busó-Rogero; Enrique Herrero; Jochen Bandlow; Aleix Comas-Vives; Timo Jacob; **CO oxidation on stepped-Pt(111) under electrochemical conditions: insights from theory and experiment**, *Physical Chemistry Chemical Physics*, Volume 15, Issue 42, Pages 18671-18677 (2013).

9. Manuel J. S. Farias; Carlos Busó-Rogero, Rubén Gisbert, Enrique Herrero and Juan M. Feliu, **Influence of the CO Adsorption Environment on Its Reactivity with (111) Terrace Sites in Stepped Pt Electrodes under Alkaline Media**, *Journal of Physical Chemistry C*, Volume 118, Issue 4, Pages 1925-1934 (2014).